TRUMOX-30 CANDU-900

ANALYSIS OF TRANSURANIC MIXED OXIDE FUEL IN A CANDU

NUCLEAR REACTOR

By

ANDREW CHRISTOPHER MORREALE, B.ENG.MGT, M.ENG

A Thesis Submitted to the School of Graduate Studies

In Partial Fulfilment of the Requirements for the Degree of

Doctor of Philosophy

McMaster University

McMaster University DOCTOR OF PHILOSOPHY (2012) Hamilton, Ontario
(Engineering Physics)

TITLE: Analysis of Transuranic Mixed Oxide Fuel in a CANDU Nuclear Reactor

AUTHOR: Andrew Christopher Morreale, B. Eng. Mgt, M. Eng
                  (McMaster University)

SUPERVISORS: Professor J. C. Luxat, Professor D. R. Novog

NUMBER OF PAGES: xiv, 269

Abstract

The reprocessing of spent fuel is a key component in reducing the end waste from nuclear power plant operations and creating a sustainable closed fuel cycle. Central to this effort is the extraction and reprocessing of actinide materials to be recycled into fast or thermal reactors. Reprocessed actinides can contribute additional energy and may be partially transmuted in current thermal systems using mixed oxide fuels before being sent to fast reactors. The use of current thermal reactors as an intermediary step significantly reduces the fast reactor infrastructure needed to handle the spent fuel inventory in the long term, and also provides a source of additional energy from existing mined resources in the short term. An optimization of the fast and thermal systems in a closed fuel cycle reduces the end cycle waste to primarily fission products which have little residual value and manageable disposal and monitoring demands. The dissertation explores the design and analysis of an actinide transmutation solution utilizing a current thermal reactor design. The TRUMOX-30 CANDU-900 system defined herein uses a mixed oxide fuel containing 3.1% transuranic actinides extracted from 30 year cooled spent fuel from a prototypical Pressurized Water Reactor (PWR) and mixed with natural uranium. A significant constraint imposed on the design is that the actinide burning is to occur in an existing CANDU design without major changes or infrastructure replacement. Hence the standard CANDU design and analysis methodology was employed to produce and evaluate the system. The phased approach includes extensive neutron transport modeling of the lattice and control device super-cell configurations, which feed forward in to a detailed full core diffusion model of the TRUMOX-30 CANDU-900 design. Suitable fuel burnup and significant actinide conversion was achieved while remaining within the prescribed operational envelope of the CANDU reactor. The design was evaluated against existing operational constraints and limits, performing well and achieving the goal of actinide transmutation with no changes to the reactor design. This effort demonstrated the adaptation of a current CANDU-900 reactor as a platform for intermediary actinide transmutation which may form part of a sustainable and efficient fuel cycle.

Acknowledgements

Contents

List of Figures

List of Tables

List of Abbreviations

Abbreviations

2D	two dimensional
3D	three dimensional
ACR	Advanced CANDU Reactor
ADS	Accelerator Driven Systems
AECL	Atomic Energy of Canada Limited
BNA	Burnable Neutron Absorber
BOC	Beginning of Cycle
BWR	Boiling Water Reactor
CANDU	Canadian Deuterium Uranium
CANFLEX	CANDU Flexible Fuelling
CVR	Coolant Void Reactivity
DUPIC	Direct Use of PWR fuel In CANDU
ENDF	Evaluated Nuclear Data Files
EOC	End of Cycle
FPD	Full Power Day
HE	Heavy Element
HWR	Heavy Water Reactor
IMF	Inert Matrix Fuel
IST	Industry standard toolset
JEFF	Joint Evaluated Fission and Fusion File
JENDEL	Japanese Evaluated Neutron Data Library
LEU	Low Enriched Uranium
LOCA	Loss of Coolant Accident
LWR	Light Water Reactor
LZCR	Liquid Zone Controller
MCA	Mechanical Control Absorbers
MOX	Mixed Oxide
NRU	National Research Universal
NU	Natural Uranium
NUE	Natural Uranium Equivalent
NUO_2	Natural Uranium dioxide
PHTS	Primary Heat Transport System
PHWR	Pressurized Heavy Water Reactor
PPF	Pin Power Factor

PRCAD	Pattern Random Channel Age Distribution
PWR	Pressurized Water Reactor
RFF	Radial Form Factor
RRS	Reactor Regulating System
RU	Reprocessed Uranium
SDS	Shutdown system
SEU	Slightly Enriched Uranium
TRUMOX	Transuranic Mixed Oxide
VE	Void Effect

Units

$ (dollars)	Reactivity /delayed neutron fraction $(\Delta\rho/\beta)$
barn	10^{-24} cm^2
eV	electron-Volt
mk	milli-k
MWD/kgHE	megawatt days per kilogram heavy element
MWD/T	megawatt days per ton
MWh/kgHE	megawatt hours per kilogram heavy element
MWe	megawatts electrical
n/kb	neutrons per kilo-barn
THM	tons heavy metal
W	Watt
wt%	weight percent

Variables

ν	Neutrons emitted per fission event
σ	Microscopic cross section, (cm^2)
Σ	Macroscopic cross section (cm^{-1})
χ	Energy distribution of fission neutrons
υ	Neutron velocity

Chapter 1

Introduction

Nuclear fission has been an important method of electrical energy generation in many countries for several decades. Nuclear energy is receiving increased interest due to the desire for low carbon energy production and the desire to replace and refurbish some of the aging nuclear fleets. This further interest brings into focus the major public concerns in the nuclear industry, specifically the desire for safe operation to address safety issues and lessons learned post-Fukushima and the need to meet the challenge of dealing with spent fuel inventories. A majority of existing nuclear energy infrastructure operates on a once-through concept, where processed ore is used in a reactor for a finite period of time and then earmarked for eventual long-term storage. Spent fuel, due to its long term radiotoxicity and heat generation, requires the design of long-term repositories capable of mitigating the associated hazards. However, spent fuel still contains a significant amount of energy that, if accessed, would provide more useful power per ton of mined ore and decrease the repository burden per megawatt (MW) of energy produced. Research into closing the once through fuel cycle and dealing with spent fuel inventories using existing thermal reactor technologies and new technologies such as Accelerator Driven Systems (ADS) and fast spectrum reactors is being promoted worldwide.

The prevalent once through fuel cycle approach used in current reactors and the "wait and see" attitude to spent fuel reprocessing and disposal may significantly impact the public attitude toward nuclear energy as a safe, clean and abundant energy source. The spent fuel can be used in recycling and reuse projects, which reprocess the fuel, extracting useful materials that can be integrated into a new fuel cycle. These actions reduce the amount of actual waste that must be stored and monitored and the length of time that the waste has serious effects. Such steps are necessary for a nuclear industry that is interested in expanding generating capacity and operators worldwide.

There are several methods that can be utilized to reuse and recycle different portions of the spent fuel inventory which are discussed in Chapter 2. A simple and direct activity is the recycle of uranium. However, the most promising efforts, in terms of impact on spent fuel storage, are the reprocessing of long lived actinides. Through combined strategies of uranium recycle and actinide reprocessing the current inventories of spent fuel can be separated out and reused such that the actual end waste of the system is reduced to primarily the fission products. For the current inventory of fuel the fission products make up about 3 to 5% of the mass of spent fuel and hence abundant energy reserves exist within the spent fuel [1]. Thus recycle and reprocessing efforts would have a significant impact on the long term management of spent fuel output from nuclear power generation. The reduction in waste volume per MW of energy produced is also supplemented by the shorter decay periods, lower heat loads and more manageable logistics of storing only the fission products. The actinides and usable uranium are sent back into the fuel cycle to be consumed. These recycle efforts provide much more efficient use of the fissile isotopes in the fuel and provide the capability to transmute the actinide components, which are the largest contributors to long term (> 500 years) radiation levels and spent fuel heat loads.

The traditional method for the destruction of actinides has been to utilize a fast reactor system to provide the necessary high energy flux to transmute the actinides. However, while many countries continue to pursue fast reactor technologies, these systems have been high cost ventures with risky reliability that are still under heavy development. This has led to the desire to develop strategies for the transmutation of actinides in standard water cooled and moderated thermal reactor systems to the greatest extent practicable. These thermal systems are to serve as an intermediary step to reduce the actinide inventory and thus reduce the future fast reactor infrastructure required. Both light water reactors (LWR) and heavy water reactors (HWR) are being explored as potential systems for actinide transmutation [2]. An approach with significant impact is the partial or full core loading of actinide fuel assemblies containing group extracted actinides suspended in an inert matrix or blended into a uranium oxide carrier. The use of dedicated actinide targets composed of separately extracted minor actinides such as americium and curium is a smaller scale alternative but is not the focus of this study.

The production of actinide fuel using group extraction of neptunium, plutonium, americium and curium from spent fuel provides the added benefit of proliferation

resistance as the plutonium is never in a pure state. The carrier materials for the actinides include inert materials or uranium oxide. The embedding of the actinides in an inert non-fertile matrix avoids the production of new actinides from uranium isotopes as occurs in mixed oxide fuels[1]. However, these inert matrix options have different thermal and neutronics characteristics than standard uranium fuels making them difficult to utilize in full core configurations in the absence of significant design changes.

The blending of the actinides with uranium in a mixed oxide format produces a fuel with very similar behavior to standard UO_2 fuel and draws on the previous research into disposal of weapons plutonium and the experience of using plutonium-uranium mixed oxide fuels used to burn plutonium reprocessed from spent LWR fuel .

Current reactors have limited abilities to transmute actinides before the fuel is sent on to a fast reactor system (i.e. only a few cycles). The limitation on the number of cycles is driven primarily by the increased complexity of reprocessing spent actinide based fuels in each subsequent recycle process. Employing advanced fuel cycles and the current reactor fleet allows additional utilization of the energy in the fuel and reduces the majority of waste to the fission products portion of the spent fuel. The reprocessed fuel would be burned in current reactors for 1 to 2 cycles and then sent to fast breeder reactors to close the fuel cycle. This use of the current thermal reactor fleet to burn the reprocessed fuel for the first cycle reduces the necessary fast reactor infrastructure.

Actinide fuels present some challenges for current thermal reactors. The first impediment stems from the technology used to reprocess the LWR spent fuel inventories in an efficient and environmentally friendly manner. Secondly, due to limited full scale operational experience the thermodynamic and materials behaviors of these fuels have not been fully proven. Finally the use of these actinides in the fuel may produce a hardened neutron spectrum which can alter the response of control systems and may have effects on accident conditions.

There has been extensive experience in using actinide fuels for partial core loadings in light water reactors. This experience is mostly in plutonium driven

---

[1] Fertile isotopes of lower actinides such as U-238 can transmute, through successive neutron capture and decay, to higher actinides such as plutonium and americium.

reactions using mixed oxide fuels containing plutonium reprocessed from spent fuel. To a lesser extent, some of boiling water and pressurized water reactor units in Europe and Japan are utilizing group extracted actinide mixed oxide fuels in partial core loads of up to 30% [3]. Building on this operational experience, analysis is being done to determine the possibility of utilizing a full core load of actinide mixed oxide fuel in a light water reactor which can have even greater impact on the transmutation of actinides [3]. Alongside these efforts, research projects are being developed to determine the possibility of utilizing heavy water reactor designs for actinide transmutation and uranium recycle [4, 5, 6].

The heavy water CANadian Deuterium Uranium (CANDU®[2]) Reactor designs offer significant benefits in the transmutation of actinides. There is extensive flexibility due to high neutron economy, a simple compact fuel design and online fueling. The neutron economy produced by the combination of heavy water coolant and separate heavy water moderator along with low-neutron absorbing materials provides for efficient harnessing of the fuel at various levels of enrichment. Online fueling reduces the need for poison loading (i.e. boron in the moderator or coolant water) to counteract fresh fuel reactivity and provides constant management of the flux profile in the core. The fuel design of 37 or 43 elements in a circular multi-ringed arrangement provides for flexible fuel content including integrated poison and varied enrichment. Bundles can be optimized for linear power rating, coolant void reactivity or differential burnup. This adaptability and flexibility make CANDU an excellent reactor system for the employment of reprocessed actinide fuel.

The use of an actinide mixed oxide fuel in a CANDU platform requires in-depth analysis and assessment to ensure that the new fuel design can be operated within the safe operational envelope of the reactor. This assessment utilizes neutron transport lattice physics models, 3D super-cell simulations and full core diffusion simulations to design and evaluate a full core model of an actinide mixed oxide fuel in a CANDU reactor. The objective is to evaluate the relevant performance of the design to demonstrate the potential to achieve acceptable levels of actinide transmutation without extensive modifications to the operation or design of the standard CANDU reactor system.

---

[2] CANadian Deuterium Uranium (CANDU) is a registered trademark of Atomic Energy of Canada Limited (AECL)

The evaluation methodology used in this assessment, as discussed in Chapter 3, closely follows the standard design, tools and analysis practices utilized in the CANDU industry. This strategy ensures consistent analysis and allows for effective comparison to standard natural uranium (NU) fuel throughout the process. The actinide based fuels are designed to run in the CANDU reactor with minimal changes to operational strategy and no changes to the reactor systems with the exception of the fuel. Using these CANDU standard analysis procedures and comparing to NU fuel allows one to demonstrate that such new fuel designs fit within the operational envelope of the reactor. The actinide based fuel used is described in Chapter 4 and is referred to as transuranic mixed oxide (TRUMOX) fuel. The fuel blends group extracted transuranic actinides (neptunium, plutonium, americium and curium) with natural uranium in order to reach a specific burnup target. The burnup target in this study is 30 MWD/kgHE which is about 3 times the standard CANDU-900 burnup of 9.5 MWD/kgHE. This specific fuel is referred to as TRUMOX-30 fuel and has an actinide oxide content of 3.1% blended with 96.9% natural uranium dioxide (NUO_2). The fissile content of the fuel is 2.53%, about 3 times that of natural uranium fuel. This fuel impacts the neutronics of the reactor and requires special fuel designs incorporating integrated burnable neutron absorbers. While the MOX fuel and use of burnable poison represent significant changes from a typical CANDU-900 fuel assembly, the remainder of the reactor infrastructure does not require significant modifications. The full core modeling and analysis, described in Chapter 5, highlights the changes in operational strategy needed to accommodate this advanced fuel design and includes a detailed evaluation of the full core behaviour.

The dissertation systematically examines the important physics aspects to actinide burning in CANDU. First a review of the relevant literature in this field is presented in Chapter 2. The fuel and reactor operation is evaluated using a four phase procedure described in Chapter 3 which can be summarized as:

1. The multi-phase analysis begins with the design of the fuel composition and bundle geometry, presented in Chapter 4. The fuel is designed to meet specific burnup, fissile content and reactivity properties using a neutron transport code that models the properties of a lattice cell that is a building block of the full core reactor model and evaluates the cell reaction rates and cross sections over the full burnup cycle.

2. The second phase uses a three dimensional (3D) transport super-cell model to determine the incremental effect of the interaction of reactor control devices on the lattice cell cross sections. The tables of cell cross sections for the full burnup cycle and the incremental cross sections that relate to each control device in the core are inputs for the next phase.

3. The third phase involves a three-dimensional, two group neutron diffusion physics code that is used to model the full core reactor design with all relevant structures, devices and geometry using the lattice cell building blocks. The full core model is performed with lattice cell properties that are an average representation of the core during the burnup cycle, known as a time-average. This solution is then evaluated using several instantaneous models to determine if it is capable of maintaining within the operational envelope for a specific core burnup configuration that mimics the fuelling ripple. The model is refined such that the fuel design implementation meets the current CANDU regulatory limits and the operational envelope of the reactor design.

4. Upon completion of the suitable full core model, the fourth phase evaluates the operational impact of the new fuel design including reactor coefficients, control system responses and operational simulations including fuelling events. Figure 1.1 shows a flow chart of the design and analysis and the analysis codes (WIMS-AECL, DRAGON, RFSP) used for each of the steps.

The fuel design and first and second phases of analysis are detailed in Chapter 4 while the full core modeling and evaluation of the third and fourth phase are presented in Chapter 5.

The full core evaluation of an actinide based fuel in a CANDU reactor has not been fully investigated previously in open literature. In particular, the complete reactor physics analysis from lattice to core physics has not been systematically explored, nor have the operational impacts been predicted. The analysis is performed using the standard procedures and methodologies for CANDU fuel and reactor analysis. The dissertation includes the physics design and evaluation of a transuranic mixed oxide fuel and the development of full core loading procedures for the safe operation of a full core actinide fuelled CANDU-900 reactor. At each stage, the models are compared to the natural uranium fuelled CANDU design so

that all differences can be evaluated. This will help to ensure that the new fuel meets all the regulatory limits and operational guidelines for a CANDU reactor system. The conclusions of this work in Chapter 6 demonstrate an important step towards the full core utilization of recycled actinides in a CANDU.
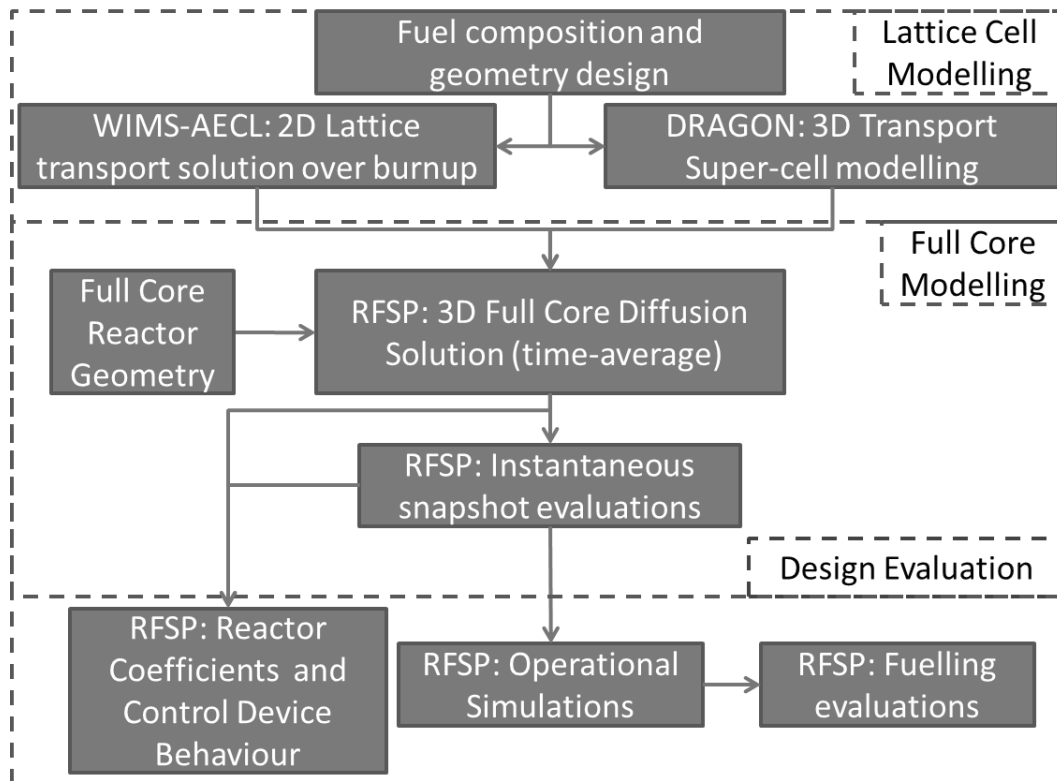
Figure 1.1: Flow Chart of Design Analysis

Chapter 2

Background and review of literature

The concept of actinide reprocessing is central to the closing of the nuclear fuel cycle and provides several benefits in both energy and resource utilization and in the streamlining of long term nuclear waste management. The benefits that motivate actinide reprocessing and the challenges faced are discussed herein along with the research and design experience that has led to the development and research into actinide burning in current thermal reactor systems. The benefits of CANDU as the reactor of choice are also explored and ultimately justify the exploration of a full core of actinide mixed oxide fuel in a CANDU reactor.

2.1 Background on actinide reprocessing

The reprocessing of actinides takes several forms with different end goals, challenges and benefits. The vast quantities of spent fuel stored on site at nuclear power instillations provide the feedstock available for reprocessing. The desire is to separate out the useful portions of the spent fuel leaving the fission products (about 3 to 5 wt% of the original heavy element (HE) mass [1]) to be disposed of. The useful material includes the remaining uranium isotopes (making up the largest portion of the spent fuel), the fissile actinides (primarily Pu-239 and Pu-241) and the minor actinides (neptunium, americium and curium). The minor actinides are not useful in the form of a feedstock for future fuel but they present long-term issues for repositories in terms of radiotoxicity and heat load. By reprocessing the minor actinides into new fuel or targets, they can be eliminated though transmutation to fissionable or shorter lived actinides that will fission and/or decay resulting in spent material with a shorter time horizon. The removal of the actinides, as discussed in Chapter 2.2, eliminates much of the long term heat and radiotoxicity loads and reduces the monitoring and disposal facility legacy to < 1000 years [7]. Thus it is important to include the minor actinides in the reprocessing scheme whether through separated target irradiation or through

grouped extraction and irradiation in a fuel carrier (e.g. uranium or an inert material such as silicon-carbide or zirconium).

Uranium driven fission in thermal systems produces actinides through neutron capture and transmutation of the uranium in the fuel. Primarily this is due to successive neutron capture starting in U-238 resulting in the production of higher plutonium isotopes which through beta decay and additional neutron capture can produce americium and curium. Neptunium is also produced in the reactor from successive neutron capture in U-235 which transmutes to U-237 and then through beta decay generates Np-237. The actinide reactions for the major isotopes are detailed in Table 2.1.

Actinides in this dissertation generally refer to isotopes of the transuranic elements: neptunium, plutonium, americium and curium. These are generated in uranium fuel that has been burned in a reactor and thus are present in the spent fuel. These actinides can be transmuted through successive neutron capture and decay reactions into fissile forms (e.g. Pu-239, Pu-241, Am-242) which through neutron fission can be eliminated resulting in the generation of fission products. This process of transmutation and fission removes the actinide isotopes from the fuel cycle, converting them to shorter lived fission products that are more easily managed. The thermal or fast reactor system utilized for actinide burning provides the neutrons that drive this process thus eliminating the actinides. The actinides are embedded in the spent fuel and in most cases must be reprocessed in order to be utilized for transmutation purposes. Reprocessing generally follows a method that separates the spent fuel into its major components which follow different paths in the fuel cycle. These components include uranium, plutonium, minor actinides (neptunium, americium and curium) and fission products.

The fission products are not useful for recycle and are stripped out and sent off for permanent disposal. They are usually converted to a stable non-leaching format using vitrification allowing the material to be safely stored and monitored on a long term basis until such time that the radiotoxicity levels of the fission products has decayed to a level similar to uranium ore. Upon extraction of the fission products, the useful materials of uranium, plutonium and the minor actinides remain to be dealt with. The uranium is generally handled separately while the plutonium and minor actinides can be dealt with either separately or together. Eventually the plutonium and actinides may be blended into uranium or other carriers in order to be utilized in the fuel cycle.

Table 2.1: Relevant Actinide Reactions [8].

Isotope	Reaction Information			
	Production (parent)	Decay [product] (half-life)	n-capture produces	Fission %
U-234	α (Pu-238)	α [Th-231] (2.5E5 y)	U-235	2
U-235	IC, n-c (U-234), α (Pu-239)	α [Th-230] (7.0E8 y)	U-236	84
U-236	n-c (U-235), α (Pu-240)	α [Th-232] (2.3E7 y)	Np-237 via U-237	5
U-238	IC, α (Pu-242)	α [Th-234] (4.4E9 y)	Pu-239 via U/Np-239	10
Np-237	n-c (U-236), α (Am-241)	α [Pa-233] (2.1E6 y)	Pu-238 via Np-238	1
Pu-238	n-c (Np-237)	α [U-234] (87.7 y)	Pu-239	1
Pu-239	n-c (U-238), α (Cm-243)	α [U-235] (2.4E4 y)	Pu-240	68
Pu-240	n-c (Pu-239), α (Cm-244)	α [U-236] (6563 y)	Pu-241	1
Pu-241	n-c (Pu-240), α (Cm-245)	β [Am-241] (14.4 y)	Pu-242	9
Pu-242	n-c (Pu-241), α (Cm-246)	α [U-238] (3.7E5 y)	Am-243 via Pu-243	2
Am-241	β (Pu-241)	α [Np-237] (432 y)	Am-242, Am-242m	0.4
Am-242	n-c (Am-241), i-t (Am-242m)	β [Cm-242] (16.0 h) e-c [Pu-242]	N/A	N/A
Am-242m	n-c (Am-241)	i-t [Am-242] (141 y)	Am-243	80
Am-243	n-c (Am-242m)	α [Np-239] (7370 y)	Cm-244 via Am-244	1
Cm-242	β (Am-242m)	α [Pu-238] (162.8 d)	N/A	N/A
Cm-243	IC	α [Pu-239] (29.1 y)	Cm-244	13
Cm-244	n-c (Cm-243)	α [Pu-240] (18.1 y)	Cm-245	0
Cm-245	n-c (Cm-244)	α [Pu-241] (8500 y)	Cm-246	86
Cm-246	n-c (Cm-245)	α [Pu-242] (4730 y)	Cm-247	7

IC = initial content, α = alpha decay, β = beta decay, n-c = neutron capture, e-c = electron capture, i-t = isomeric transfer, N/A = not applicable
U-237, U-239, Np-238, Np-239 Pu-243, and Am-244 are transition products that transmute through beta decay to long lived products of neutron capture.
Fission % denotes the likelihood of fission occurring due to neutron capture.

Uranium makes up the bulk of spent fuel, and once extracted can be reused in the original once-through fuel cycle as reprocessed uranium (RU). RU functions as an additional feedstock that can supplement newly mined uranium and can be enriched or blended with natural or depleted uranium stockpiles that are currently available to produce new reactor fuel. The RU fuels can be tailored to a desired composition such that they are nearly identical to standard new fuel. Thus integrating them into the front end of the fuel cycle for thermal systems is accomplished with little challenge.

Plutonium, like uranium can be adapted into the current nuclear fuel cycle in a mixed oxide (MOX) form that is primarily made up of fissile isotopes such as Pu-239 and Pu-241 and the fertile isotope Pu-240 along with various isotopes of uranium. Plutonium MOX fuels were developed extensively and utilized to burnup plutonium recycled from spent fuel in light water thermal reactors. The plutonium can also be used to provide initial fuel loadings for fast breeder reactor designs. There is potential for embedding plutonium in an inert matrix fuel (IMF) for use in current reactors or as fuel for Generation IV designs such as high temperature gas reactors.

The remaining elements, neptunium, americium and curium, are the minor actinides in spent fuel and generally require successive neutron captures before they are transmuted into a fissile form. Thus the minor actinides represent a neutron absorbing material that can be blended into the fuel or separately combined to produce dedicated transmutation targets. It is easier to extract the neptunium with the plutonium isotopes and produce Np-Pu MOX or IMF fuels and if blended properly to account for the capture properties of neptunium the operation of the fuel has little affect the fuel performance compared to Pu-MOX fuel [9]. The americium and curium can be easily adapted into Am-Cm targets that can be placed in reactors for direct transmutation or utilized as burnable neutron absorbers in a fuel assembly or control device.

The separation of the neptunium, plutonium, americium and curium into different reprocessing streams allows for direct disposal in a manner tailored for the specific material but presents an issue in the form of proliferation concerns, specifically the extraction of pure plutonium. The combined extraction of plutonium and the minor actinides from spent fuel avoids most proliferation concerns and produces a grouped actinide mixture with both fissile isotopes and neutron absorbing material that can be utilized in a MOX or IMF design.

Most of the experience in actinide reprocessing has come from the use of mixed oxide fuels where the actinides are blended with uranium to produce a fuel with similar thermal and neutronics properties as the standard fuels low enriched uranium (LEU) fuels used in LWRs and HWRs. Research has progressed with inert matrix fuels which provide another option for the transmutation of actinides.

An inert matrix carrier, such as silicon carbide or zirconium provides the most efficient and direct option for actinide burning because the carrier material is inert so the neutron interactions in the fuel are focused on transmutation and fission of the actinides. The inert carrier also does not produce any new actinides, which is a benefit over MOX designs. MOX fuels primarily utilize uranium as the carrier material which is fertile and can generate new actinides during the burnup cycle. However, IMF fuels do produces challenges in terms of fuel manufacture and operation. There is enhanced complexity in properly distributing the actinides in the inert material in order to manufacture fuel assemblies with similar power and burnup characteristics to standard LEU and NU fuels. As a result, IMF configurations are more easily utilized in advanced designs such as the high temperature gas reactor which is configured to use fuels that distribute the fissile material in an inert or moderating matrix (usually silicon-carbide and graphite) [10]. Operational challenges may arise due to the different neutronics and heat transfer characteristics of IMF designs compared to uranium oxide fuels. There has been some study regarding the use of a few outer channels in a CANDU core to burn IMF bundles. This is useful as it would allow for small scale actinide transmutation without significant effects on the overall power distribution [4].

The grouped extraction method is simpler and less costly to perform from a partitioning point of view [11] and the resulting fuel is still suitable for use in thermal reactor systems as an intermediary step before reaching a fast reactor. The challenge of grouped extraction is balancing the neutron absorption from the minor actinides and the increased production of higher actinides in the fuel, which affects the radiotoxicity and heat loads of spent actinide MOX fuels (as discussed, IMF bundles have less problems due to the lack of actinide production in the carrier material). The MOX fuel types most closely resemble standard fuel in their thermal properties, neutronics and power densities and are a viable option for creating a full core actinide fuel in a current thermal reactor system. If a full sustained cycle is employed, the spent actinide fuel bundles will also be partitioned and the actinides will be fed forward to a fast reactor system for ultimate disposal.

Fast reactors are the end of cycle system that is used to transmute the actinides into fission products and completely remove them from the fuel cycle. These reactors operate with a higher energy (faster) neutron spectrum and do not use a moderator like a thermal reactor. Due to lower fission cross sections and increased leakage, the fuel enrichment level required is increased over a thermal system (~20% compared to ~4% in PWR). However, the high neutron energy creates a favorable atmosphere for the breeding of fuel, Pu-239. Thus with an initial driver amount and the use of a U-238 fertile blanket the reactor can breed its own fuel with a conversion ratio > 1.0 thus allowing it to be self-sufficient after the initial loading. The breeding ratio of > 1.0 is possible because at high energies fission of Pu-239 is much more prevalent that the neutron capture and transmutation to Pu-240 (>100 times) and the neutron yield of Pu-239 fission is about 19% higher than for U-235 [12]. Additionally, the neutron capture of U-238 which produces Pu-239 is also more prominent in a fast spectrum. For the purposes of actinide transmutation, the fast reactor systems are also more favorable for the conversion of transuranic isotopes. The fission cross sections for the actinide isotopes (especially Np-237, Am-241 and Cm-244) are larger in a fast spectrum, especially above 1 MeV, see Figure 2.1. Thus there is more direct conversion and less generation of higher actinides through capture.
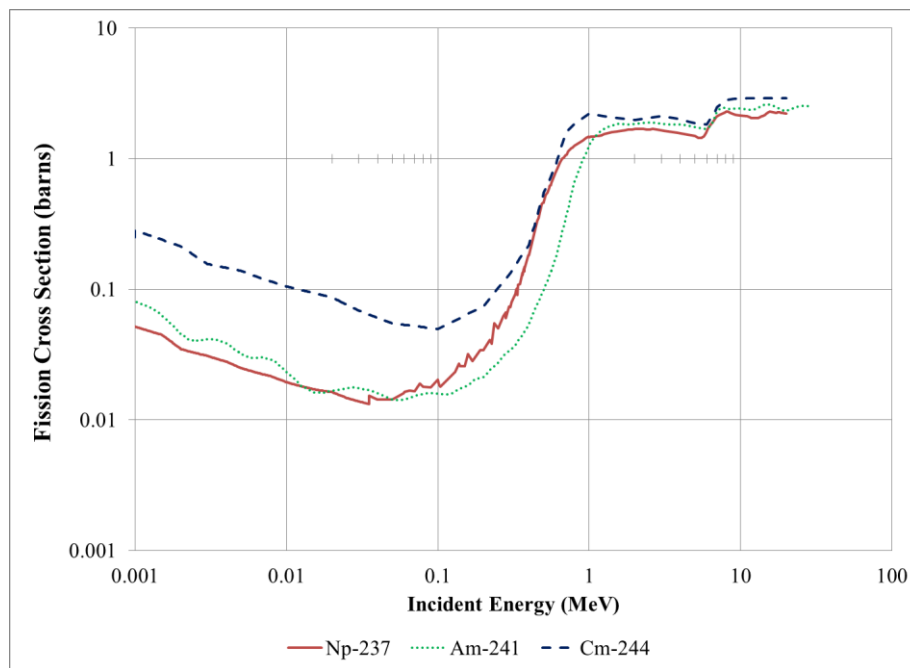
Figure 2.1: Actinide fission cross sections at high neutron energies [13].

The advantages of the fast spectrum systems make them ideal for actinide burning and they could theoretically be solely employed for the transmutation of actinides in the spent fuel produced by once through thermal system. However, fast reactor systems are more complicated than thermal systems and have had limited operational success. Thus the cost of employing fast reactors in this manner would be excessive. The alternative option, which this dissertation is associated with, is to utilize current thermal reactors to transmute some of the actinides before going to a fast reactor system. This reduces the amount of fast reactor infrastructure required. Also the thermal step provides a net removal of actinides from the fuel cycle, reducing the actinide inventory and avoiding the additional actinide production that would result from standard fuel use in these reactors.

2.2   Decay heat behaviour of spent fuel

Removing the actinides from the spent fuel and recycling them back into the fuel cycle, first in thermal and then in fast reactor systems, until they transmute and fission has a major effect on long term spent fuel management. Taking out the actinides even partially reduces the heat load, radiotoxicity and monitoring time for the spent material as only the fission products remain to be stored and monitored in the depository. The transuranic actinides are primarily responsible for the long term decay heat load of spent fuel and dictate the need for very long term disposal requiring deep geologically stable repository facilities. As seen in Figure 2.2, the decay heat power profile of spent nuclear fuel is dominated by fission products in the short term (< 100 years) and by actinides in the longer term [14]. These contributions are laid out numerically in Table 2.2.

The long term heat contributions and radiotoxicity loads from actinides are what spent fuel reprocessing seeks to address by reusing the actinides into new fuel or recycling them into reactors as burnup targets. The recycle of the actinides into new thermal reactor fuel seeks to transmute some of the actinides over the burnup cycle and to eventually transfer the spent actinides that remain into a fast reactor system that would be used to completely transmute them. This combined thermal-fast reuse cycle would see the spent fuel material reduced to the fission products which can be vitrified and stored for the ~500 years necessary for the radiotoxicity to return to the levels of regular uranium ore.
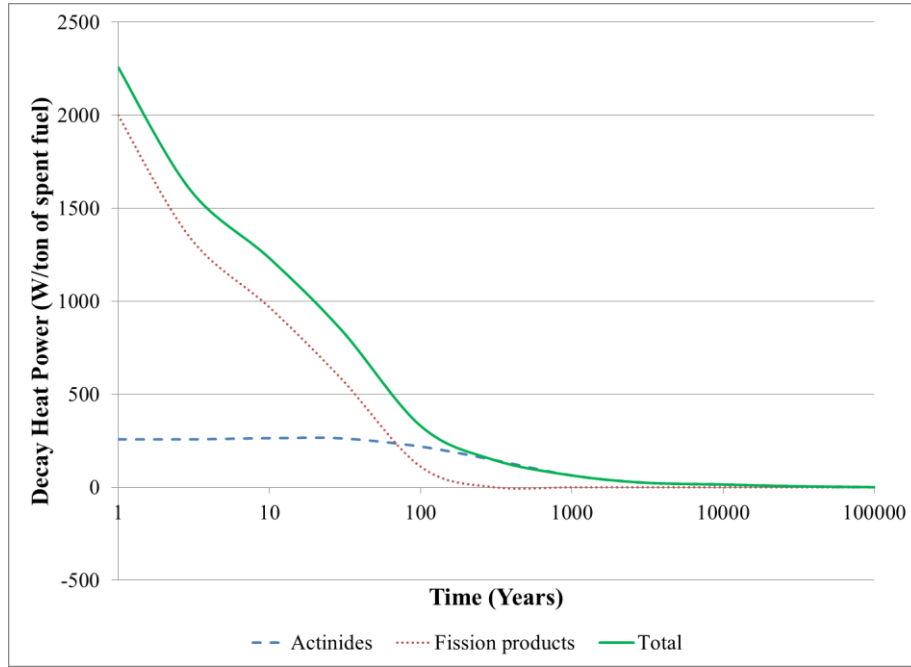
Figure 2.2: Contributions to spent fuel heat load [14].

Table 2.2: Contributions to Spent fuel heat load [14].

Time (Years)	Decay Heat Contribution (W/ton of spent fuel)		
	Actinides	Fission Products	TOTAL
1	258	2000	2258
3	258	1340	1598
10	264	968	1232
30	263	582	845
100	219	111	330
300	148	1.04	149.04
1000	63.8	0.0211	63.8211
3000	24.9	0.0209	24.9209
10000	14.7	0.0202	14.7202
30000	5.58	0.0183	5.5983
100000	0.846	0.0132	0.8592
300000	0.233	0.00573	0.23873

It is possible for all the actinide transmutation required for the spent fuel inventory to be done directly with fast reactor systems. However, the current success rate and operational experience with fast reactors is limited thus the spent

fuel inventories continue to build while fast reactor actinide burning technologies are researched and perfected.

The goal of the TRUMOX CANDU-900 system, described herein, and other thermal actinide burner designs is to provide an intermediary first step to transmute a portion of the actinides in the near future, reducing the current inventory before moving on to a fast spectrum system. This reduces the amount of fast reactors required and provides additional development and construction time for the fast systems. Thermal reactor actinide transmutation results in a significant reduction of the actinide content (> 30%) and offsets the production of new actinides that would result from using standard uranium fuel in the reactor.

As a first stage for fuel-reuse and for the intermediary cycle of burning actinide fuels in a thermal system there will be some transmutation and some production of actinides, especially using a MOX format with a fertile carrier such as uranium. Overall the actinide concentration will be reduced by a significant amount but by introducing actinides into the reactor system there is a net production of higher actinides such as curium in the fuel coming from the transmutation of neptunium, plutonium and americium isotopes. The curium production is not a major issue in the long run as most of the isotopes are shorter lived and can be eventually transmuted in the fast reactor system that is used to close the fuel cycle.

If the TRUMOX-30 CANDU-900 system is considered as a stand-alone process there are still benefits in terms of actinide destruction. The net actinide content decreases over the irradiation period and there is only a buildup of curium (almost entirely Cm-244 and lower). These primary curium isotopes produced are short lived when compared to the other actinides and have similar decay heat and radiotoxicity behaviour to that of the fission products. For example, Figure 2.3 displays the decay heat behaviour for the prominent actinide isotopes for a LWR spent fuel (VVER in this case). The portion of the decay heat from actinides is initially dominated by curium (especially Cm-244) for a period of about 10 years. After this period the decay heat becomes dominated by the production of Am-241 from the decay of Pu-241. The decay heat contributions of curium are very minor after 100 years and hence it behaves much like the fission products seen in Figure 2.2. If desired, the shorter lived curium isotopes (Cm-244 and lower) could be extracted from the fuel individually and vitrified along with the fission products but this individual extraction may be expensive and complicated. Thus movement of the curium into the fast reactor stage with the other actinides is preferred.

Therefore, the production of curium during the irradiation in thermal reactors is not a major issue in the reprocessing of spent fuel for the recycle of actinides.

In the event fast reactor system development is significantly delayed, there is a possibility to recycle the MOX fuel again in the thermal actinide burners. However, the build-up of higher isotopes of the actinides can limit the number of recycles and complicates the partitioning process that extracts the actinides. This stage is generally limited to about 2 iterations in the thermal system at which time the MOX fuels would have to be stored until such a time that a fast system becomes available to burn the actinides. In this case, the heat load and radiotoxicity of spent actinide MOX fuel would be of short-term concern as it will eventually be reprocessed into fast reactor fuel. Spent MOX fuels tend to have more actinide content with larger concentrations of higher actinide isotopes. This causes the radiotoxicity and decay heat power of a uranium-plutonium MOX fuel to be as much as 2.5 times higher than for that of uranium fuel [15]. Thus there will be a larger handling burden for the spent MOX fuel while it is stored awaiting the availability of fast reactor actinide burning capacity.
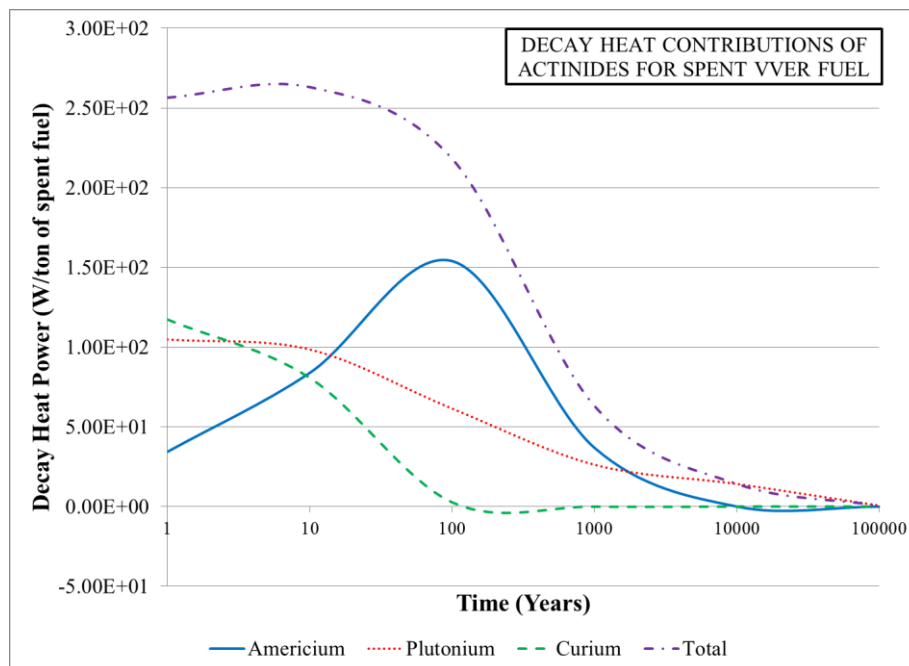
Figure 2.3: Contributions of actinide isotopes to spent fuel heat loads [14].

2.3   Fuel cycles

The classic nuclear fuel cycle of once-through fission of mined uranium, seen in Figure 2.4, is open ended and produces long term waste concerns. As discussed, the goal of actinide reprocessing is to extract both the useable fuel materials and the long lived actinides from the once through spent fuel so the materials can be reused thus reducing the end output of the fuel cycle to the fission products. Various methods can be employed to burn the actinides and reintroduce the fuel material into the cycle. These approaches can be classified as limited or continuous depending on the extent of the recycle of actinides and the number of reprocessing steps utilized.
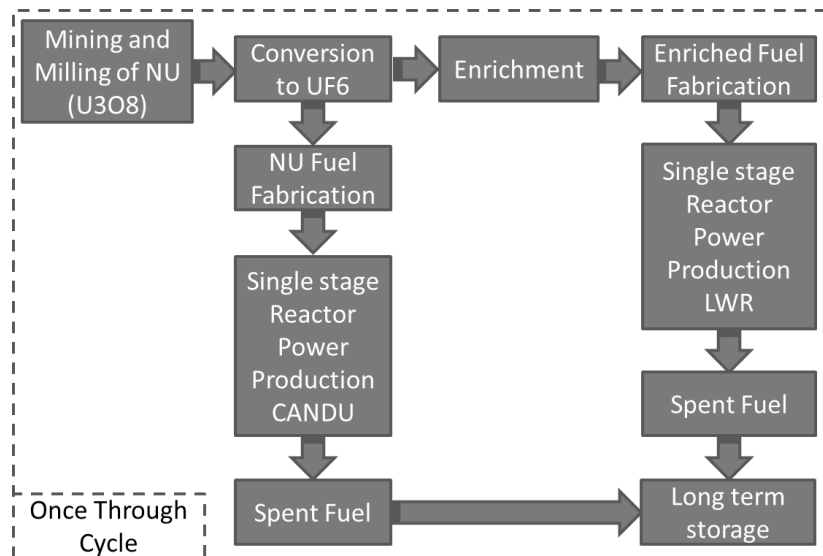
Figure 2.4: Flow diagram of the once through fuel cycle in CANDU in LWR

A limited cycle, displayed in Figure 2.5, extracts usable actinides and uranium from cooled spent fuel and integrates it with newly mined ore to be run through reactors. The uranium cycle combines the reprocessed uranium with newly mined ore or depleted uranium stockpiles and through blending or enrichment produces equivalent fuels for use in the single stage reactors of the once through fuel cycle. This includes processes like the direct use of recovered uranium from LWR spent fuel in CANDU reactors (CANDU-RU) and the lower risk short term method of natural uranium equivalent (NUE) which blends in depleted uranium to make a fuel that is equivalent to natural uranium [16]. The actinide cycle partitions the transuranic isotopes out of the spent fuel and blends them with newly mined or

reprocessed uranium to produce actinide MOX fuels or embeds them in inert materials so that they can be burned in thermal systems. The MOX options include the TRUMOX-30 CANDU-900 system, detailed in this thesis, and LWR fuel designs such as the CORAIL system [17]. Inert material options are also available in CANDU and LWR [4, 18].

Another set of procedures that fit into this limited cycle are those that do not partition the spent fuel into uranium, actinides and fission products but directly recycle the fuel material into reactors. These include the direct use of PWR fuel in CANDU (DUPIC) [19] and the combination of the spent fuel with enriched uranium to produce new PWR fuel, referred to here as PWR-DR [20]. The DUPIC process takes the cooled spent PWR fuel and through a dry process grinds it up and re-sinters the fuel into new pellets that are loaded into a 43 element CANDU bundle [19]. The PWR-DR process takes similar steps but blends in additional enriched uranium before sintering to increase the fissile content to normal PWR levels [20]. The minor actinide concentration increases with each recycling operation, affecting the fuel neutronics and complicating the spent fuel separation efforts. Thus, in the limited cycle, the fuel is recycled for a few iterations and then the end stage spent fuel is sent to a long term depository.
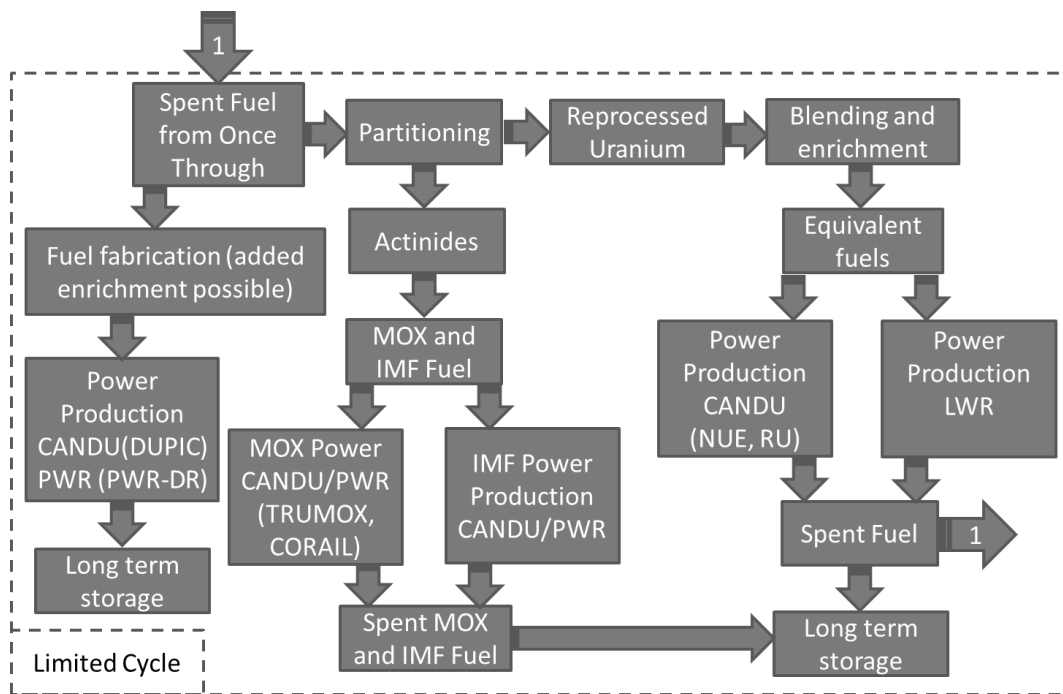
Figure 2.5: Flow diagram of limited cycle reprocessing

A sustained cycle, shown in Figure 2.6, extracts the actinides from spent fuel coming out of the once through process or any of the limited cycle processes and recycles them directly in to a fast breeder reactor. The actinides are burned in the fast reactor until they are totally consumed and fission products are the only output from of this closed cycle. The fast reactor used is a breeder reactor which uses a fertile blanket of U-238 to produce Pu-239 fuel and can achieve breeding ratios of greater than 1 such that the system is self-sufficient. The feedstock into the fast breeder system after the initial fissile content is the U-238 for the fertile blanket and the actinides that are being incorporated into the fuel to transmute and fission. The fertile blanket produces Pu-239 fuel which is reprocessed out and blended with the actinides to produce the new fuel for the fast reactor. Since more fuel is produced through the breeder blanket than is consumed the reactor can maintain sustained operation without added fissile material.
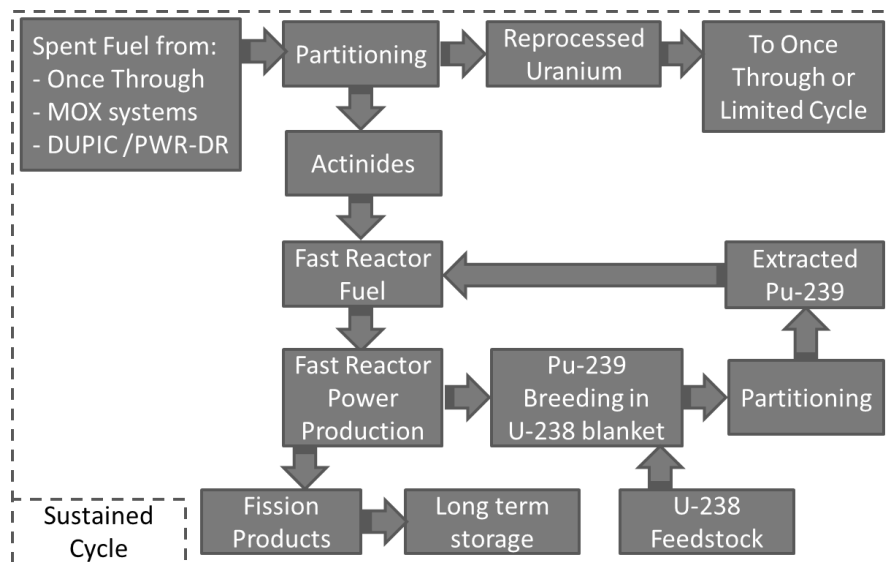
Figure 2.6: Flow diagram of continuous cycle

Thermal systems such as pressurized water, boiling water and pressurized heavy water reactors (PWR, BWR and PHWR) are plentiful and readily available worldwide but are unable to cope with more than a few iterations of actinide recycle before safe operation concerns arise [1]. Thus they are only viable for the limited cycle described above. As the separation efforts are more complex for each additional cycle it is ultimately necessary to progress to a sustained cycle

using a fast reactor system to eliminate the remaining actinides. Otherwise limited cycle spent fuel would be sent to an end repository for monitored storage.

The sustained cycle using a fast spectrum breeder reactor can be directly appended to the once-through cycle performing repeated and continuous recycle of fuel with minimal reprocessing steps and allowing the elimination of all the actinides. However, as discussed in Chapter 2.1, fast breeder designs are somewhat more complex, have higher capital and operational costs and there are only a limited number of demonstration plants in operation around the world (e.g. BN-600 in Russia, MONJU in Japan, etc. [21, 22]). Thus a significant amount of time is needed to improve the designs and develop the necessary fast reactor infrastructure to handle the actinide inventory that currently exists and the actinides that will continue to be produced by the current thermal reactor fleet.

Since the sustained cycle can also follow any of the limited cycle processes, there is the potential for synergy. Specifically, by using a limited cycle with thermal reactors first the spent fuel and actinide volume is reduced and less fast reactor infrastructure is required. The thermal reactors therefore shoulder some of the actinide burning load before fast reactor systems are employed. This coupled cycle provides the ability to start dealing with once-through spent fuel inventories using currently available thermal reactors while providing the development and construction time required for the establishment of the fast reactor infrastructure that will be used in the sustained cycle.

By employing the continuous or coupled recycle procedures described, the actinides are removed from the waste stream and all that remains are the fission products reducing the physical amount of waste per MW, radiotoxicity levels and heat load. This reduces demands on long term storage facilities and shortens the required monitoring time.

2.4 Benefits and challenges of reprocessing

The reprocessing and recycling of spent fuel and the movement away from a once-through fuel cycle to limited and continuous recycle strategies, presented in Chapter 2.3, provides significant benefits to the nuclear industry. These include reductions in overall waste volumes per MW, decreases in repository lifetimes and more efficient utilization fuel materials. The current once-through nuclear

generation cycle in the United States outputs about 100 GW of electrical energy resulting in 2200 tons of heavy metal (THM) of spent fuel per year [7]. The proposed long-term repositories have storage volume and heat load limits, which in turn dictate the volume of spent fuel that can be accommodated. For example, the Yucca Mountain project had an administrative maximum capacity of 70,000 THM and a temperature limit between adjacent waste rows of 96 °C (the local boiling point of water) [7, 23, 24]. Using these limits as a guideline, and assuming the current rate of nuclear power production remains constant, a repository of the size of Yucca Mountain would need to be opened every 32 years [7]. Considering the swell of interest in nuclear energy as a non-fossil and low-carbon emission power production strategy, there is a potential for expanded nuclear power usage and hence demands for repository space may increase.

As discussed, actinide extraction and the use of limited and continuous recycle operations can reduce the total end waste to only the fission products resulting is less waste per MW and lower heat loads and time horizons for fuel monitoring and storage. Proper use of a coupled or continuous strategy, explained in Chapter 2.3, could increase the repository loading by a factor of 200, reducing the demand for large repository facilities [23]. These estimates are at the extreme end of the success rate and rely on extensive fast reactor technology and a continuous recycle strategy to attain maximum benefit. As discussed, the limited cycle methods provide an intermediary step that can help to deal with the actinide inventory while buying time for the development of fast reactor infrastructure.

Considering limited cycles as a stand-alone one-iteration process that reuses the spent fuel of the once through systems there are still benefits. The partitioning of the spent fuel into the actinide materials and the uranium reduces the end spent fuel volume. In order to manufacture MOX fuel the actinides from a larger amount of once through spent fuel is needed. In the case of TRUMOX-30 fuel each ton of MOX fuel requires the actinide content from about 2.9 tons of spent PWR fuel. For MOX recycle in PWRs the actinide content is higher in PWR-MOX requiring about 4.9 tons of spent PWR fuel as feedstock for each ton of heterogeneous CORAIL-TRU fuel bundles that contain 30% MOX fuel rods which have transuranic loadings of about 20% [17]. This is similar for other recycle cases in LWRs which require about 5 once through UO2 elements for 1 MOX element [7]. The reduction in waste volume is supplement by the efficiency gains from using the fuel material more than once.

The recycle cases generate power from burning the actinides and feed the reprocessed uranium into the fuel cycle to be used a second time. The increased amount of MWe/kg of fuel is also complimented by the fact that the limited cycle methods are actinide burners and thus reduce the actinide inventory in the fuel cycle rather than generating more actinides as a once through system would, resulting in lower amount of actinides produced per MWe.

A direct cycle like DUPIC has similar benefits coming from burning the fuel material twice but has less impact on the spent fuel inventory as all the fuel material is directly recycled into the new DUPIC fuel and the inclusion of the fission products reduces the transmutation efficiency. The reuse of fuel materials allows current inventories of spent fuel to supplement freshly mined sources; thus allowing the nuclear industry to cope better with increased fuel demand.

Reprocessing, despite its efficiency and economic benefits, presents unique challenges. Partitioning and transmutation activities required to extract the actinides from spent fuel are complex, involve extensive chemical processing and must employ various safeguards. At all times criticality and radiation protection concerns must be addressed combining the hazards of large scale chemical processing and nuclear fuel production as well as the associated waste streams generated. Current methods require stringent controls and have high costs which are important issues in determining the viability of reprocessing. Reprocessing methods technology and costs are not explored here as the focus of this work is on the feasibility of utilizing reprocessed spent fuel not its fabrication.

Additional challenges arise with the spent MOX fuels which, with higher actinide content, have higher heat loads and require more space in repositories than regular spent fuel. Thus a limited cycle that does not move on to a sustained cycle will require more repository space for its MOX fuel inventory than for the equivalent amount of once through fuel. Additional challenges can arise with some MOX fuels that have high plutonium and minor actinide content as neutron absorbing materials may be needed in the spent fuel containers to avoid criticality concerns [7]. These issues bolster the argument that combined and sustained cycles are best at effectively dealing with long term fuel management concerns.

Current reprocessing of actinides is confined to light water reactors that utilize mixed oxide bundles in a portion of the channels of the core (10-30%). This method has been well studied and employed and thus is considered a mature

technology [3]. Other areas that are developing include research into direct burning of PWR fuel in CANDU reactors. DUPIC work has included research reactor test irradiations of the fuel and operational feasibility and safety calculations of a DUPIC CANDU system have been performed using conventional design and analysis tools [19]. The direct burning processes, like DUPIC, avoid any partitioning of the fuel into the uranium, actinides and fission products. This avoids some of the challenges of chemical reprocessing but has fewer benefits to the fuel cycle as there is less reduction in the spent fuel generated per MW. Also since the fission products are still in the fuel there is increased neutron loss and thus lower transmutation of actinides. On the uranium recycle side, the use of NUE fuels in CANDU has been developed as a low risk method for reusing reprocessed uranium and for utilizing stockpiles of depleted uranium from the enrichment process. This method has included extensive calculations and small scale tests of NUE fuel in a CANDU reactor performed in 2010 [16].

The current smaller scale reprocessing activities are providing extensive operational experience but currently have limited impact on long term waste concerns. The next step is to expand actinide transmutation with more reactors utilizing actinide based fuels, larger core loadings, increased use of minor actinide targets and eventually the development of fast reactor systems to close the cycle. The challenges involved in this expansion include designation of suitable reactor systems that can operate with a full actinide core and still achieve suitable transmutation rates. A fuel design using a mixed oxide or inert matrix carrier must be produced along with other target designs to be used in reactor control devices or accelerator systems. The objective herein is to design and evaluate a mixed oxide actinide fuel to be employed full core in a CANDU-900 pressurized heavy-water reactor.

2.5   Plutonium mixed oxide fuels

Current thermal reactor designs were first employed in actinide transmutation through the use of plutonium/uranium mixed oxide fuels. Research was initiated as an avenue to consume plutonium from nuclear weapons material as a method of eliminating some of the stockpiles that had accumulated during the cold war and was expanded to utilize plutonium reprocessed from spent fuel. Plutonium burning using MOX has been fully explored in both light and heavy water reactor systems and there has been extensive operation experience with partial core

loadings (10-30%) of plutonium MOX in many PWR and BWR reactors [3]. This experience with mixed oxide fuels has been essential in the development of actinide based MOX fuels containing both plutonium and group extracted minor actinides. Plutonium derived from weapons material is primarily Pu-239 (~93.8%) with some Pu-240 (~5.8%) and traces of Pu-241 and Pu-242 [25]. The Pu-239 is fissile and the Pu-240 is easily transmuted into Pu-241 which is also fissile. The weapon's plutonium is usually in metallic format and is almost purely fissile material. It must be converted into plutonium oxide and then blended with natural or depleted uranium oxide to produce MOX with an enrichment level suitable for a light water or heavy water system. Plutonium feed stock from the recycle of spent fuel is obtained through separated extraction methods and is still primarily Pu-239 (66.6 wt%) [26]. The content of the higher plutonium isotopes is increased (Pu-240 = 23.8 wt%, Pu-241 = 3.6 wt%, and Pu-242 = 4.5 wt%) adding more fertile material and increasing the production of higher actinides in the MOX fuel [26]. The reprocessed spent fuel plutonium is still quite simple to use for MOX fuel and is currently employed in LWRs in many European countries and Japan. The production of mixed oxide fuel for LWR reactors is quite mature and the fabrication technologies for such fuels are well developed and employed on an industrial scale [3].

The plutonium mixed oxide fuels are a natural building block for the grouped recycle of actinides from spent nuclear fuel. In the case of separated extraction, the plutonium was fed into the MOX feedstock and the other minor actinides were collected and either stored or fabricated into direct irradiation targets. However, the use of grouped extraction methods to produce MOX is also being explored due to their increased simplicity and proliferation resistance [11]. The bulk of the actinide material is plutonium (~84.5 wt%) providing the necessary fissile content but the minor actinides and the larger Pu-240 content increase neutron capture and thus effect the loading necessary for a fuel with suitable burnup [26]. Actinide based MOX fuels are being employed extensively in LWR systems with partial core loadings of up to 30% and studies into 100% core loadings are being conducted [3].

For heavy water reactor designs, there has been significant exploration into the use of CANDU reactors for plutonium disposal from nuclear weapons materials or spent LWR fuel conducted by Ontario Hydro and Atomic Energy of Canada Limited (AECL) [25]. AECL has more than 30 years of experience in Pu-MOX fuel research and development [27]. Fuel fabrication and irradiation testing has

been conducted on plutonium MOX CANDU fuels in the ZED-2 reactor and the National Research Universal (NRU) reactor [3, 28]. A detailed analysis of the possibility of using some of the Bruce CANDU reactor units as plutonium burning avenues was performed [29]. The evaluation determined that through the employment of certain design factors such as integral burnable neutron absorber material the MOX fuel could be designed to mimic NU fuel as much as possible and avoid introducing new safety issues. The study concluded that reactor safety was unaffected by the introduction of the plutonium MOX fuel.

Related work that benefited from the research into plutonium disposal in CANDU was the DUPIC cycle which expanded the synergy options available between LWRs and CANDU systems. The DUPIC system, mentioned in Chapter 2.3 and 2.4, provides the capability to essentially "twice-burn" PWR or BWR fuel, once in the LWR and then once in CANDU. DUPIC uses a dry process that does not partition the LWR spent fuel but only grinds it up and sinters it into pellets to produce CANDU type bundles. This method is a simple form of actinide burning but the fact that all the fuel material is present for the second burn cycle including the fission products makes it a less efficient transmutation method.

Complementary to actinide transmutation strategies that include partitioning is the use of reprocessed uranium. The use of reprocessed uranium partitioned from LWR spent fuel in CANDU has been heavily researched and includes direct use of RU and the blending with depleted uranium to produce natural uranium equivalent fuel. The NUE method, discussed previously in Chapter 2.3 and 2.4, is currently under development and has undergone detailed analysis and in reactor testing [16]. CANDU-RU fuel programs are also being explored and the use of RU-43 fuel in CANDU is currently at the stage of final design assessment and will move towards experimental trials [30].

This initial work in MOX fuels and LWR-CANDU synergy options lead the way for the development of MOX fuels from group extracted actinides taken from LWR spent fuel and the analysis described in this dissertation. Additional avenues such as direct Am-Cm targets and burning of actinide inert matrix fuels in CANDU were also developed from this work.

2.6 Thermal reactor and fuel choice for actinide burning

The governing factors of reprocessing in thermal systems include the type of target or recycled fuel matrix and the reactor type. The fuel matrix can be inert material or uranium oxide and can be employed in an LWR or HWR system.

The fuel design choices include blending the actinide materials into an inert fuel matrix such as zirconium or silicon or into uranium to form a mixed oxide fuel. The IMF carrier material is non-fertile and hence does not generate new actinides during burnup. However, the fuel has different thermal characteristics and neutronics properties from existing fuels [31]. Thus, it is likely better suited to advanced reactor designs rather than current systems. The MOX fuel option more closely retains the thermal and neutronics properties of standard fuel and has been extensively studied and utilized in plutonium reprocessing efforts. The fuel mixture can be utilized in homogenous elements with all the pins the same or heterogeneous configurations designed to optimize power profiles and/or burnup. Direct actinide targets, specifically Am-Cm, are another method of actinide destruction. This method goes along with a MOX cycle which combines the neptunium and plutonium into MOX fuel and utilizes the separated extraction of americium and curium to produce dedicated targets that are bombarded with neutrons in a reactor or accelerator. In reactor technologies currently being explored include single target elements integrated in a regular bundle acting as a neutron absorber (e.g. central absorber pin of Am-Cm), full bundles of Am-Cm target elements placed in a periphery channel and targets that are separate from fuel such as control devices composed of Am-Cm [4, 32].

Thermal reactors are an ideal option for the initial burning of actinides since they have been proven commercially for the last 40 years. The use of thermal water-moderated reactors as a first stage in improved utilization allows 1 to 2 iterations of reprocessed spent fuel to be burned before using fast breeder reactors to close the cycle or disposing of the fuel. This intermediary step increases the energy extracted per ton of fuel and can significantly reduce the fast breeder infrastructure needed in the near term. As discussed in Chapter 2.3, one actinide MOX bundle requires the actinide content of several regular spent fuel bundles. The majority of the remaining materials in these bundles can be recycled (e.g. uranium) while the fission products are sent to long term disposal. The focus is on current thermal systems, both LWR and CANDU, which are able to utilize a flexible fuel cycle without major changes to design or operations, making for an

easy transition to partial or full loadings of recycled fuels. Research and development efforts in reprocessing plutonium from spent fuel have produced MOX fuels that have been employed in current reactors with 10-30% of the fuel in the core being MOX [13].

Comparisons of plutonium burning in heavy and light water reactor designs have been explored previously and both technologies show promise in the area of initial actinide burning [2]. Therefore, the first step of thermal reactor utilization for actinide burning can be developed from the plutonium disposition technologies already used in PWR and BWR systems and those explored and tested in PHWR designs such as CANDU.

The CANDU design as a result of its optimization for natural uranium fuel use provides advantages for actinide burning. The low parasitic neutron absorption in the core provided by the heavy water moderator and coolant allows for increased levels of actinide transmutation and accommodation of a wide range of fuel enrichments. The CANDU fuel bundle design is highly flexible allowing the inclusion of varied enrichments in different elements or integral absorber material. The concentric ring design provides a compact and simple fuel bundle that can be optimized for a variety of parameters including differential burnup, void reactivity or linear power rating. The CANDU reactor utilizes online fuelling providing an extensive capability for the management of the core flux profile. Online fuelling also means that fresh fuel reactivity is balanced by neutron absorption in older fuel in the core rather than by adding large amounts of neutron absorbing materials into the core (e.g. neutron poison loading in PWR and BWR systems with boron or gadolinium) resulting in more actinide transmutation. The objective of this dissertation is to demonstrate the adaptability and flexibility of CANDU in the utilization of reprocessed actinide fuel.

2.7   Partitioned actinide burning research in CANDU

Actinide burning research in CANDU has been primarily driven by the benefits of the reactor design including the neutron economy and compact fuel design as discussed in Chapter 2.6. Earlier work in using Pu-MOX from weapons material, LWR and CANDU synergy and complimentary uranium reuse studies, explained in Chapter 2.5, has provided the necessary basis and experience to explore partitioned actinide burning in CANDU. This area has been explored as a

subsection of the greater CANDU fuel cycle for more than 15 years as CANDU is an excellent venue for the burning of plutonium [33, 34].

Partitioned actinide burning is different from the DUPIC method discussed earlier in this chapter since it separates the LWR spent fuel feedstock into uranium, transuranic actinides (Np, Pu, Am, Cm) and fission products rather than processing it directly as a whole. The partitioned components are then sent to different fuel manufacturing processes or in the case of the fission products to long term monitored storage for disposal. The grouped actinides are placed in an inert matrix fuel or blended with uranium to produce a mixed oxide. The uranium is sent for reuse with methods like CANDU-RU or blended with depleted uranium for use as NUE fuel for CANDU. If desired, the actinides can be further separated to extract Am-Cm which can be produced into dedicated targets while the Np-Pu is used directly in fuel.

Straight plutonium-uranium recycle has been explored for PHWR with both NU and DU carrier materials. The NU case used 0.45% Pu while the DU case used 0.9% Pu [35]. The NU case actually generated plutonium through neutron capture in Pu-239 but the DU case provided a modest reduction of 0.11% of the plutonium in the fuel [35]. These efforts were focused on savings in natural uranium resources and used low concentrations of plutonium resulting in less successful amounts of transmutation than the group extracted actinide studies or the previous studies with plutonium from weapons material [25, 29].

The direct transmutation of separately extracted americium-curium (Am-Cm) from spent fuel was investigated in a few heterogeneous forms including target pin and target channel designs. The target pin study placed Am-Cm in the center element of a low enriched uranium 43 element bundle allowing it to function as a burnable neutron absorber and help to reduce coolant void reactivity. Simulations for this design were performed using lattice cell simulations. The target pin was designed to be demounted from the bundle so it could be run through multiple cycles enhancing transmutation [4]. The target channel method for direct Am-Cm transmutation utilizes fuel bundle sized inert matrix targets which would be placed into dedicated periphery channels of a CANDU 6 core fuelled with recycled uranium (0.9% fissile). The Am-Cm is embedded in silicon carbide and a variety of bundle designs were simulated with 21 to 43 elements. Full core diffusion calculations with the Am-Cm target bundles were evaluated and the channel and bundle powers of the system were found to stay within normal

CANDU reactor operating conditions [4]. An additional feasibility study using lattice simulations was performed for select channels with targets containing Am-Cm in graphite with normal CANDU 37 element fuel bundle proportions and the system was found to be able to transmute significant amounts of the minor actinides. For a transmutation time of 7 year the use of 20 target channels was able to transmute about 28.5 kg/year or enough minor actinide burnup to support three VVER-1000 type PWRs [36]. In a homogeneous study, pure americium was mixed with recycled uranium and slightly enriched uranium and loaded in a CANDU Flexible-fuelling (CANFLEX®[3]) 43 element bundle and simulations were performed in a lattice code for various loadings [4].

Americium elimination using CANDU is being assessed using a blended fuel containing americium, depleted uranium and separated civilian grade plutonium. This approach uses a full core of Am-Pu-DU mixed oxide fuel with an exit burnup of 20 MWD/kgHE that can transmute 680 kg/y of americium, 980 kg/y of plutonium and will consume about 38 tons/year of depleted uranium [5]. This approach is similar to MOX fuels with grouped actinides blended with NU but relies almost entirely on plutonium fission as the U-235 content in depleted uranium is usually less than half that of natural uranium. CANDU is a desirable vector for minor actinide removal as the fuelling feasibility of the system is relatively insensitive to impurities such as americium [6].

The inclusion of actinides in CANDU type fuel is also being studied for the potential to enhance the proliferation resistance of spent fuel. A minor actinide reduction study in the heavy water moderated, light water cooled advanced CANDU reactor (ACR) found that the inclusion of the transuranic actinides Np-237 and Am-241 in the fuel would result in significant increases in the ratio of Pu-238 to total plutonium content. In this case the fuel is composed of neptunium and americium blended into enriched uranium (either separately or together up to about 0.2% total with 2.3% U-235 enrichment) [37]. The inclusion of Am-241 or Np-237 in the fuel results in end of burnup (~20 MWD/kgHE) Pu-238 ratios of ~10% of total plutonium, which increases spent fuel proliferation resistance.

Another area of future interest is the integration of minor actinide burning into a thorium fuelled CANDU system. In this case, plutonium and minor actinides would be blended with thorium to produce an oxide fuel. The initial fissile

---

[3] CANFLEX is a registered trademark of Atomic Energy of Canada Limited (AECL) and the Korean Atomic Energy Research Institute (KAERI)

content comes from the Pu-239 in the actinides and the Th-232 provides the fertile carrier matrix that generates U-233 fissile content via neutron capture. The minor actinides of neptunium and americium provide some integrated neutron absorption that helps to flatten flux. Multi-cycle scheme with combined burnup of 20-30 times regular CANDU is envisioned to take full advantage of the production of U-233 which will likely require re-cladding activities [38].

Preliminary studies with inert matrix actinide fuel have been undertaken and show large conversion rates for the actinides (~60%) [39]. The net destruction efficiency for the plutonium is higher than for a MOX case but the minor actinide conversion for a Pu-MA loaded in silicon carbide is about 38% which is comparable to MOX [18]. IMF options are still under full investigation especially in the areas of materials research and irradiation testing but have great potential as a future follow-on to MOX systems [40].

Group extracted actinide transmutation with MOX is a subject of great interest and the main focus of this dissertation. A detailed feasibility analysis was performed for the use of a group extracted actinide MOX fuel in a CANDU 6 reactor [4, 41]. This study utilized a long burnup high actinide content fuel with a fissile content of 3.5% and an actinide loading of 4.75% which utilized a modified CANFLEX type bundle and was used in the full core load of a CANDU 6 reactor system with minimal changes in operational procedures. Full core calculations demonstrated that the channel and bundle powers were within the normal CANDU limits and that the fuelling of channels was within the control device capabilities [41].

As this was a feasibility study, the incremental cross sections of the fuel were not updated and standard natural uranium fuel values were used. In addition, the fuel utilized was found to be very active and stretched the operational limits of the control systems in the CANDU design. Abnormal liquid zone levels were observed that exceeded the desired envelope which imposes potential limits on the fissile content (and hence actinide loading) of the actinide MOX fuel [41]. This study was the direct forerunner for the research presented in this dissertation and helps to establish the feasibility of actinide mixed oxide fuels in a CANDU reactor. The dissertation builds on this study by redesigning the fuel to a more suitable actinide loading, including a full treatment of the incremental cross sections and moving to the larger CANDU-900 reactor design with higher neutron economy and increased actinide transmutation potential. Portions of this analysis

and some initial designs and procedures for the full actinide core that have been refined within this dissertation are presented in reference [42, 43].

2.8   Dissertation Objectives

The goals of this dissertation are to build on the previous work done with actinide transmutation in current thermal systems, specifically CANDU. The focus is the exploration and evaluation of a 100% full core loading of a CANDU-900 reactor design with an actinide based mixed oxide fuel. The physics design of a suitable fuel composition and bundle geometry and the full core loading procedures and operational guidelines necessary for safe operations is described. The impacts of the actinide fuel on the neutronics properties of the system and the effects on reactor operations are studied in detail. The analysis methods and simulation procedures are in line with the standard practices in CANDU reactor design and analysis. The full core model is evaluated and compared to a standard natural uranium fuelled CANDU to ensure that the new fuel meets operational limits and guidelines.

This dissertation aims to evaluate the capability of a CANDU-900 fueled with group extracted actinide based mixed oxide fuel to achieve a significant level of actinide transmutation while maintaining a comparable operational envelope to a standard NU fuelled configuration. This is an important step towards the full core utilization of recycled actinides in a CANDU.

Chapter 3

Methodology

The process of CANDU fuel design and assessment is multi-phased beginning with lattice and super-cell calculations to determine homogenized cross sections which are then subsequently fed forward to a full core diffusion model to define operating constraints and simulate standard reactor operations to evaluate the compatibility of the fuel with the reactor design. Finally the diffusion models are used to assess the safety margins and to perform design basis analyses. Each phase is described separately in the sections within this chapter. A flow chart of the analysis method is provided in Figure 3.1.

The investigation of the feasibility of employing advanced actinide fuel designs in a standard CANDU-900 reactor design follows the same methods and procedures used in current analysis for standard natural uranium fuels and other recent advanced fuel designs. Given the proven reactor design of CANDU, it is fitting that the analysis and modelling suite and methods that have been used to evaluate the design with natural uranium fuel are employed to assess the use of an actinide based fuel. This ensures that the analysis is consistent with standard practices and the actinide fuel can be evaluated and compared to natural uranium fuel throughout the process.

The lattice calculations determine the neutron distribution in group-wise energy and space within a unit cell, along with the reaction rates for the materials within the cell. The lattice cells are assembled into a repeated grid that is a suitable representative of the full core reactor system. The base lattice cell in CANDU is a single channel of fuel surrounded by moderator. This cell is arranged in an two dimensional infinite grid replicating the configuration in the center of the full core, which is a suitable building block to be inserted into a full core model with more detailed boundary conditions and in-core structures. The neutron distribution and reaction rates are determined through a solution of the neutron transport equation (see Chapter 3.1) based on the specific material, geometry and fundamental neutron-nucleus interaction data.
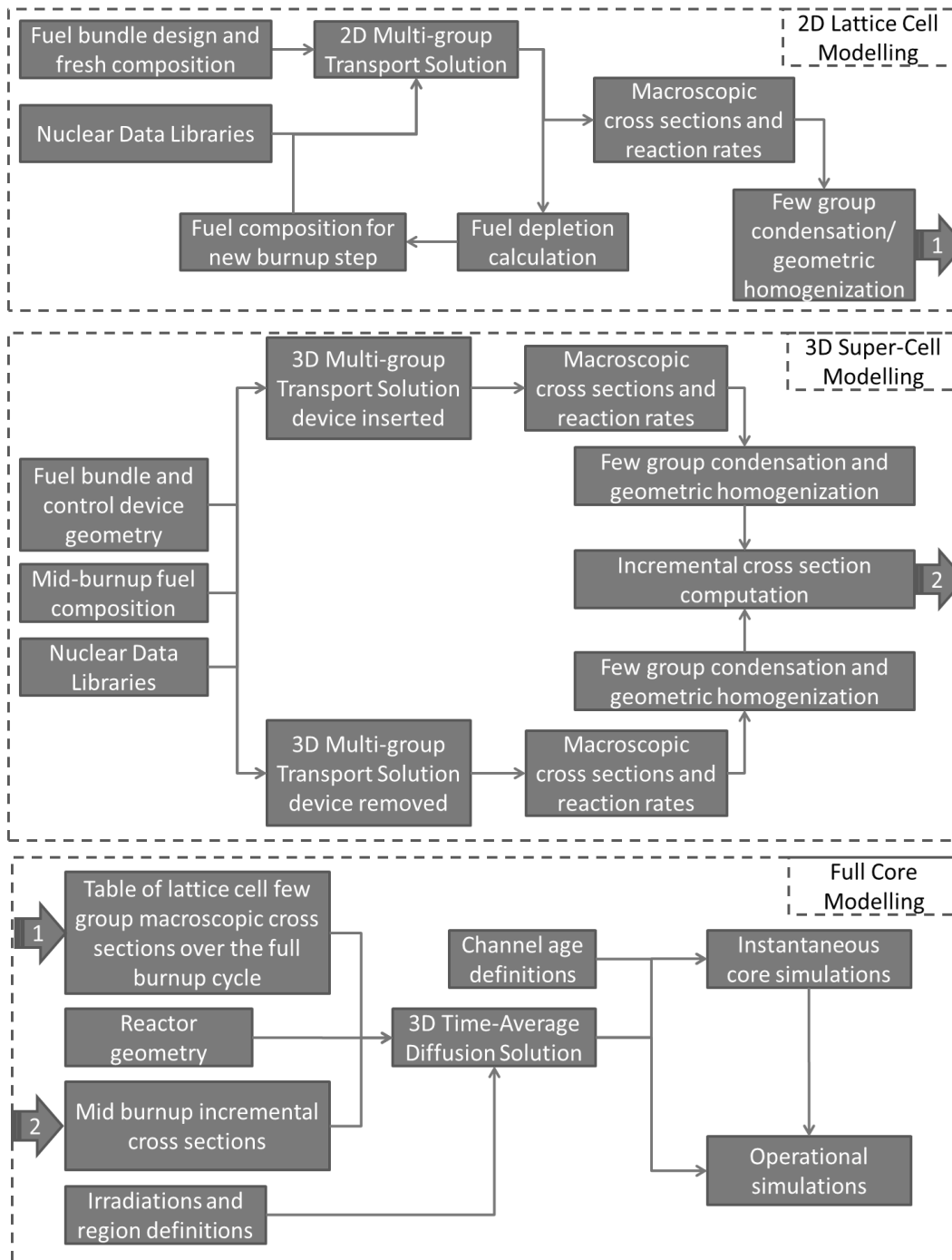
Figure 3.1: Flow chart of analysis method

The lattice cell cross sections are computed for detailed geometry and many energy groups (e.g. 44, 69, or 89) for a single fuel composition. The computed

reaction rates, power level, and neutron distribution are used to determine the changes in the fuel composition over the irradiation time. The varying compositions of the lattice over the burnup are used to produce a set of cross sections at numerous intervals over the full burnup cycle accounting for the composition changes in the lattice cells as the neutrons interact with the fuel, fission products and actinide materials. These cross sections are then homogenized to produce few group macroscopic cross sections that describe the lattice cell. The reaction rates are weighted using the neutron distribution in the cell and the energy groups are condensed to produce the macroscopic cross sections of the homogenized lattice cell for two groups, thermal and fast. The set of two group macroscopic cross sections for the fuel is post processed to provide a table of lattice cell cross sections and diffusion constants (determined using a buckling search) for use in a diffusion model built out of the lattice cell building blocks. The lattice cell simulation, burnup computations and homogenization are discussed in Chapter 3.2.

The interaction of control devices with the lattice cell is modeled using a super-cell configuration and calculating the neutron transport equation with the control device inserted and removed from the system to determine the incremental change necessary to the lattice cell properties to account for the interaction of the control device. Unlike most light water reactors, the CANDU super-cell models must be 3 dimensional as the control devices insert perpendicular to the fuel channels. The 3D super-cell calculation is done for a mid-burnup fuel composition that represents the average fuel composition that a control device will interact with in an equilibrium full core. The changes in microscopic cross sections are homogenized for the geometry and energy group interaction to produce two-group homogenized incremental cross sections. These incremental values are used to modify the standard lattice cell (no control device) cross sections in the full core model to account for the interaction of the control devices (see Chapter 3.3)

The full burnup homogenized macroscopic lattice cell cross sections, along with the set of homogenized incremental cross sections from the super-cell calculations for all the control devices, are passed along to the full core modeling code and provide the cross sections of the lattice cell building blocks of the full core diffusion solution.

The full core model uses a detailed 3D representation of the reactor core and all its internal structural components using the homogenized lattice and super-cell

cross sections as building blocks to faithfully reproduce the core configuration and solve the diffusion equation (see Chapter 3.4) to determine the neutron flux distribution within the core. Full core modelling, described in Chapter 3.5, is used first to determine an optimal "equilibrium" core configuration that will be suitably within the operational envelope of the core. The key inputs used to determine this envelope are the time-average properties at each bundle location in the core (average bundle depletion, average coolant, fuel and moderator temperatures and densities). This provides important information about the fuel design including fissile content and burnup levels to determine if the fuel will be sufficiently active to maintain operations while maintaining the necessary constraints on the flux shape and power levels defined for the reactor system. The examination and design of a time-average model is detailed in Chapter 3.5.3.

The CANDU reactor system uses a continuous online fuelling scheme in order to maintain the reactivity in the core, in contrast to LWRs which tend to be batch fuelled. Therefore, the equilibrium or "time-average" calculation is used to define suitable specific irradiation levels and fueling scheme and frequencies to achieve the desired fuel burnup level while maintaining the proper core reactivity and operational power and flux profiles. The specific characteristics of the full core model including the responses to changes in conditions such as temperature and moderator composition are evaluated along with the full core responses to the different control devices present in the core.

Upon the completion of a suitable "time-average" model the specific effects of instantaneous snapshot cores with random channel ages are then evaluated to ensure the design will remain within the desired operational envelope. Specifically, the online fuelling nature of the CANDU reactor means that the core at each instant in time will show small deviations from the time-average conditions described earlier. The method for examining these instantaneous effects is detailed in Chapter 3.5.4. The online fuelling of the CANDU design puts specific demands on the control system and fuelling events must be studied in detail to ensure that the reactor remains in the operational envelope during fuelling events which is detailed in Chapter 3.5.6. The finalized model is then evaluated for specific scenarios of normal and accident operations to determine the response of the system and ensure acceptable behaviour under the defined conditions. More detailed operational and accident scenarios can be accomplished through a multi physics simulation by coupling the full core reactor

physics model with a suitable thermalhydraulics model to creating a more realistic representation of the reactor.

3.1   Prediction of neutron transport in a CANDU lattice

At the center of any nuclear reactor analysis is the movement of neutrons through the specific reactor geometry. All processes and behaviour of a reactor are governed by the distribution of neutrons in space, energy and time within the lattice cells. There are several methods for determining the nature of this distribution of neutrons, one of the most widely used being neutron transport theory. The basis of transport theory is the transit of neutrons with specific energies through a given volume. Primarily, this is a counting problem where an arbitrary volume, V, contains a number of neutrons, n, with a trajectory within an angle $d\widehat{\Omega}$ of $\widehat{\Omega}$ and with an energy interval of dE about energy E. The change in neutron population in V is the sum of the gain and loss terms. The following explanation of the neutron transport equation is adapted from the derivation provided in Duderstadt [44].

The gain terms within the volume include neutron sources within the volume (fission, non-fission, delayed neutrons), the scattering of neutrons into the energy range of interest within the volume, and neutrons within the energy range entering into the volume through the surface, S.

$$neutron\ source\ term: \left[\int_V s\left(r, E, \widehat{\Omega}, t\right) d^3 r\right] dE d\widehat{\Omega} \tag{1}$$

$$fission\ source\ term: \left[\int_V d^3 r \frac{\chi(E)}{4\pi} \int_{4\pi} d\widehat{\Omega}' \int_0^\infty v(E')\Sigma_f(r, E')n\left(r, E', \widehat{\Omega}', t\right) dE'\right. \tag{2}$$
$$\left. + s\left(r, E, \widehat{\Omega}, t\right)\right] dE d\widehat{\Omega}$$

$$scattering\ in\ term: \left[\int_V d^3 r \int_{4\pi} d\widehat{\Omega}' \int_0^\infty v\Sigma_s\left(r, E' \to E, \widehat{\Omega}'\right.\right. \tag{3}$$
$$\left.\left. \to \widehat{\Omega}\right) n\left(r, E', \widehat{\Omega}', t\right) dE'\right] dE d\widehat{\Omega}$$

For the fission source term, equation 2, the fission neutrons will have an energy distribution given by the fission spectrum, $\chi(E)$.

The loss terms include neutrons that are absorbed while interacting with a nucleus in the volume, neutrons that undergo a scattering interaction within the volume shifting their energy or trajectory out of the interval of interest and the leakage of neutrons out of the surface S, where v is the neutron velocity.

$$absorption\ term: \left[\int_V v\Sigma_t(r,E)n(r,E,\widehat{\Omega},t)d^3r\right]dEd\widehat{\Omega} \qquad (4)$$

The interaction term combines both absorption and scattering out of the realm of interest due to interaction within the volume and is accounted for using the total cross-section, Σ_t, while the leakage into an out of the volume are combined into a net leakage term.

$$net\ leakage\ term: \left[\int_V v\widehat{\Omega}\cdot\nabla n\left(r,E',\widehat{\Omega}',t\right)d^3r\right]dEd\widehat{\Omega} \qquad (5)$$

The above terms are true for any arbitrary volume V and will follow the balance relation below expressed using angular flux, φ, rather than number of neutrons. This is the integral form of the transport equation.

$$\frac{1}{v}\frac{\partial\varphi}{\partial t} + \widehat{\Omega}\cdot\nabla\varphi + \Sigma_t(r,E)\varphi(r,E,\widehat{\Omega},t) \qquad (6)$$

$$= \int_{4\pi} d\widehat{\Omega}' \int_0^\infty \Sigma_s\left(r,E'\rightarrow E,\widehat{\Omega}'\rightarrow\widehat{\Omega}\right)\varphi\left(r,E',\widehat{\Omega}',t\right)dE'$$

$$+ \frac{\chi(E)}{4\pi}\int_{4\pi} d\widehat{\Omega}' \int_0^\infty v(E')\Sigma_f(r,E')\varphi\left(r,E',\widehat{\Omega}',t\right)dE' + s(r,E,\widehat{\Omega},t)$$

The initial condition is the initial value of angular flux for all positions, energies and directions $\widehat{\Omega}$ while the boundary condition is dependent on the surrounding medium with the surface treated as a "non-re-entrant surface". A common condition for the boundary is that of a vacuum where a neutron that leaks out will not be scattered back into the volume. The more common boundary condition for

use in lattice cell calculations is the Albedo or white boundary condition where a portion of the outgoing neutrons is assumed to return to the volume isotropically entering at the outer surface, the influx of neutrons can be treated as a source term. These initial and boundary conditions are displayed in equations 7, 8 and 9.

$$IC: \varphi(r, E, \widehat{\Omega}, 0) = \varphi_0\left(r, E', \widehat{\Omega}'\right) \tag{7}$$

$$BC \ (vacuum): \varphi(r_s, E, \widehat{\Omega}, t) = 0 \ if \ \widehat{\Omega} \cdot \hat{e}_s < 0, all \ r_s \ on \ S \tag{8}$$

$$BC \ (albedo): \varphi(r_s, E, \widehat{\Omega}, t) = \alpha \int\limits_{\widehat{\Omega}'\hat{e}_s < 0} \left|\widehat{\Omega}'\hat{e}_s\right| \varphi\left(r_s, E, \widehat{\Omega}', t\right) d\widehat{\Omega}', \widehat{\Omega}'\hat{e}_s \tag{9}$$
$$> 0, all \ r_s \ on \ S$$

3.1.1   Solution of the transport equation

There are several methods to solve the integral form of the transport equation that are used for modeling specific lattice geometry.   The primary deterministic methods include discrete ordinates, functional expansion and the collision probability method.   These methods are procedures for discretizing the neutron transport equation in order to solve the system numerically.   The explanations of these methods of solution follow the descriptions within Duderstat [44] for the first two methods.   The theory manuals for the WIMS-AECL [45] and DRAGON [46] codes are used for the explanation of the collision probability method with the assistance of the distillation by Buijs [47].

The discrete ordinates method represents the function of neutronic flux, $f(\varphi) = 0$, with its value at a discrete set of specific points of the flux.   The lattice cell in question is first discretized into a space-time coordinate grid then the function for flux is replaced with its value at each of these mesh points.

$$f(\varphi) \to f(\varphi_i) \equiv f_i, i = 1, \dots, N \ \ or \ alternatively: \varphi(\widehat{\Omega}) \to \varphi(\widehat{\Omega}_n) \equiv \varphi_n \tag{10}$$

The neutron flux at these discrete locations is not known but it transforms the function of flux to a column vector of discrete fluxes, resulting in the algebraic system being possible to express as a matrix equation.   The operators within $f(\varphi)$ are then converted to their discretized counterparts (e.g. derivatives become finite

difference, integrals become numerical quadratures, weights = $\Delta\widehat{\Omega}_{n'}$ being small cones about the discrete angles) and the system becomes a numerically solvable coupled set of N equations.

$$\frac{1}{v}\frac{\partial}{\partial t}\varphi_n + \widehat{\Omega}_n \cdot \nabla\varphi_n + \Sigma_t\varphi_n(r,E,t) \tag{11}$$
$$= \sum_{n'=1}^{N}\Delta\widehat{\Omega}_{n'}\int_0^\infty \Sigma_s\left(r,E'\to E,\widehat{\Omega}'_{n'}\to\widehat{\Omega}_n\right)\varphi_{n'}(r,E',t)dE'$$
$$+ s_f(r,E,t) + s_n(r,E,t)$$

The second method is a functional expansion which represents the original flux function with a finite series of known functions, commonly polynomials. This results once again in the conversion of the function to a column vector and the coupled set of equations being expressible as a matrix equation. The angular functions are expanded as a finite series of spherical harmonics with Legendre polynomials resulting in a flux expression in 1D based on $P_l(\mu) = P_l(\cos\theta)$.

$$\varphi(x,E,\mu,t) = \sum_{l=0}^{N}\left(\frac{2l+1}{4\pi}\right)\varphi_l(x,E,t)P_l(\mu) \tag{12}$$

This expression is subbed into the neutron transport equation resulting in a 1D expression for neutron transport which is closely related to the expressions used for diffusion theory.

$$\frac{1}{v}\frac{\partial}{\partial t}\varphi_l + \left(\frac{l+1}{2l+1}\right)\frac{\partial}{\partial x}\varphi_{l+1} + \left(\frac{l}{2l+1}\right)\frac{\partial}{\partial x}\varphi_{l-1} + \Sigma_t\varphi_l(x,E,t) \tag{13a}$$
$$= \int_0^\infty \Sigma_{sl}(E'\to E)\varphi_{l'}(x,E',t)dE' + s_{fl}(x,\mu,E) + s_l(x,\mu,E)$$

The angular components of the differential scattering term are:

$$\Sigma_{sl}(E'\to E) \equiv 2\pi\int_1^{+1}\Sigma_s(E'\to E,\mu')P_l(\mu')\,d\mu', \qquad where\ \mu' \equiv \widehat{\Omega}'\cdot\widehat{\Omega} \tag{13b}$$

There is still an area that must be addressed before the above methods can be used to solve the transport equation, the integrals over energy. The energy utilized in both is still continuous and must be suitably discretized in order to be numerically computable while still suitably covering the full range of neutron energies. Neutron energies in a nuclear reactor span a vast range with fast neutrons born from fission at a few tens of MeV scattering down to thermal energies of 1 meV or lower resulting in a range more than 10 orders of magnitude wide. Additionally, the neutron spectrum does not follow a constant function over the energy range it is dependent on different processes differing in each area of interest; thermal, resonance, fast. In order to represent the continuous energy spectrum of neutrons we use the discrete ordinates method described earlier. A collection of specific energies is not suitable so the energy is split into bins or groups. The neutron transport equation is then integrated over each group to produce the appropriate averaged values for the cross sections or other properties for each discrete energy group.

$$\Sigma_{ag} \equiv \frac{\int_{E_g}^{E_{g-1}} \Sigma_a(E)\varphi(E)dE}{\int_{E_g}^{E_{g-1}} \varphi(E)dE} \tag{14}$$

Provided the group structure chosen is fine enough, the cross sections can be considered constant over the group range and hence effectively independent of the weighted spectra used to generate them. Lattice calculations are done with many groups (44, 69, 89, etc.) to properly represent the energy spectrum. The term "multi-group" is used to distinguish this energy discretization from the continuously varying nuclear data detailing the fundamental neutron-nucleus interaction. The flux spectrum from these calculations along with the predicted interaction characteristics can then be used to condense down the group structure and recalculate the cross sections for a smaller number of groups. These condensed values are used for full core diffusion calculations usually using two energy groups taken from the condensation of the multi-group data (e.g. 89 groups) used in the transport solution. The term "few-group" is used to describe cross section information that has been condensed down to 2 to 8 groups from the multi-group data.

It is useful to take note of the major assumptions that are made in solving the neutron transport equation.

a) The first assumption is that the neutron flux is approximated by piecewise constant functions in energy and space. The energy discretization described earlier is one half of this assumption while the spatial discretization method (e.g. discrete ordinate, collision probability) is the remainder.

b) The second assumption is that the time dependent processes are slowly varying in time meaning that the only time dependent process is depletion. Depletion is performed in small time steps where the flux profile and fuel compositions remain constant.

c) The third assumption is that neutron scattering is isotropic in the laboratory coordinate system meaning that the scattering from one angular coordinate to another will be equally likely, removing the angular dependence of the scatter term. This is usually combined with a transport corrected total cross section which sufficiently mitigates the isotropic inaccuracies for a thermal reactor.

$$\Sigma_s \left(r, E' \to E, \widehat{\Omega}' \to \widehat{\Omega} \right) = \frac{1}{4\pi} \Sigma_s (r, E' \to E) \qquad (15)$$

These above assumptions are sometimes paired with the simplification that the medium is invariant in one dimension resulting in a two dimensional (2D) problem. Most lattice calculations are performed in 2D with the exception of super-cell calculations for CANDU which must be performed in 3D due to the control devices being perpendicular to the fuel channel axis. The most popular method of discretizing and solving the transport equation, collision probability, is described in the following section and takes into account the above assumptions.

3.1.2   The collision probability method

The collision probability method is a very widely used method for solving the integral form of the transport equation and is present in the dominant transport codes (e.g. DRAGON and WIMS). It is a method of approximating the spatial dependence of the neutron flux with a region based discretization. The basis is that the flux at a given point, a, is proportional to the neutron source at any point b multiplied by an exponential attenuation factor that acts over the path taken by the neutron from b to a. This optical path, τ, is given in equation (16).

$$\tau = \int_{a}^{b} \Sigma(R)dR, \quad or\ more\ specfically:\ \tau_g(s) = \int_{0}^{s} \Sigma_g(r - s'\Omega)ds \quad (16)$$

Therefore by defining specific regions within the lattice cell that the neutrons will travel through during their lifetime, each with a specific probability of interaction, we can obtain the probable path for neutrons leaving a specific region and interacting with surrounding regions. The computation for fast multiplication relies on the probability of the neutron having its first collision in the region it is born in (i.e. fuel). If the first collision occurs within the moderator region it is likely that the neutron will scatter down in energy and have its next collision within fuel again, but at a thermal energy. The domain in question is divided into N regions with specific volumes and the external boundary is composed of N_S surfaces with specific surface areas, the simplest system is that of two regions: fuel and moderator.

Utilizing the assumptions listed earlier and the energy discretization along with the region based spatial discretization of the collision probability method we can generate the full matrix of equations for neutron transport. The system follows the losses and multiplication connected by the neutron multiplication factor k.

$$L\varphi = \frac{1}{k}M\varphi, \quad (17)$$

$with\ L\ and\ M\ taken\ from\ reference\ [46,47]\ with\ discrete\ energy\ groups$

$$L = \widehat{\Omega} \cdot \nabla\varphi_g\left(r,\widehat{\Omega}\right) + \Sigma_{t,g}(r)\varphi_g\left(r,\widehat{\Omega}\right) - \sum_{g'=1}^{G} \Sigma_{s,g'\to g}(r) \int_{4\pi} \varphi'_g\left(r,\widehat{\Omega}'\right)d^2\widehat{\Omega}' \quad (18)$$

$$M = \chi_g \sum_{g'=1}^{G} \nu_{g'}\Sigma_{f,g'}(r) \int_{4\pi} \varphi'_g\left(r,\widehat{\Omega}'\right)d^2\widehat{\Omega}' \quad (19)$$

The collision probability comes into play with the integrated angular flux, φ'_g, terms in L and M. The integrated flux for a specific volume is computed based on the summation of the collision probability times the neutron source density, Q. Using the probability that a neutron born in any region V_i of the lattice will undergo its first collision in region V_j of a unit cell or assembly, $P_{ij,g}$, and the total cross section in V_j of $\Sigma_{j,g}$ for group g we can compute the reduced collision

probability. The source in volume V_j for group g is then combined to compute the integrated flux for V_i for group g.

$$\phi_{i,g} = \int_{4\pi} \varphi'_g\left(r,\widehat{\Omega}'\right) d^2\widehat{\Omega}' = \sum_i Q_{j,g} p_{ij,g} \tag{20}$$

$$p_{ij,g} = \frac{P_{ij,g}}{\Sigma_{jg}} = \frac{1}{4\pi} \int_{V_i} d^3r' \int_{V_j} d^3r \frac{e^{-\tau_g(s)}}{s^2} \tag{21}$$

$$Q_{j,g} = \sum_{\substack{g'=1 \\ g' \neq g}}^{G} \Sigma_{s0,j,g\leftarrow h}\, \phi_{i,h} + \frac{1}{k}\chi_g \sum_{g'=1}^{G} \nu\Sigma_{f,g'}\phi_{i,g'} \tag{22}$$

The collision probability method follows three steps:

1. A tracking grid is applied over the lattice geometry to span a sufficiently large number of neutron trajectories.
2. Numerical integration is used to determine the collision probabilities using the tracking information and the microscopic total cross sections for each region. This is performed for each energy group.
3. Once the collision probabilities are known then the integrated flux terms can be computed from the equation 20 to 22 and the matrix system can be solved.

The components of L and M can be written in matrix form since they are a coupled set of G equations, $\widehat{\Omega} \cdot \nabla$ is a scalar operator; the flux, $\nu\Sigma_f$, and χ are vectors; the total and scattering cross sections are matrices (Σ_t is diagonal). The scattering cross section matrix and the vector $\nu\Sigma_f$ are operators.

$$(\widehat{\Omega} \cdot \nabla)\varphi + \Sigma_t\varphi - \Sigma_s\varphi = \frac{1}{k}\chi\left(\nu\Sigma_f\right)^T\varphi \tag{23}$$

The individual group equations, within group transport, are usually solved with a two level iteration with the outer determining the group k and the inner accounting for up-scatter in the thermal region with the coupled source defined in equation 22. The convergence is on the eigenvalue, k, and the eigenvector is flux.

3.2   The CANDU lattice cell

The CANDU lattice cell is the base unit for modeling the full reactor system and contains fuel pins arranged in concentric rings contained within a coolant region surrounded by a pressure tube, an annulus gas gap, a calandria tube and a rectangular area of moderator. This base cell replicates a single channel and is simulated in an infinite lattice which effectively represents a central channel in the core surrounded on all sides by other fuelled channels.

There are several fuel bundle designs that can be employed in CANDU with different numbers and sizes of fuel elements. The standard fuel arrangement for natural uranium fuel is the 37 element bundle with concentric rings of 1, 6, 12 and 18 elements. The bundle has 120° symmetry with all element sizes being the same and the fuel composition being identical in each element. The standard CANDU lattice cell is composed of natural uranium fuel (0.71% U-235) with a zirconium sheath, heavy water coolant and moderator, zirconium alloy pressure and calandria tubes and CO_2 annulus gas. The standard lattice pitch is ~28.6 cm. A standard 2D lattice cell with a 37 element fuel bundle is provided in Figure 3.2.
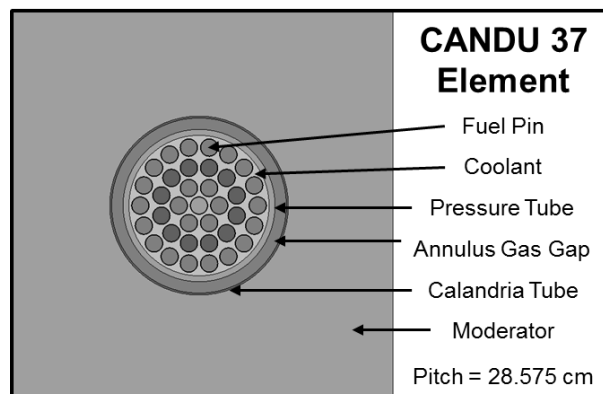
Figure 3.2: A 2D CANDU 37 element lattice cell

The base lattice cell calculations are performed using a 2D transport solution, most commonly with the WIMS-AECL code [48]. A library of nuclear data, containing the interaction cross sections for the set of isotopes (adapted from experimental nuclear databases, such as ENDF, JEFF and JENDEL, for the specific transport code) is utilized along with the geometry and material composition in the lattice cell to produce the microscopic cross sections. These

dictate the neutron-nucleus interactions in the lattice cell for multiple energy groups (e.g. 44, 69, or 89) and are the main inputs to the transport solution.

The transport solution takes in the cross section information and is used to determine the neutron flux distribution, reaction rates, relative pin powers, and calculate the multiplication constant, k, for the lattice cell for a given composition. A depletion model is also included in the code to track the changes in lattice cell composition over the fuel burnup cycle. The depletion calculation uses the reaction rates along with interaction data to alter the composition of the fuel over a given irradiation time step. During the irradiation time step the flux distribution is assumed to be constant. Consecutive transport solutions over a full burnup cycle at regular small intervals thus produce the reaction rates and neutron distribution of the lattice cell over the burnup time along with the specific material composition. This information is aggregated in the lattice cell cross sections for each irradiation step over the full burnup cycle. The lattice cross sections are then homogenized over the geometry and energy groups to produce macroscopic cross sections that describe the lattice cell as a whole at each of the irradiation steps over the burnup cycle. These few-group macroscopic lattice cell cross sections are then fed forward to be utilized in full core diffusion simulations that are constructed from the lattice cell blocks. A similar method is performed for the reflector cells on the periphery of the core. These cells contain only moderator and represent the water in the calandria tank that surrounds the lattice of fuel channels. This information is sufficient for a simple full core simulation that does not take into account any reactor structures or control devices. To produce a more realistic and accurate model, the effects of the reactor control devices on the lattice cells must be included. This is accomplished with super-cell calculations which yield incremental cross sections that detail the effect of the interaction of these components with the base lattice cell.

3.3 Lattice super-cell computations in CANDU

The CANDU system is unique among other reactor types as it is designed with horizontal pressurized fuel channels residing in a large tank of moderator at atmospheric pressure with the control devices, instruments and structures residing in the moderator section. As a result the control devices interact with the core perpendicular to the fuel channels. This creates a complication in modeling the interaction of control devices with the core. In light water reactors the fuel is

vertically oriented as are the control devices and as such, the control interaction can be implemented in the lattice cell model and simulated using a 2D transport solution. In the case of CANDU, the orthogonal orientation of the fuel channels to the control devices and structures requires a full 3D treatment of the system to capture the variations in neutron flux along the length of the fuel channel and locally near reactivity control device components.

The control device interaction is modeled using a 3D structure known as a super-cell which simulates an infinite repeated network of a base cell with two fuel channels and the control device. The cell has two fuel channels with the surrounding moderator (essentially the 2D lattice cell representation) side by side with an axial length of 1 fuel bundle (49.50 cm). The control device interacts orthogonal to the fuel channels centered at the interface between the two cells, midway along the length. A depiction of a typical CANDU super-cell arrangement is seen in Figure 3.3.
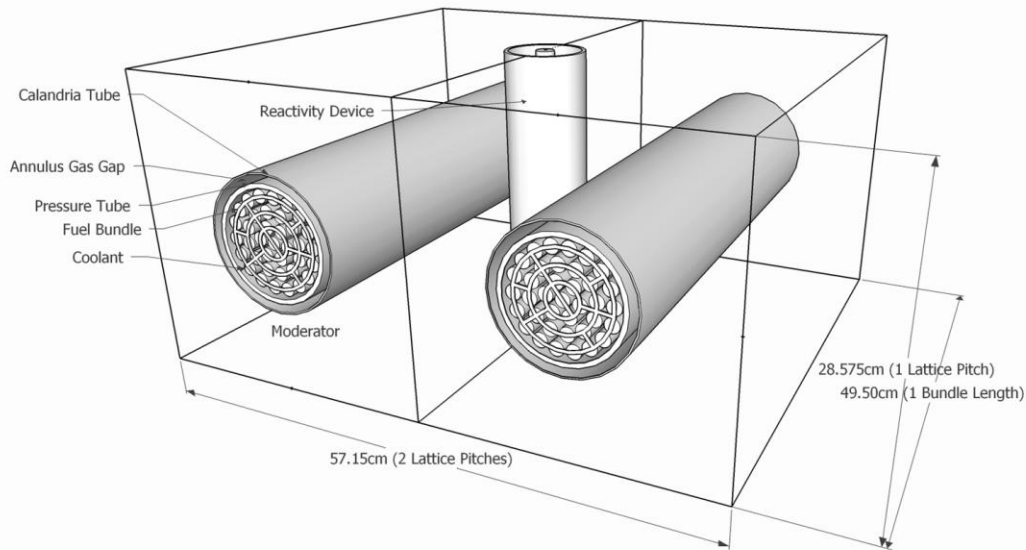
Figure 3.3: A 3D CANDU super-cell model (37 element bundle with adjuster)

The CANDU design has four different control device systems; the liquid zone controllers (LZCRs), adjuster rods, mechanical absorber (MCA) rods and shutdown system (SDS) rods. Each control device has its own separate super-cell model which depicts the interaction with the fuel channels. The self-shielding calculation for the fuel channels is performed using the standard 2D lattice cell

arrangement. The primary 3D transport software currently utilized in most CANDU applications is the DRAGON 3D transport code [49]. The end goal of the simulations is to produce two sets of cross sections for the system with the control device removed and fully inserted. The cross sections are homogenized for the full height and depth over the inner area of the model from the centre of the left fuel channel to the centre of the right fuel channel including the control device. The differences in the two sets of homogenized cross sections are then computed, producing the incremental cross sections for the specific control device that are required for the diffusion calculation. These incremental cross section values are included as an additional input in the diffusion calculation to adjust the reference lattice cell cross sections in order to appropriately account for the control device configuration at any one time.

The 3D transport solution is quite complex and is computationally intensive, as such the geometry of the fuel channel and some of the control devices are simplified for the calculation. The legacy codes and previous versions of DRAGON (v3.04 and earlier) were unable to solve the 3D transport equation for the nested cluster geometries present in a CANDU fuel channels with full bundle detail and thus the use of an annular simplification was required. The newer versions of DRAGON, such as 3.06 used herein, are capable of handling the nested cluster geometry but still have quite high computational complexity [50]. The use of an annular simplification will change the physics of the model slightly as the heterogeneity and separation of the fuel into individual pins is removed. The goal of the 3D super-cell simulation is to determine the change in cross sections when the control device interacts with the two full lattice cells. Studies on the effects of using an annular simplification for fuel bundles in CANDU 3D super-cell calculations have been performed and show that the differences in the incremental reactivity between 3D cluster and 3D annular simulations are negligible (< 10 pcm or 0.1mk) [51]. The minor accuracy differences with the annular simplification are acceptable as it greatly reduces the computational time for the simulation. Hence, this study utilizes the accepted technique of annular homogenization of fuel rings that has been used in a substantial amount of prior CANDU safety analysis [52].

The cluster geometry of the fuel bundles is represented with concentric homogenized annuli as depicted in Figure 3.4. Specifically, the outer rings (rings 2, 3, 4) are represented by annuli of homogenized fuel coolant and sheath in proportion with the correct volume and are separated by rings of pure coolant.

The annular fuel rings maintain the volume of fuel, coolant and cladding to represent the fuel elements at the common radial distance from the centre of the bundle. The thicknesses of the annuli are equal to the diameter of the clad fuel elements and the centres of the annuli are located at the radial distance of the elements in the ring to the centre of the bundle.
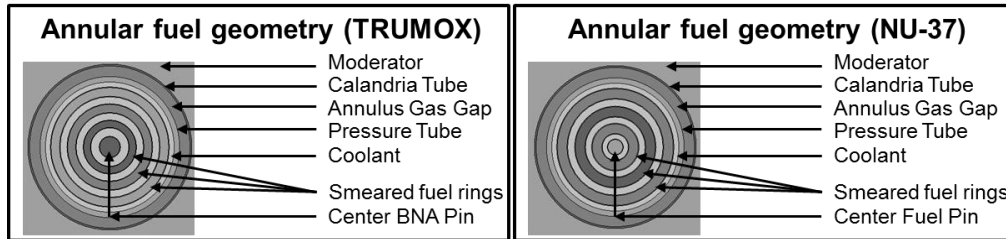
Figure 3.4: CANDU annular fuel geometry (front view)

The rod geometry control devices (adjusters, MCA and SDS) are concentric annuli and can be faithfully reproduced in the 3D transport models. The adjuster rods in CANDU are a pin in tube design with a central pin of varying thickness composed of usually stainless steel or titanium contained within a hollow stainless steel tube of varying thickness that is filled with moderator. The pin in tube rod assembly is consistent along the full length and moves within a perforated zirconium alloy guide tube. The MCA and SDS rods are of the exact same design with a hollow tube that has a layer of cadmium sheathed between stainless steel and moderator within the tube. The MCA/SDS tube is also consistent over the length and contained within a perforated zirconium alloy guide tube. These geometries are reproduced exactly based on the real system requiring no simplification for the modelling and are depicted in Figure 3.5.
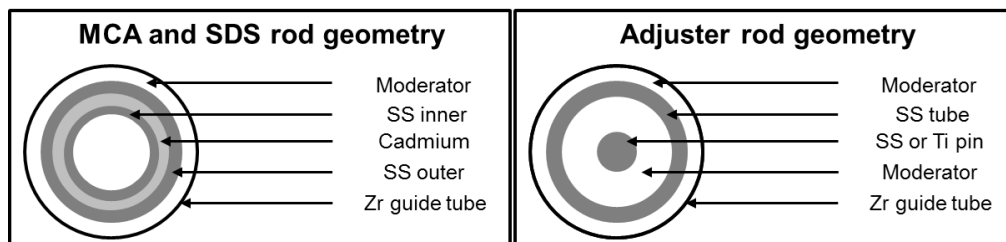
Figure 3.5: CANDU control rod geometry (top view)

The adjuster and MCA/SDS rods have permanent guide tubes that are in the core so the cross sections with the rod removed and the guide tube present are

subtracted from the cross sections with the guide tube present and the rod fully inserted. The guide tubes themselves also need incremental cross sections which are computed by subtracting the cross sections for a cell with only the fuel channels (no control devices or guide tubes present) from the cross sections with the guide tubes present.   This produces one set of incremental cross sections for each adjuster and MCA/SDS type and each guide tube type, in the case of CANDU 9 there are a total of 7 sets (4 adjuster types, 1 MCA/SDS type, and 2 guide tube designs).

The final control devices modeled are the liquid zone controller tanks which are a more complex geometry and require some simplification.   There are three different liquid zone designs depending on the vertical location in the core. The zone controllers are arranged in three columns across the core at two different axial positions as shown in Figure 3.6 for the core face view. The two outer columns consist of two liquid zone tanks stacked on top of each other with feeder and scavenger pipes for both the light water and the helium cover gas.   The central column has the same two tank stack as the outer configuration with the addition of a third tank on top of the stack. This configuration results in three different liquid zone tanks which only differ by the number of feeder and scavenger pipes that pass through the tank.
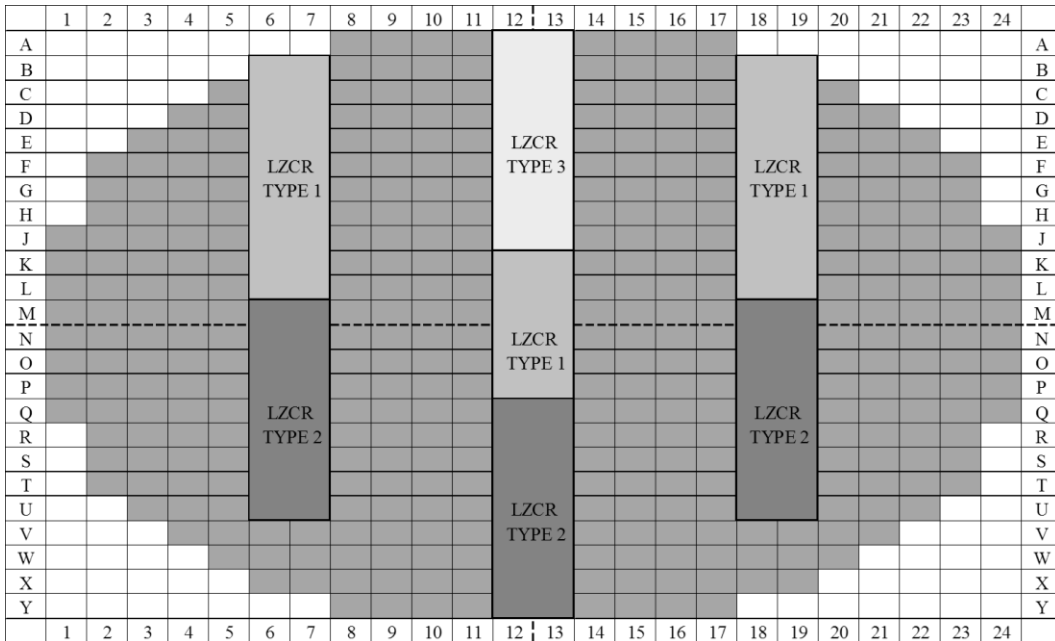
Figure 3.6: CANDU liquid zone controller locations (core face view)

The liquid zone tank at the top of the outer columns and the middle of the center column is LZCR type 1 and has two feeder pipes (one for water and one for helium) and four scavenger pipes (water and helium for this zone and water and helium for the zone below). The liquid zone tank at the bottom of all three columns is LZCR type 2 and has no feeder pipes and two scavenger pipes (one for water and one for helium). The tank at the top of the centre column is LZCR type 3 and has four feeder pipes (water and helium for each of the two zones below) and six scavenger pipes (water and helium for each of the three zones in the stack). The helium pipes are smaller than the water pipes and are located inside their diameter for both feeders and scavengers. For each liquid zone type the area where the feeder and scavenger pipes are located is smeared into a homogenous ring with a thickness equal to the largest pipe diameter that maintains the volume of pipe material, helium and water present in the original geometry. This serves to change the cluster configuration of the liquid zone in to a series of concentric annuli much like the adjuster rods. A sample of the liquid zone geometry for LZCR type 1 is provided in Figure 3.7.
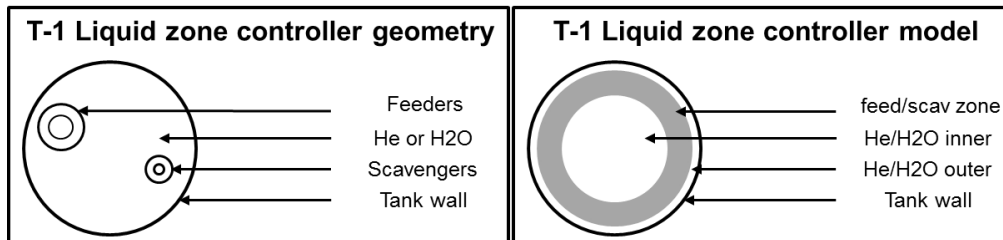
Figure 3.7: CANDU liquid zone controller geometry and model (top view) [52].

The liquid zone controllers require incremental cross sections to apply to both the light water and the helium cover gas and hence have two sets of incremental cross sections for each zone controller type. The incremental computation for the helium case, also referred to as the zone controller guide tube, is performed by subtracting the cross sections for the fuel channel only cell from the cell with the zone modeled and full of helium. The incremental cross section for the water filled case is similarly computed by subtracting fuel channel only cell cross sections from those of the liquid zone full of water. This results in 2 sets of incremental cross sections for each liquid zone controller type, a total of 6 sets for a CANDU-900 design.

The configurations for all the different control devices are modeled in 3D as described to produce incremental cross sections. For the CANDU-900 design there are 4 adjuster types, 1 MCA/SDS type, and 3 liquid zone types. As discussed earlier, the cross sections used for the incremental values are homogenized both in energy and geometry. The multi-group cross sections from the transport calculation are homogenized into two energy groups, fast and thermal. Also there is only a specific portion of the super-cell that is included in the cross section calculation, the inner region of the super-cell which contains one half of each fuel channel and the full control device. By homogenizing this inner region, seen in Figure 3.8, the cross sections computed for the fast and thermal groups align with the standard base lattice cell geometry that is used in the diffusion code and the incremental values are applicable to the base cross sections for the lattice cell.
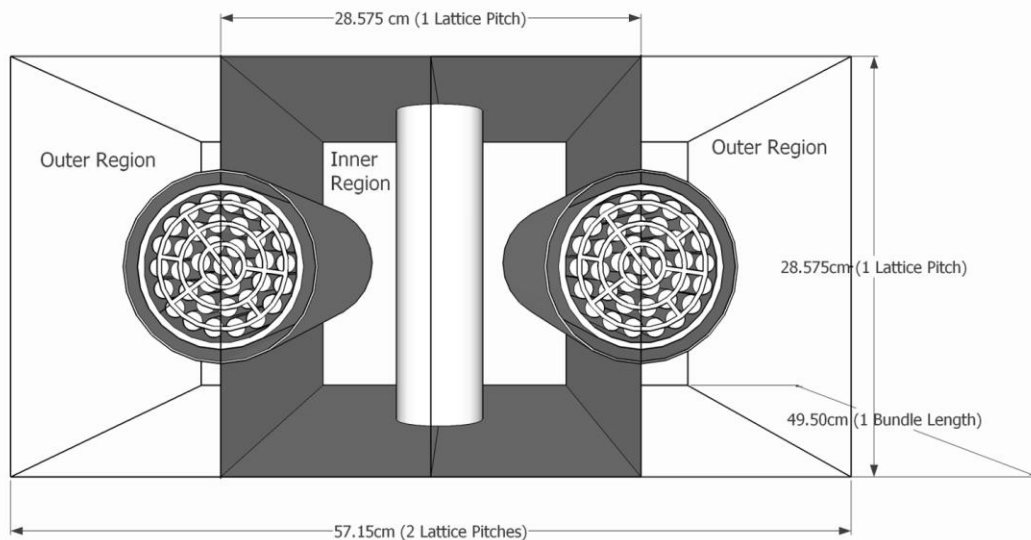
Figure 3.8: CANDU 3D super-cell face view, inner region is homogenized.

The homogenized cross sections are used to compute the incremental cross section values for the control devices as discussed and are passed on to the diffusion code. This provides the information necessary to modify the base lattice cell cross sections to properly account for the control device interaction. Table 3.1 provides the set of 11 incremental cross sections that are passed on to the diffusion code for each specific super-cell calculation.

With the homogenous few-group cross sections from the lattice cell transport calculations for the full burnup cycle determined and the few-group incremental

cross sections computed with the 3D super-cell transport simulations at mid-burnup complete the information is fed forward to the full core model. The 3D full core diffusion model is assembled from lattice cell building blocks surrounded by reflector cells with the proper control devices and in core structures included in the model. The solution of the diffusion equation for the 3D geometry predicts the neutron flux distribution in the full core and the reaction rates allowing the computation of the fuel burnup for each bundle in the core.

Table 3.1: Incremental cross section inputs required for the diffusion code [53]

Incremental	Description of cross section
2GTR1	Fast group transport corrected
2GTR2	Thermal group transport corrected
2GSA1	Fast group absorption
2GSA2	Thermal group absorption
2GNF1	Fast group $\nu\Sigma_f$ (production)
2GNF2	Thermal group $\nu\Sigma_f$ (production)
2GS12	Transfer from group 1 to 2 (down-scattering)
2GS21	Transfer from group 2 to 1 (up-scattering)
2GF	Ratio of fuel flux to cell flux (F factor, thermal only)
2GH1	Ratio of bundle power produced by the epithermal spectrum to the fast cell flux (H1 factor)
2GH2	Ratio of bundle power produced by the epithermal spectrum to the fast cell flux (H2 factor)*
$* H_{g,cell}(10^{-11} kW\ cm^2 s) = 10^8 V_{bundle}\Sigma_{f,g,cell}E_{fission}$	

3.4   Solution of the diffusion equation

A full core reactor model that includes all in core structures and devices is too complex and computationally intensive to efficiently model with a transport code. The solution for full core modeling is to utilize the homogenized cross sections taken from the transport solutions to build the full core model out of lattice cell building blocks and compute the two group diffusion solution to determine the neutron flux distribution in the core. The two energy groups used in this solution are the fast and thermal groups (the separation energy is 0.625 eV) and the equation solved is the finite difference diffusion equation.

The treatment of the diffusion equation follows that of Duderstadt [44] and is similar to that of neutron transport where the production and losses of neutrons in an arbitrary volume, V, are tracked such that the time rate of change is described for a one speed diffusion system.

$$\frac{d}{dt}\left[\int_V d^3r \frac{1}{v} \phi(r,t)\right] = \int_V d^3r \frac{1}{v}\frac{d\phi}{dt} = Production - absorption - Leakage \tag{24}$$

Given a neutron source density, $S(r,t)$, an absorption cross section, $\Sigma_a(r)$, and the neutron current density, $J(r,t)$, we can define the production absorption and leakage terms.

$$Production\ (source)term: \left[\int_V S(r,t)d^3r\right] \tag{25}$$

$$Absorption\ term: \left[\int_V \Sigma_a(r)\phi(r,t)d^3r\right] \tag{26}$$

For the leakage case we start with the surface integral form where the neutron current density leading to the leakage through a small surface element dS at position r_s is $J(r_s,t)dS$. The resultant total net leakage through the surface of the volume V is described in equation 27.

$$leakage\ term: \left[\int_S J(r,t) \cdot dS\right] = \left[\int_V \nabla \cdot J(r,t)d^3r\right] \tag{27}$$

Using the above terms and the fact that the volume is arbitrary (thus the integrand will vanish) will result in the following relation for the time dependence of flux.

$$\frac{1}{v}\frac{d\phi}{dt} = -\nabla \cdot J - \Sigma_a \phi + S \tag{28}$$

The above result has both unknown flux and unknown current such that these two variables must be related through a second equation. This is where the diffusion approximation comes into play. As known from gaseous diffusion, the flow of particles from high concentration regions to low concentration regions is at a rate

proportional to the negative concentration gradient (the flux). Fick's law accomplishes this mathematically using a constant of proportionality known as the diffusion coefficient, D(r).

$$J(r,t) \cong -D(r)\nabla\phi(r,t) \tag{29}$$

The diffusion coefficient is defined directly from the neutron transport equation via the macroscopic transport cross section (Σ_{tr}) as seen in equation 30 with $\bar{\mu}_0$ being the average cosine of the scattering angle in a neutron scatter collision.

$$D = \frac{1}{(3\Sigma_{tr})} = \frac{1}{[3(\Sigma_t - \bar{\mu}_0 \Sigma_s)]} \tag{30}$$

The diffusion approximation is only valid several mean free paths away from boundaries or from sharp changes in flux (absorbers or sources). These limitations are acceptable given the common use of lattice cell codes to resolve these regions using transport theory. The homogenized cross sections from the transport solution provide a more accurate diffusion representation. The one speed neutron diffusion equation is now expressed in equation 31.

$$\frac{1}{v}\frac{d\phi}{dt} = \nabla \cdot D(r)\nabla\phi - \Sigma_a(r)\phi(r,t) + S(r,t) \tag{31}$$

The initial condition of a specific flux at time zero, $\phi(r,0) = \phi_0(r)$, for all r. The boundary condition is chosen at the point where the diffusion theory flux vanishes at a distance and is an extrapolated boundary at $z_0 = 0.7104\lambda_{tr}$. Extrapolation length is frequently ignored in large scale reactor systems as it is on the order of a few centimeters when the reactor sizes are several meters.

The one speed diffusion equation made two major assumptions that must be accounted for. First the assumption that the angular flux is only weakly dependant on angle (linearly anisotropic actually) so that the diffusion approximation is valid. This is usually valid in a large reactor system if the areas near strong absorbers, interfaces and boundaries are treated to account for transport effects. This is the main use of an assembled system that uses a transport code to analyze the base lattice cell and generate homogenized cross sections. The use of super-cell simulations to compute incremental cross sections for an absorber accounts for the transport effects and builds them into the

assembled diffusion solution. For proper treatment of boundary cells in the reactor, detailed cell models can be made and solved with the transport equation similar to the base lattice or to the super-cells. The use of this integrated information from the transport solutions by way of the homogenized cross sections allows the diffusion model to have acceptable accuracy while avoiding the computational complexity of a full core transport solution.

The second assumption of one speed (energy) of the neutrons strains to properly simulate actual reactor conditions since the energies span ten orders of magnitude (0.001 eV to 10 MeV). Like the transport solution, the energy for the diffusion case is separated into groups producing a few-group diffusion solution.

The source term in a reactor system is the production of neutrons from fission which is described, as in transport, as $\nu_g \Sigma_{fg}$ with χ_g as the fission spectrum for the specific group. The cross sections for each group are assembled in the same manner as in the transport equation, by collapsing down from the number of groups in the transport solutions down to the number of groups in the diffusion solution as per equation 14 in Chapter 3.1. This treatment will yield the multi-group diffusion equation for g = 1, 2, …, G, where Σ_{tg} includes scatter-out.

$$\frac{1}{v_g}\frac{\partial \phi_g}{\partial t} - \nabla \cdot D_g \nabla \phi + \Sigma_{tg}\phi_g(r,t) = \sum_{g'=1}^{G} \Sigma_{s\,g'g}\phi_{g'} + \chi_g \sum_{g'=1}^{G} \nu_{g'}\Sigma_{fg'} + S_{g'} \quad (32)$$

The few-group solution is usually performed with 2 energy groups for full core simulations and is the method used in the RFSP diffusion code [54]. The two group solution for a time invariant system is the most common form of the diffusion equation that is solved. The static 2 group neutron equation used in RFSP in shown in Equation 33 [53].

$$-\nabla \cdot D_1(\vec{r})\nabla\phi_1(\vec{r}) + \left(\Sigma_{a1}(\vec{r}) + \Sigma_{1,2}(\vec{r})\right)\phi_1(\vec{r}) - \Sigma_{2,1}(\vec{r})\phi_2(\vec{r})$$
$$-\frac{1}{k_{eff}}\left(\nu\Sigma_{f1}(\vec{r})\phi_1(\vec{r}) + \nu\Sigma_{f2}(\vec{r})\phi_2(\vec{r})\right) = 0$$
$$(33)$$
$$-\nabla \cdot D_2(\vec{r})\nabla\phi_2(\vec{r}) + \left(\Sigma_{a2}(\vec{r}) + \Sigma_{2,1}(\vec{r})\right)\phi_2(\vec{r}) - \Sigma_{1,2}(\vec{r})\phi_1(\vec{r}) = 0$$

The two groups treated are the fast (1) and thermal (2) with the energy division taken as 0.625eV. It should be noted that $\chi_1 = 1$ and $\chi_2 = 0$ thus all neutrons produced from fission are born in the fast group whether from fast or thermal fission. The k_{eff} value is the reactor multiplication constant and is the inverse of the eigenvalue of the above equation.

The matrix representation for the two group solution can be expressed as an eigenvalue solution problem with $\lambda = 1/k_{eff}$.

$$M\Phi = \left(\frac{1}{k_{eff}}\right)F\Phi, \tag{34}$$

$$with\ M = \begin{pmatrix} -\nabla \cdot D_1(\vec{r})\nabla + \Sigma_{a1} + \Sigma_{1,2} & -\Sigma_{2,1} \\ -\Sigma_{1,2} & -\nabla \cdot D_2(\vec{r})\nabla + \Sigma_{a2} + \Sigma_{2,1} \end{pmatrix}$$

$$and\ F = \begin{pmatrix} v\Sigma_{f1} & v\Sigma_{f2} \\ 0 & 0 \end{pmatrix}$$

Numerical solution of the diffusion equation is performed using finite difference where the derivatives are approximated by a finite difference ratio and is described as per the RFSP treatment [53]. The solution must satisfy the above equations at all points in the reactor. The finite difference method is employed at the midpoints of the homogeneous cells that define the reactor. The homogeneous properties of the cells are taken from the lattice calculations and modified by incremental cross sections if necessary.

The finite difference equation is obtained by integrating equation 33 over the node volume using the homogeneous properties [53].

$$\int_{node\ 0} \left\{ -\nabla \cdot D_1^0 \nabla \phi_1(\vec{r}) + \left(\Sigma_{a1}^0 + \Sigma_{1,2}^0 - \frac{v\Sigma_{f1}^0}{k_{eff}} \right)\phi_1(\vec{r}) - \left(\Sigma_{2,1}^0 - \frac{v\Sigma_{f2}^0}{k_{eff}} \right)\phi_2(\vec{r}) \right\} d\vec{r}$$

$$= 0$$

$$\tag{35}$$

$$\int_{node\ 0} \left\{ -\nabla \cdot D_2^0 \nabla \phi_2(\vec{r}) + \left(\Sigma_{a2}^0 + \Sigma_{2,1}^0 \right)\phi_2(\vec{r}) - \Sigma_{1,2}^0 \phi_1(\vec{r}) \right\} d\vec{r} = 0$$

The two types of integrals found in equation 35 are those that involve the divergence operator and those that do not. The terms without the divergence

operator are evaluated by pulling the cross section terms out of the integral and making the assumption that the average flux over the node is equal to the flux at the center of the node. This results in a treatment as shown with the $\left(\Sigma_{a2}^{0} + \Sigma_{2,1}^{0}\right)$ term in equation 36, where V^{0} is the volume of the node.

$$\int\limits_{node\ 0} \left(\Sigma_{a2}^{0} + \Sigma_{2,1}^{0}\right)\phi_{2}(\vec{r})\,d\vec{r} = \left(\Sigma_{a2}^{0} + \Sigma_{2,1}^{0}\right)\phi_{2}^{0}V^{0} \tag{36}$$

The treatment of the integrals containing a divergence term which represent the leakage between the node and its neighbours is more complicated. The volume integral is converted back to a surface integral to determine the current out of the surface of the node. This surface integral is evaluated over the interfaces of the node and its 6 neighbours (see Figure 3.9) and the current at the interface is assumed to be equal to the average interface current then the general surface integral for a given interface is calculated using equation 37.
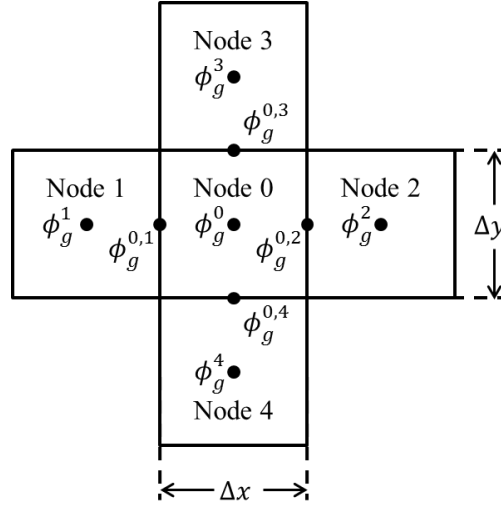
Figure 3.9: Node coupling schematic in diffusion model (X-Y view) [53].

$$\int\limits_{node\ 0} \left\{-\nabla \cdot D_{g}^{0}\nabla\phi_{g}(\vec{r})\right\}d\vec{r} \equiv \int\limits_{\substack{surface \\ of\ node\ 0}} J_{g} \cdot \hat{n}dS = \sum_{n=1}^{6} A_{g}^{0,n}\left(\phi_{g}^{0} - \phi_{g}^{n}\right)$$

$$\tag{37}$$

$$with\ A_{g}^{0,n} = \frac{2D_{g}^{0}D_{g}^{n}\Delta^{0}y\Delta^{0}z}{D_{g}^{0}\Delta x^{n} + D_{g}^{n}\Delta x^{0}}$$

The $A_g^{0,n}\left(\phi_g^0 - \phi_g^n\right)$ terms represent the group g leakage out of node 0 across the interface with the neighbouring node n. The final form of the finite difference diffusion equation then becomes equation 38 [53].

$$\sum_{n=1}^{6} A_1^{0,n}(\phi_1^0 - \phi_1^n) + \left(\Sigma_{a1}^0 + \Sigma_{1,2}^0 - \frac{\nu\Sigma_{f1}^0}{k_{eff}}\right)\phi_1^0 V^0 - \left(\Sigma_{2,1}^0 - \frac{\nu\Sigma_{f2}^0}{k_{eff}}\right)\phi_2^0 V^0 = 0$$

$$(38)$$

$$\sum_{n=1}^{6} A_2^{0,n}(\phi_2^0 - \phi_2^n) + \left(\Sigma_{a2}^0 + \Sigma_{2,1}^0\right)\phi_2^0 V^0 - \Sigma_{1,2}^0\phi_1^0 V^0 = 0$$

Therefore for a system with P nodes the finite difference form of the 2 group diffusion equation produces a coupled set of 2*P linear homogeneous equations of the type defined by equation 38 [53]. This system produces a sparse matrix eigenvalue problem which is then solved iteratively in a two loop scheme. The overall normalization of the flux is arbitrary in the homogeneous diffusion equation and thus only relative fluxes can be determined. Therefore a predefined total power is provided to allow the normalization to absolute flux. The outer loop converges on k_{eff} while the inner loop converges on the flux. Upon convergence of the full two loop system the relative fluxes are normalized based on the total power value to obtain the absolute flux distribution in the reactor.

The boundary conditions for the system deal with the nodes that are not fully surrounded by other homogeneous nodes. In this case there is a need to account for the extrapolation length at which the flux vanishes. Essentially, the border nodes are treated by adding on a dummy node at the interfaces at the edge of the core to account for the extrapolation length, d_{extr} as seen in Figure 3.10.
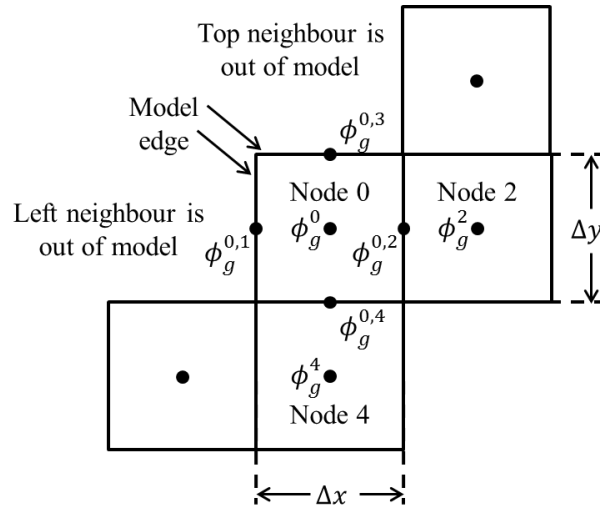
Figure 3.10: Node coupling schematic for edge cell (X-Y view) [53].

The $A_g^{0,n}(\phi_g^0 - \phi_g^n)$ terms are computed for the node interacting with its fictitious neighbour node n with $\phi_g^n = 0$, $D_g^n = D_g^0$, and $\Delta x^n = 2 \cdot d_{extr}$. The boundary is evaluated as flat or circular into a vacuum or can be user defined (see Figure 3.11). The circular condition is common for the x and y edges of the core, the circular extrapolation radius is defined in relation to the inner radius of the reactor calandria vessel and the x and y extrapolation distances are evaluated based on this circle. The flat condition is common in an axial direction and for a vacuum boundary condition extrapolation length is defined as $d_{extr}^g = 2.1312 D_g^0$ [53].
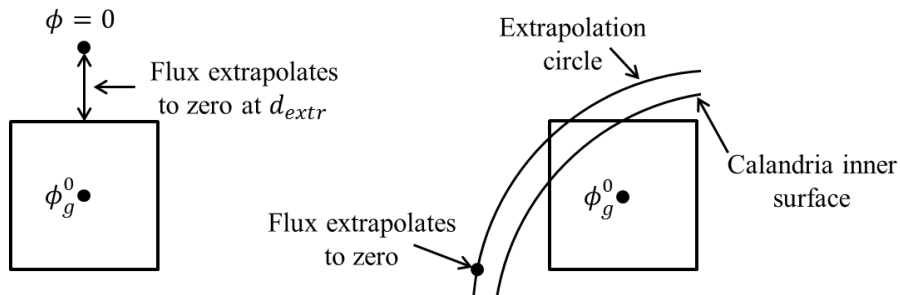
Figure 3.11: Boundary extrapolation for flat (axial) and circular (X and Y) [53].

3.5 Full core CANDU modeling

Once the homogenized cross sections for the requisite burnup length and incremental cross sections for the control devices are produced by the lattice cell code simulations they are fed into the full core modelling software to perform a 3D detailed diffusion solution. As mentioned previously, the main code used in CANDU full core diffusion analysis is RFSP [54]. The full core modelling includes the definition of model geometry and the designing of a time-average model which is then tested and refined through the use of instantaneous snapshots and short and long term fuelling simulations to ensure the specific operational limits of CANDU are being met.

3.5.1 Full core geometry

The geometry is defined based on the reactor system being modeled to the level of fidelity deemed necessary. The model usually includes all the fuel and in core structures along with the control devices and includes the specific meshing in all 3 dimensions. In addition, the grouping of fuel channels into regions of similar characteristics and the specific fuelling scheme for each region (e.g. 4 or 8 bundle shift) is defined in this step.

3.5.2 CANDU reactivity control devices

The main systems of reactor control in a CANDU were touched on in Chapter 3.3 and include the liquid zone controllers, the adjuster, MCA and SDS rods and in some cases low levels of moderator poison. Figure 3.12 displays the locations of the control devices in the horizontal and axial directions.

The liquid zone controllers are the primary control system in the core and used to fine tune the spatial flux distribution during normal operations including fuelling and to provide control for changes in bulk reactor power. The constant adjustment of the liquid zones balances the flux throughout the core and maintains a stable power profile. The 14 liquid zone compartments contain light water with a helium cover gas (previously described in Chapter 3.3). Since they are located within the heavy water moderator the light water in the zone controllers has a negative effect on reactivity such that when the zones are filled the reactivity in the individual zone and in the full core decreases. The zones provide bulk control

of the core reactivity through coordinated movement and also provide spatial control to keep the 14 zones close to their target power levels.
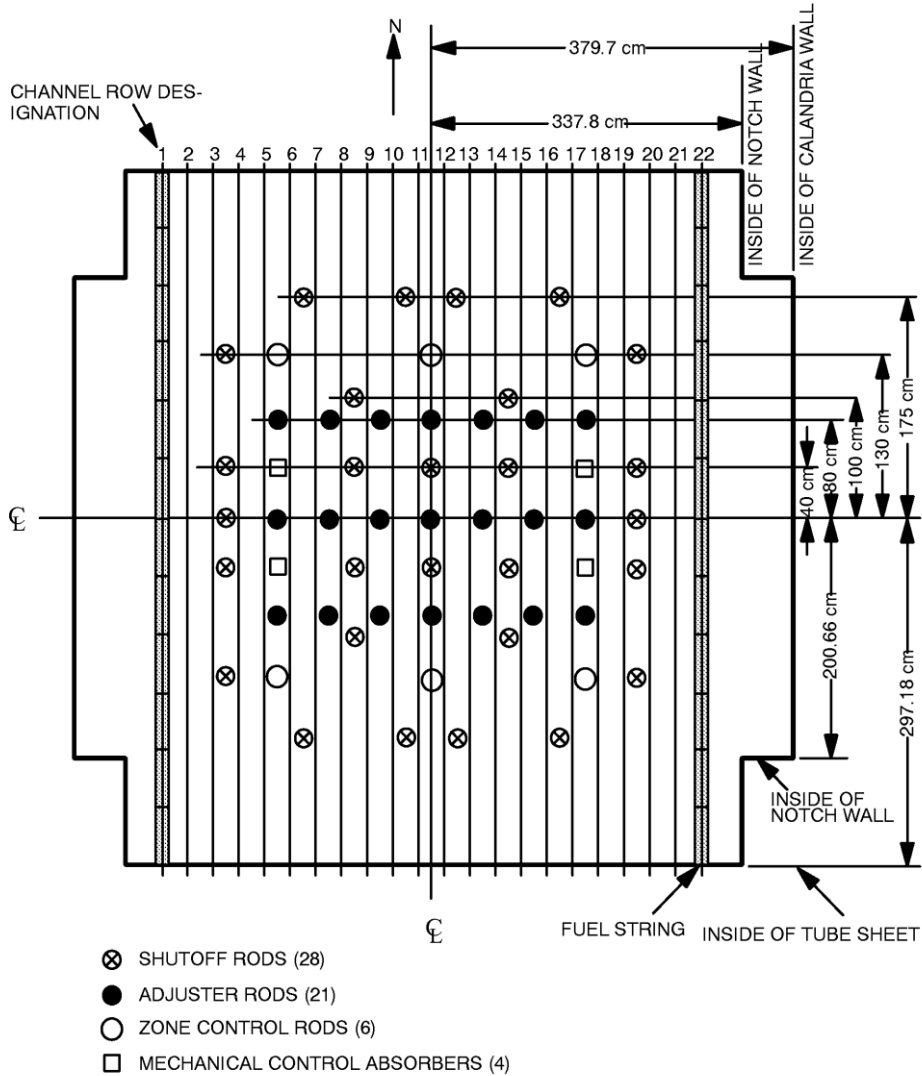
Figure 3.12: CANDU control device locations in core, top view [55].

The adjuster and MCA rods are primarily used for more coarse control manoeuvers and recovery from abnormal conditions. The adjusters are composed of stainless steel or titanium[4] and have a pin in tube design as described previously in Chapter 3.3. They are usually fully inserted into the reactor core

---

[4] Some CANDU designs utilize cobalt pins in the adjusters for isotope production, but the generic CANDU-900 utilizes only titanium or stainless steel pins for its adjuster assemblies.

providing a reserve of positive reactivity in the core that can be used to overcome issues such as the buildup of neutron absorbing fission products (e.g. xenon-135) and to assist the liquid zones to control the core. There are 21-24 adjuster rods (depending on CANDU reactor type) contained in 7 banks across the core. These rods can provide some level of spatial control but their worth and movement speeds make only coarse adjustment possible and they are not specifically designed for this purpose. In addition to the adjuster assemblies, there are the 4 mechanical control absorbers (MCAs), which are hollow tubes of cadmium sandwiched between two layers of stainless steel, see Chapter 3.3. They are the same configuration as the rods used in shutdown system 1 (SDS 1) rods and are usually positioned outside the core. The 4 rods are divided into two banks and are located near the center of the core. The MCAs do not provide much assistance in spatial control and are primarily designed to allow the reactor regulating system to provide negative reactivity to rapidly lower power during a malfunction or accident condition. The MCAs provide bulk control capability that can supplement the liquid zone controllers.

Occasionally, a moderator poison such as boron or gadolinium may be used to provide a reserve of negative reactivity in the core. This is primarily for instances when the station desires to fuel the core ahead of schedule to accommodate a fuelling machine outage or to avoid fuelling over a weekend or holiday period. This may also done to mitigate the xenon free effects encountered after a long duration outage. Small amounts of moderator poison are added to keep the reactivity in the core down and maintain the balanced criticality. Since the poison is added directly to the moderator and diffuses throughout, this is a bulk effect in the core.

The core reactivity control in a CANDU is accomplished through day to day fuelling activities which maintain the reactivity in the core while the liquid zones provide the necessary spatial balancing to maintain the desired flux/power profile in the core. As the fuel in the channels burns up the reactivity in the core decreases which is replenished by fuelling some of the channels each day. In general a CANDU reactor must fuel about 15 bundles/full-power-day [55].

3.5.3   Time-average simulation

Once the geometry and regions are defined, the time-average calculation is performed. The time-average model, when completed, provides the targets for 3D

flux, power, burnup and fuelling frequency for standard operations. The CANDU reactor is fuelled online and maintains core reactivity by fuelling a few channels each day rather than using batch refuelling which is common in light water reactors. The fuelling frequency of a channel or group of channels is defined based on the irradiation level chosen. For each of the defined regions of fuel channels defined in the model a specific exit irradiation is set determining the fuelling frequency. A sample diagram of irradiation regions utilized in CANDU is provided in Figure 3.13.
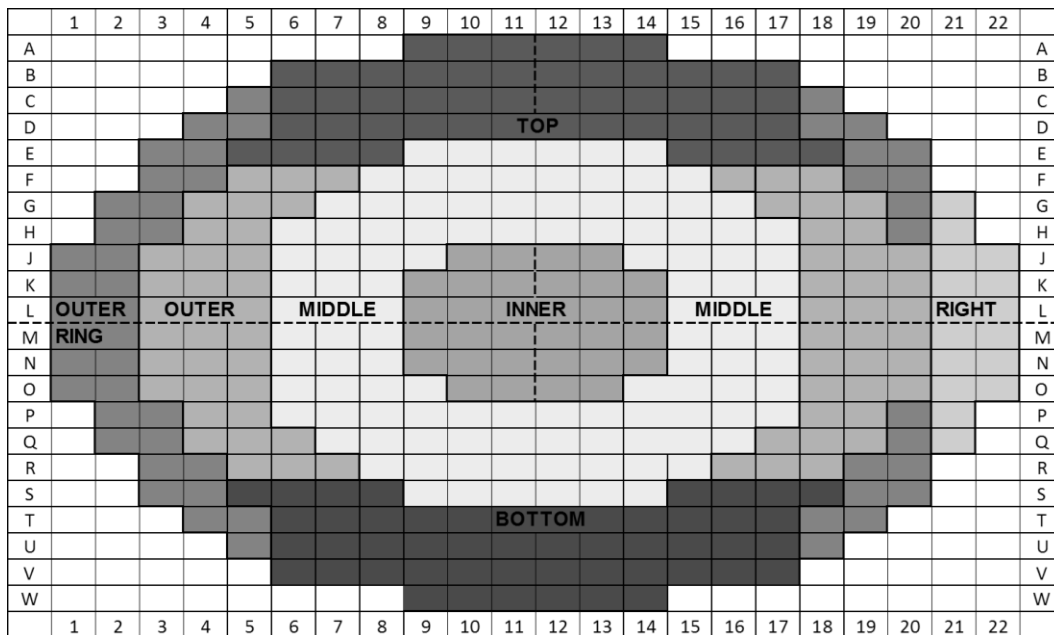
Figure 3.13: Multi-region time-average model for CANDU 6.

The definition of regions provides the ability to alter the irradiation or fuelling scheme for a specific set of channels. In principle, a different region can be defined for every single fuel channel (480 in a CANDU-900) thus allowing a unique irradiation or fuelling scheme to be defined. The process of grouping channels into regions reduces the number of inputs and allows a simpler core layout that is manageable. The regions group channels of similar power levels or locations in the core that would have common exit irradiations. For example, in Figure 3.13 we see groupings based on power levels (inner, middle, outer) and on geometric symmetry (top, bottom, right). The definition of a specific region can also be used to account for differences in the core in that area, the right region in Figure 3.13 is different from the outer ring region because the liquid neutron

absorber injection nozzles for the shutdown system 2 (SDS 2) are located in this region. The top and bottom zones are defined differently because of differences in the core structures at the top and bottom of the core such that the irradiations must be different to achieve a symmetrical channel power distribution. The goal of the regions is to provide symmetry across the core to account for differences in the geometry and to allow higher power regions to burn longer. In principle, the more irradiation regions the greater the control the designer has over the power distribution but, in difference to operational constraints, the number of regions must be manageable. The net result of a properly executed region and irradiation definition is a symmetric channel power profile that is flat over much of the core which promotes even burnup and distribution of power.

The region definitions and exit irradiations are modulated until a core configuration is reached where the channel and bundle powers and the reactivity of the core are suitable and the fuel burnup targets for the core have been reached. The higher the exit irradiation, the longer the fuel spends in the channel and the higher the burnup. The exit irradiation is limited by the activity of the fuel since at later stages of burnup the fuel will impose a negative reactivity on the core. The goal is to choose the irradiations such that the time-average full core reactivity is about zero ($\pm < 1$ mk) resulting in a critical geometry. The control devices are usually modeled at their average positions for a time-average core, for natural uranium fuelled CANDU this usually means that the adjuster rods are fully inserted and the liquid zone controllers are held at about 50% full.

The time-average-model calculates the lattice properties that are averages of their values over the burnup cycle and provide a target power distribution. The time-average power distribution, channel fuelling frequencies and the fuel discharge burnup values provide a guide line for core follow simulations. The time-average lattice properties are calculated at each bundle location such that they are averages over the residence time of the fuel at that location, essentially reproducing the number of reactions that will occur there on average. Using the time-average properties in the solution of the neutron diffusion equation therefore produces the aforementioned target flux, power, burnup and fuelling frequency distributions. The production of the time-average cross section (x) for a position (channel, bundle or c, b) in the core is a function of the integral of the cross section over the burnup and the entry and exit burnup as per equation 39 [56].

$$\Sigma_{x,cb,tav} = \frac{\int_{\omega_{entr,cb}}^{\omega_{exit,cb}} \Sigma_{x,cb}(\omega)d\omega}{\int_{\omega_{entr,cb}}^{\omega_{exit,cb}} d\omega} = \frac{\int_{\omega_{entr,cb}}^{\omega_{exit,cb}} \Sigma_{x,cb}(\omega)d\omega}{\left(\omega_{exit,cb} - \omega_{entr,cb}\right)} \tag{39}$$

The cross sections for each position in the time-average are then fed into the neutron diffusion equation which is solved to find the time-average flux. The irradiations and regions are then adjusted to produce a core with a symmetric power distribution that has acceptable radial flattening and maintains suitable core reactivity. The fine tuning of the time-average model produces a target distribution that maintains the bundle and channel powers well within their operational envelope while meeting specific burnup goals. The time-average parameters that are defined can then be tested and validated using full core simulations based on the defined average behaviour and by using snapshot simulations of the core.

3.5.4 Instantaneous snapshot simulations

Once the time-average properties are defined, it is possible to explore the effects of individual fueling events and realistic channel age patterns. The next stage after the time-average model is to produce a snapshot core that contains specific ages for each of the channels in the core. On average, these channels will be at the equilibrium age but will be different across the core creating local variances which can be used to approximate the core a specific point in time. A random snapshot of the core at a given time is generated with some channels recently fuelled, some in the middle of the fueling cycle and some high burnup channels that are to be fuelled soon. A random aging pattern is provided which dictates the stage in the fueling cycle for each channel and must be representative of the range of fuel burnup possible. Furthermore, the output of these simulations provide data to ensure the bundle and channel power limits are met for a given set of random channel ages. It is very important to produce a realistic distribution of ages for the channels such that they actually represent a configuration which the core would attain after a long period of fuelling based on the operational parameters defined by the time-average model.

The production of a realistic random age pattern is complex and could be unique to each fuel design. A stylized approach is taken to provide a general and consistent method for generating channel ages. A matrix of random ages between 0 and 1 (usually of 6x6 or 7x7 size) is generated and referred to as a "pattern

random channel age distribution" (PRCAD) matrix. One of the 49 (7x7 = 49) elements in the matrix is assigned the highest number and is hence next to be fueled. The values within this "patterned" matrix are not just random numbers they are based on an operating history to realistically represent the ages of channels near each other [57]. In the absence of a fuel history one could use a uniform random distribution over the interval (0, 1) with a different value for each channel. However, this method will frequently produce exaggerated maximum bundle and channel powers compared to a more accurate core history where fuelling engineers take great care in optimizing and constraining the channel powers. For example, a random number generator may place several channels of the same age together, while a fuelling engineer avoids fuelling adjacent channels at the same time especially for higher power regions of the core. Therefore, the elements of the PRCAD matrix are based off of a real fuelling history for the group of channels to provide a more realistic pattern of channel aging and avoid unrealistically excessive bundle and channel powers. The channel ages over the full matrix and over several smaller portions average out to be close to 0.5 such that the full core burnup level will be near equilibrium. A sample 7x7 PRCAD matrix based on CANDU operational experience is shown in Table 3.2.

Table 3.2: Sample PRCAD Matrix with Element (1) as the Oldest Channel.

	5	6	7	8	9	10	11
M	(1) 0.98	(2) 0.24	(3) 0.66	(4) 0.84	(5) 0.38	(6) 0.92	(7) 0.50
N	(8) 0.60	(9) 0.46	(10) 0.04	(11) 0.30	(12) 0.56	(13) 0.10	(14) 0.80
O	(15) 0.34	(16) 0.88	(17) 0.14	(18) 0.76	(19) 0.22	(20) 0.68	(21) 0.26
P	(22) 0.72	(23) 0.06	(24) 0.44	(25) 0.54	(26) 0.96	(27) 0.02	(28) 0.48
Q	(29) 0.58	(30) 0.28	(31) 0.82	(32) 0.16	(33) 0.42	(34) 0.64	(35) 0.86
R	(36) 0.20	(37) 0.94	(38) 0.12	(39) 0.70	(40) 0.08	(41) 0.18	(42) 0.32
S	(43) 0.74	(44) 0.40	(45) 0.62	(46) 0.36	(47) 0.90	(48) 0.52	(49) 0.78

The PRCAD matrix pattern is repeated across the array that encompasses all of the channels in the CANDU core. Adjacent matrices are the transpose of those next to them and the application across the core of the channel ages produces a single "snapshot" of the channel burnup profile at an instant in time.

Using multiple PRCAD matrices, several random channel age patterns can be produced which generate multiple core snapshots. These snapshots represent possible instantaneous core configurations, each having their own channel ages, bundle powers and channel powers. Given the limits on these quantities, the

results of the core snapshot simulations are used to evaluate and refine the irradiation times and fuelling patterns, such as to meet the overall limits. The desired result is that an adequate k-effective value is maintained over these simulations and that the maximum bundle and channel powers are kept under the desired limits. Following the snapshot simulations, a more detailed tracking of the effects of fuelling is performed through direct simulation of the reactor throughout its operational cycle. In these simulations the core snapshot is selected as a possible initial condition and then a channel is selected for fuelling. A detailed fuelling simulation is performed with the reactor control system logic modeled to execute the selected fuelling operation. The results of this simulation allow the evaluation of criteria related to bundle and channel powers as well as linear ramp rates.

3.5.5 Reactor characteristics and coefficients

The full core simulations also provide information on the characteristics of the control devices and the reactor coefficients for a change in the bulk reactor properties. The specific reactivity worth of each of the control devices, even down to individual rods and specific liquid zones, can be assessed using the time-average core. This helps to provide guidelines for operations and determine if the system is sufficient to maintain reactor control. A base simulation of the time-average is performed and the irradiation histories for all the fuel bundles are retained. The perturbation simulation that follows uses the stored irradiation values for the bundles and perturbs a selected control device. The comparison of the core reactivity for these two simulations will provide the reactivity worth of the perturbed control device. These computations are different than the reactivity changes determined from control device insertions in the 3D super-cell calculations which model an infinite lattice. The leakage of the core and the actual spacing and number of control devices is modeled faithfully in the 3D diffusion calculation and thus produces a more accurate device reactivity worth. Running several sets of perturbation simulations for each control device provides the operational capabilities of the devices in terms of their reactivity worth. These simulations can help determine the operational strategies and any restrictions that may be required due to specific controller properties. For instance, the worth of the adjusters or absorbers will dictate the number of rods inserted or removed to deal with a specific reactivity injection or power change. The worth of the liquid zones dictates the reactivity insertions from fuelling that can be managed by the system.

An additional capability of the full core simulation is the computation of important reactivity coefficients such as temperature coefficients for fuel, coolant and moderator and purity coefficients for moderator and coolant. By providing multiple input tables from the lattice cell calculations that are performed with different fuel, coolant and moderator properties. Multiple simulations with a wide range of temperatures, purities and densities allow the computation of reactor coefficients. These tables are referred to as micro-depletion tables in the case of RFSP. These reactivity coefficients can be computed using 2-D lattice cell models over the burnup cycle for the fuel but they are not directly applicable to full core predictions. The use of an equilibrium full core model to compute the temperature and purity coefficients is considered to yield results which most closely match the actual behaviour of the reactor core [58]. Additionally, the coolant void reactivity can be computed for the full core by comparing a voided (coolant density is reduced by a factor of $\rho_{liquid}/\rho_{vapour} \approx 1000$) and non-voided simulation. Specific channels or portions of the core can be selectively voided to simulate a desired scenario. Void reactivity is an important factor in loss of coolant accidents as are the fuel and moderator temperature coefficients. These properties of the full core design are useful in determining the response of the system to operational and accident scenarios and can be used to dictate operating procedures in different situations.

3.5.6   Operational simulation of the reactor

The simulation of reactor operations is primarily designed to perform a core follow, meaning a reactor physics simulation of the daily fuelling operations of a CANDU over a period of a single day, several days or months. This involves simulating the fuelling of channels in accordance with standard operating procedures and the parameters determined in the time-average model. This allows the testing of the effects of fuelling through a study of the instantaneous responses of the liquid zone controllers and the channel and bundle powers. The full core simulations include the response of the liquid zones as per standard control logic for bulk and spatial control. The CANDU reactor regulating system (RRS) will manipulate the fill levels in the liquid zone controllers and the positions of the adjuster and absorber rods in order to maintain reactor power or change it to a specified level (bulk control) or to maintain a specific target power distribution in the core in terms of zone powers or fluxes (spatial control). RFSP does not solve the time-dependent diffusion equation using the SIMULATE module but it can mimic the RRS actions in a quasistatic manner [53]. Bulk

control at a constant power is mimicked by manipulating the zone fills equally to maintain criticality. Spatial control is mimicked by altering the individual zone fills independently to best reproduce a target flux distribution. The automated bulk and spatial controls only apply to the liquid zone controllers and an external algorithm in conjunction with the capability to alter the rod positions in the input file are necessary to model the proper movement of the adjuster or absorber rods.

The bulk and spatial control options are invoked in the SIMULATE module diffusion calculation which involves both the eigenvalue computation and the resolution of the self-consistency problem between the flux shape and the zone fill levels [53]. The bulk control function seeks to maintain a specified reactivity in the core by changing all the zone fills uniformly as per equation 40 [53].

$$\Delta Z_i = \alpha_i \big[k_{eff}(current) - k_{eff}(target) \big] \quad for\ i = 1, \dots, N_z \qquad (40)$$

The maneuvering constant for the individual zone, α_i, is usually identical for all the zone compartments ($N_z = 14$) and is equal to 1.0 / total worth of LZCRs (for NU the LZCR worth is about 7 mk so $\alpha_i = 1/0.007 \approx 140$) [53]. The spatial control algorithm is more complicated as it changes the individual zone fills separately to achieve a desired target zone flux distribution. The modifications to the individual zone fills are dictated by equation 41 [53].

$$\Delta Z_i = \alpha_i \left\{ \beta_i \left[\frac{\phi_i}{\phi_{i,ref}} - \langle \frac{\phi}{\phi\ ref} \rangle \right] - \frac{K_h}{K_t}(1 - \beta_i)[Z_i - \langle Z \rangle] - \frac{K_l}{K_t}[Z_i - \langle Z \rangle] \right\}$$
$$for\ i = 1, \dots, N_z \qquad (41)$$

The maneuvering constant for the individual zone, α_i, is usually identical for all the zones and the same as the bulk constant. The β_i value regulates the fade out of the zone controllers as they reach the upper and lower fill limits. The K values are constants in the valve lift/percent-flux-tilt-error. The chevron bracketed values, $\langle Z \rangle\ and\ \langle \frac{\phi}{\phi\ ref} \rangle$ are averages of the current zone fills and the flux ratio across the core, respectively. These simulations can mimic actual operations including fuelling, power manoeuvres, some abnormal conditions or accident scenarios. These core follow simulations are generally started from an initial point dictated by a snapshot core as described in the Section 3.5.4.

For a simulation with short time intervals, the response of the liquid zones to fuelling events can be measured to ensure that the fuelling shifts are within the operational capabilities of the control system. Additionally, by observing the bundle and channel powers around a fuelling site before and after the fuelling, the effects of fuelling on the bundle powers or the fuel ramp rate can be assessed. This information is used to determine the probability of fuel defects that can be encountered if the bundle powers get too high or the fuel experiences excessive power ramps. These effects are assessed within 6 to 12 hours of a fuelling event so the full simulation length is usually about 1 to 2 days. The study of longer operational periods can be performed with a chain of sequential simulations that follow core operations with user defined fuellings and schedules, which can be based on operational and fuelling histories from actual station records.

3.6 Safety analysis for CANDU systems

The full core model provides a detailed and realistic system that can be manipulated and tested upon to replicate conditions and determine the reactor response. This is a vital tool for evaluating a reactor or fuel design and ensuring that an acceptable operating envelope is achieved. Safety analysis of the reactor system using computer models is beneficial in both the design and operational stages of the reactor system.

The objectives of CANDU safety analysis at the design stage are to establish the safe operating envelope for plant operation, verify the adequacy of the design to mitigate the consequences of accidents and to ensure the key safety objectives of a nuclear reactor system are maintained. The safety objectives are based on the three principles of nuclear safety: control, cool and contain.

The control aspects involve ensuring that the reactor can remain within proper limits and be capable of being managed with the associated control systems at all times Also it must be ensured that the reactor has an acceptable shutdown capability at all times during operation. The cool principle requires that the system maintains effective cooling of the fuel and adequate transport and rejection of heat from the reactor at all times. This includes maintaining adequate water inventory in the steam generator system to provide sufficient time to establish an alternative heat sink. The heat transport system integrity should be unimpaired during normal operations and abnormal situations should be accounted for with auxiliary systems. This is explored through thermalhydraulics

modelling. The final principle dictates effective containment of radioactive material released from reactor and associated systems through a defence in depth containment strategy. This ensures multiple barriers to the release of radiation to the public including the fuel matrix, sheath, heat transport system, containment structure and the local exclusion zone around the reactor facility. The fuel matrix and sheath barrier must be carefully designed and monitored to avoid fuel defects and failure during both normal operations (fuelling and power changes) and abnormal or shutdown events with rapid power excursions. The heat transport system and especially the fuel channels must be compatible with the fuel envelope such that fuel overheating is avoided and does not impede channel integrity. The prevention of fuel centerline melting and excessive heat transport system pressures is critical to maintaining these barriers to the release of radiation.

This dissertation describes the design of an advanced fuel design that is adapted into an existing proven reactor system and thus is focused on maintaining the standard operating procedures and keeping modifications to reactor systems at a minimum. The safety analysis portions of this work are primarily concerned with ensuring that the fuel design has a similar or more favorable response than standard fuel in the important operational and simulated accident conditions that are encountered in a CANDU reactor system.

Full safety analysis requires several different analysis codes and coupled assessments to cover all aspects of the system from physics to thermalhydraulics to material integrity. The fuel design explored is to operate within the same heat generation and power envelopes of standard fuel. Therefore, the bulk of the operational differences will be related to the neutronics of the fuel and reactor system. Changes in neutronics behavior can impact thermalhydraulics and other areas of the analysis but if thermal outputs are maintained similar to those of standard fuel as much as possible the differences in these sections of the analysis should be minimized.

The safety analysis methodology utilized in CANDU does include some practical constraints on the situations to promote conservatism. These include accounting for malfunctions in the shutdown and safety systems such as ensuring shutdown even with the two most effective shutdown rods inoperable. Both single and dual failures in the reactor system are important. The handling and management of the fuel outside of the core is also of concern such as ensuring that the decay heat, criticality and radiological activity can be managed by the spent fuel bay system.

Chapter 4

Fuel design and description

The fuel design used in this analysis is a balance of the many operational constrains and has the objective of maximizing the transmutation of the actinides in the system. The desire is to maintain the standard reactor design, operating envelope and procedures to the greatest extent practicable while still enabling the reuse of fuel and an appreciable level of actinide transmutation. There are to be no physical changes to the reactor design except the new fuel. The lattice physics parameters of the fuel design are assessed and compared to standard fuel in order to help refine the design such that it can meet the above objectives. The fuel design process first requires investigation into the effects of the actinides on the physics properties of the fuel followed by design considerations such as the bundle geometry, burnable neutron absorber use and actinide concentration.

The following chapter utilizes two neutron transport codes, WIMS-AECL v3.1.2.1 for 2D lattice cell modelling and DRAGON v3.06f for 3D super-cell modelling. WIMS-AECL uses an 89 energy group structure and a tracking mesh of 11 angles and 53 lines/cm^2. The 3D DRAGON super-cell model (described in Chapter 3.3) uses 69 energy groups and a tracking mesh of 12 angles and 20 lines/cm^2 for both 3D and the 2D self-shielding calculation. Both of the codes use the ENDF-BVII nuclear data library. The WIMS-AECL meshing accuracy was tested from 50-5000 lines and 11-31 angles and the k-infinity value stays within 0.8 mk. The 3D dragon meshing accuracy was tested for similar limits and the k-infinity remained within 0.65 mk. Model qualification is discussed in chapter 4.3.

4.1   Actinide effects on physics properties

The use of actinide MOX fuel will alter the physics properties as compared to the standard natural uranium fuel utilized in CANDU. The objective of the fuel design stage of this work is to minimize and detail these changes. The neutronics behaviour in the lattice cell is defined primarily by the fuel design including the

fuel composition, bundle design, lattice geometry and presence of absorbers within the bundle. The inclusion of actinides in the fuel will affect the cross sections, neutron energy spectrum, delayed neutron fraction, lifetime depletion characteristics and the power distribution within the bundle. Additionally, there will be changes to the neutronic behaviour of the fuel when interacting with control devices or experiencing coolant voiding.

It should be noted here that the comparisons made in the following section use a few commonly available specific bundle geometries, which may not represent the most efficient utilization of resources as compared to a complete optimization where the bundle and lattice geometry may be altered. Such an optimization is beyond the scope of this study as it would involve significant changes to the CANDU-900 design. The three bundle geometries used for the comparisons are: I) the standard 37 element bundle (described in Chapter 3.2), II) a 43 element slightly enriched uranium (SEU) void effect (VE) bundle and III) a 43 element TRUMOX bundle. The lattice spacing, pressure and calandria tube design and moderator characteristics are identical for all the designs considered. Both the 43 element designs arrange their elements in concentric rings of 7, 14 and 21 elements around a central pin. In the SEU-VE bundle the center element and first ring elements are of a larger diameter than the elements in the outer rings. The center element also contains a burnable neutron absorber (BNA) that is 15% dysprosium blended with natural uranium. The TRUMOX bundle has a similar concentric arrangement but only the center element is thick and the remaining 42 elements are of a smaller diameter. The thick central pin in the TRUMOX bundle contains a strong dysprosium-zirconium-oxide (67% Dy_3O_2) BNA to offset the high initial enrichment. The three bundle geometries are shown in Figure 4.1 in a standard CANDU lattice cell.
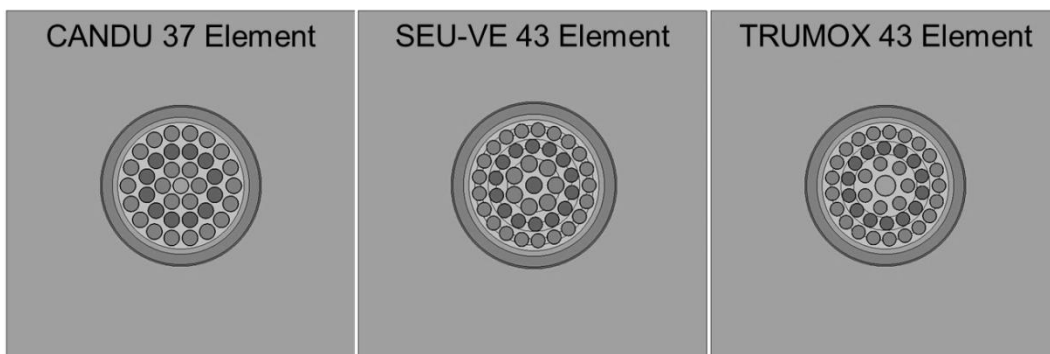
Figure 4.1: Various bundle designs in a CANDU type lattice cell.

The CANDU 37 element bundle is used for basic fuel composition comparisons while the SEU-VE 43 element bundle is a low coolant void reactivity design that is used to compare the effects of burnable neutron absorbers. The TRUMOX 43 element bundle with its larger number of elements and thick centre pin of BNA material is designed to utilize enriched actinide MOX fuel (e.g. TRUMOX). The larger enrichments of the TRUMOX fuels allow for longer burnup intervals which increases actinide transmutation and reduces the amount of fuelling required thus improving the economics of the TRUMOX implementation[5].

4.1.1 Fuel and cell cross sections

The inclusion of actinides alters the initial fuel composition and depletion isotopes considerably and these differences will alter the cross sections of the fuel and those of the homogenized lattice cell used in subsequent full core calculations. The changes in the cross section will affect the neutron flux, energy spectrum and distribution. The major difference between actinide blended fuel and standard natural uranium is the presence of plutonium and the minor actinides (Am, Cm and Np) in fresh fuel and the subsequent differences throughout the burnup cycle. Natural uranium will begin as U-238 and U-235 and as it burns will build up plutonium isotopes from neutron capture in U-238 and will also build up small amounts of minor actinides. The actinide presence will cause differences in the absorption cross sections of the fuel and will affect the fission cross section due to the increased amounts of the fissile element Pu-239.

A simple change that will affect the cross sections of the fuel would be an increase in the level of enrichment (the ratio of U-235 to U-238) or the presence of plutonium isotopes in the fuel. The fission cross section of the fuel increases with a larger U-235 concentration. For example, increasing the enrichment of natural uranium fuel from 0.71% to 1.00% U-235 (a 43% increase) will cause the thermal $\nu\Sigma_f$ cross section and the thermal absorption cross section to increase by 27% and 13% respectively. The increase in U-235 enrichment displaces some U-238 from the fuel and reduces the neutron capture and transmutation of U-238 to Pu-239 over the burnup period. An increase in enrichment also brings the fuel closer to that used in LWR systems (3-5 wt% enrichment) resulting in more fissions coming from uranium and less plutonium buildup. Natural uranium

---

[5] The economics of the fuel improve due to the higher burnup for a given bundle (~3 times standard NU) as well as the reduction in volumetric spent material per MWe produced due to the fuel reuse.

CANDU reactors have increased plutonium production throughout the burnup cycle compared to LWR systems with higher fuel enrichments. About 80-90 atoms of plutonium are produced per 100 U-235 fissions compared to 60-65 in LWRs [59]. This increased plutonium production is important as about 50% of the power over the burnup cycle in CANDU is produced from plutonium fission.

The TRUMOX fuel blends an actinide mixture with natural uranium in specific proportions to achieve a desired burnup level and fissile content. The proportions of the actinide isotopes that are extracted from cooled spent LWR fuel dictate the composition of the actinide mixture (in this case, the actinides are consistent with prototypical PWR fuel irradiated to 45 MWD/kgHE and cooled for 30 years). The actinides are then blended with natural uranium to produce a specific fuel design. For example the TRUMOX-45 fuel (designed for 45 MWD/kgHE of burnup) is a blend of 4.75% actinide oxide and 95.25% natural uranium oxide. The lower burnup TRUMOX-30 fuel (30 MWD/kgHE) has 3.1% actinide oxide. The composition of the TRUMOX type fuels is displayed in Table 4.1.

Table 4.1: Actinide and Natural Uranium Composition for TRUMOX fuels [26].

Actinides			Uranium Mix		
Isotope	**Type**	**Wt %**	**Isotope**	**Type**	**Wt %**
Np-237	Actinide	4.698	U-234	U Mix	0.0054
Pu-238	Actinide	1.301	U-235	U Mix	0.7110
Pu-239	Actinide	56.243	U-238	U Mix	99.2836
Pu-240	Actinide	20.099			
Pu-241	Actinide	3.040	**Actinide Oxide (AOX)**		
Pu-242	Actinide	3.800	Actinides	88.207	wt %
Am-241	Actinide	9.907	Oxygen	11.793	wt %
Am-243	Actinide	0.763			
Cm-243	Actinide	0.001	**Uranium Oxide (UO2)**		
Cm-244	Actinide	0.072	Uranium	88.150	wt %
Cm-245	Actinide	0.012	Oxygen	11.850	wt %
Cm-246	Actinide	0.001			

The actinide mixture in the TRUMOX fuel displaces some natural uranium reducing the impact of the transmutation of U-238. A comparison of NU fuel to an actinide mixed oxide fuel, TRUMOX-30, over their respective burnup cycles

displays a marked difference in the dominant fissile content and the plutonium content of the fuel over the burnup cycle. The composition changes over the burnup cycle, especially of the fissile elements (U-235, Pu-239 and Pu-241) will affect the neutronics and cross sections of the fuels. The fissile composition over the burnup cycle is computed using WIMS-AECL and presented in Figure 4.2 for both fuels. The NU fuel is modelled in the standard 37 element CANDU bundle while the TRUMOX-30 fuel is modelled in the 43 element TRUMOX bundle with the integrated burnable neutron absorber as described earlier in Chapter 4.1.
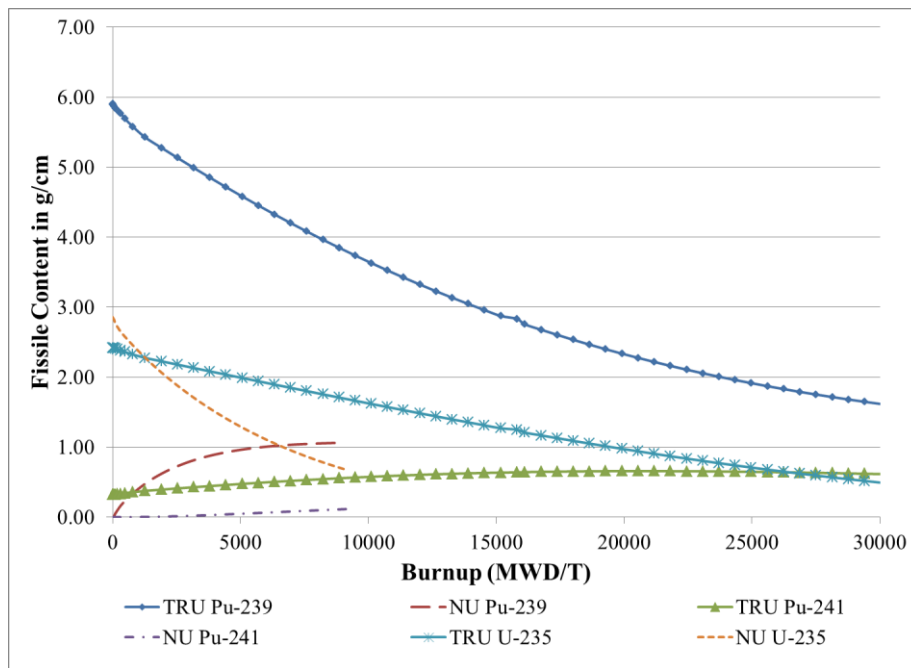
Figure 4.2: Concentrations of fissile isotopes over the burnup cycle.

The major composition changes in the NU fuel are the burnup of U-235 through fission and the transmutation of U-238 to Pu-239 though neutron capture. The Pu-239 adds fissile content to the depleting amount of U-235 and also undergoes further neutron capture that produces transuranic species. As seen in Figure 4.2, the fissile content in NU is dominated by U-235 for the first portion of the burnup up until ~6, 800 MWD/T (about 75% of CANDU-900 NU burnup) where it is exceeded by the Pu-239 content which is dominant for the remainder of the burnup. For NU, the initial fissile content is 100% U-235 which is burned up throughout the cycle down to 35% at the end of the cycle. The Pu-239 and Pu-241 content climb from zero to 58% and 7% of the fissile content.

For TRUMOX-30 the transmutation of U-238 is overshadowed by dominant Pu-239 content throughout the burnup. The U-235 burns in a more linear fashion beginning at 28% of the fissile content and declining to 18% over the burnup. The Pu-239 starts at 68% of the fissile content and is depleted continually through fission and transmutation through neutron capture to higher transuranic isotopes down to 59% of the fissile content at the end of burnup. Neutron capture in Pu-239 contributes to the larger build-up of Pu-241 which builds linearly from 3.7% to 22.6% of the fissile content during the cycle. The total plutonium content at the end of the burnup cycle is 3.5 times higher in the TRUMOX-30 fuel than in NU (5.9 g/cm vs 1.68g/cm). This results in higher spent fuel heat load and radiotoxicity relative to NU, as discussed in Chapter 2.2.
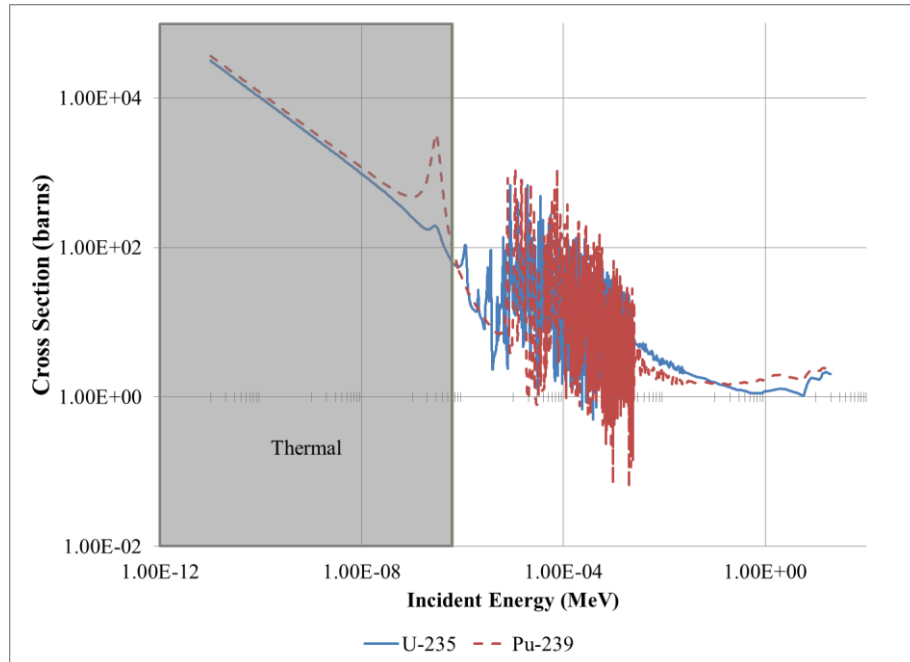
Figure 4.3: Neutron fission cross sections for U-235 and Pu-239 [13].

The presence of plutonium will affect the composite cross section of the fuel as seen in the differences in the fission cross sections of U-235 and Pu-239 (Figure 4.3) Plutonium has a much higher thermal absorption peak (between 0.1 and 1 eV) and different resonance characteristics than U-235. The dominance of plutonium has major impact on the fission and n-gamma reactions in the fuel, altering the proportions of thermal and fast flux in the system.

The actinide mixed oxides such as TRUMOX are also designed for longer burnup cycles and have higher fissile content resulting in a more active fuel that is less affected by parasitic absorption within the lattice cell. The actinide content in fuels such as TRUMOX is primarily Pu-239 (1.54 wt% of fuel, for TRUMOX-30) but also includes several non-fissile minor actinides with significantly different capture cross sections than U-238 which makes up the bulk of any fuel. These non-fissile minor actinides such as Np-237, Pu-242, Pu-240 and Am-241 (~1.1 wt% of the fuel in total) will alter the capture cross section of the fuel. This increases the total parasitic absorption and reduces the U-238 capture (thus reducing the Pu-239 production) relative to natural uranium fuel necessitating some of the higher fissile content. The capture cross sections of these non-fissile minor actinides are provided in Figure 4.4 (thermal energies are ≤ 0.625 eV).
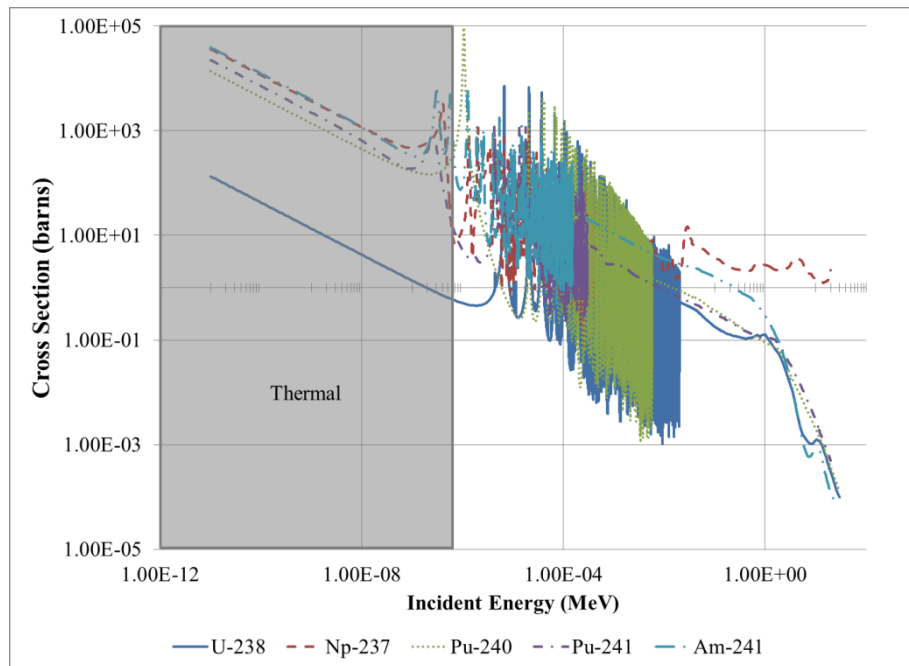
Figure 4.4: Neutron capture cross sections for U-238, Np-237, Pu-240, Pu-242 and Am-241 [13].

The presence of the non-fissile minor actinides increases neutron capture for energies of less than 10 eV and introduces resonance peaks into the thermal region resulting in a different capture cross section for TRUMOX fuel than NU. The largest effects are from Pu-240 and Am-241 which are the largest components of the actinide mix (for capture) and have high capture cross sections

and thermal peaks. The increase in capture cross section is 2-3 orders of magnitude over that of U-238 meaning that even though U-238 still makes up the bulk of the fuel the overall capture cross section will be dominated by the presence of the actinide elements. For example, the aggregated capture cross section for U-238, Pu-240 and Am-241 (given the TRUMOX-30 composition) at ~0.625 eV is 5.549 barns compared to 0.597 barns for U-238 at this energy (9.3 times higher). This demonstrates the significance of the presence of these non-fissile minor actinides and their effect on the thermal absorption for fresh fuel.

4.1.2 Neutron spectrum

Due to the changes in isotopic composition and the presence of the higher actinides in the TRUMOX fuel there may be significant changes in the neutron spectrum within the lattice cell when compared to standard natural uranium. The presence of plutonium and minor actinides alters the neutron spectrum through the increased thermal absorption, larger portion of Pu-239 fission (resulting in higher average neutron energy and higher neutron yield per fission, see Chapter 4.1.2.1) and increased fissile content in the fuel. These composition differences result in a different ratio of thermal to fast neutron flux for TRUMOX than NU.

The neutron spectrum refers to the energy distribution of the neutrons within the lattice cell and is strongly affected by the fuel composition. The specific fissile composition will dictate the energy of neutrons born in fission, the number of neutrons yielded per fission and their resonance absorption. Spectrum hardening occurs when the distribution of neutron energies is shifted higher causing the proportion of fast neutrons to increase while the thermal portion decreases. The division between thermal energies and fast energies is generally 0.625 eV and the proportion of thermal to total flux is an important neutronics characteristic of a fuel or lattice cell. Changes in the energy spectrum can affect fission rates, resonance absorption and the effectiveness of control devices. Additionally, the changes in energy spectrum may also affect some modeling assumptions and uncertainties since many simulation codes and approximations were not specifically designed to handle variances in the neutron spectra (in particular for the low lying resonances of plutonium).

The neutron spectrum changes during fuel burnup as the composition changes. Natural uranium, due to the burnup of U-235 through fission and the production

of Pu-239 through neutron capture, will experience a change in the spectrum over its burnup cycle. The beginning of cycle (BOC) and end of cycle (EOC) cell spectrum for NU 37 element fuel using WIMS-AECL is provided in Figure 4.5.
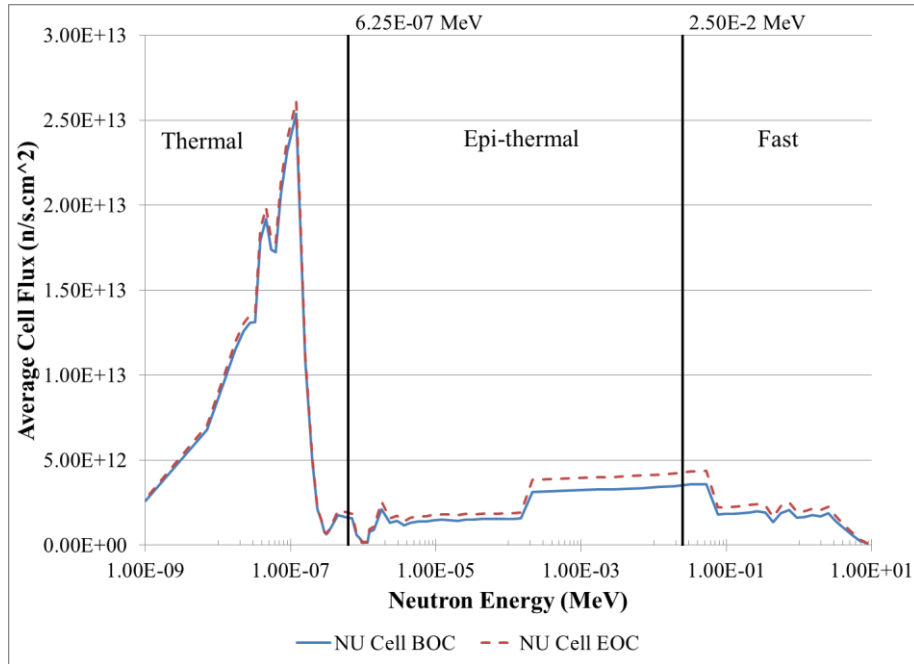
Figure 4.5: Neutron Spectrum for 37 element NU Lattice Cell

The thermal flux in NU lattice cell is higher at the end of the cycle below approximately 0.15 eV but the total flux is also higher due to lower U-238 absorption. Overall, the ratio of thermal to total flux drops by about 3% (from 67.1% to 64.1%). The differences in the flux come from the increased plutonium in the fuel and the presence of minor actinides transmuted from U-238 through successive capture. This is similar to the differences between NU and TRUMOX which has more plutonium and minor actinides.

The spectrum hardening effect in TRUMOX results in a lower portion of thermal neutrons compared to the total flux due to differences in: I) the fission energy, II) the number of neutrons per fission, and III) changes in the absorption, primarily in the thermal region. Points I) and II) are due to the presence of Pu-239 and Pu-241 which have higher average fission neutron energies and larger numbers of neutrons produced per fission. Point III) is due to the increase absorption resulting from the presence of the non-fissile minor actinides. Given these

differences, there are fewer thermal neutrons that interact in fission events than for a comparable NU system and a lower overall flux. However, the lack of thermal neutrons is compensated for by the increased enrichment in the fuel resulting in more potential targets for neutrons to induce fission (also there is increased fission in the range of the low lying Pu-239 fission cross section peak). The resultant system, as seen with TRUMOX, is able to remain critical and balance the lower proportion of thermal neutrons and increased absorption with higher fissile content. In general, the result will be a lower total neutron flux which has a higher proportion of neutrons in the epithermal and fast region.

It is useful to investigate the effects from both these attributes (plutonium content, transuranic actinide presence) and to determine their overall influence on the neutron spectrum. This is performed with various fresh fuel lattice simulations using the WIMS-AECL code. The goal is to identify the comparative magnitude of the two effects on the spectrum specifically on the thermal to total flux ratio.

4.1.2.1 Effect of plutonium

The fissile material in the fuel will dictate the energy of the neutrons being produced. Plutonium isotopes have average neutron kinetic energies from fission that are 23-25% higher than uranium (Pu-239 = 5.90MeV, Pu-241 = 5.99MeV, and U-235 = 4.79MeV) [60]. These higher energies result in a lower ratio of thermal neutrons in the system and harden the spectrum shifting flux toward fast energies reducing the portion of thermal flux and increasing the probabilities of resonance capture for epithermal neutrons. Additionally, the thermal absorption peaks that are prevalent in plutonium isotopes (see Figure 4.3) will result in more interaction with plutonium in the 0.1 to 1eV range.

To examine the direct effect of the presence of plutonium in fuel, a comparison was made between the two types of fissile material. Fresh fuel configurations of U-235 and a plutonium composition (Pu-239 = 94.8721% and Pu-241 = 5.1279%) diluted in an inert ZrO_2 matrix within a standard CANDU 37 element bundle and lattice cell were compared for different amounts of fissile content.

The fresh fuel total flux and thermal flux for a given fissile content is provided in Figure 4.6 for both cases. The U-235 case has consistently higher thermal flux of about 40% more over the range of fissile content. The total flux is higher for the U-235 case but narrows with increasing fissile content (from 22% down to about 8% more for U-235). The thermal flux ratio is shown for both cases in Figure 4.7.
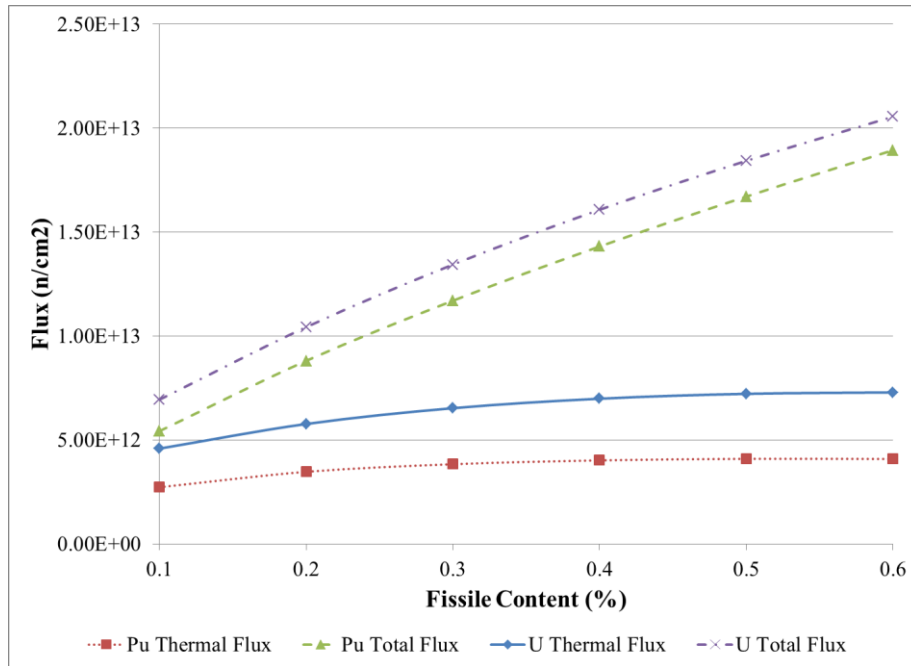
Figure 4.6: Thermal & Total Flux Vs. Fresh Fuel fissile content (U-235 and Pu-Mix in ZrO2).
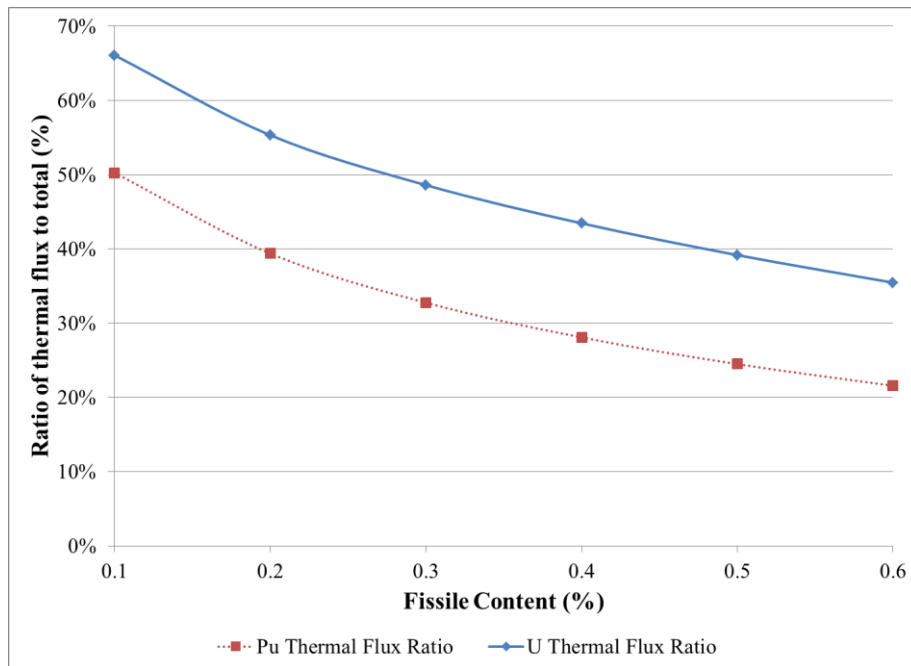
Figure 4.7: Thermal Flux Ratio Vs. Fresh Fuel fissile content (U-235 and Pu-mix in ZrO2)

The U-235 case has a higher thermal flux ratio than the plutonium case for a given fissile content, starting out at 16% higher and narrowing to about 14% at the higher fissile content. These results are as expected from looking at the average neutron kinetic energies and from the resulting spectrum which is harder for plutonium driven systems. When considering only the flux, and since the total flux is lower, it would seem that the multiplication factor for the plutonium case would be lower than for a U-235 case with an equivalent fissile content. However, the k-infinity for the plutonium case is higher (see Figure 4.8). This is due to the higher fission neutron yield for plutonium that must also be considered.
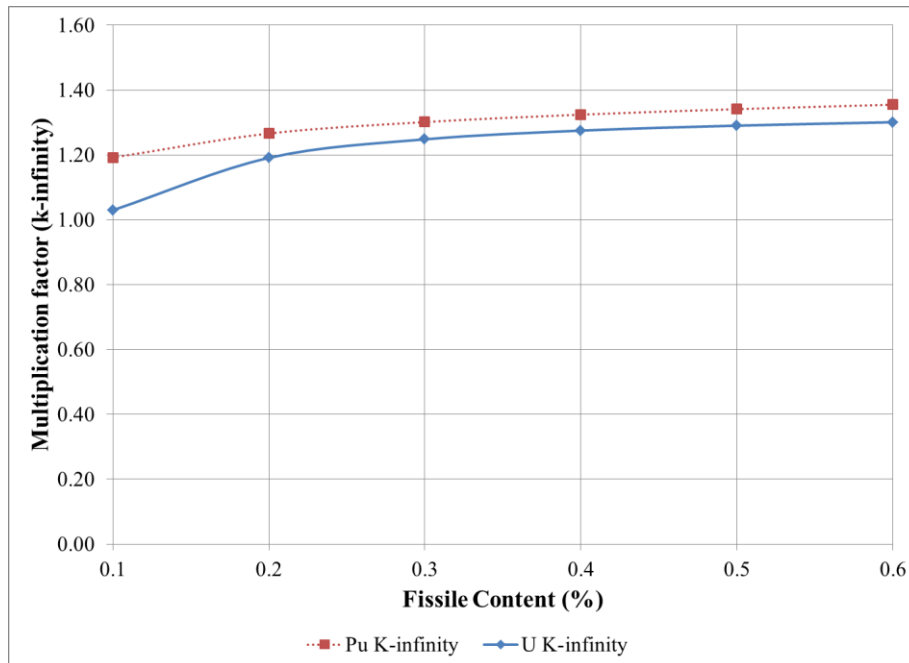
Figure 4.8: Fresh Fuel k-infinity Vs. fissile content (U-235 and Pu-mix in ZrO2)

The k-infinity for the two cases is interesting as the U-235 values are consistently below that of the plutonium mix. Initially, the gap is 130 mk and narrows to a more consistent 30 mk for fissile content > 0.2%. This gap is explained by the differences in the average number of neutrons produced for each fission event.

The average total fission yield, number of neutrons produced per fission (ν), for plutonium isotopes is higher than for uranium ($\nu_{Pu-239} = 2.8799$ and $\nu_{Pu-241} = 2.9340$ while $\nu_{U-235} = 2.4229$) [12] resulting in a larger number of neutrons produced by an equivalent number of fissions in the plutonium case. This effect

is seen in a comparison of the fissile content at a specific multiplication constant value. For example, the U-235 case needs a fissile content of 0.21% to reach a level of criticality of k-infinity = 1.2, while the plutonium mix only needs a fissile content of 0.11%. The higher neutron yield per fission is the reason for the offset in these results. The plutonium mix explored here (94.8721% Pu-239, 5.1279% Pu-241) has a $\nu_{Pu-Mix} = 2.8827$ which is about 19% higher than the U-235 value.

The comparison can also be made of the thermal flux ratio for each of two fuels at specific multiplication factors as displayed in Figure 4.9. The uranium cases have a higher thermal flux ratio for a given multiplication factor by several percent. In the case of a k-infinity = 1.2 the thermal flux ratio is 49% for the plutonium case and 54.5% for the uranium case, a difference of 5.5%. Therefore, the fissile material in the fuel does affect the neutron energy spectrum. The inclusion of plutonium will harden the spectrum, decreasing the ratio of thermal to total flux as the higher neutron energies shift the flux towards fast energies.
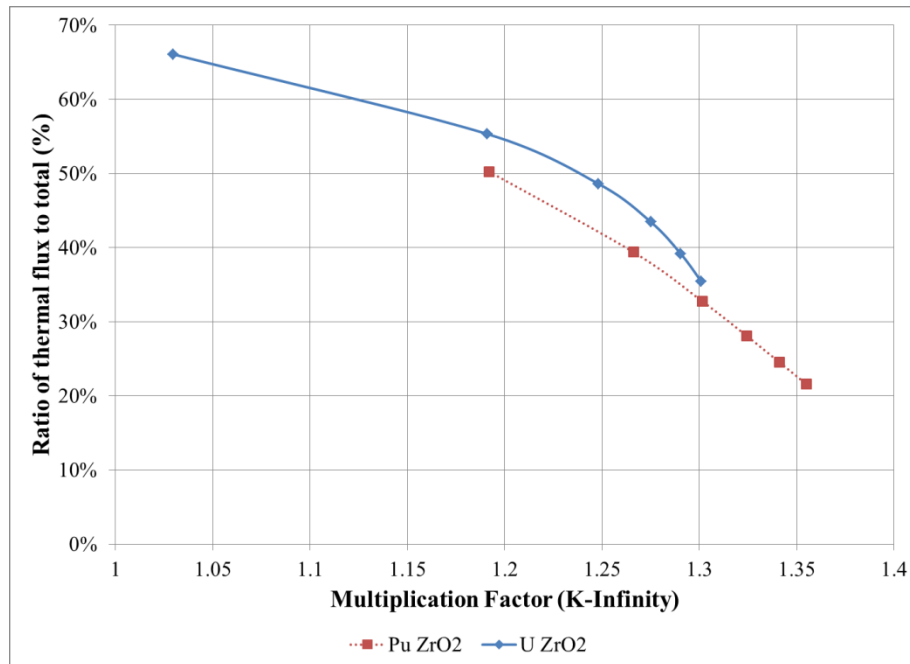
Figure 4.9: Fresh Fuel Thermal flux ratio Vs. k-infinity (U-235 and Pu-mix in ZrO2)

4.1.2.2 Effect of non-fissile minor actinides in the fuel

The second effect that changes the neutron spectrum in TRUMOX type fuels compared to NU is the higher presence of the non-fissile minor actinides including neptunium, americium, curium and some non-fissile plutonium isotopes. These have large thermal absorption cross sections (primarily within the 0.1-1.0 eV range) resulting in increased thermal absorption and a generally higher average neutron energy. This parasitic absorption of thermal neutrons further reduces the ratio of thermal to total flux in the fuel and lattice cell.

As seen earlier in Figure 4.4, the Np-237, Pu-242, Pu-240 and Am-241 isotopes have large thermal capture cross sections and some thermal resonance peaks. In TRUMOX this parasitic thermal capture is driven by Pu-240 and Am-241 which are the larger portions of the actinide mix. To directly measure the effects of the actinides on the neutron energies in the system, fresh fuel trials with a TRUMOX type actinide material mixed with inert ZrO2 are compared to the plutonium mixture trials from earlier. The actinide mix case has more absorption since there is non-fissile material that parasitically absorbs neutrons. As a result the fissile content must be higher in order to achieve a similar level of criticality in the system. The actinide mixture and the plutonium mixture that are diluted with the inert ZrO2 in this trial are detailed in Table 4.2

Table 4.2: Actinide and Plutonium mixture information for test case

Actinide Mix			Pu Mix		
Isotope	**Type**	**Wt %**	**Isotope**	**Type**	**Wt %**
Np-237	Actinide	4.698	Pu-239	Pu Mix	94.872
Pu-238	Actinide	1.301	Pu-241	Pu Mix	5.128
Pu-239	Actinide	56.243	Am-243	Actinide	0.763
Pu-240	Actinide	20.099	Cm-243	Actinide	0.001
Pu-241	Actinide	3.040	Cm-244	Actinide	0.072
Pu-242	Actinide	3.800	Cm-245	Actinide	0.012
Am-241	Actinide	9.907	Cm-246	Actinide	0.001

The multiplication factor for various fissile contents of the two cases is provided in Figure 4.10. The actinide case, due to the increased absorption requires much more fissile content to become critical. For example to achieve a multiplication

factor of 1.2 the fissile content in the actinide case would need to be 2.82% compared to only 0.11% for the plutonium case.
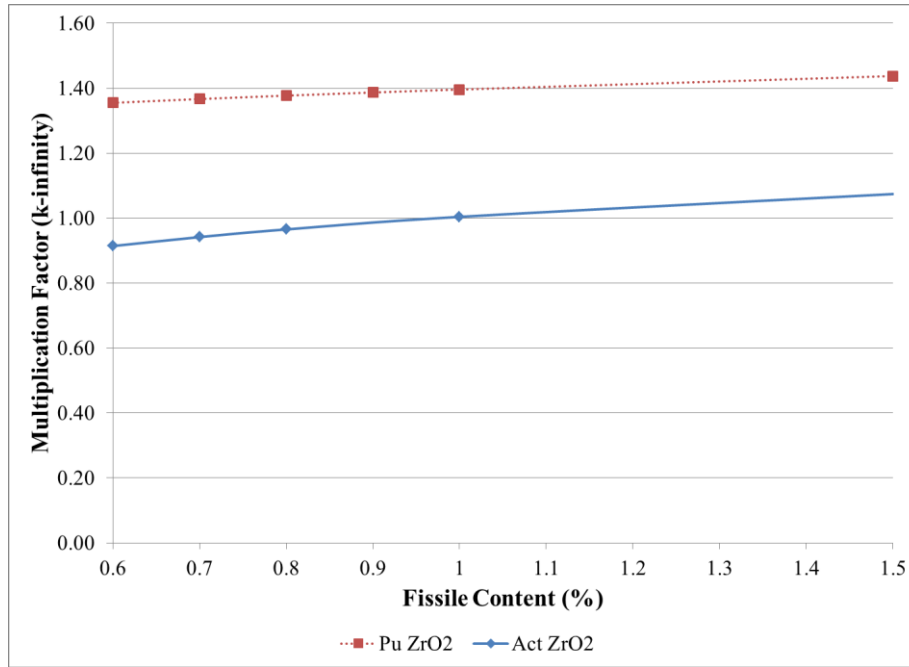
Figure 4.10: k-infinity for various Fresh Fuel fissile contents (Actinide and Pu-mix in ZrO2)

The presence of the actinides also alters the thermal and total flux in the cell. The amount of total and thermal flux is higher in the actinide case resulting from the availability of delayed neutron emission from some of the actinide material. The actinide mix case has higher absolute values for the thermal and total flux for a given fissile content and the ratio of thermal flux to total is higher. These relationships are seen in Figure 4.11 and 4.12.

However, if we compare the Pu-mix case and the actinide case with the same multiplication factor, the ratio of thermal to total flux is much lower for the actinide case, see Figure 4.13. For example, given a multiplication factor of 1.2 the plutonium case has a thermal flux ratio of 49% while the actinide case has a ratio of only 12.5%, a difference of 36.5%. The thermal absorption in the actinide case causes a harder spectrum over the plutonium case for each specific multiplication factor.
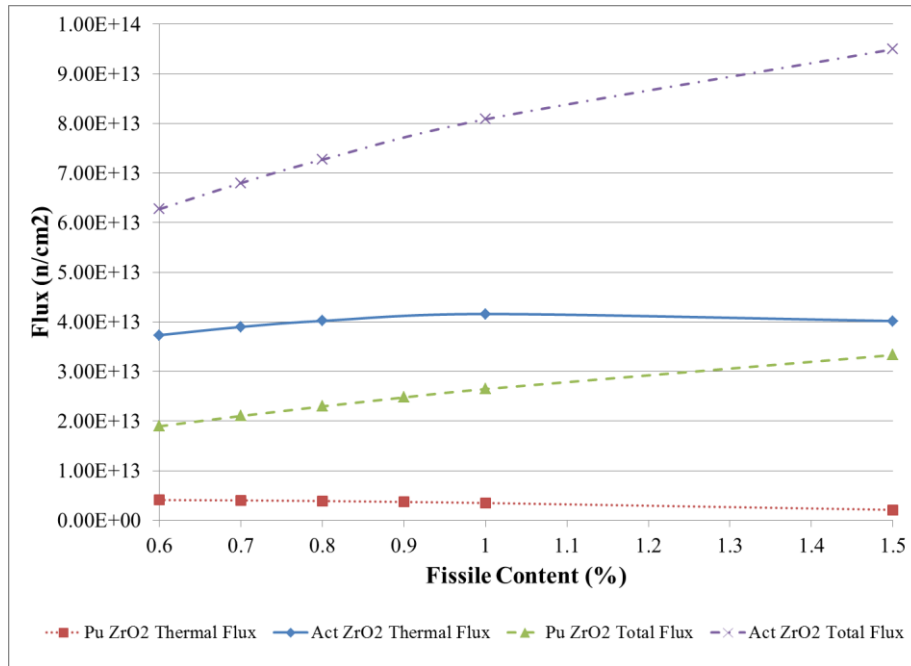
Figure 4.11: Thermal and Total Flux Vs. Fresh Fuel fissile content (Actinide and Pu-mix in ZrO2)
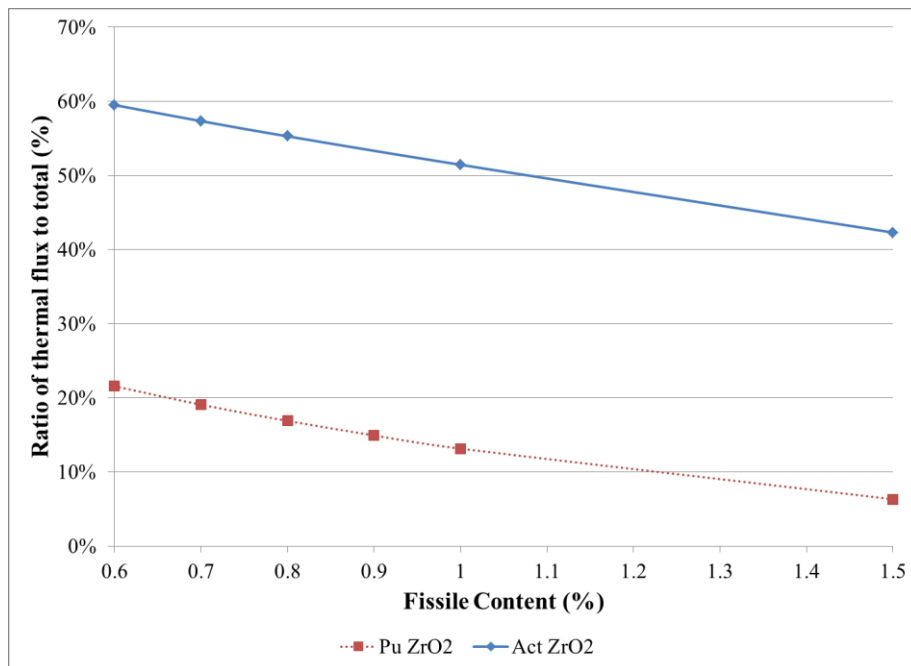
Figure 4.12: Thermal Flux ratio Vs. Fresh Fuel fissile content (Actinide and Pu-mix in ZrO2)

The data presented here illustrates the flux hardening resulting from the actinide materials is a result of the increased thermal absorption from the nuclides present in the actinide mixture, specifically Pu-240 and Am-241. The ratio of thermal flux is much lower in the actinide cases by 36.5% for a multiplication factor of k-infinity = 1.2. For the TRUMOX fuel, the neutron spectrum is hardened by this factor and from the presence of plutonium fissile material (Pu-239, Pu-241) making the spectrum harder than for a uranium based system. It should be noted that the non-fissile minor actinides will be consumed during the fuel burnup and thus their effects will be reduced over the burnup cycle. The effects of burnup are examined for the TRUMOX fuel in Chapter 4.1.2.3.
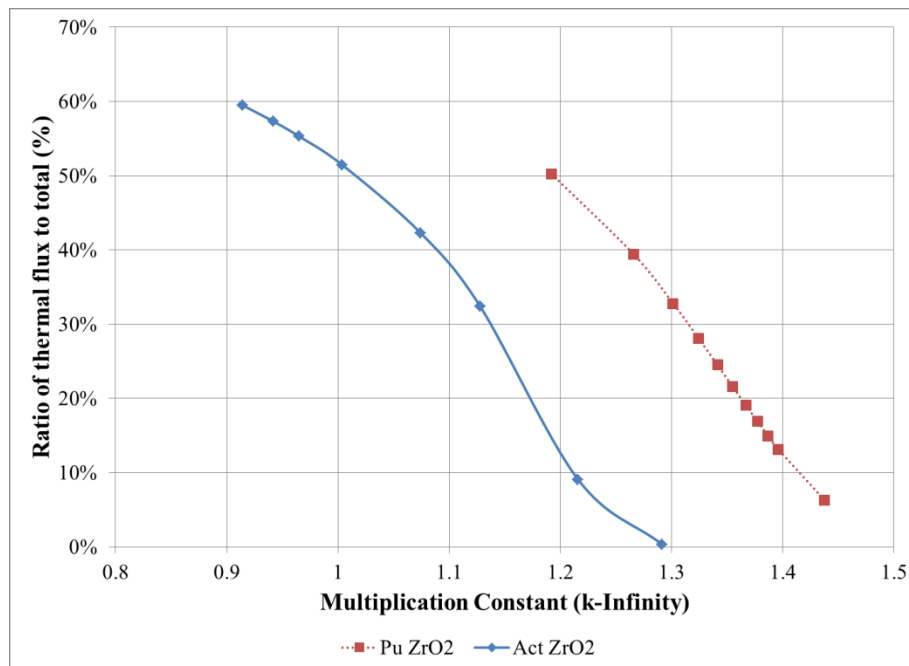
Figure 4.13: Fresh Fuel Thermal Flux ratio Vs. k-infinity (Actinide and Pu-mix in ZrO2)

4.1.2.3 Combined effects of plutonium and minor actinides

Of the two effects discussed that attribute to the harder neutron spectrum the increased thermal absorption from the actinide materials has a much larger effect than the hardening from the plutonium fissile material (nearly 7 times). To obtain the combined effect of both these attributes a comparison can be made between the actinide mixture and U-235 both diluted in ZrO_2. The comparison of the ratio of thermal flux is made for a given multiplication factor in Figure 4.14. The

example comparison made for the individual inspections of actinides and plutonium effects was at k-infinity = 1.2 and is applied to this combined effects test. The thermal flux ratio for k-infinity = 1.2 was 54.5% for U-235 and 12.5% for the actinide mixture, a difference of 42%. Therefore, the bulk of this difference in the thermal flux ratio, 36.5%, comes from the absorption caused by the actinide mixture with the remaining effect, 5.5%, coming from the higher energy plutonium fissile content.
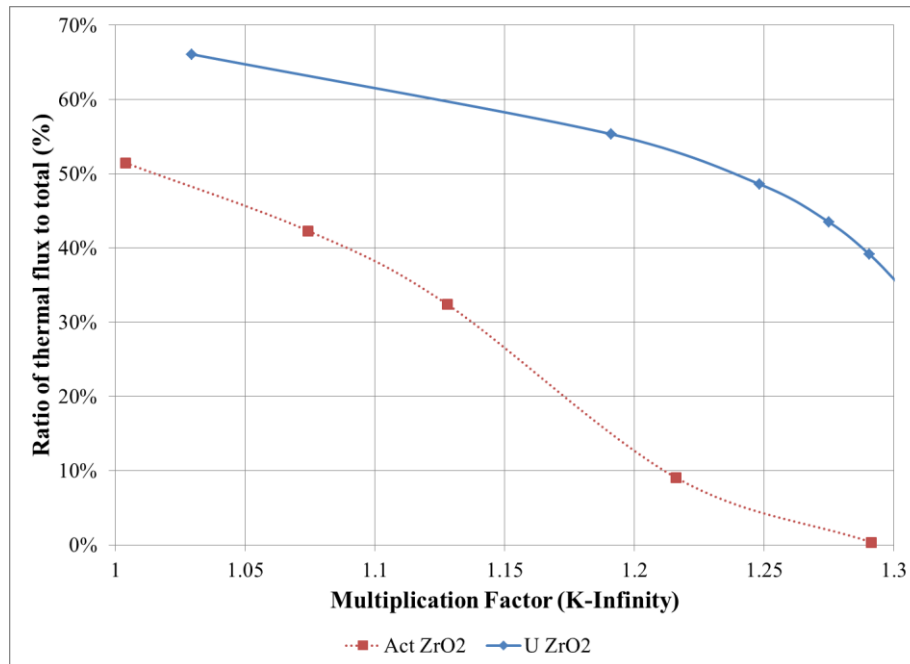
Figure 4.14: Fresh Fuel Thermal Flux Ratio Vs. k-infinity (Actinide and U-235 in ZrO2)

4.1.2.4 Direct comparison of TRUMOX and NU neutron spectrum

In order to evaluate this effect for the actual fuel design a comparison is made between the actinide mixture blended with natural uranium, TRUMOX, and standard natural uranium fuel as used in CANDU reactors. This comparison is made using the TRUMOX-30 fuel (3.1% actinides) in both a 37 element arrangement and the 43 element geometry with an integrated burnable absorber.

The proportions of fissile elements in the TRUMOX-30 fuel result in an average thermal fission neutron kinetic energy of 5.60MeV compared to 4.79MeV for NU fuel. Also the average number of neutrons produced per thermal fission, ν, in

TRUMOX-30 fuel is 2.7573 compared to 2.4229 for U-235 thermal fission. Since the plutonium fissions make up more than 72% of the fissions in TRUMOX-30 fuel more neutrons are generated for each fission event and these neutrons have higher energies than the uranium fission neutrons. Therefore, the average energy produced per fission ($E_{kinetic} * \nu$) is 33% higher for TRUMOX than NU for fresh fuel (15.44 MeV/fission Vs. 11.61 MeV/fission).

Table 4.3: Thermal and total flux comparison for NU and TRUMOX-30 fuel.

Bundle Type	Thermal Flux (n/cm^{2}s)	Total Flux (n/cm^{2}s)	Portion of Total
37 NU/NU	2.28E+14	3.41E+14	67.02%
37 NU/TRU-30	1.02E+14	2.15E+14	47.54%
43 TRU/TRU-30[*]	9.57E+13	1.96E+14	48.96%
* this bundle contains BNA in the central pin			

The higher neutron energy reduces the proportion of thermal flux, as seen in Table 4.3, with the TRUMOX-30 fuel having a 19.48% lower portion of thermal flux than NU when compared as fresh fuel in the 37 element bundle. Since the 43 element TRUMOX bundle contains an integrated burnable neutron absorber in the central pin, the portion of thermal flux is slightly higher resulting in an overall difference of 18.06% from standard NU 37 element fuel. The BNA presence increases the thermal flux ratio (by 1.42%) mainly due to the disposition of some flux to the outer areas of the bundle making it more likely to reach the moderator and scatter down to thermal energies. The total flux in the lattice cell for the two fuel cases is also of note as the TRUMOX-30 fuel has a much lower value, 37% less than NU given the common 37 element configuration. The total flux is even lower (42.5% less than NU-37) with the 43 element TRUMOX-30 bundle design where the integral BNA increases absorption.

The results of the comparisons of the average energy per fission and thermal flux ratio are evident in a comparison of the fresh fuel neutron energy spectrum for the 43 element TRUMOX-30 (with BNA) and the 37 element NU designs. The differences in the two designs are primarily within the fuel and thus the neutron spectrum in the outer fuel ring of each of the designs is provided in Figure 4.15.
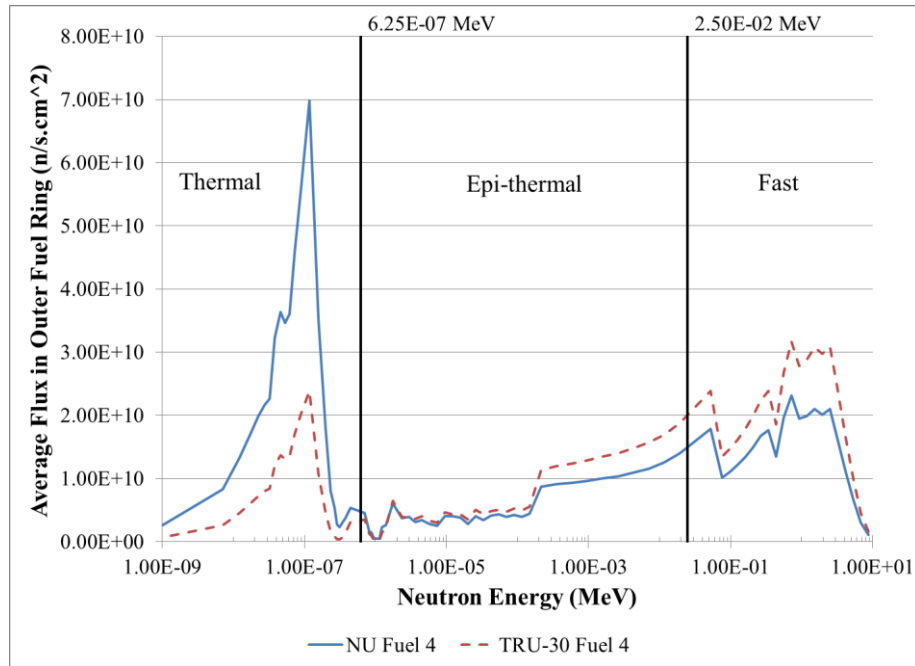
Figure 4.15: Fresh Fuel Neutron Spectrum in Outer Ring for 37 Element NU and
43 Element TRUMOX-30

The fresh fuel neutron spectrum in the outer ring is quite different with the TRUMOX-30 case having higher flux in the fast region and lower flux in the thermal region. In the epithermal region the spectrums are similar with the TRUMOX-30 spectrum jumping up above about 150 eV.

The previous descriptions focused on fresh fuel but the changes in composition over the burnup will affect the flux. The proportion of thermal flux is tracked for the 37-NU fuel and the 43-TRUMOX-30 fuel for their respective burnup cycles in Figure 4.16.   The changes in composition, as discussed in Chapter 4.1.1, are due to burnup of fissile content, production of higher actinides through neutron capture and the burnup of some actinides.   As seen in Figure 4.2 previously, TRUMOX is plutonium driven while NU fuel is primarily dominated by U-235 until plutonium builds up and overtakes it near to the end of the cycle.
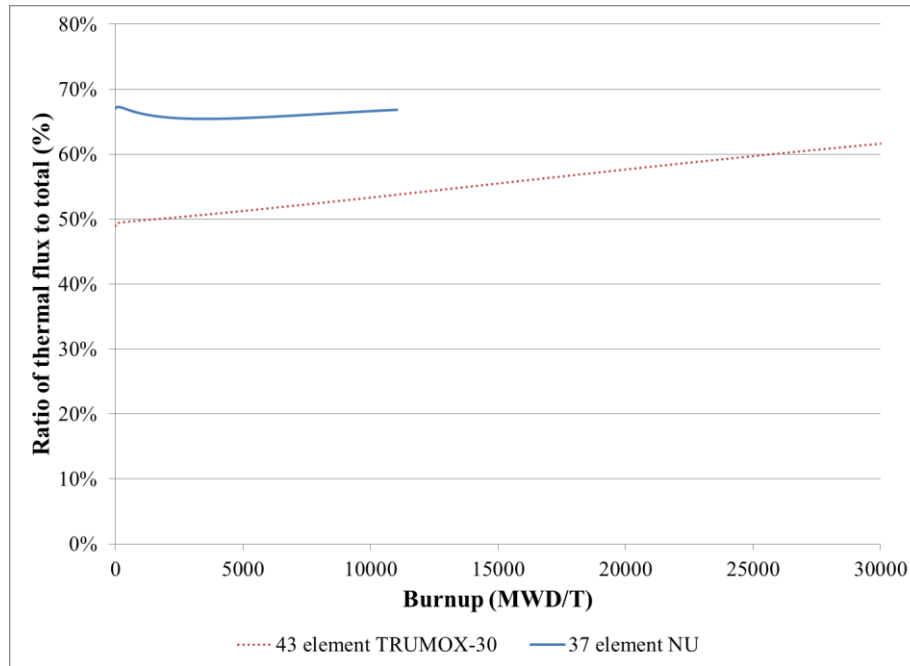
Figure 4.16: Thermal Flux Ratio Vs. Burnup (43-TRUMOX-30 and 37-NU)

The proportion of thermal flux is relatively constant for NU fuel dipping in early burnup and leveling back out near the initial value with a range of 1.84%. The TRUMOX-30 case sees a linear increase of 12.68% in the proportion of thermal flux over the 30, 000 MWD/T burnup cycle (48.96% to 61.64%). This increase in thermal flux is the result of reduced thermal absorption as the minor actinides are transmuted. There are other effects common to both fuels, especially from fission products such as Xe-135 which has a large thermal capture cross section.

The effect of the actinide burnup is evident in the beginning of cycle (BOC) and end of cycle (EOC) neutron spectrum for the TRUMOX-30 fuel which is displayed in Figure 4.17. The ratio of thermal flux increases by about 9.5% due to the reduced absorption from the actinides that have been burned up. The overall flux is 52% higher and the thermal flux is significantly higher, below 0.1 eV while the rest of the spectrum sees a similar smaller increase in flux.

Overall, actinide based fuels like TRUMOX have higher average neutron energies and increased thermal absorption resulting in a hardening of the neutron energy spectrum. Based on the assessments in Chapters 4.1.2.1 to 4.1.2.3 the ratio of the strength of the two effects on hardening was 13% for the plutonium energy

increase and 87% for the increased absorption by the actinides. If we apply this to the fresh fuel differences between the 43 element TRUMOX-30 fuel and the 37 NU fuel we see that the difference in the thermal flux ratio of 18.06% can be split into approximately 15.71% from the actinide absorption and 2.35% from the plutonium effect.
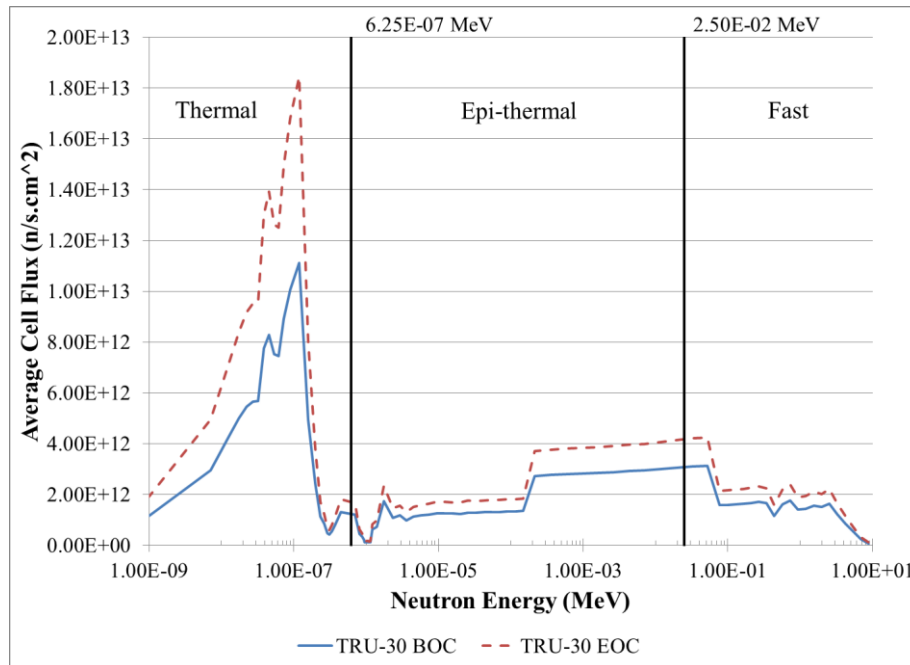
Figure 4.17: TRUMOX-30 Lattice Cell Neutron Spectrum for BOC and EOC

It should be noted that there is an additional source of spectrum hardening (or softening) from increases (or decreases) in fuel temperatures which will be driven by the fuel bundle geometry and fuel composition. Larger numbers of elements in the bundle will distribute the power but the increased surface area and smaller sub-channels in the geometry reduce flow. Thus even though power is better distributed the local fuel temperatures may be higher. These local effects require a sub-channel level thermalhydraulics code to properly be assessed. There also may be some heat transfer effects due to slightly differences in the thermal conductivity of plutonium and uranium oxides but as the bulk of the fuel is uranium they should be minor. Overall the temperature hardening effects are minor compared to the two main causes discussed earlier.

4.1.3 Bundle power distribution

Actinide mixed fuels such as TRUMOX, will also affect the flux/power distribution in the bundle due to increased enrichments, the presence of minor actinides and changes in the absorption and flux characteristics across the bundle. The distribution of fission power across the fuel bundle is denoted by the pin power factors in each of the regions of the bundle. In general for CANDU, the pins with the lowest powers are in the center and those with the highest are in the outer ring. The power distribution in the bundle is expressed by the pin power factor (PPF) which relates the specific pin powers in the ring to the average pin power in the bundle.

Using WIMS-AECL lattice simulations of a 37 element bundle in a CANDU lattice cell the pin power distributions for different fuel compositions were examined and the results are presented in Figure 4.18. It was seen that higher enrichment levels tend to push the power towards the outer ring and reduce it within the center. SEU (1% U-235) produced a reduction in PPF of 2-5% in the inner rings (highest in the center) and an increase in the outer ring PPF of 2.2% compared to the NU case. The increased fissile content in the outer rings increases the bundle spatial self-shielding effects redistributing power to the outer edges. Fuels containing plutonium, such as an actinide mixture, will result in a similar but more pronounced redistribution of bundle power to the outer rings.

It should be noted that many enriched fuel or actinide based designs also include a burnable neutron absorber (BNA) in the bundle which can affect the power distribution. Generally the BNA is placed in the central pin of the bundle which will cause a flux depression in the middle of the bundle displacing the fission and increasing the PPF values in the outer ring. This fuel design decision is discussed in Chapter 4.2. It is important to note the effect here since it will further increase the power displacement to the edge of the bundle and reduce the margin to the linear rating limit in the outer elements. In these cases, the use of larger numbers of elements can mitigate this effect since the power is spread over more elements with lower pin powers and lower fuel temperatures.
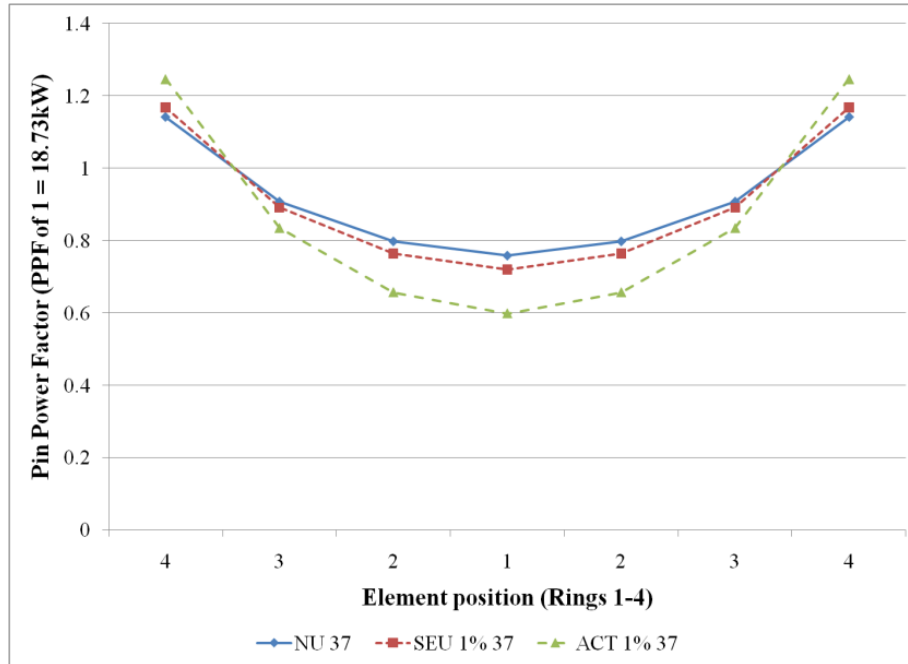
Figure 4.18: Pin power factors across a CANDU bundle.

4.1.4 Delayed neutron fraction

The different isotopic composition of the actinide mixed oxide fuel has an effect on the basic physics properties such as the delayed neutron fraction, β, due to the varied fissile content. The β value will change over the burnup as per the changing fuel composition described in Chapter 4.1.1. The changes in the delayed neutron fraction affect the relative dollar worth of control devices $(\Delta\rho/\beta)$.

A direct comparison is made between standard 37 element natural uranium fuel and the 43 element TRUMOX-30 fuel (BNA included) in the CANDU lattice. The delayed neutron fraction is tracked over the relevant burnup cycle for each fuel based on the composition of fissile isotopes generated from a WIMS-AECL lattice cell simulation and is displayed in Figure 4.19.
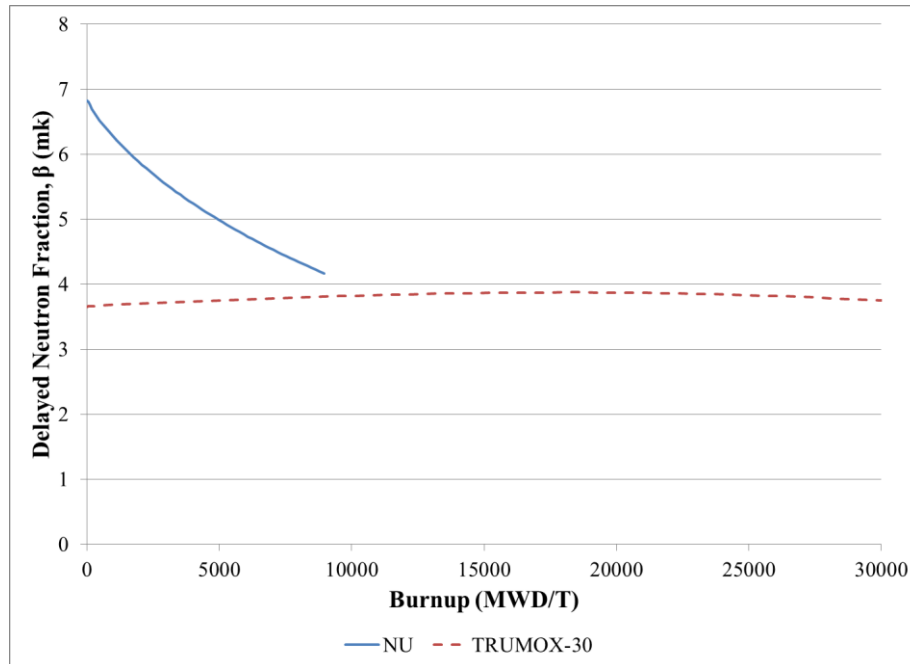
Figure 4.19: Burnup effects on delayed neutron fraction, β (infinite lattice case)

For the infinite lattice case, the NU β value is initially high at 6.82 mk and decreases as more plutonium is produced in the fuel down to 4.15 mk at 9000 MWD/T (typical CANDU-900 exit burnup), a drop of 2.67 mk over the burnup cycle. The TRUMOX fuel has higher plutonium content and thus lower β values throughout (~3 mk less than NU). The β value starts at 3.66 mk and rises slightly to a peak of 3.88 mk and then decreases to 3.75 mk at 30000 MWD/T, a range of only 0.22 mk, less than 10% of the range for NU. The TRUMOX lattice delayed neutron fraction is more stable over the burnup cycle than NU but it is consistently lower. It should be noted that a full core with many channels all at different burnup levels will produce an average β for the full core based on the overall fuel composition in the core (for NU CANDU $\beta_{NU\,Full\,Core} = 5.82\,mk$) [61]. The full core β for TRUMOX-30 would be close to the mid-burnup value which is 3.86 mk making the delayed neutron fraction in TRUMOX is about 34% lower than the NU value.

This effect is in line with what is seen in PWRs that use plutonium MOX fuels. For a VVER with a core loading of 1/3 MOX the delayed fraction is 5.1-5.3 mk which is about ~10% lower than for a regular full core of UO_2 [62].

This lower delayed neutron fraction will have an effect on the control device responses. A comparison of the full core worth of the control systems (computed in RFSP) for TRUMOX and NU in CANDU is made in Table 4.4.

Table 4.4: Comparison of full core reactivity worth of control devices

Device	TRUMOX-30 Worth (mk)	NU Fuel CANDU Worth (mk) [55]
LZCRs 0% to 100% Full	3.90, $1.01	~7, $1.20
Adjuster Rods	3.14, $0.81	~ 15.0, $2.58
Mechanical Absorbers (MCAs)	4.38, $1.13	~ 10.0, $1.72
Shutdown System (SDS#1)	60.27, $15.61	~ 80.0, $13.75
β values: TRUMOX-30 = 3.86 mk, NU = 5.82 mk		

The lower absolute device worth values and the lower delayed neutron fraction of the TRUMOX fuels combine to produce relative dollar worth values, $(\Delta\rho/\beta)$, that are similar to NU. The effect of the actinide presence on the control devices is further explored in Chapter 4.1.8.

4.1.5 Prompt generation time and neutron lifetime

The presence of the actinides in the fuel will also alter the prompt generation time and neutron lifetime in the fuel. The prompt generation time, Λ, is regarded as the time between the birth of a neutron and its subsequent absorption inducing fission. Thus prompt generation time is primarily dependent on the velocity of the neutrons within the reactor system and the fission production factor ($\nu\Sigma_f$). Using the infinite lattice simulations performed with WIMS-AECL for the TRUMOX-30 and NU fuel at mid-burnup it is possible to compute the estimated prompt generation time. Within the lattice cell, the fission yield cross section ($\nu\Sigma_f$) for each of the 89 energy groups is related with the average velocity of the neutrons in each energy group using a flux squared weighting function to produce the infinite lattice prompt neutron generation time through equation 42 [63].

$$\Lambda_\infty = \frac{1}{\bar{\nu}\nu\Sigma_f} = \sum_{g=1}^{89} \phi_g^2 \frac{1}{\nu_g} \bigg/ \sum_{g=1}^{89} \phi_g^2 (\nu\Sigma_f)_g \qquad (42)$$

The infinite lattice prompt generation time for the TRUMOX-30 case was found to be $\Lambda_{TRUMOX-30} = 0.427ms$ while the NU value was $\Lambda_{NU} = 0.688ms$. The TRUMOX prompt generation time is about 38% lower than NU. The harder spectrum of the TRUMOX fuel results in higher neutron energies increasing the average neutron energy. Also the larger amount of fissile material in the fuel increases the likelihood for fission. The lower prompt generation time means that the TRUMOX core will be quicker to respond to reactivity insertions which may have implications on reactor control. The control systems, designed for the slightly slower responding NU core, will have the same system lags (e.g. electronics, rod drop actuation, and spring, motor and gravity driven decent times) but be interacting with the quicker responding TRUMOX-30 core.

The infinite lattice neutron lifetime, l_∞, can also be computed for both the core designs in a similar fashion to the prompt generation time. The lifetime is the time from when a neutron is born to the point where it is absorbed and as such is dependent upon the neutron velocity and the absorption cross section. Similar to the prompt generation time computation in equation 42, a flux square weighting is used to relate the point kinetics formulation for infinite neutron lifetime to the multi-group transport system in WIMS-AECL. The infinite neutron lifetime formulation is provided in equation 43 [63].

$$l_\infty = \frac{1}{\bar{v}\Sigma_a} = \sum_{g=1}^{89} \phi_g^2 \frac{1}{v_g} \bigg/ \sum_{g=1}^{89} \phi_g^2 (\Sigma_a)_g \tag{43}$$

The resultant infinite neutron lifetimes for the TRUMOX-30 and NU systems are: $l_{TRUMOX-30} = 0.495ms$ and $l_{NU} = 0.766ms$. The TRUMOX value for infinite lattice neutron lifetime is approximately 36% lower than the NU value. The prompt generation time and neutron lifetime are related through the infinite multiplication factor as per equation 44 [63].

$$l_\infty = \Lambda_\infty k_{infinity} \tag{44}$$

The slight differences in the mid-burnup k-infinity values in TRUMOX-30 and NU account for the difference in the percentage reductions in prompt generation time and neutron lifetime from NU. The reductions in prompt generation time and neutron lifetime for the TRUMOX core are in line with the MOX loaded PWRs (VVER-1000) which experience a 10% reduction in prompt lifetime for a

1/3 MOX core over a standard UO_2 loading [62]. The standard PWR prompt lifetime is around about 20 µs depending on the point in the burnup cycle compared to about 766 µs for NU CANDU or 495 µs for TRUMOX CANDU.

4.1.6 Lattice cell reactivity

The fuel composition will affect the lattice cell reactivity through the fissile content and the parasitic absorption within the fuel. In the case of NU fuel, the fissile content is low and there are small amounts of parasitic loss in the fuel as the bulk of the fuel is U-238 which transmutes to the fissile isotope Pu-239 through neutron capture. The TRUMOX fuel has higher fissile content which will increase reactivity but it also has minor actinides within the fuel that contribute to higher levels of parasitic absorption. In general, the reactivity of the lattice cell will decrease over the burnup cycle as the fission content is steadily depleted. A comparison of the infinite lattice cell multiplication factor, k-infinity, for standard 37 element NU fuel and 43 element TRUMOX-30 fuel was made over their full burnup cycles and is provided in Figure 4.20 (performed using WIMS-AECL).
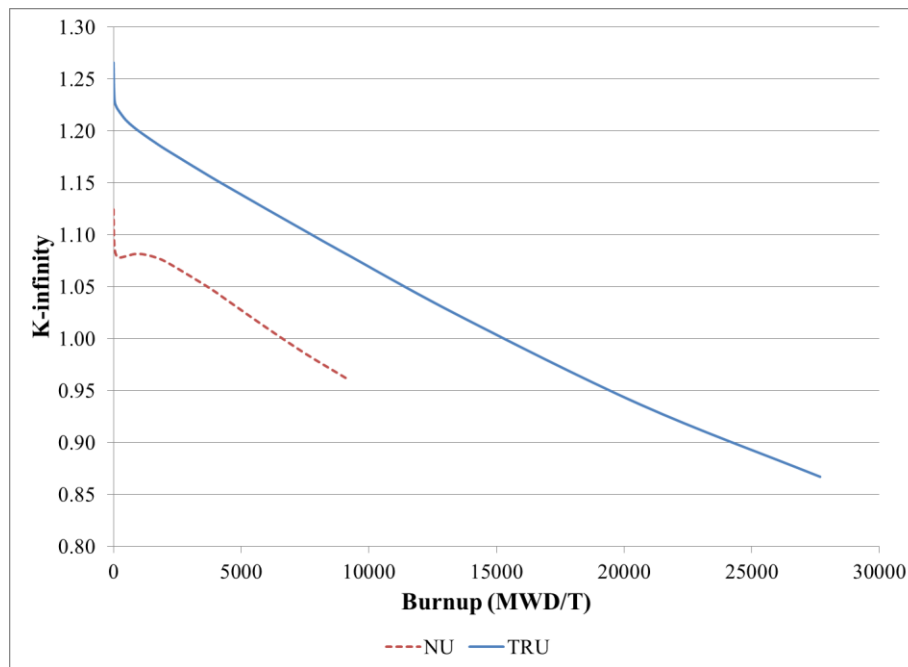
Figure 4.20: k-infinity Vs. burnup, NU and TRUMOX-30 fuels.

The general reactivity response over the burnup cycle is similar for both fuel types, an initial strong reduction followed by a gradual linear decline. The initial decrease results from the production of neutron absorbing fission products, such as Xe-135, which build-up to a steady state value in the first week of operations. The NU case experiences a reactivity peak at about 1,100MWD/T due to the build-up of Pu-239 which transmutes from U-238 adding fissile content to the fuel. Early in the cycle these gains outpace the losses due to burnup producing a reactivity peak. TRUMOX fuel has a much higher fissile content, much of it plutonium and a reduced U-238 content which makes transmutation to Pu-239 a less dominating effect on the fuel reactivity and hence there is no reactivity peak.

The TRUMOX fuel has a fissile content of 2.53% compared to the 0.71% in NU fuel and thus is more active. This is evident in the higher k-infinity for most of the burnup. The initial k-infinity is 12.6% higher in TRUMOX and at 1120 MWD/T is 10.7% higher while at the end of burnup it is 9.9% lower than that of NU. For a critical operating reactor with fuels at all burnup levels, the active new fuel will balance out the older fuel. Since the TRUMOX fuel is more active to begin with it is able to stay in the core longer and reach a lower k-infinity value while overall full core criticality is maintained.

The lattice cell reactivity is directly dependent on the fissile content and parasitic absorption and is therefore directly related to the amount of actinide mixture in the fuel. The actinide mixture used in TRUMOX results in a net increase of reactivity as the fissile content outweighs the parasitic absorption.

4.1.7 Coolant voiding behaviour

The fuel composition will also alter the response of the lattice to the voiding of the coolant. This effect is important for CANDU reactors as the coolant void reactivity (CVR) is usually a positive value. The different neutron spectrum and distribution dictated by the composition of the fuel and the possible presence of neutron absorbers within the bundle will alter the coolant voiding behaviour.

Coolant void effect in CANDU is an important phenomenon as the pressure tube design separates the coolant and moderator and thus allows the possibility of a core configuration with the moderator present but no coolant (usually due to a loss of coolant from a break in the heat transport system). This situation is not

possible in a pressure vessel type reactor (e.g. PWR) as the moderator and coolant are one fluid and thus a loss of coolant will result in a loss of moderator.

The voiding of the coolant produces several energy specific reactivity effects which sum together to determine the reactivity difference between a cooled and voided lattice configuration. These effects on neutron multiplication are via the components of the four-factor equation, (45 [44]), and thus change reactivity, ρ.

$$k = \eta f p \epsilon \tag{45}$$

- η is the neutron reproduction factor: the average number of neutrons produced per absorption in fuel = $\left. \nu \Sigma_f^{FUEL} \middle/ \Sigma_a^{FUEL} \right.$

  Since most fuels contain a mixture of many isotopes, the macroscopic fission and absorption cross sections include all isotopes, j, in the fuel.

  $$\nu \Sigma_f^{FUEL} = \sum_j \nu_j \Sigma_f^j \ and \ \Sigma_a^{FUEL} = \sum_j \Sigma_a^j$$

- f is the thermal utilization factor: the probability that if a neutron is absorbed, it will be absorbed in the fuel material = $\left. \Sigma_a^{FUEL} \middle/ \Sigma_a \right.$

- p is the resonance escape probability: the fraction of fission neutrons that manage to slow down from fast to thermal without being absorbed.

- ϵ is the fast fission factor:

  $$\frac{\text{the total number of fission neutrons (from fast and thermal fission)}}{\text{the number of fission neutrons from thermal fissions}}$$

The effects of coolant voiding on neutrons leaving and re-entering the fuel channel are detailed below along with their effects on the components of the four factor formula and thus the reactivity.

1. **Leaving the channel**: Fission neutrons are born in the fuel within the channel and as they escape towards the moderator some of them are slowed by the coolant in the channel into the resonance energy region and absorbed.
   - **Effects of coolant voiding:**
     - Fewer fast neutrons are slowed into the resonance region resulting in more opportunities for fast fission. $\epsilon \uparrow$, **so** $\boldsymbol{\rho} \uparrow$
     - More fast neutrons escape resonance capture. $\boldsymbol{p} \uparrow$, **so** $\boldsymbol{\rho} \uparrow$

2. **Re-entering the channel**: Some of the thermal neutrons coming back into the channel can be scattered to higher energies by the hot coolant and absorbed in the resonance energy region.
   - **Effects of coolant voiding:**
     - Increased escape from the U-238 resonances $p_U \uparrow$, so $\rho \uparrow$
     - Reduced scatter into the Pu-239 fission resonance peak at ~0.3 eV, see Figure 4.3, reduces the overall fission in the lattice cell. $\downarrow p_{Pu}$, so $\rho \downarrow$

The net result of these four effects, 3 positive and 1 negative, in NU CANDU is a net positive increase in reactivity due to coolant voiding, CVR > 1. The lattice cell reactivity change produced by the coolant voiding is computed by comparing a simulation of the cooled lattice cell (the base case, 0) and the voided lattice cell (the void case) in CANDU lattice cell simulation as per equation 46.

$$CVR \ [mk] = \left(\frac{1}{k_0} - \frac{1}{k_{Void}}\right) * 1000 \tag{46}$$

The net CVR will decrease with the buildup in the Pu-239 in the fuel that occurs during burnup. The changes to the neutron spectrum for voiding in an NU CANDU lattice cell at mid-burnup (~4.5 MWD/kgHE) are shown in Figure 4.21.

Upon voiding, the spectrum in the full cell decreases for thermal energies below about 0.1 eV and increases slightly for fast energies between 0.1 MeV and 5 MeV. These differences are the result of the reduced moderation in the cell from the voiding of the coolant. The coolant voiding effects described above focus on changes in the full cell but there is an important local effect within the fuel channel. Specifically, the voiding of coolant causes the thermal flux to increase in the center of the fuel bundle and decrease at the outer edge. Thus, thermal flux is redistributed into the center of the bundle due to the loss of scattering from the coolant. The thermal flux at different points across the lattice cell for both the cooled and voided cases for NU CANDU at mid burnup is seen in Figure 4.22
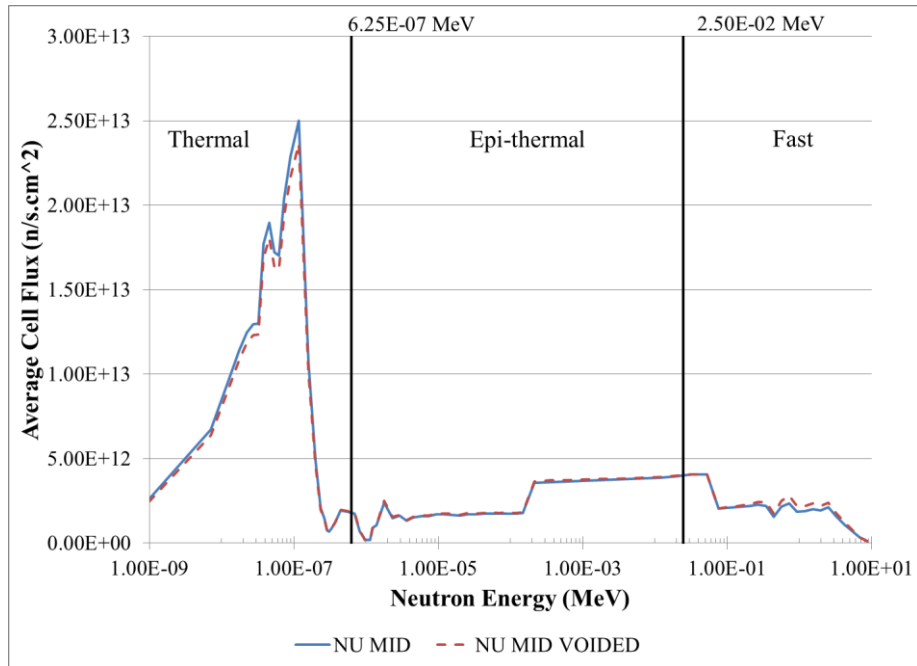
Figure 4.21: Neutron Spectrum for Mid-Burnup NU CANDU (Cooled and Voided)
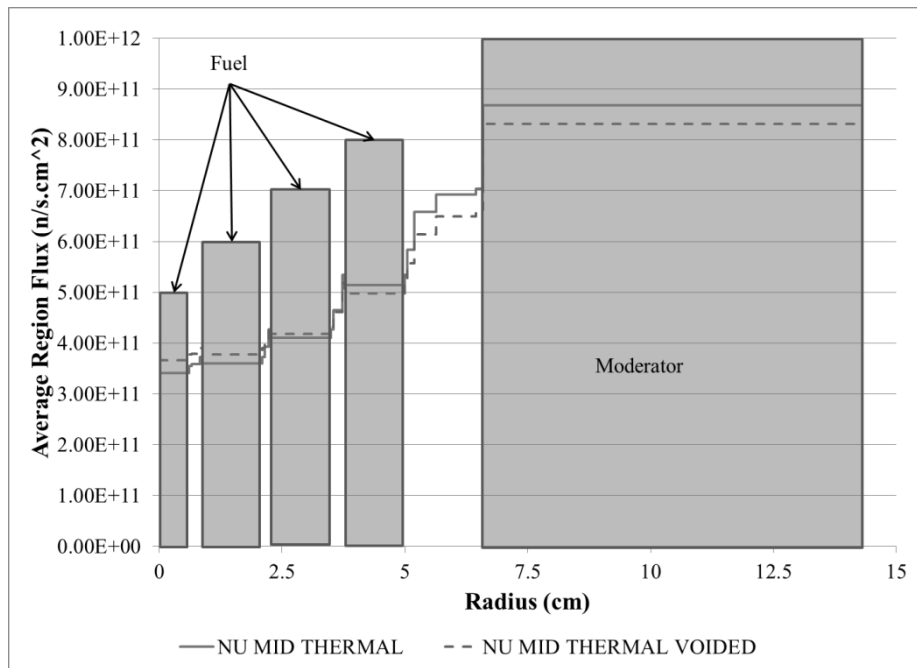
Figure 4.22: Thermal Regional Average Flux for Mid-Burnup 37 Element NU in CANDU 9 Lattice Cell (Cooled and Voided)

Figure 4.22 displays the thermal flux redistribution during coolant voiding showing an increase of 8.5% in thermal flux and 2.4% of total flux in the center fuel element. In the outer fuel ring, the thermal flux drops by 2.0% and by 3.3% in the moderator (total flux increases by 0.4% in the outer fuel ring and decreases by 0.1% in the moderator). This local effect of the voiding increases thermal flux and hence absorption and fission in the center fuel element.

A central burnable neutron absorber is designed specifically to take advantage of the flux redistribution in order to reduce the coolant void reactivity. In a regular bundle the fuel in the center see a higher flux and as a result has higher absorption and fission increasing reactivity in the voided case. By placing a BNA in the center of the bundle this flux redistribution yields increased thermal absorption in the lattice cell reducing the reactivity.

The effect of fissile content on CVR is assessed by comparing standard NU fuel with slightly enriched uranium fuel (SEU, 1% U-235) and with the TRUMOX-45 fuel (4.75% actinides) and the TRUMOX-30 fuel (3.1% actinides) in the same bundle configuration without a BNA present. This comparison is performed using fresh fuel in standard CANDU 37 element bundle lattice cell simulations performed in DRAGON. The results are seen in Table 4.5.

Table 4.5: Measurements of CVR for various fresh fuel configurations in a 37 element CANDU lattice cell [64].

Fuel Type	2D k-infinity		Coolant Void Reactivity (mk)	% Difference From NU
	Reference	*Voided*		
NU	1.12816	1.14469	12.80	0.0
SEU	1.26483	1.28162	10.36	-19.09
TRUMOX-30	1.33839	1.35491	9.10	-28.91
TRUMOX-45	1.35397	1.37009	8.69	-32.18

The fuel composition does have a significant effect on the coolant void reactivity of the lattice cell. The increase in U-235 enrichment from NU to SEU (0.7% to 1.0%) results in a 19.1% reduction in CVR. The larger enrichment in the SEU fuel displaces U-238 and hence the positive reactivity effect from the increased U-238 resonance escape in point 2 is reduced lowering the overall CVR.

The actinide mixed oxide fuels, TRUMOX-30 and TRUMOX-45, are plutonium based and have lower coolant voids than the NU case. TRUMOX-30 reduces CVR by 28.9% while the TRUMOX-45 fuel reduces the CVR by 32.2% in the absolute measure. There are two effects at play here reducing the coolant void response. First, like the SEU case, there is less U-238 in the TRUMOX fuel which is displaced by the actinide mix thus reducing the positive reactivity effect from U-238 resonance escape in point 2. Second, the plutonium content in the TRUMOX fuels increases the negative effect of the loss of scattering into the thermal fissile resonance of plutonium at 0.3 eV. The TRUMOX-45 has a lower CVR because the larger amount of actinide material in the fuel displaces more of the U-238 and has more plutonium content.

The absolute coolant void reactivity is important to look at for the effects on the neutron multiplication factor but for reactor control aspects it is important to account for the differences in the fresh fuel delayed neutron fractions, β, of the different fuels. As discussed earlier in Chapter 4.1.4 the plutonium in the TRUMOX fuels results in a lower delayed fraction (fresh fuel: $\beta_{NU} = 6.82$ mk, $\beta_{TRUMOX-30} = 3.66$ mk, $\beta_{TRUMOX-45} = 3.30$ mk,). The relative CVR, $(\Delta\rho/\beta)$, for the three fuel types are: NU = \$1.88, TRUMOX-30 = \$2.49 and TRUMOX-45 = \$2.63. Interestingly, the relative CVR for the TRUMOX fuel is actually higher by 32% for TRUMOX-30 and 40% for TRUMOX-45 than NU given the same 37-element bundle. This is because of the lower delayed fraction of these fuels.

To study the effect of the inclusion of a burnable neutron absorber a comparison is made between the SEU fuel in the 37 element bundle and in a 43 element SEU-VE bundle which contains a central burnable neutron absorber pin. The BNA in the SEU-VE bundle is composed of 15% Dy-Zr and 85% natural uranium. The results of the DRAGON lattice simulations are provided in Table 4.6.

Table 4.6: Measurements of (CVR) for SEU fuel in various bundle configurations in a CANDU lattice cell [64].

Bundle Type	2D k-infinity		Coolant Void Reactivity (mk)	% Diff from 37 element
	Reference	*Voided*		
37 element	1.26483	1.28162	10.36	0.0
43 element SEU-VE	1.13681	1.14070	3.00	-71.0

The BNA in the SEU-VE configuration reduces the CVR by 71% compared to the 37-element SEU design and results in an overall decrease of 76.6% from the 37-element bundle fuelled with NU. This effect is due to the displacement of fuel volume from the center by the BNA which takes advantage of the thermal flux redistribution caused by voiding.

The TRUMOX fuels are also designed to be used with a 43 element bundle that contains a BNA in the central pin. This bundle design uses a BNA that is Dy-Zr-oxide (67% Dy_3O_2) and is much stronger than the SEU-VE configuration. This is necessary because the fissile contents in the TRUMOX fuels are much higher than SEU (2.5-3.5% Vs. 1%). The TRUMOX-30 fuel comparison is explored in Table 4.7 while the TRUMOX-45 fuel is explored in Table 4.8.

Table 4.7: Measurements of (CVR) for TRUMOX-30 fuel in various bundle configurations in a CANDU lattice cell.

Bundle Type	2D k-infinity		Coolant Void	% Diff from
	Reference	Voided	Reactivity (mk)	37 element
37 element	1.33839	1.35491	9.10	0.0
43 element TRUMOX	1.26832	1.27015	1.14	-87.5

Table 4.8: Measurements of (CVR) for TRUMOX-45 fuel in various bundle configurations in a CANDU lattice cell [64].

Bundle Type	2D k-infinity		Coolant Void	% Diff from
	Reference	Voided	Reactivity (mk)	37 element
37 element	1.35397	1.37009	8.69	0.0
43 element TRUMOX	1.30160	1.30593	2.54	-71.0

The result of the use of BNA in the TRUMOX bundles is similar to that of the SEU-VE bundle with a large reduction. The TRUMOX bundles use a much stronger BNA which counteracts their higher fissile contents and large plutonium content. The effect is an 87.5% reduction for the TRUMOX-30 fuel and a 71% reduction for the TRUMOX-45 fuel from their 37 element bundle values. The change in CVR from the original 37 element NU case is significant with a 91.1% reduction for TRUMOX-30 and an 80.1% reduction for TRUMOX-45. The same amount and strength of BNA is used in both TRUMOX cases so the TRUMOX-

30 fuel with its lower fissile content is more affected by the BNA. The same BNA is counteracting a lower amount of fissile content resulting in a stronger coolant void response. An additional benefit of the BNA is that it holds down the bundle power during online fuelling and helps to maintain the fuel ramp rate limit.

The relative reactivity changes (accounting for fresh fuel β) in the 43 element case with a BNA also show the improvement and help compare the control effects of the CVR between the different fuel designs. The relative CVR values of two 43 element TRUMOX designs with the BNA are much lower than the base NU value of $1.88 with TRUMOX-30 achieving $0.31 (83.5% lower) and the TRUMOX-45 achieving $0.77 (59% lower). The BNA in the center pin took advantage of the flux redistribution described earlier and the increased absorption in the voided state resulted in a lower coolant void reactivity.

The above studies focused on fresh fuel cases which, while able to show the changes in coolant void response between fuel types, do not provide insight on the coolant voiding response over the burnup cycle. To accomplish this, a comparison of lattice cell simulations in WIMS-AECL for 37 element NU and the 43 element TRUMOX-30 fuel (with central BNA pin) in the CANDU-900 lattice was performed. The coolant void reactivity was measured at different points along the burnup cycle for the two fuels and is provided in Figure 4.23.
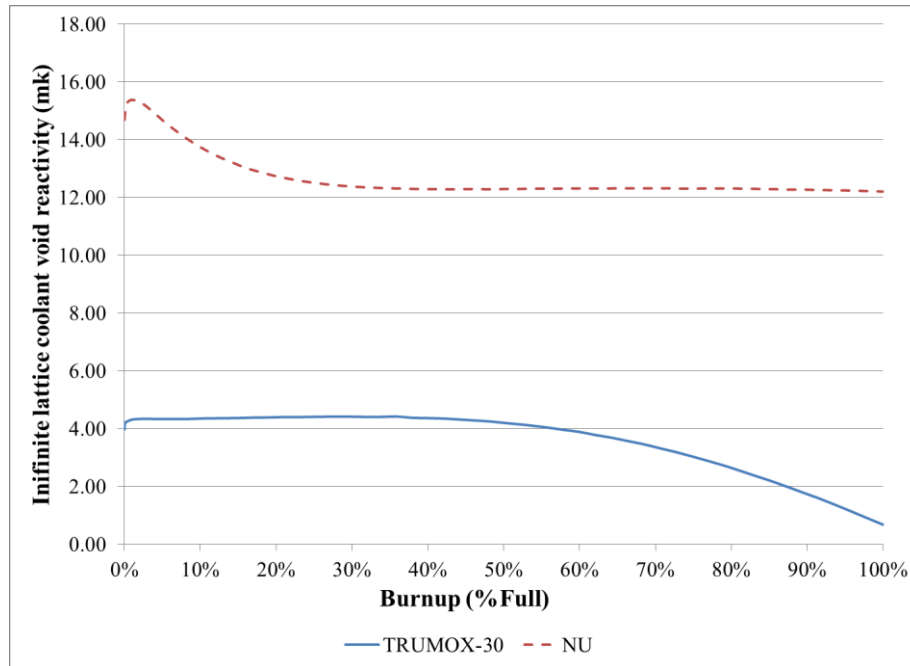
Figure 4.23: Lattice cell coolant void reactivity for TRUMOX-30 and NU.

The coolant voiding response is quite different between the two fuels over the burnup cycle with the TRUMOX fuel CVR being consistently lower than that of NU. For NU, the CVR rises to a peak of 15.4 mk at 99.13 MWD/T or about 3 days of iteration time (~1.1% of burnup). Following this peak the CVR declines steadily until about 12 mk at about 35% of the full burnup, after which it declines very slightly until reaching the end of burnup. The TRUMOX-30 fuel conversely maintains a constant value of about 4.3 mk for the first half of the burnup and then descends down to 0.7 mk by the end of the cycle. The end of cycle burnup for the NU fuel is 9000 MWD/T and is 30,000MWD/T for the TRUMOX-30 fuel. For a full core system, the fuel burnup will be close to equilibrium across the core meaning the void will be closer to the 50% burnup values of 12.3 mk for NU and 4.2 mk for TRUMOX-30. However, the void in a full core simulation will be lower as the leakage in the core will be included.

The CVR differences over the burnup cycle are mainly due to the inclusion of the BNA in the central pin of the 43 element TRUMOX-30 configuration which reduces the coolant void reactivity significantly, 66% at mid-burnup. The thermal flux in the regions of the lattice cell for the cooled and voided case for mid burnup TRUMOX-30 in the 43 element TRUMOX bundle is   provided in Figure 4.24.
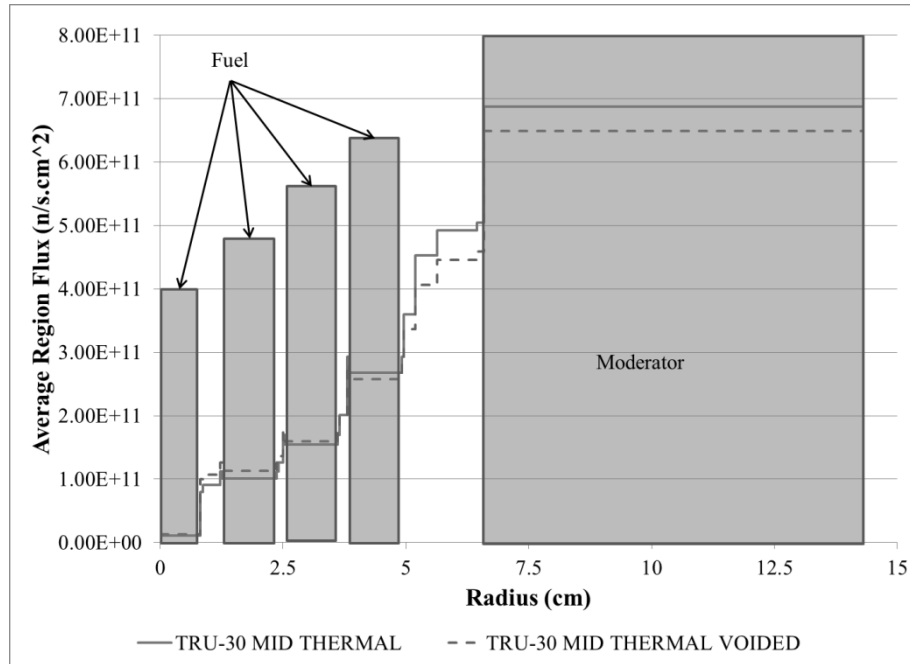
Figure 4.24: Thermal Regional Average Flux for Mid-Burnup 43 Element TRUMOX Bundle with TRUMOX-30 Fuel in CANDU 9 Lattice Cell (Cooled and Voided)

The flux displacement towards the center of the bundle is visible and the voiding results in an increase of 22.9% in the thermal flux in the central BNA. This results in more absorption and a negative reactivity component which helps to keep the CVR for this configuration low. The total flux in the BNA region increases very slightly by 0.1%. The thermal flux in the outer fuel ring drops by 3.6% and by 5.4% in the moderator (total flux in the outer fuel ring increases by 0.7% while the moderator total flux decreases by 0.1%). The flux displacement is the main factor driving the effectiveness of the central BNA for controlling CVR. The increased fissile material in the TRUMOX fuel is also a factor as described in the fresh fuel cases. The difference in CVR is significant but must be tempered by the difference in the delayed neutron fraction. Recalling the full core β for NU of 5.82 mk and the estimated full core β for TRUMOX-30 of 3.86 mk, the dollar value for the relative CVR can be computed for the mid-burnup values [61]. The relative mid-burnup CVR works out to be $2.11 for the NU case and about $1.15 for the TRUMOX-30 fuel. The inclusion of the delayed neutron fraction in the

coolant voiding calculation has reduced the separation between the two fuels but the TRUMOX-30 CVR is still 46% lower than NU at mid-burnup.

4.1.8 Control device interactions

The effects of the actinide content on the interaction with CANDU type control devices are explored through the use of 3D super-cell simulations with the DRAGON transport code (See Chapter 3.3 regarding super-cell modeling in CANDU). These simulations are used to determine important information such as incremental cross sections and the reactivity change produced by the insertion of the control device. The reactivity change is computed by comparing a simulation of the device fully removed (the base case, 0) and fully inserted (the perturbed case) in a 3D CANDU super-cell as per equation 47.

$$\Delta\rho\,[mk] = \left(\frac{1}{k_0} - \frac{1}{k_{Perturbed}}\right) * 1000 \qquad (47)$$

4.1.8.1 Preliminary investigation of effects on reactivity change

The reactivity change for control device insertion was explored using a 3D super-cell model with a simple stainless steel tube for the control device with no guide tube involved. This simplistic system was modeled in DRAGON and is used to see the general effects of adding enrichment, including burnable neutron absorbers and using actinide based fuel. The bundle and fuel configurations explored are similar to those investigated in the CVR study found in Chapter 4.1.7 and are described in the beginning of Chapter 4.1. The three fuels explored in this case are NU, SEU (1%) and the TRUMOX-45 fuel. The bundles are the standard 37 element bundle, the 43 element SEU-VE bundle and the 43 element TRUMOX bundle. The control device is a stainless steel tube with an inner radius of 3.51 cm and a thickness of 0.3 cm, the composition is as shown in Table 4.9.

Table 4.9: Composition of stainless steel tube used for simplified trial.

Material	Wt %	Material	Wt %	Material	Wt %
C	0.05	Si	0.62	Mn	1.60
Fe	69.34	Ni	9.93	Cr	18.46

The effect of the fuel composition on the reactivity change for a common bundle is explored first. All three fuel types were modelled as fresh fuel in a 37 element bundle in the CANDU lattice to determine the effect of the fuel composition on the reactivity change from inserting the stainless steel tube (see Table 4.10).

Table 4.10: Reactivity change for various fuel types in the 37 element CANDU lattice cell [64].

Fuel Type	3D k-infinity		Reactivity	% Difference
	Reference	*Rodded*	Change (mk)	From NU
NU	1.12503	1.03772	74.79	0.0
SEU	1.26170	1.17335	59.68	-20.20
TRUMOX-45	1.35771	1.29928	33.12	-55.72

The use of higher enrichment like the SEU fuel reduces the reactivity change by 20% diminishing the strength of the control device. The TRUMOX-45 fuel with its even higher fissile content and plutonium in the fuel has a larger effect decreasing the reactivity change from rod insertion by 56%. The reduction in effectiveness of the control device is driven by two factors, the fissile content and the energy spectrum of the neutrons. The larger fissile content increases the ratio of neutrons produced in fission per absorption ($\nu\Sigma_f/\Sigma_a$) at thermal energies. This is a combination increase in both the η and *f* components of the four factor formula (see equation 45 in Chapter 4.1.7). Thus a fission neutron is more likely to be absorbed in fuel in the TRUMOX case than for NU reducing the impact that the control device will have on the lattice cell. This is seen in the SEU fuel where increasing the fissile content by 0.29% (0.71% to 1.00%) results in a 20% decrease in the reactivity change with no change in the fissile isotope composition (both fuels use U-235 only).

The second effect is found in the TRUMOX-45 fuel as it has a harder (higher average energy) neutron spectrum than the NU or SEU fuels. The fissile content of the TRUMOX-45 fuel is 3.5% (2.8% of which is Pu-239 and Pu-241) producing a harder neutron spectrum with a lower ratio of thermal to total flux. A comparison of the spectrum in the moderator region (i.e. where the control device will be interacting with the cell) of a 43 element TRUMOX/TRUMOX-30 lattice cell configuration for mid burnup to that of 37 NU at mid-burnup is provided in Figure 4.25 (using WIMS-AECL).
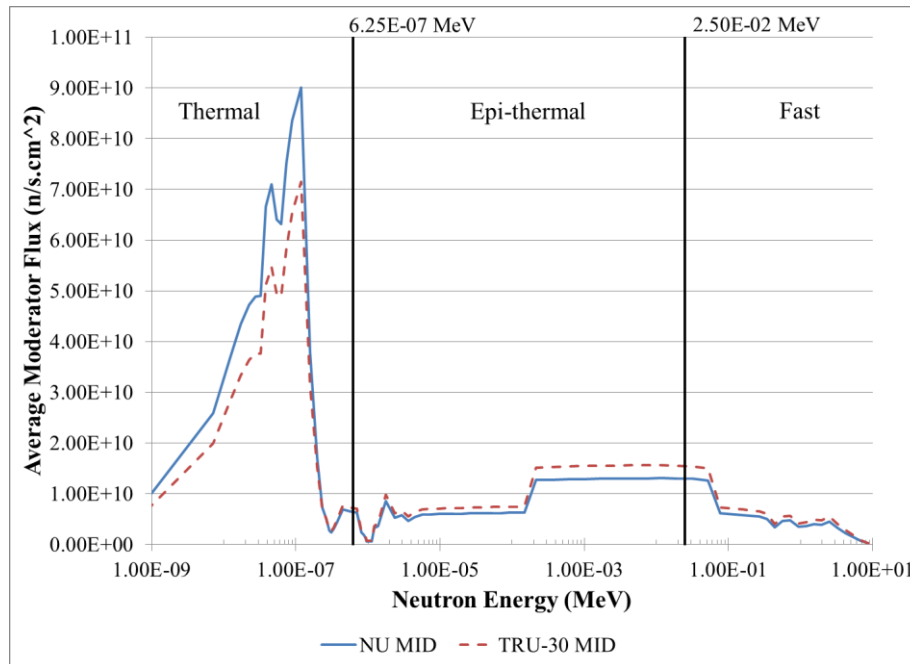
Figure 4.25 Flux Spectrum for 43 element TRUMOX-30 and 37 element NU both at mid-burnup

There is a marked difference in the thermal flux with the TRUMOX-30 values being 12.6% lower overall and about 12-15% lower for energies less than 0.1 eV. Additionally, the epithermal and fast flux in the TRUMOX-30 case are higher than NU especially between 130 eV and 67.4 keV. The control device modeled here is primarily composed of iron and thus the absorption cross section will be dominated by this element. The neutron capture cross section for iron (Fe-56), shown in Figure 4.26, decreases linearly until resonances appear at neutron energies of 1000 eV. Therefore, the redistribution of flux resulting in lower thermal flux and higher fast/epithermal flux will result in lower neutron capture in the control device. There will be an additional contribution from the thermal absorption peak from the plutonium content in TRUMOX-30 (seen in Figure 4.3).
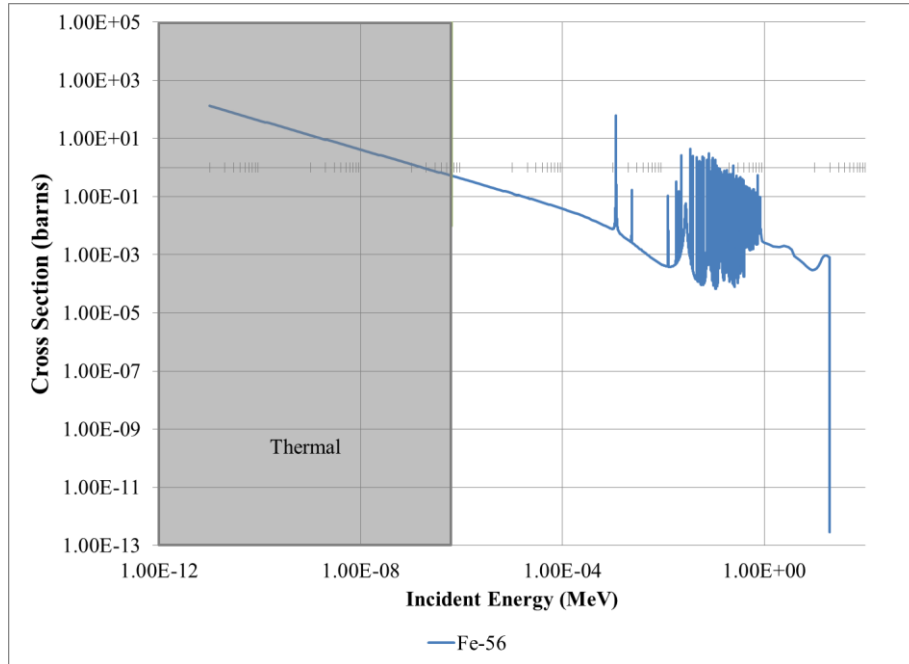
Figure 4.26: Neutron capture cross section for iron (Fe-56)

The effects of the inclusion of the BNA in the fuel design are seen when the 37 element bundle loaded with SEU fuel is compared to the 43 element SEU-VE bundle fuelled with SEU fuel. The 43 element SEU-VE bundle contains a BNA in the centre element that is 15% dysprosium and 85% natural uranium. The comparison of the reactivity changes in made in Table 4.11

Table 4.11: Reactivity change for various bundle types fuelled with SEU in a CANDU lattice cell [64].

Bundle Type	3D k-infinty		Reactivity	% Diff From
	Reference	*Rodded*	Change (mk)	37 element
37 element CANDU	1.26170	1.17335	59.68	0.0
43 element SEU-VE	1.13739	1.05914	64.96	8.85

The inclusion of the BNA in the 43 element SEU-VE bundle produces an 8.85% increase in the reactivity change from the insertion of the control device. This is due to the fact that the BNA is absorbing some of the neutrons in the lattice cell and helping to offset the effects of increased enrichment from the use of SEU fuel on the $(v\Sigma_f/\Sigma_a)$ ratio. Additionally, the central flux depression produced by the

114

presence of BNA displaces fissions toward the outer ring placing more neutrons closer to the moderator, where the control device is interacting, increasing the control device strength. Overall, the 43 element SEU-VE bundle fuelled with SEU has a 13% lower reactivity change than the standard 37 element NU case (64.96 mk vs. 74.79 mk).

The effect of BNA inclusion can also be tested by comparing the 37 element bundle loaded with TRUMOX-45 fuel with the 43 element TRUMOX bundle containing the same fuel. The 43 element TRUMOX bundle contains a strong BNA of dysprosium-zirconium in the centre element. The comparison of the reactivity changes for the TRUMOX-45 fuel is provided in Table 4.12.

Table 4.12: Reactivity change for various bundle types fuelled with TRUMOX-45 in a CANDU lattice cell [64].

Bundle Type	3D k-infinty		Reactivity Change (mk)	% Diff From 37 element
	Reference	Rodded		
37 element CANDU	1.35771	1.29928	33.12	0.0
43 element TRUMOX	1.31103	1.25438	34.45	4.02

The difference in reactivity change for the inclusion of the BNA using the 43 element TRUMOX bundle produces a smaller increase of only 4.02% due to the fact that there is more fissile content in the TRUMOX-45 fuel that must be offset and the harder spectrum dilutes the flux displacement effect. Overall, the 43 element TRUMOX bundle fuelled with TRUMOX-45 has a 54% lower reactivity change than the standard 37 element NU case (34.45 mk vs. 74.79 mk).

As with the investigation in to the effects on CVR, it should be noted that reactivity change due to absorber insertion is not always comparable as an absolute measure. When comparing between different fuels the reactivity change should be expressed with respect to the delayed neutron fraction, β. This is a measurement of the reactivity required for the reactor to reach prompt criticality. The relative worth or "dollar value" of an absorber is the absolute reactivity change divided by the β for the specific fuel design, (Δρ/β). The end objective of the device is to control reactivity which changes on the order of β essentially factoring in the "time" for the device to take effect. This is useful when comparing different fuel compositions and bundle types.

Given the fresh fuel delayed fraction values, $\beta_{NU} = \beta_{SEU} = 6.82$ mk and $\beta_{TRUMOX-45}$ = 3.30 mk the dollar values of the stainless steel absorber for the different fuels in the 37 element bundle (Table 4.10) are as follows. 37 element NU = \$10.97, 37 element TRUMOX-45 = \$10.04. Therefore, the relative dollar value only decreased by 8.5% rather than the 55.7% seen in the absolute reactivity changes described above. Thus the full difference between the 37 element NU fuelled bundle and the 43 element TRUMOX bundle fuelled with TRUMOX-45 fuel is a 4.8% decrease in relative reactivity change (\$10.44 for TRUMOX-45 vs. \$10.97 for NU). The differences are caused by the higher fissile content and harder neutron spectrum but the overall difference in reactivity change between the two fuels is small meaning that an NU control system should be able to handle a TRUMOX fuel design. There are many interacting factors that affect reactivity changes and their impact on reactor operations.

4.1.8.2 Detailed investigation of effects on reactivity change

Further examination of the effects of actinide based fuels on the interaction of control devices with the lattice cell is performed using a detailed comparison between a 37 element NU fuelled system and a 43 element TRUMOX bundle (BNA included) fuelled with TRUMOX-30 (3.1% Actinides) for the interaction of an actual CANDU stainless steel adjuster rod. The simulations are again done with 3D super-cells in the DRAGON transport code. Unlike the preliminary investigation performed in the previous section, this detailed comparison is made at several stages throughout the burnup cycle of the two fuels to show the effect of fuel burnup on the reactivity changes resulting from adjuster insertion (within a guide tube).

The control device utilized in these trials is a standard CANDU-900 type stainless steel adjuster. It is a pin in tube design with both components made of 304L stainless steel alloy with a composition as described in Table 4.13. The solid pin is has a 0.8 cm radius and is held inside the 3.8 cm outer radius tube that is 0.124 cm thick. The tube is open at both ends allowing moderator to fill the inner gap and surround the solid pin. The adjuster assembly (pin and tube) is moved within a perforated zirconium guide tube that is fixed within the core.

Table 4.13: Composition of CANDU-900 stainless steel adjuster (detailed trial).

Material	wt %	Material	wt %	Material	wt %
C	0.037	Si	0.460	Mn	1.282
Fe	72.671	Ni	8.430	Cr	17.120

The 3D incremental cross section simulations consisted of a simulation with the rod fully inserted and with the rod fully extracted. The perforated zirconium alloy guide tube is present in both models. The k-infinity values for the rod in and rod out models and the associated reactivity changes for both the NU and the TRUMOX-30 fuels are provided in Table 4.14 and the reactivity change over the burnup is graphed in Figure 4.27

Table 4.14: Effects of Burnup on Super-cell Reactivity Change from Adjuster Rod Insertion.

Natural Uranium Fuel				
Burnup (MWD/T)	*Rod out k-infinity*	*Rod in k-infinity*	*Reactivity change (mk)*	*$\Delta\rho/\beta$ ($)*
0	1.110372	1.04895	52.7	7.23
1760	1.068021	1.013743	50.1	8.41
3680	1.040618	0.989219	49.9	9.36
4480	1.027027	0.97665	50.2	9.81
7520	0.975944	0.928873	51.9	11.71
9120	0.952263	0.906633	52.9	12.77
TRUMOX-30 Fuel				
Burnup (MWD/T)	*Rod out k-infinity*	*Rod in k-infinity*	*Reactivity change (mk)*	*$\Delta\rho/\beta$ ($)*
0	1.258476	1.217424	26.8	7.33
4480	1.142152	1.104555	29.8	7.96
9120	1.077236	1.040713	32.6	8.54
13600	1.017082	0.98161	35.5	9.21
20640	0.932344	0.898479	40.4	10.44
27680	0.863062	0.830615	45.3	11.93

There are distinct differences in the reactivity changes for adjuster insertion between the NU and TRUMOX-30 fuels over their burnup cycles. The reactivity change for NU decreases initially and then after a flat period begins to linearly

increase as the middle of the burnup cycle is reached. The range of NU reactivity change is small (~3 mk) over the entire burnup cycle. The reactivity change of the adjuster rod in TRUMOX-30 fuel undergoes a linear increase throughout the full burnup cycle that increases from 26.8 mk to 45.3 mk, a range of 18.5 mk. For a comparison of the reactivity change at the same burnup the TRUMOX-30 fuel is consistently lower: 50% less for fresh fuel, 41% less for 4480MWD/T and 38% less at 9120 MWD/T.
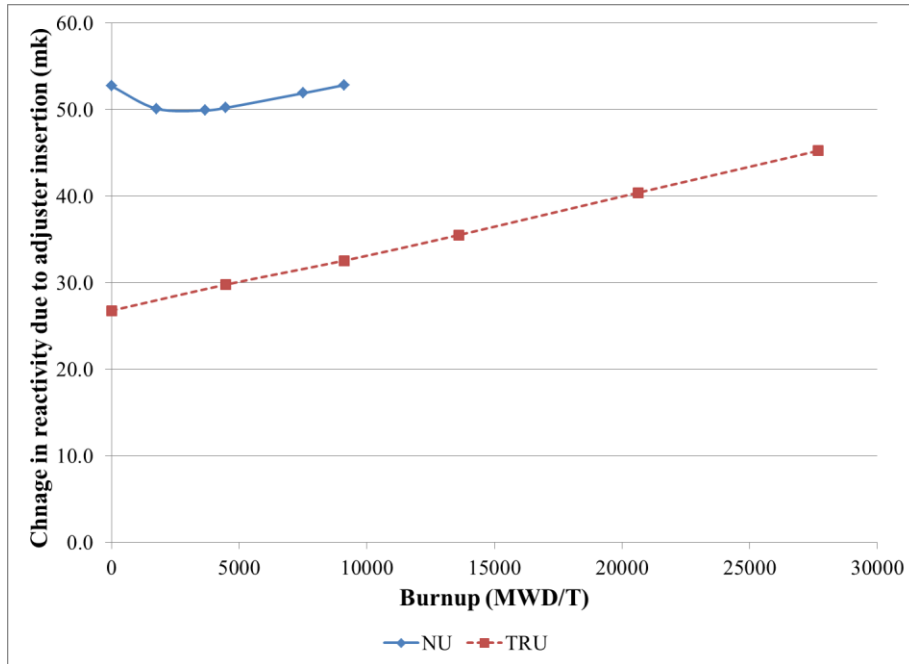
Figure 4.27: Effects of fuel burnup on reactivity change due to rod insertion for NU and TRUMOX-30.

In TRUMOX, the larger fission content and lower amount of U-238 means that transmutation to Pu-239 has less effect on the fission content and the Pu-239 and U-235 content decreases continuously during burnup (see Figure 4.2). The ratio of Pu-239 to U-235, the two primary fissile elements in the fuels, is a driver of the differences in reactivity change during rod insertion for the two fuels. In the NU case the ratio increases exponentially as the initial concentration of Pu-239 starts at zero and builds as the U-238 in the fuel is transmuted to Pu-239 causing the ratio to increase from zero to a ratio of about 1.53 at the end of the NU burnup cycle. Alternatively, the TRUMOX fuel begins at 2.44 and dips downward to 2.24 at 11,400 MWD/T then rises back up to 2.44 at 21,000 MWD/T and

continues to rise during the next 6,500 MWD/T to 2.98 and reaches 3.28 at 30,000 MWD/T, the approximate end of the TRUMOX burnup cycle. This difference in Pu-239 behaviour explains the more constant nature of the reactivity change for the TRUMOX fuel and the initial dip seen at low burnup levels for the NU fuel.

Additionally, the rod effectiveness at a fixed burnup is reduced for TRUMOX because of its harder neutron spectrum (due to the higher plutonium and minor actinide content, discussed in Chapter 4.1.2). The harder spectrum reduces the strength of the adjuster rod due to the 1/velocity nature of the absorption cross section for Fe-56, the main component of stainless steel (as discussed in Chapter 4.1.8.1). The largest difference between NU and TRUMOX occurs for fresh fuel as the differences in both plutonium content and the spectrum are largest here.
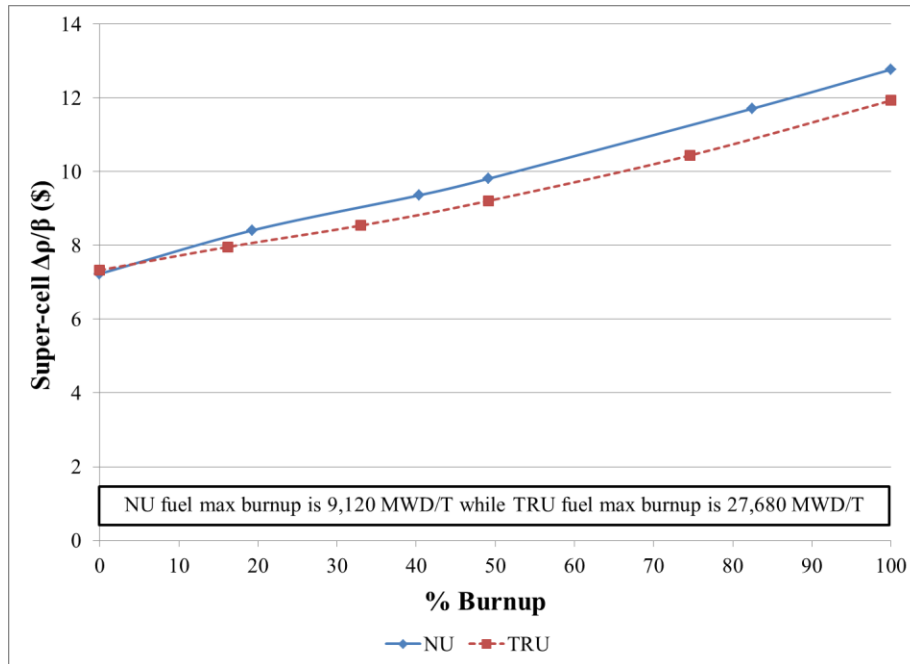
Figure 4.28: Effects of fuel burnup on relative reactivity change $(\Delta\rho/\beta)$ for NU and TRUMOX-30.

Using the β values computed in Chapter 4.1.4, the relative reactivity change, $(\Delta\rho/\beta)$, was computed for each of the burnup steps. Comparing $(\Delta\rho/\beta)$, the two fuels show different results for a specific burnup with the TRUMOX being 1.38% higher for fresh fuel, 18.9% lower at 4480MWD/T and 33.1% lower at 9120 MWD/T. In order to assess these differences further, the results are also compared

at similar relative burnup (fraction of burnup relative to end of cycle discharge burnup) in Figure 4.28. Both fuels experience a generally linear increase from about $7 to $12-$13 at the end of burnup. The dollar values for TRUMOX are 1.38% higher than NU for fresh fuel, 6.12% lower at the mid burnup stage and 6.58% lower at the end of burnup.

A comparison of the infinite lattice reactivity worth of the liquid zones was also made at mid burnup for the two fuels and showed similar results. The reactivity change between a simulation with the liquid zone filled with the helium cover gas and filled with water was measured for a CANDU 9 core configuration with both the 37 element NU fuel and the 43 element TRUMOX-30 fuel. The results for the three liquid zone types (see Chapter 3.3 for a description of the liquid zones) are provided in Table 4.15. The absolute reactivity change from filling the zones with water for both fuel types is different but including the delayed fraction results in similar dollar values for each zone. The dollar worth of the NU fuel is 2.1% to 7.5% higher than the TRUMOX value which is in line with the 6.1% seen at the mid-burnup stage for the adjuster rod.

Table 4.15: Liquid Zone Infinite Super-cell Reactivity Change

Liquid Zone	Mid-Burnup NU		Mid-Burnup TRUMOX-30	
	Reactivity change (mk)	$\Delta\rho/\beta$ ($)	Reactivity change (mk)	$\Delta\rho/\beta$ ($)
LZCR 1	92.04	17.99	66.23	17.17
LZCR 2	103.05	20.15	71.93	18.64
LZCR 3	79.95	15.63	59.05	15.31

Despite significant differences in the two fuel types, their relative reactivity performance is quite comparable over their burnup cycle. This suggests that the current NU control system would be able to continue to be used with the TRUMOX-30 fuel with minimal changes to the physical system and/or operational procedures. This is an important issue when considering the use of TRUMOX fuel in an NU CANDU system as modifications to the reactor design are complicated and can be costly.

4.1.8.2 Detailed investigation of effects on incremental cross sections

The comparison between the 37 element NU fuelled bundle and the 43 element TRUMOX bundle fuelled with TRUMOX-30 also included the effects of the actinide mixture on the incremental cross sections over the full burnup cycles. The adjuster incremental cross sections are calculated by running a simulation with the adjuster rod fully out and then fully in and then subtracting the 2 group condensed cross sections for the rod out case from the rod in case. The adjuster incremental cross sections examined in these trials include fast and thermal $\Delta\Sigma_{Total}, \Delta\Sigma_{absorption}, \Delta\Sigma_{N-Gamma}$ and $\Delta\nu\Sigma_f$ along with the $\Delta\Sigma_{scatter\ 1\rightarrow2}$ and $\Delta\Sigma_{scatter\ 2\rightarrow1}$. These were computed at several burnup steps for each of the fuel types and are provided in Table 4.16 and 4.17 along with the percentage change of the cross section from the beginning to the end of the burnup cycle.

Table 4.16: Effects of Burnup on Adjuster Incremental Cross Sections (ΔΣ), NU.

Burnup (MWD/T)	GROUP 1 (Fast) – NU FUEL (cm⁻¹)				Down Scatter Gr1 to Gr2
	Total	Absorption	N-Gamma	NU-SIGMA-F	
0	5.55E-04	1.10E-05	1.10E-05	-2.12E-07	-1.89E-05
1760	5.55E-04	1.09E-05	1.10E-05	-2.26E-07	-1.89E-05
3680	5.56E-04	1.09E-05	1.10E-05	-2.39E-07	-1.88E-05
4480	5.56E-04	1.09E-05	1.10E-05	-2.43E-07	-1.88E-05
7520	5.56E-04	1.09E-05	1.10E-05	-2.52E-07	-1.88E-05
9120	5.56E-04	1.09E-05	1.09E-05	-2.54E-07	-1.88E-05
% Change	0.24%	-0.87%	-0.73%	19.77%	-0.54%
Burnup (MWD/T)	GROUP 2 (Thermal) – NU FUEL (cm⁻¹)				Up Scatter Gr2 to Gr1
	Total	Absorption	N-Gamma	NU-SIGMA-F	
0	2.31E-04	2.45E-04	2.42E-04	7.70E-06	4.64E-06
1760	2.47E-04	2.51E-04	2.45E-04	1.49E-05	4.72E-06
3680	2.54E-04	2.53E-04	2.47E-04	1.80E-05	4.72E-06
4480	2.56E-04	2.54E-04	2.47E-04	1.87E-05	4.72E-06
7520	2.60E-04	2.55E-04	2.48E-04	1.99E-05	4.70E-06
9120	2.62E-04	2.55E-04	2.48E-04	2.01E-05	4.69E-06
% Change	13.12%	4.15%	2.56%	161.18%	1.08%

Table 4.17: Effects of Burnup on Adjuster Incremental Cross Sections ($\Delta\Sigma$), TRUMOX-30.

Burnup (MWD/T)	GROUP 1 (Fast) – TRU FUEL (cm^{-1})				Down Scatter Gr1 to Gr2
	Total	Absorption	N-Gamma	NU-SIGMA-F	
0	5.61E-04	1.08E-05	1.09E-05	-2.24E-07	-1.88E-05
4480	5.61E-04	1.08E-05	1.09E-05	-2.21E-07	-1.88E-05
9120	5.61E-04	1.08E-05	1.09E-05	-2.29E-07	-1.88E-05
13600	5.61E-04	1.08E-05	1.09E-05	-2.37E-07	-1.88E-05
20640	5.60E-04	1.08E-05	1.09E-05	-2.47E-07	-1.88E-05
27680	5.60E-04	1.08E-05	1.09E-05	-2.53E-07	-1.88E-05
% Change	-0.23%	-0.21%	-0.10%	13.04%	-0.28%
Burnup (MWD/T)	**GROUP 2 (Thermal) – TRU FUEL (cm^{-1})**				**Up Scatter Gr2 to Gr1**
	Total	Absorption	N-Gamma	NU-SIGMA-F	
0	3.36E-04	2.78E-04	2.66E-04	3.43E-05	4.67E-06
4480	3.31E-04	2.76E-04	2.65E-04	3.21E-05	4.66E-06
9120	3.24E-04	2.74E-04	2.63E-04	2.99E-05	4.64E-06
13600	3.18E-04	2.72E-04	2.62E-04	2.79E-05	4.62E-06
20640	3.09E-04	2.69E-04	2.60E-04	2.52E-05	4.59E-06
27680	3.01E-04	2.66E-04	2.58E-04	2.32E-05	4.57E-06
% Change	-10.20%	-4.16%	-2.87%	-32.32%	-2.26%

For both fuel cases, there is very little change in the group 1 (fast) $\Delta\Sigma_{Total}$, $\Delta\Sigma_{absorption}$ and $\Delta\Sigma_{N-Gamma}$ values with the differences being less than $\pm1.0\%$ and the directions are similar for both with the exception of the $\Delta\Sigma_{Total}$ value which increases by 0.24% in NU but decreases by 0.23% in the TRUMOX case. The $\Delta\Sigma_{scatter\ 1\rightarrow2}$ values for NU and TRU both decrease by a small amount over their burnup cycle with the NU fuel decreasing by 0.54% while the TRU only decreases by 0.28%. The group 1 (fast) $\Delta\nu\Sigma_f$, values both increase with the NU case increasing by 6.8% more than the TRUMOX case.

In group 2 (thermal) the two fuel types have opposite responses, the percentage changes in the NU fuel cases are all positive while the changes in the TRUMOX case are all negative. The behavior over the burnup for the two fuels is very different for the $\Delta\Sigma_{Total}$, $\Delta\Sigma_{absorption}$ and $\Delta\Sigma_{N-Gamma}$ values (Figure 4.29). In the NU case the adjuster incremental values generally increase sharply at the beginning and plateau during the last half of the burnup while the TRUMOX values decrease linearly with burnup. In general, these differences are caused by

the plutonium build up in the NU fuel as the adjuster incremental cross sections tend to follow the Pu-239 concentration during burnup (Figure 4.2). In TRUMOX, plutonium content steadily decreases during the burnup cycle which is reflected in the adjuster incremental cross sections. In the specific case of adjuster incremental cross section for thermal absorption with TRUMOX fuel, the decrease over burnup is driven by actinides with high thermal absorptions that have been transmuted to other isotopes with lower absorption cross sections. Over the full burnup cycle, about 35% of the higher actinides, which have high thermal absorption cross sections, will be transmuted.
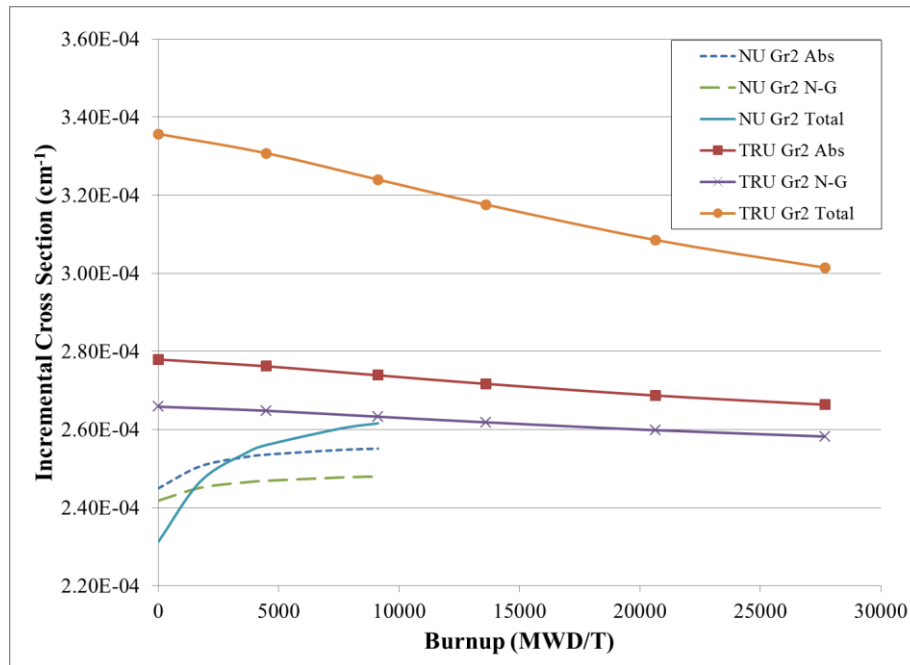
Figure 4.29: Change in Group 2 (Thermal) incremental cross sections over the burnup cycle.

The adjuster incremental cross section for up-scatter in the NU case increases sharply to a maximum in the early burnup, plateaus, and then decreases linearly for the last half of the burnup. In the TRUMOX case, the adjuster incremental up-scatter cross section maintains a steady decline that is less linear than for other values but is still fairly consistent (Figure 4.30). The overall change in up-scatter for the TRUMOX case is a loss of 2.26%. In the NU case the overall change from BOC to EOC is 1.08% while the change from the peak value (occurring at about 40% burnup) is -0.68%. The linear decrease in the NU case during the

second half of the burnup is driven by the fact that plutonium is becoming the dominant fissile isotope in the fuel.
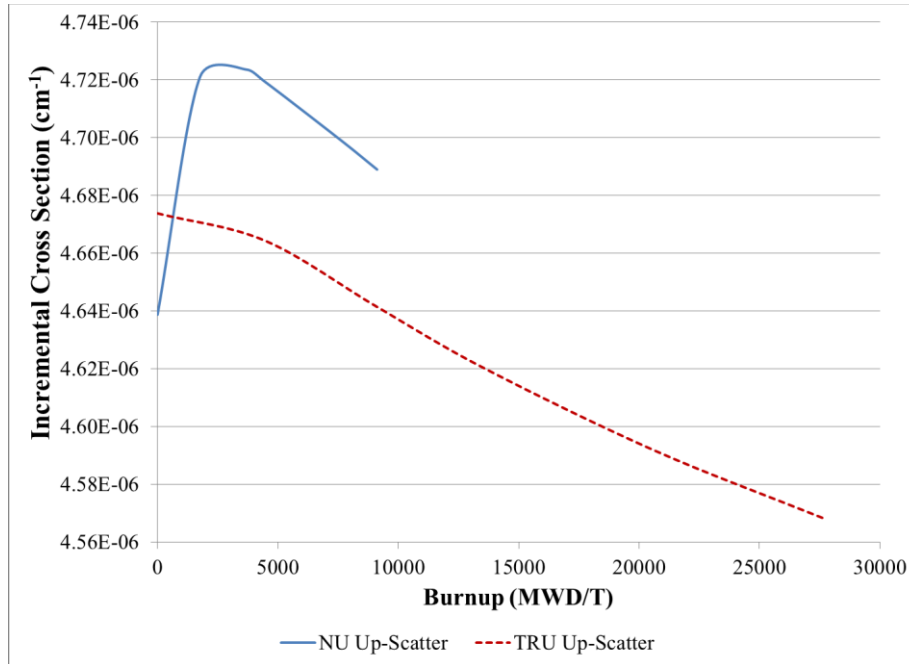
Figure 4.30: Change in the up-scatter incremental cross sections over the burnup cycle.

Comparison between the adjuster incremental cross sections for NU and TRUMOX fuel can also be made either at specific burnup levels or at the relative places in the burnup cycle (e.g. Fresh, mid, end), similar to the comparison from Chapter 4.1.8.1 in Figure 4.28. The percent difference of the adjuster incremental cross section values for the TRUMOX case are computed with respect to those of the NU case for both types of comparisons in Tables 4.18 and 4.19.

The results of the comparisons of the adjuster incremental cross sections for the two fuel types are consistent over the two methods with the mid and end burnup values being larger than the direct burnup numbers due to the larger burnup cycle of TRUMOX. Group 1 (fast) values for $\Delta\Sigma_{Total}, \Delta\Sigma_{absorption}$ and $\Delta\Sigma_{N-Gamma}$ are relatively small (all within ±1.2%) as are the values for down scattering.

In the burnup stage comparison, the up-scatter differences change to -2.1% and -2.6% due to the higher burnup of TRUMOX. Additionally, the group 1 $\Delta\nu\Sigma_f$

value comes closer to NU in the burnup stage comparison by 7 to 9%. The biggest differences from the NU case are in the group 2 (thermal) values for $\Delta\Sigma_{Total}$ and $\Delta\nu\Sigma_f$. The total values have differences as high as 45% for fresh fuel that decrease down to 15% over the burnup cycle.

Table 4.18: Comparison of NU and TRUMOX-30 Adjuster Incremental Cross Sections at Specific Burnup.

Burnup	Gr 1 (Fast) – % diff from NU (TRU-NU)/NU				Down Scatter
(MWD/T)	Total	Absorption	N-Gamma	NU-SIGMA-F	Gr1 to Gr2
0	1.17%	-1.50%	-1.47%	5.57%	-0.52%
4480	0.97%	-0.94%	-1.01%	-9.06%	-0.19%
9120	0.81%	-0.70%	-0.79%	-9.75%	-0.09%
Burnup	Gr 2 (Thermal) – % diff from NU (TRU-NU)/NU				Up Scatter
(MWD/T)	Total	Absorption	N-Gamma	NU-SIGMA-F	Gr2 to Gr1
0	45.15%	13.46%	9.94%	345.20%	0.76%
4480	29.19%	8.92%	7.26%	72.23%	-1.16%
9120	23.86%	7.36%	6.17%	48.71%	-1.01%

Table 4.19: Comparison of NU and TRUMOX-30 Adjuster Incremental Cross Sections at Burnup Stage.

Burnup	Gr 1 (Fast) – % diff from NU (TRU-NU)/NU				Down Scatter
Stage	Total	Absorption	N-Gamma	NU-SIGMA-F	Gr1 to Gr2
Fresh Fuel	1.17%	-1.50%	-1.47%	5.57%	-0.52%
Mid Burnup	0.86%	-1.07%	-1.09%	-2.44%	-0.33%
End of Burnup	0.69%	-0.84%	-0.84%	-0.37%	-0.26%
Burnup	Gr 2 (Thermal) – % diff from NU (TRU-NU)/NU				Up Scatter
Stage	Total	Absorption	N-Gamma	NU-SIGMA-F	Gr2 to Gr1
Fresh Fuel	45.15%	13.46%	9.94%	345.20%	0.76%
Mid Burnup	24.05%	7.15%	6.06%	49.31%	-2.10%
End of Burnup	15.23%	4.41%	4.12%	15.37%	-2.58%
NU Mid Burnup = 4480 MWD/T, NU End of Burnup = 9520 MWD/T					
** TRU Mid Burnup = 13600 MWD/T, TRU End of Burnup = 27680 MWD/T					

The adjuster incremental cross section for group 2 (thermal) $\Delta\nu\Sigma_f$ is very different between the two cases for fresh fuel (345%) due to the much higher fissile content of the TRUMOX fuel which is about 3.5 times that of NU (2.53% vs 0.71%). As the fuel burns, the fissile content decreases explaining the differences between the

specific burnup and burnup stage comparisons. By the time both fuels reach the end of their burnup cycle the difference in the values is about 15% since the TRUMOX fuel has a burnup cycle length that is 3 times as long as NU which utilizes the higher fissile content.

In summary, the incremental cross sections of the adjusters for the two fuels do behave differently over the burnup cycle of the fuels. The NU case shows an increase and then plateau while the adjuster incremental cross sections in the TRUMOX case undergo a continual decline. The main cause for the difference in behaviour is the different plutonium concentrations and build-up in the fuel types during the burnup cycle that alters the neutron spectrum. The NU fuel begins with no plutonium which builds from the transmutation of U-238 to become more than half the fissile content by the end of burnup. In the first part of the NU burnup cycle the Pu-239 concentration builds, adding fissile content to the steadily decreasing U-235 concentration faster than it is burned off producing a reactivity peak at approximately 1,100 MWD/T. From this point on, the reactivity constantly declines until the end of the cycle. The TRUMOX fuel has a much higher fissile content and a lower U-238 concentration and thus this transmutation effect has a lower impact resulting in a more linear reactivity and fissile content that decreases throughout the full burnup cycle.

4.2 Design Considerations

The design considerations for the use of actinide based fuels in CANDU contain several elements that are altered to achieve the design objectives of the fuel. The specific goal of the actinide fuels is to provide a similar operating envelope to NU fuel while maintaining a low coolant void reactivity and maximizing the conversion of actinides in the bundle. The bundle geometry must be compatible with the CANDU fuel channel and suitable for the higher fissile content and burnup of the new fuel. The complementary relationship between the strength of a burnable neutron absorber and the actinide concentration level must be balanced to achieve the maximum actinide conversion given a specific target exit burnup. The burnup target of the fuel is a balance between the actinide transmutation goals and the limitations of the CANDU control devices in maintaining their operation envelope and design. Figure 4.31 shows a flow chart of the design considerations.
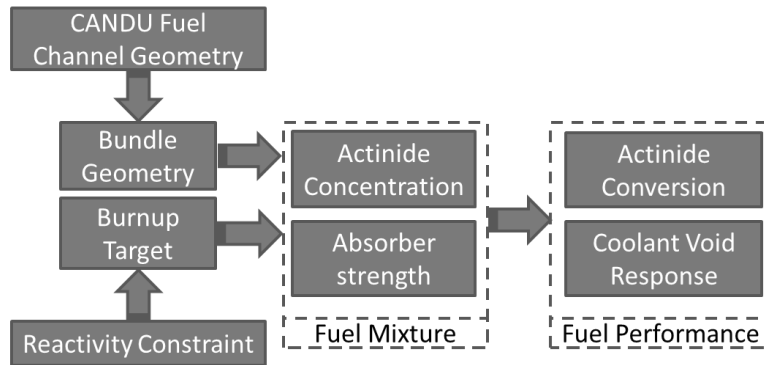
Figure 4.31: Flow Chart of the Fuel Design Considerations

4.2.1 Bundle geometry

The use of an advanced fuel composition may dictate the need for an alternative bundle configuration. The CANDU reactor design utilizes fuels that are of a circular geometry with concentric rings of fuel elements. This general orientation aside, there are several other factors of the fuel bundle design to consider including the number of fuel elements, element diameters, heterogeneity, the inclusion of burnable poisons or water sites and the bundle lengths.

The actinide MOX fuel, as described in the previous sections, has specific neutronics characteristics and thus requires a modified bundle design. Considering the CANDU design constraints it is required that any advanced bundle design maintain the outer dimensions of standard 37 element CANDU fuel (overall diameter ~10 cm, bundle length = 49.53 cm) and the cluster geometry of concentric rings of fuel elements. The lattice spacing is also fixed at the standard CANDU value (28.575 cm). This reduces the design problem to the number of elements in the bundle, their specific diameters, the radial locations of the element rings and the degree of heterogeneity in the bundle.

The number of elements utilized in a bundle is an important design characteristic as it affects the individual element power densities, sub-channel thermalhydraulic geometry and the surface area available for heat transfer. There is a limit to the number of elements due to the overall size of the bundle, the necessary separation and the minimum element diameter possible (from a manufacturing standpoint). Given a fixed bundle power, a larger the number of elements will reduce the

linear element ratings. Actinide based fuels with higher enrichments and plutonium content tend to run hotter than natural uranium fuel and thus benefit from the better heat transfer and lower individual element powers that come with a larger number of fuel elements in the bundle.

The specific element diameter is an important consideration along with the spacing of concentric rings and the number of elements. These factors dictate the sub-channels present in the fuel bundle significantly affecting the thermalhydraulic behaviour of the bundle [65]. Given the diameter constraint of CANDU fuel, in order to increase the number of elements in the bundle the element diameters must be reduced to keep suitable spacing. It is also necessary to determine if different sized elements should be included in the same bundle. Symmetry of the bundle is also important as the bundle orientation in the radial direction cannot be controlled. The bundle heterogeneity involves varied enrichments in each ring, the inclusion of a burnable neutron absorber and the combination of elements of different diameters in a single bundle design. Fuel bundle design is intensive from a thermalhydraulics point of view as the design must ensure that the coolant flow is adequate throughout the bundle sub-channels to properly cool the fuel. The scope of this study was limited to a single fuel geometry design to be evaluated with the TRUMOX fuel.

The 43 element TRUMOX bundle is an evolution of the 37 element design and CANFLEX like designs similar to the SEU-VE bundle described above. The higher fissile content and actinide presence of the TRUMOX fuels required a bundle with more individual elements and thus smaller diameters. The desire to reduce coolant void reactivity also dictated the need to include a burnable neutron absorber in the bundle. The specific considerations of the actinide proportion and the strength of the burnable absorber material are discussed in Chapter 4.2.2. In order to best reduce the CVR of the bundle, the BNA should be located in the centre pin where it is able to counteract the voiding effect and has the least negative effect on the average fuel burnup in the bundle. The bundle design of the 37 element fuel evolved into the 43 element SEU-VE fuel which provided an increased number of elements and the availability to include a BNA. This change in geometry accommodated slightly enriched uranium fuels (1-2% U-235).

The SEU-VE design can be evolved further for use with an actinide fuel such as TRUMOX. The 43 element configuration is satisfactory but changes in certain the element diameters would be beneficial. The centre pin of the SEU-VE design

should be enlarged to provide more room for the BNA. This will help to counteract the high fissile content of actinide fuels designed for high burnup (>20,000 MWD/T). The thicker elements in the second ring are too tight to accommodate a larger center pin and should be shrunk to maintain suitable element spacing and sub-channel size. Therefore, the 43 element TRUMOX fuel design increased the diameter of the centre element and maintained a uniform smaller diameter in all the other 42 elements. This provides the necessary volume for the BNA, the larger sub-channel size for increase heat transfer and reduced manufacturing complexity in that all the elements containing fuel are the same size. The geometry of the 43 element TRUMOX bundle has been adapted from the 37 element design and CANFLEX designs providing a proof of concept design that will be a suitable carrier for actinide mixed oxide fuel.

4.2.2 Actinide and neutron absorber concentrations

The desire to maximize the actinide conversion in the fuel requires the balancing of the concentration of actinides in the fuel and the strength of the burnable neutron absorber present in the fuel. The goal is to achieve the highest actinide for a given burnup/reactivity constraint. This constraint is dictated by the level of fuel activity that the control systems and the operational envelope are capable of handling and is discussed in Chapter 4.2.3. In general, increasing the percentage of actinides in the fuel with a constant amount of burnable neutron absorber material will increase the percentage and quantity of actinides burned over the cycle. Higher actinide content contains more fissile material which results in a higher reactivity fuel with a larger end of cycle burnup level.

The burnup level at the end of life is computed based on an integrated k-infinity value of 1.03 in WIMS-AECL. Integrated k-infinity is an average value that equals the excess reactivity in the core from leakage and absorption in the reactivity devices and other core structures. In an NU CANDU system this value is 45 mk (integrated k-infinity = 1.045) with the adjuster rods inserted in the core [66]. The adjusters are generally worth about 15 mk for NU CANDU [55]. Thus the reactivity corresponding to the prescribed end of cycle for an online fuelled NU CANDU system with the adjusters removed from the core is 15 mk less or k-infinity = 1.03. This value accounts for the leakage and the effects of the in core structures and liquid zone controllers still present in the core.

The TRUMOX fuel, due to the differences in composition and neutron spectrum discussed earlier, will likely have less absorption in the in core structures but higher leakage so the optimal k-infinity value may be different from the NU case. In the interim, for the fuel design studies, the NU k-infinity constraint of 1.03 is being adopted to define the end of the burnup cycle. The actual k-infinity constraint for TRUMOX would need to be computed from a full core simulation that includes the structural material and leakage effects. Thus once the fuel design choice has been narrowed down iteration between the full core model and the lattice model can correct any discrepancy.

The correlation between actinide concentration and end of cycle burnup was explored in a series of 2D WIMS-AECL lattice cell simulations using a 43 element TRUMOX bundle design with full 100% Dy-Zr-oxide BNA in the centre pin and several different actinide content amounts in the fuel, see Figure 4.32.
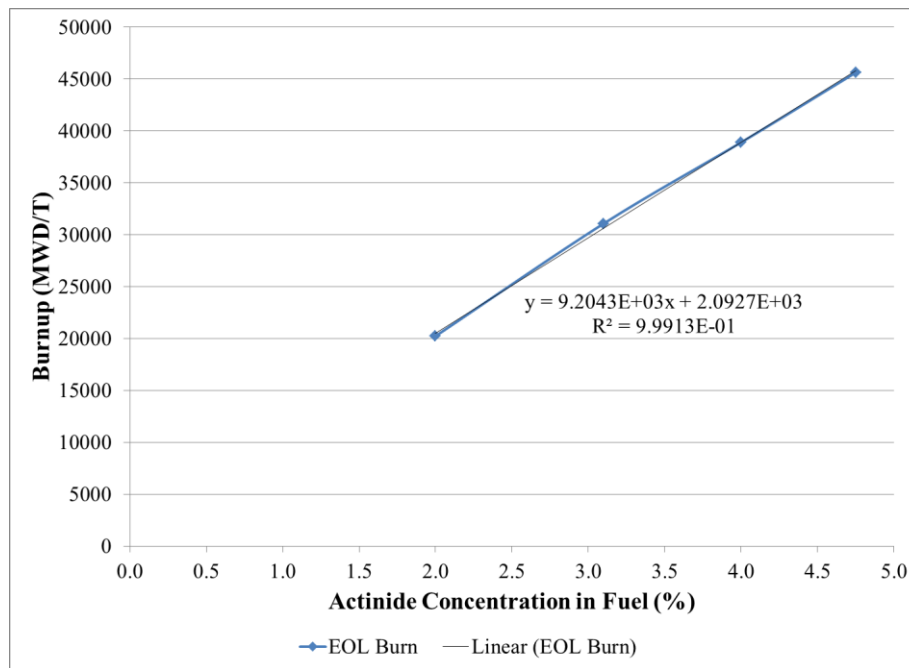
Figure 4.32: End of cycle burnup for different actinide concentrations with a fixed 100% Dy-Zr-O2 BNA in the central element.

The end of cycle (EOC) burnup is linearly dependent on the actinide concentration in the fuel The burnup is as high as 45,635 MWD/T for 4.75% actinide content and as low as 20,231 MWD/T for 2% actinides. The actinide mix

being added to the fuel contains 52.3 wt% fissile material (Pu-239 and Pu-241) compared to natural uranium which has a fissile content of 0.627 wt% (U-235). Thus the addition of the actinide mix increases the fissile content in the fuel by 0.517 wt% for each 1% increase in the actinide content. Since the end of cycle burnup is dependent on the fissile content in the fuel, for a 1% increase in the actinide content the EOC burnup increases by ~9200 MWD/T. The fissile content determines the reactivity of the fuel and thus is what is constricted by the control system capabilities and the desired operational envelope.

For the actinide burning reactor system designed here the desire is to obtain the highest actinide burnup in the fuel considering the other trade-offs discussed above (i.e. the burnup/reactivity constraint). The actinide burnup is tracked for the various actinide contents in Figure 4.33. The actinide burnup follows a second order polynomial curve with the burnup increasing with the higher concentration of actinides. In the portion of the curve near an actinide concentration of 3%, the average change in the conversion ratio is about 1% for every 0.1% increase in actinide concentration or a factor of 10.
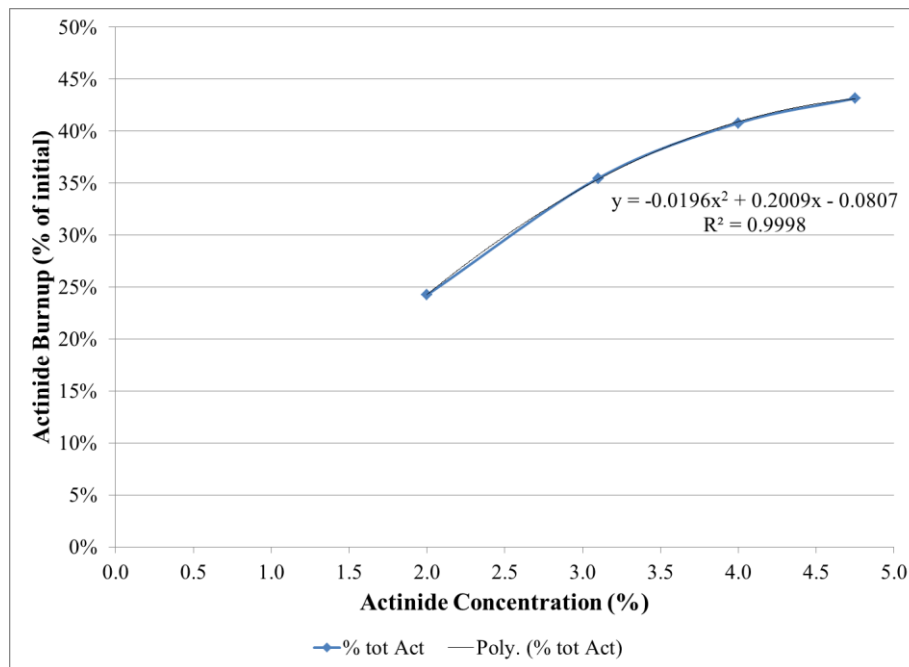
Figure 4.33: Actinide burnup for different concentrations with a fixed 100% Dy-Zr-O2 BNA in the central element.

Therefore, the higher the actinide content the more the actinide burnup ratio and the larger the exit burnup and reactivity of the fuel. The fuel reactivity in these studies was explored with a full strength (100% Dy-Zr-O2) BNA. However, the strength of the BNA will also affect the end of cycle burnup possible and hence the actinide conversion ratio. The desire is to determine the optimal BNA strength given a specific actinide concentration.

The BNA material is a dysprosium-zirconium-oxide mixture (67 wt% Dy_3O_2), which can be mixed with natural uranium or an inert material like more zirconium oxide to achieve a specific absorber strength. The dysprosium absorbs neutrons creating a central flux depression and reducing the CVR of the system. The BNA has a dramatic effect on the CVR of the lattice cell and these effects should be recognized as an additional constraint in this optimization.

The earlier comparison of multiple actinide levels with a constant BNA strength showed the actinide conversion increasing with more actinides in the fuel. The actinide conversion level can also be raised by reducing the parasitic absorption in the lattice cell by reducing the amount of BNA in the center pin. Two methods of reducing absorber strength, diluting with NU and with an inert material (e.g. ZrO_2) were explored in WIMS-AECL 2D CANDU lattice cell simulations with a 43 element TRUMOX bundle fuelled with 3.1% actinide fuel. The two diluting materials have similar effects on the initial fresh fuel reactivity and the ultimate exit burnup of the design as shown in Figures 4.34 and 4.35.

The fresh fuel k-infinity values follow a similar trend in both cases with the NU dilution values slightly below those of the inert dilution. The more diluted the absorber is, the higher the fresh fuel k-infinity due to the decreased parasitic absorption. The effects on fresh fuel reactivity of diluting the central absorber are quite large with reactivity increases of about 0.1 mk for each percent that the absorber is diluted. Therefore, for a 40% dilution (60% black) the fresh fuel k-infinity has been increased by about 0.006 or an increase in reactivity $(1/k_1 - 1/k_2)$ of 3.65 mk in the lattice cell.

The burnup reached at the end of the cycle also increases as the absorber is diluted but the pattern is different depending on the dilution method. As seen in Figure 4.27, inert dilution with zirconium dioxide causes a linear increase in end of cycle burnup which is much higher than that of the NU dilution case. The NU dilution produces a parabolic curve that peaks at 98.4% of the inert dilution value.
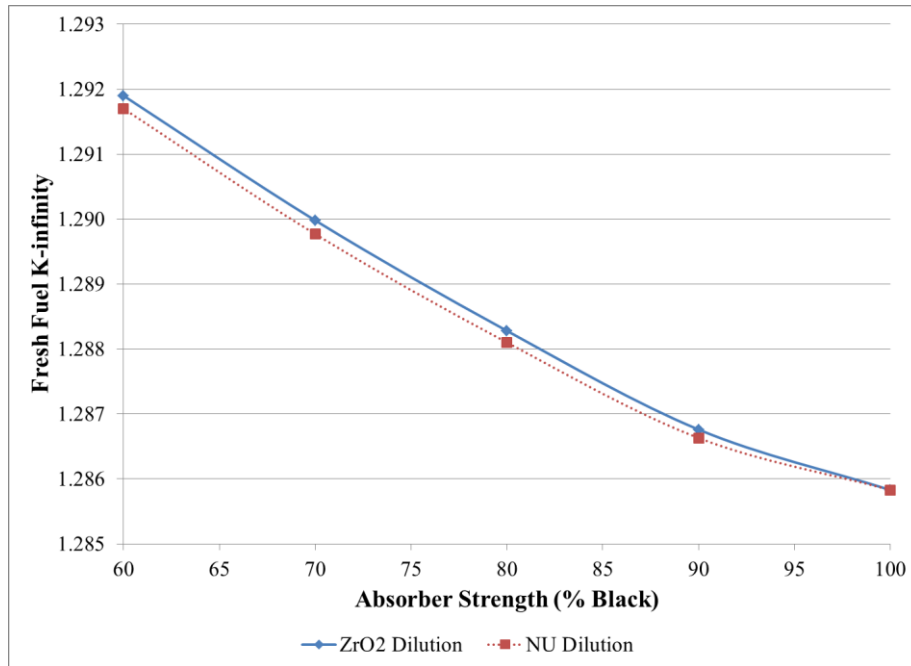
Figure 4.34: Effects of central absorber element strength on fresh fuel k-infinity at a fixed actinide concentration of 3.1%.
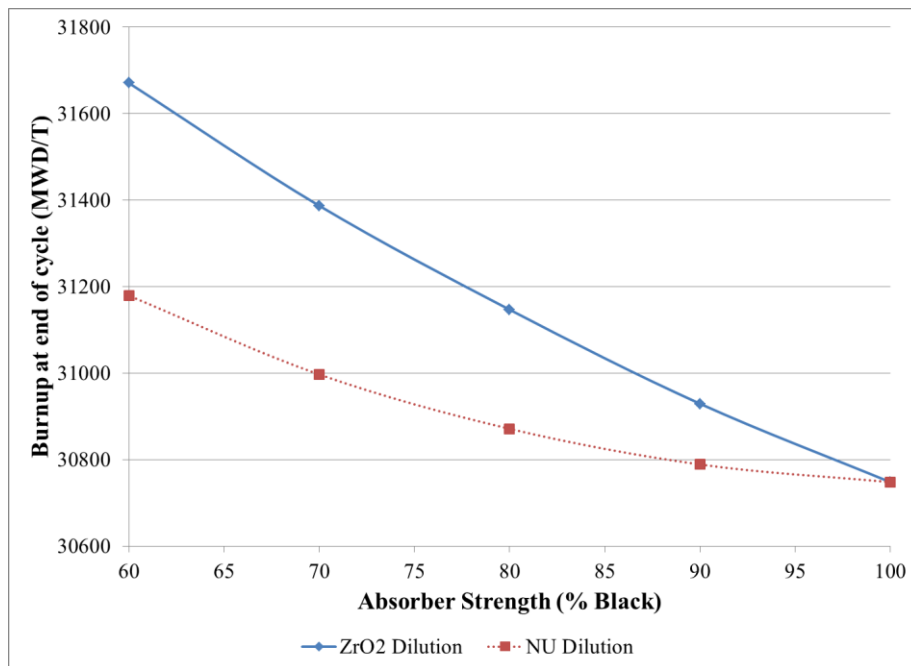
Figure 4.35: Effects of central absorber element strength on end of cycle burnup for a fixed actinide concentration of 3.1%

The inert dilution increases end of cycle burnup by about 23 MWD/T for each % of dilution. The NU dilution increases burnup by about 13 MWD/T for each % dilution. Over the 40% of dilution the inert case increases its end of cycle burnup by 923 MWD/T while the NU case increases by 431 MWD/T, increases of 3.0% and 1.4% in the overall burnup. These burnup increases are small resulting in only minor gains in actinide conversion.

The two dilution methods will reduce the parasitic absorption in the cell to the dysprosium but have different effects on the actinide conversion over the burnup cycle. The dilution of the poison pin with NU adds more uranium to the system which is transmuted into actinides. As a result the actinide conversion percentage is reduced. Diluting with an inert material such as ZrO_2 does not introduce new actinides and therefore the reduction in the parasitic absorption goes directly to increased actinide conversion. These effects are seen in Figure 4.36.
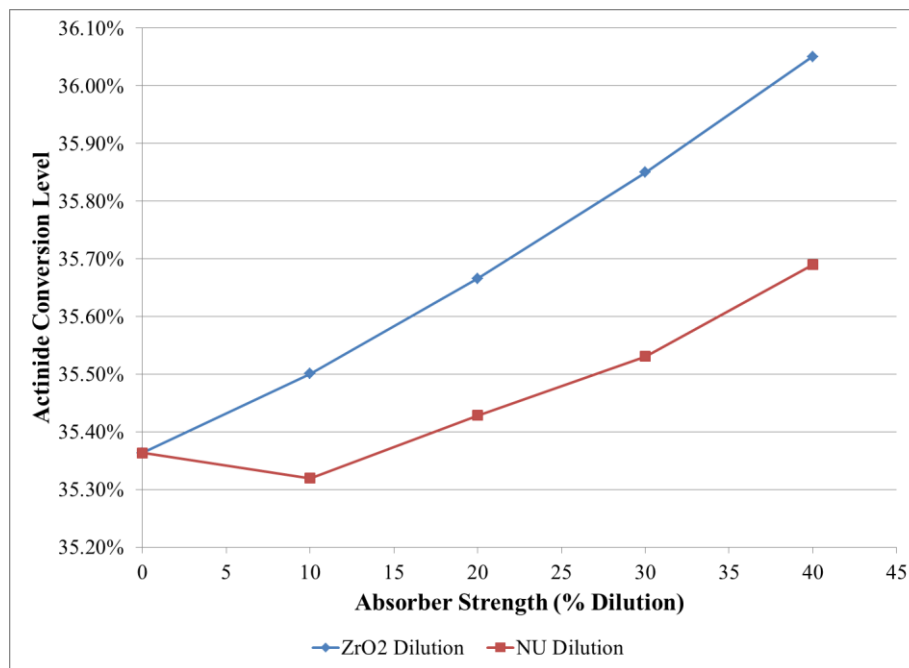
Figure 4.36: Effects of central absorber element dilution method on actinide conversion for a fixed actinide concentration of 3.1%.

In the NU dilution case the actinide conversion ratio decreases by a small amount initially and then increases at about 15% dilution. Over the course of the full dilution (up to 40%) the NU case only gains about 0.33% in actinide conversion

while the inert case gains about 0.69%. In both cases, the gains in actinide conversion are relatively small so the benefit is minor relative to the consequences on the coolant voiding behaviour of the system as discussed below.

The effect of the dilution methods on coolant void reactivity in the lattice cell is shown in Figure 4.37. The inert dilution method increases the CVR by 11-20% as the absorber is diluted up to 40%, while the NU dilution is even worse increasing CVR by 12-24% over this dilution range. The NU dilution method has a larger impact on CVR because of the introduction of fuel material into the central pin (NU) rather than an inert filler material. The effects on CVR are 0.008 to 0.012 mk for each percent that the absorber is diluted. While this is small, in order to gain a 0.1% increase in the actinide conversion ratio the central absorber would need to be diluted by 6% with the inert material causing an increase of 0.048 mk or 1.6% in the CVR of the fuel. Thus the gains in actinide burnup from BNA dilution are overshadowed significantly by the drawbacks of increased CVR.
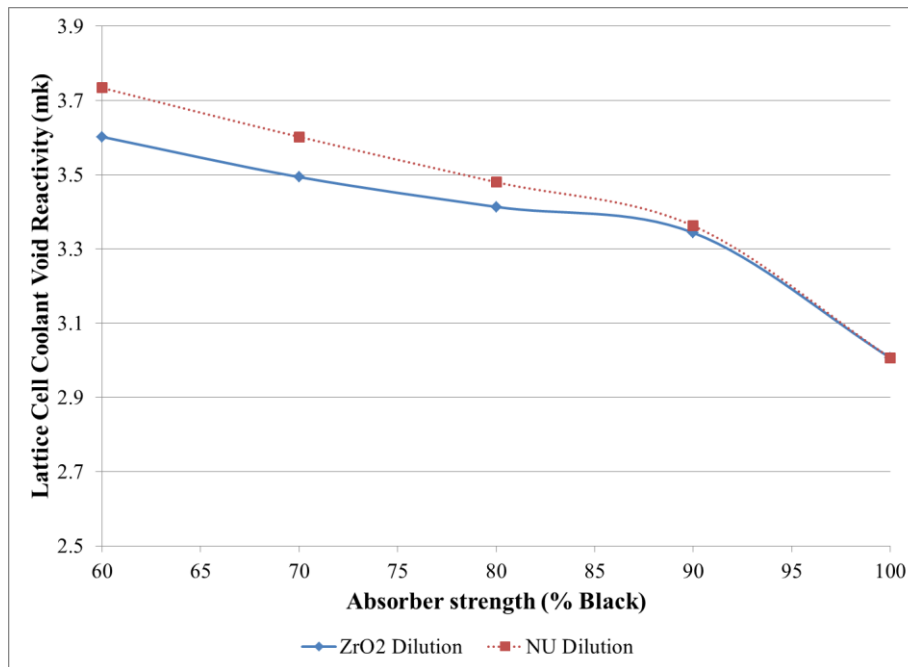
Figure 4.37: Effects of BNA dilution on coolant void reactivity.

As discussed above diluting with NU is less effective than using an inert material such as ZrO_2. The inert dilution has better results for actinide conversion ratio, end of cycle burnup and less effect on the coolant void reactivity of the cell.

However, even with an inert dilution method, the very small gains in actinide conversion from diluting the central absorber change the CVR making dilution of the absorber an ineffective choice. It should be noted that in order to accurately meet the desired fuel reactivity and exit burnup level the actinide concentration and the absorber dilution would have to be considered as part of a larger optimization study.

The initial case of the full strength (100% Dy-Zr-O2) central absorber rod (no dilution) required an actinide concentration of 3.1% to reach the desired exit burnup at the end of cycle of 30,748 MWD/T and had a fresh fuel k-infinity of 1.28583. In order to achieve a similar end of cycle burnup level and fresh fuel k-infinity the actinide concentration would have to be lowered as the central absorber is diluted to maintain the cell reactivity.

For example, with a dilution of 20% to the central absorber (80% Black) the actinide concentration would need to be lowered to 3.01% (a reduction of 0.09%). The resulting fresh fuel k-infinity of this configuration is 1.28568 (a difference of -0.09 mk). The burnup at the end of cycle is a bit smaller at 30, 309 MWD/T a reduction of 439 MWD/T or 1.43% from the reference case. The necessary reduction in actinide concentration reduces the conversion ratio which comes out 0.37% lower than the reference.

Therefore, the savings in parasitic absorption from the dilution of the absorber are outweighed by the losses due to the required reduction in actinide concentration to maintain the fuel reactivity. The losses in actinide conversion are minor but as discussed, the dilution of the absorber has a large effect on coolant void reactivity driving it up by 0.295 mk or 9.8% resulting in a less controllable system. Table 4.21 displays the relevant values for the reference and composite case described.

The simulations and analysis performed lead to the conclusion that to achieve the highest actinide conversion ratio, the fuel design should have the highest actinide content possible (given the reactivity and burnup constraint) and should utilize a central absorber with no dilution since the penalties incurred from a strong absorber are still more favorable than the results of dilution. The burnup reactivity target is defined based on the reactor control system capabilities and the desired operational envelope of the fuel as discussed in Chapter 4.2.3 below.

Table 4.20: Comparison of the reference and Composite fuel designs.

Value	Reference*	Composite**	Difference
Absorber Dilution (%)	0	20	20
Actinide Concentration (%)	3.10	3.01	0.09
EOL Burnup (MWD/T)	30748	30309	-1.43%
Fresh Fuel k-infinity	1.28583	1.28568	-0.01%
Actinide Conversion (%)	35.36%	35.00%	0.36%
Coolant void (mk)	3.01	3.30	9.80%

Actinide concentration of 3.1% with no dilution of the BNA.

** Actinide concentration of 3.01% with a 20% inert dilution of the BNA.

4.2.3 Burnup target

The specific burnup target of the fuel is, as discussed in the previous section, a balance between the desire to maximize the actinide burnup and maintain the fuel reactivity within the limits of the control system and the desired operational envelope[6]. The evaluation of the acceptable fuel reactivity is complicated and actually requires full core analysis to ensure that the design constraints such as zone level response, maximum channel and bundle powers and fuel power ramp rates are properly met. As a result there is an iterative component that requires the fuel be designed, modeled in the full core and then possibly altered to better the performance of the control devices in the core. This change in the fuel composition is a global change that has a core wide effect. Within the context of full core implementation, the channel specific target exit irradiations (or region specific sizes and targets) can also be adjusted so as to maintain an acceptable result. For example, spatial power tuning is accomplished by altering the region definitions, irradiation levels and the fuelling scheme for the channels in the core.

The iteration between the lattice calculations and the full core simulations can be classified as minor and major.

- The minor iteration step can occur when the activity of the fuel is too much or too little to satisfy the time-average diffusion solution or the

---

[6] For example, too high a fissile content may make online fuelling difficult or impossible as the capabilities of the liquid zone controllers could be exceeded or the fuel power ramp rates may become too high.

associated instantaneous simulations. This requires an alteration to be made in the enrichment of the fuel design (in the case of TRUMOX this means altering the amount of actinide mix in the fuel). Changing the fuel enrichment is a last resort after all the degrees of freedom in the full core simulations such as adjustment of the target exit irradiations or average zone level. This is the "minor" iteration as the alterations are usually small for this case and the result of a miscalculation in the enrichment level needed to produce the desired burnup or from excess leakage in the full core model that is not accounted for in the infinite lattice simulation[7].

- The major burnup target/reactivity iteration is related to the ability of the reactor control system to handle the fuel reactivity. This usually requires a larger change in the fuel enrichment (actinide content) and burnup target to ensure the fuel does not exceed the operational capabilities of the control systems. Details of the reactor control system and fuel loading modelling and how they impact the fuel design iteration are discussed below.

The reactor control system response to the new fuel design is evaluated utilizing full core diffusion simulations of common events such as fuelling. Since CANDU uses online fuelling to maintain the reactivity in the core, the fuelling of channels is a daily occurrence and the control systems must be able to handle the reactivity transients associated with fuelling operations. The fuelling of a channel will cause the liquid zone controller levels to fluctuate in the area of the fuelling and throughout the core. If the fuel is too active, the liquid zones will exceed their operational envelope and begin to get close to the maximum and minimum fill limits in the individual zones. Other considerations involve the limits on maximum bundle and channel power and reactivity ramp rates. Thus while the minor iterations are usually small changes in fuel composition to align with a specific burnup target the major iteration step has to do with aligning the specific fuel reactivity with the capabilities of the reactor control system. The lattice cell simulations and super-cell models do provide some insight into the effect the fuel may have on the control systems but the actual performance is only accurately modelled with the full core simulations that account for the fuelling of channels.

---

[7] In particular, since the lattice calculations assume the criticality to be k-infinity of 1.03 based on CANDU NU fuel, the different composition of the TRUMOX may require changes in the amount of excess reactivity that may be needed due to differences in leakage or absorption effects.

Initial studies with the TRUMOX type fuel used a mixture designed for a burnup of 45 MWD/kgHE. This fuel, referred to as TRUMOX-45 and described earlier in Chapter 4.1, contained a mixture of 4.75% actinide oxides and 95.25% natural uranium oxide [41]. These studies were performed with the CANDU 6 reactor system and the reactor control systems were found to be stressed during fuelling events and tended to exceed the limits of the desired operational envelope. A further study compared TRUMOX-45 fuel to a less reactive design with 3.1% actinide oxides and a burnup target of 30 MWD/kgHE called TRUMOX-30 [67]. This study showed that the TRUMOX-30 fuel was much easier on the CANDU 6 reactor control system and was ultimately more controllable. Since the CANDU 6 and CANDU-900 have similar control systems and operation envelopes, the TRUMOX-30 fuel was utilized as the fuel design in the current studies of actinide mixed oxide fuel in the CANDU-900 reactor. The burnup target/reactivity goal is first defined as a reactivity limit based on the control system, in this case as the TRUMOX-30 fuel, and then can be adjusted slightly (<0.2% changes to the actinide content) to align with the actual burnup target for the full core simulation that includes leakage.

4.3   Fuel Design and Lattice Modelling

The final fuel design utilized for the actinide based mixed oxide fuel TRUMOX in the CANDU reactor system was modelled as per the standard methodology described in Chapter 3.2. The standard CANDU lattice cell was utilized in conjunction with and advanced 43 element TRUMOX bundle design. The fuel design takes neptunium, plutonium, americium and curium, extracted from 30 year cooled spent LWR fuel and blends them with natural uranium. The fuel, referred to as TRUMOX-30, blends 3.1 wt% actinide mix with 96.9 wt% natural uranium to meet a burnup target of 30 MWd/kgHE, 3 times the burnup level of standard natural uranium fuel in the CANDU-900 (~9.0 MWd/kgHE). The actinide mixture composition is based on data from Oak Ridge National Laboratories that predicts the probable yields of actinides from spent fuel reprocessing [26] and was provided in Table 4.1 in Chapter 4.1.1.

The burnup target of the fuel is designed to provide an acceptable level of actinide conversion while not having too much reactivity in the fuel such that it exceeds the capabilities of the reactor control system and operational constraints.

The 2D infinite lattice modelling and simulation was performed using the WIMS-AECL v3.1.2.1 [48] multi-group neutron transport code with the ENDF/B-VI library modified with patches for dysprosium (a burnable neutron absorber) and curium (a minor actinide). The bundle design utilized is a 43-element bundle with mixed actinide fuel in all elements except the center pin which contains a burnable poison that is used to reduce coolant void reactivity (CVR) effects. The fuel bundle design is the 43 element TRUMOX bundle described in Chapter 4.1 and is based off of the 43-element CANFLEX design with dysprosium burnable neutron absorber in the central element. The composition of the burnable neutron absorber is described in Table 4.21.

Table 4.21: Dysprosium zirconium BNA composition.

Dysprosium Zirconium Oxide		
Isotope	**Type**	**Wt %**
Dy-160	Absorber	1.346
Dy-161	Absorber	10.943
Dy-162	Absorber	14.858
Dy-163	Absorber	14.597
Dy-164	Absorber	16.633
Zr-90	Zr Mix	12.388
Zr-91	Zr Mix	2.732
Zr-92	Zr Mix	4.221
Zr-94	Zr Mix	4.371
Zr-96	Zr Mix	0.719
O-16	Oxygen	17.192

The bundle design has one thick central pin and 42 smaller elements of the same size. The central pin is about 1.5 times thicker than the other pins which are arranged in three rings of 7, 14 and 21 elements around the central pin. The central pin poison diameter is 17.4 mm (16.38 mm poison diameter and 0.523 mm clad thickness) and the fuel pin diameter is 11.4 mm (10.7 mm fuel diameter and 0.323 mm clad thickness). The bundle arrangement was depicted in Figure 4.1.

The WIMS-AECL transport models used 89 energy groups with a meshing of 53 lines and 11 angles within the calandria tube [48]. The numerical accuracy of this meshing was explored and for meshing from 50 to 5000 lines and 11, 13, 23, and 31 angles, the k-infinity value stays within 0.80 mk of the original mesh.

The TRUMOX-30 fuel design has a heavy element fissile content of 2.53% compared to 0.711% for natural uranium fuel. The mass of fuel in each bundle is 19.719 kg, contained in the outer three rings, and the centre pin contains 741 g of Dy-Zr-oxide (67% Dy_3O_2) burnable neutron absorber. The mass of heavy elements per bundle is 17.383 kg. In comparison a 37 element NU bundle has a fuel mass of about 22.61 kg and a heavy element mass of 19.93 kg. The specific lattice properties used are detailed in Table 4.21.

Table 4.22: Specific lattice properties for WIMS-AECL and DRAGON simulations, TRUMOX-30 in CANDU-900.

Property	Value
Coolant density (g/cm^3)	0.8074
Coolant Temperature (°C)	288.13
Coolant Purity (% D_2O)	98.764
Average Moderator Density (g/cm^3)	1.0887
Moderator Temperature (°C)	63.00
Moderator Purity (% D_2O)	99.918
Fuel Temperature (°C)	586.83
Fuel Density (g/cm^3)	10.5419
Fuel volume per bundle (cm^3)	1870.57

The final reactor design chosen was the standard 900 MWe heavy water moderated CANDU type reactor (CANDU-900) [68]. The full core is fuelled with the TRUMOX-30 fuel bundles. Previous studies in the CANDU-6 reactor have been successful in determining the feasibility of utilizing a TRUMOX type fuel [41] and further efforts investigated the operational properties and behavior of TRUMOX fuel in the larger CANDU-900 system [42, 43]. The standard 900 MWe CANDU design has an 8 m diameter calandria, 6 m long fuel channels, 24 adjusters and 480 fuel channels. The control systems include 14 light water liquid zone controller zones, the adjusters, 4 mechanical control absorbers and 32 shutdown system #1 rods. These control devices were modeled with the TRUMOX-30 fuel using 3D super-cells using the methodology described in Chapter 3.2.

The super-cell calculations are performed in the DRAGON 3-D transport code with all the relevant control devices using the ENDF/B-VII library [49]. The 3D

super cells simulations are performed with the control devices at 0% and 100% inserted and the 2 group homogenized cross sections are computed. The incremental cross sections of $\Delta\Sigma_{Trans}, \Delta\Sigma_a, \Delta\Sigma_{s\,1\rightarrow2}, \Delta\Sigma_{s\,2\rightarrow1}\ and\ \Delta\nu\Sigma_f$ are computed for both the fast and thermal energy groups. The 3-D models use a tracking mesh of 12 angles and 20 lines/cm^2. The self-shielding is performed in 2-D with similar meshing of 12 angles and 20 lines/cm. The numerical accuracy of the lattice cell meshing was evaluated in a similar manner to the WIMS-AECL cases and k-infinity value was maintained within 0.65 mk of the original value. The 2-D simulation uses full cluster geometry while the 3-D geometry is defined using annular fuel rings that preserve sheath and fuel volume as previously described in Chapter 3.2. The super-cell calculations were performed with mid-burnup TRU-30 fuel which represents the control device interaction in a full core situation best. These incremental cross sections are supplied to the diffusion simulation along with the cross sections generated by WIMS-AECL to produce the full core model.

The burnup target of 30 MWD/kgHE is a compromise to balance a suitable level of actinide burnup with a fissile content/reactivity that is controllable. As discussed in Chapter 4.2.3, high fuel reactivity can cause problems with control during fuelling shuffles and excessive amounts of actinides can reduce the effectiveness of the control devices. Additionally, very high burnup levels increase the probability of fuel failure. The burnup of 30 MWD/kgHE has been selected to match expected fuel utilization in Generation III+ designs such as the Advanced CANDU reactor (ACR-1000), [69]. The TRUMOX fuel is more reactive than natural uranium with about 3.5 times the fissile content and 3 times the burnup (in CANDU-900). The mean CVR target for this study is < +5 mk (Note: 1 mk = 100 pcm = 0.001 Δk/k) and the power limits are 935 kW/bundle and 7.3 MW/channel (operational limits for CANDU-900 type reactors).

The full core modelling of the TRUMOX-30 fuel design in the CANDU-900 reactor system, fully described in Chapter 5, utilized the RFSP-IST v3.04 2-group neutron diffusion code [54]. The inputs of the lattice cell macroscopic properties were taken from the WIMS simulations and the 2 group incremental cross sections for the control devices came from the DRAGON simulations. WIMS-AECL, DRAGON and RFSP are part of the industry standard toolset (IST) for reactor analysis in Canada [70].

The lattice cell modelling was qualified to ensure an accurate representation that yielded appropriate results. The WIMS-AECL models for the TRUMOX-30 fuel were originally developed with AECL and have been benchmarked off of a similar TRUMOX design with a common bundle configuration and similar compositions for the components of the fuel and lattice cell (e.g. actinide mix, NU composition, clad, coolant and moderator). Thus the TRUMOX models were well qualified with the previous data. The WIMS-AECL models for natural uranium utilized the same lattice cell properties as the TRUMOX models but with a 100% NU fuel composition and a 37 element standard CANDU bundle configuration. The NU fuel composition was the same as that used in the TRUMOX models and the 37 element bundle geometry was taken from literature.

The calculations in DRAGON were built off the WIMS-AECL model information using the same geometry and composition data. Cross code comparisons for 2D lattice cells ensured that the information was correctly transferred. The 3D super-cell calculations were modeled using the standard methods prescribed within the DRAGON manual and by reactor physics personnel specializing in CANDU super-cell calculations at Ontario Power Generation. The 3D super-cell models were evaluated and qualified by comparing the computed NU incremental cross section values to those defined in the full core RFSP-IST model of the NU CANDU-900. Full core time average calculations with both the reference and calculated incremental cross section values were compared to ensure that the super-cell calculations were employed properly and produced suitable values for the 37 element NU fuel case.

The full core RFSP-IST simulations were based off of the standard NU CANDU-900 model and modified for the TRUMOX-30 fuel design. The standard analysis procedures for full core CANDU modeling were followed and comparisons were made with NU simulations throughout the process.

Chapter 5

Full Core Design and Analysis

The majority of fuel design is accomplished using infinite lattice cell simulations, as described in Chapter 4, which designate the material and dimensional properties of the fuel, moderator and coolant. The final phase of the design feasibility assessment is to perform full core simulations to demonstrate the large scale behaviour of the core with the new fuel design. In particular such simulations allow for the determination of leakage, reactivity coefficients, radial and axial core power profiles, fuelling ripples and control device capability. These simulations also allow comparison of the fuel design to the existing 37 element NU fuelled CANDU-900 behaviour. The use of a specific fuel design in a reactor system requires taking into account the full core geometry including various lattice physics results, reflector geometry, reactivity device configuration and other in-core structures and equipment. Thus the full core model is quite detailed and large becoming prohibitively costly, from a computational sense, to apply a transport solution for these simulations.

Therefore, full core modeling and simulations are performed using a diffusion code, as discussed in Chapter 3.5, which models the core using discrete 3D blocks or lattice cells (approximately 7500 blocks in a 100,000 cell meshing for a CANDU-900 core). Each hexahedral lattice block requires information on its location and connectivity to other blocks as well as the neutronics properties (i.e. cross sections) that represent the materials and interactions which can take place within the lattice cell. The lattice cell properties are derived from the neutron transport solutions discussed in Chapter 4, by determining the effective few-energy-group cross sections (2 energy groups in this case) for the lattice cell volume that approximate the reaction rates and neutronic interactions determined in the multi-energy-group transport solutions. This process of determining the few-group volume average cross section is termed homogenization, since it represents an averaging process wherein the neutronics properties of the cell are homogeneous within the cell volume.

The lattice cell transport solutions in Chapter 4 are used to provide the 2-energy group homogenized cross sections for the building blocks used in the full core. As a first approximation, the entire core is modeled by assembling the appropriate lattice cells with no reactivity devices or structural materials and accounting for the local burnup (or depletion) at each fuel location. Subsequently the specific lattice cell locations that contain reactivity devices are then incrementally adjusted to account for the configuration of the device in that cell. The 3D super-cell calculations in Chapter 4 provide the incremental information that dictates how the control devices interact with the base lattice cells.

The reactor model must first be discretized in space including the necessary meshing, control device locations and in-core structures. Following the reactor discretization, the homogenized properties derived from the transport solution of the fuel design must be included in the system as well as the local fuel irradiation expected in each cell (based on the assumed fuelling rates and fuelling shift pattern) and the coolant and moderator properties. The CANDU system uses continuous online fueling rather than the batch fuelling common in light water reactor designs. This allows for fine control of the core radial and axial power shape and fuel burnup through the appropriate selection of the fuelling rates, channel fuelling order and the frequency and number of bundles fuelled at a given time. Therefore, the full core simulation must define the fuelling rate for each channel, the axial shift scheme and the fuelling sequence for the channels during normal operation. After a long period of time and with a high number of fuelling operations the core and its constituent channels will exhibit an average behaviour. Hence the objective of the first stage of full core modeling is to generate these time-average properties of the core. The methodology of the time-average model was discussed in Chapter 3.5.3 and the production of it is detailed Chapter 5.2.

The time-average model is tested and refined by examining the time dependent behaviour of the core. This involves the generation of several full core instantaneous snapshots which represent differing specific core states and burnup levels. The methodology of this instantaneous snapshot analysis is described in Chapter 3.5.4. Each snapshot model provides a set of channel ages (and hence local instantaneous bundle irradiations) for the core. These instantaneous snapshot simulations allow the assessment of the effects of channel to channel interactions and are able to identify possible local hot spots or asymmetries in the core through channel and bundle powers that are not readily identifiable in the time-average examination. Thus the snapshots are used to refine the time-average

irradiation values and region definitions to ensure that the core design remains within a suitable operational envelope. Upon refinement with the snapshots, the time-average reactor core model is fully designed and can be assessed for quasi-equilibrium behaviour and evaluated using operational simulations such as the fuelling of channels.

Once complete, the time-average full core model allows for the examination of the quasi-equilibrium behaviour of the reactor including the assessment of reactivity coefficients, fuel utilization, control device effectiveness, coolant voiding and modal flux behaviour. These characteristics can then be compared to reference cases performed for the 37 element NU fuelled CANDU-900 core. The results of these assessments are presented in Chapter 5.2 to 5.7 below.

The operational simulations involve the selection of a suitable instantaneous snapshot for more detailed fuelling studies. In these studies, the snapshot is an initial condition for the fuelling transient simulation. The diffusion code is used to irradiate the initial condition for a period of time up until the next fuelling operation (typically on the order of hours). A selected channel(s) is then fueled by altering the irradiation profile in the fuelled channel such that fresh fuel with zero depletion is inserted at the beginning of the channel, all bundle irradiations are shifted axially along the channel and the irradiated bundles at the discharge of the channel are removed. Then the entire core is transiently simulated again until the next fueling operation is required. In addition, the reactor control system will adjust the control devices in such a way as to balance core power, flux tilt and reactivity (i.e. the average and local liquid zone controller levels may be altered, modifying the incremental cross sections being utilized by the affected cells by the diffusion code). The selection of the channels for fuelling, burnup time between fuellings and the irradiation shifting within a channel are performed for a short term (~1 day) evaluation (described in Chapter 5.8). The short-term fuelling events are also assessed to determine the fuel ramp rates associated with the transient to determine if there is any increased probability of fuel defects being induced. This ramp assessment is performed in Chapter 5.9. These simulations are important since, due to the higher fissile content, the reactivity changes and required fuelling patterns for the TRUMOX-30 fuel may be significantly different than 37 element NU fuel.

The reactor characteristics are assessed with both the time-average model and more detailed simulations that account for specific properties such as

temperatures and purities of the fuel, coolant and moderator. The evaluation of the reactor coefficients provides useful information on the behaviour of the reactor under a variety of circumstances including coolant voiding. The worth of the specific control devices also determines the capabilities of the reactor design to handle both normal and accident conditions.

A full core model of the TRUMOX-30 fuel in the CANDU-900 reactor was produced for a specific combination of channel regions and irradiation levels. This time-average full core model was subsequently evaluated and assessed following the general procedures for CANDU. The time-average burnup and power distribution characteristics were determined, the worth of the control devices and the reactor coefficients were calculated and the impact of coolant voiding and fuelling was assessed. The results of this evaluation are described in reference [42, 43] and represent a satisfactory configuration of TRUMOX-30 fuel in a CANDU-900. However, in order to demonstrate more realistic behaviour, this design was refined with more rigorous region and irradiation definitions to produce a core with a flatter power profile and higher burnup level. This refined configuration is described and evaluated in the following sections and is an enhanced option for a TRUMOX-30 fueled CANDU-900 reactor system.

5.1 Full core reactor model definition

The full core model is a detailed representation of the actual reactor system assembled from blocks defined by the lattice cell properties. The model includes all relevant control devices, in-core structures and detectors present in the reactor as well as the fuel characteristic, coolant and moderator properties and material temperatures. The modeling done in this study was performed with a detailed full core model of the generic CANDU-900 reactor with no changes to the physical geometry of the system such that the TRUMOX-30 fuel was evaluated for use in existing operating reactors such as Darlington and Bruce Nuclear Power Plants.

The CANDU-900 reactor design was chosen due to its larger core size, higher average burnup (~9.0 MWD/kgHE) and lower leakage than the smaller CANDU 6 reactor. This leads to an increased capability for actinide destruction as demonstrated in Chapter 5.2. There is also extensive experience in operating with no adjusters in the core and controlling the reactor primarily with the liquid zone controllers and fuelling strategy (e.g. the Bruce-A units) [71].

The core was modeled using a 3D cell structure (or mesh) of 50 by 50 by 40 (x, y, z) with an approximate individual lattice size of 14.2875 cm by 14.2875 cm by 12.700 cm. The fuel is arranged in a subset of these volumes with 480 fuel channels in a 24 by 24 lattice with 13 bundles in each channel[8] (resulting in 6240 bundles in the core). The lattice spacing is the standard CANDU value of 28.575cm by 28.575 cm with an axial length of one bundle (49.53 cm). The fuel channel lattice is the bulk of the core model but the necessary structural, control device and detector components are included. Each of the devices, detectors and core structures are located within the relevant mesh cells. The control devices are fully modeled including the drive springs and cabling.

Each of the 480 fuel channels of the CANDU-900 reactor may have a different fuelling rate and fuelling shift scheme. Channels with a similar geographic location in the core and/or a common power level are usually assigned similar fueling rates. The fuelling shift scheme is usually defined for the inner and outer channels in the core and is limited to one or two schemes in the core so as to minimize the possibilities of operator errors during fuelling.

It should be noted that the region definitions and irradiation values are selected in conjunction with each other and there are iterations back and forth between the model definition and irradiation definitions to help refine the time-average power distribution shape.

The specific region definitions used here evolved from a simple two region model with the higher power inner regions of the core in one group and the lower power outer regions in another. This two-region model was modified by subdividing the original inner and outer regions to enhance the capability for flattening and allow refinement of the domed shape. Additionally, regions were created to increase the top-to-bottom and left-to-right symmetry. Symmetrical top and bottom regions were defined to allow different irradiation values which can be used to balance out the differences in the structural materials present in the top and bottom of the core. A region was created on the right edge of the core to account for the asymmetry of the poison injection nozzles of SDS-2 being located in that area. Finally, a small top-center region was created to correct for a depression in the channel powers in that location. These regional subdivisions could conceivably be continued up until all 480 channels have their own region. In this study the

---

[8] Approximately ½ of a bundle (~25 cm) sits outside the active core region at each end of the channel as the fuel string length is approximately 6.5 m while the active core region is 6 m long.

regions were split up enough to account for the major differences in the in-core structures and to provide an acceptable level of flattening.

The axial fuelling scheme is dependent upon the activity of the fuel and the location of the channels in the core. Higher power channels in the inner regions of the core may be unable to accept larger fuelling shifts without stressing the control system or exceeding the power or ramp rate limits. The TRUMOX-30 fuel is much more active than standard NU fuel so smaller fuelling shifts were necessary. The power and ramp rate must be kept beneath the limits and the liquid zone controller system must be able to properly compensate for the reactivity change from fuelling. The axial fuelling scheme was defined based on the channel powers into two regions with the high-power inner area being one region and the lower power periphery channels being the other.

The axial fuelling scheme for TRUMOX-30 was estimated based on the fuelling scheme used in the NU CANDU-900 with the number of bundles per shift scaled down such that the average reactivity insertion for the fuelling was about the same. Based on the fissile content in the TRUMOX-30 fuel being 2.53% rather than 0.71% the reactivity injection difference should be similar for a fuelling. Thus the 4 and 8 bundle shift used in the NU CANDU would be comparable in reactivity injection to a 1 and 2 bundle shift of TRUMOX-30 fuel[9]. Two different axial fuelling schemes are used to ensure that an appropriate amount of reactivity is injected with each fuelling. Fuelling the inner region of the core with a 2 bundle shift would inject too much reactivity in to the region that could exceed the power or ramp rate limits and the capability of the liquid zones. One axial fuelling scheme with the smallest number of bundles (the lowest reactivity injection) could be applied to every channel in the core (1 bundle in the case of TRUMOX-30, 4 in the case of NU) and the fuelling rates could just be adjusted. However, this would increase the number of channel visits required to accomplish the fuelling in the core and may exceed the capabilities of the fuelling machine. For example, using a 4 bundle axial shift scheme in all channels of an NU CANDU-900 would increase the number of channel visits per day by about 9%. Additionally, the use of two different fuelling regions can help control radial flattening in the power distribution.

---

[9] The actual reactivity injection is based on the irradiation level and the flux shape of the core in addition to the fissile content of the fuel. In general, fuelling a bundle in the periphery channels injects less reactivity than fuelling a bundle in the channels in the middle of the core.

The channel regions and the axial fuelling scheme are defined in the reactor model. The refined TRUMOX-30 fuelled CANDU-900 described herein has 12 different regions over the 480 channels and uses a 1 or 2 bundle shift axial fuelling scheme. This is in contrast to a standard natural uranium fuelled CANDU design that uses about 7 to 8 regions with a 4 to 8 bundle shift strategy [55]. The region and fuelling shift information for this core is seen in Figure 5.1.

FUELLING SCHEME CORE MAP- 12 REGIONS, 1 & 2 BUNDLE SHIFTS,

	1	2	3	4	5	6	7	8	9	10	11	12	13	14	15	16	17	18	19	20	21	22	23	24	
A								2BS			TOP	EXT				2BS									A
B							2BS				TOP	MID				2BS									B
C											TOP														C
D									1BS				1BS												D
E																									E
F										1BS															F
G										TOP															G
H										CENT															H
J																									J
K		2BS		1BS		1BS				1BS				1BS				1BS		1BS		2BS			K
L	OUTER																	MIDDLE				RIGHT			L
M	RING											INNER													M
N																									N
O			OUTER																OUTER						O
P										1BS				1BS											P
Q																									Q
R																									R
S																									S
T																									T
U																									U
V										1BS	BOTTOM		1BS												V
W																									W
X						2BS				BOTTOM	MID					2BS									X
Y								2BS	BOTTOM	EXT					2BS										Y
	1	2	3	4	5	6	7	8	9	10	11	12	13	14	15	16	17	18	19	20	21	22	23	24	

Figure 5.1: Fuel irradiation regions and associated axial fuelling scheme map

The fuelling pattern has six regions (in the inner core area) using the one-bundle-shift fuelling scheme encompassing 344 channels and six regions using the two-bundle-shift fuelling scheme covering the remaining 136 channels. The time-average irradiation level for each of the regions (and subsequently each bundle) can then be determined as described in the following section.

5.2   Time-average-model

The time-average-model is designed to calculate lattice properties at each bundle location which are averages over the residence time of the fuel at that location. The time-average properties are then used to determine the time-average core distributions for flux, power, burnup and fuelling rate producing the equilibrium operational target for the core. The time-average simulation is performed with the control devices at their normal positions during operation. The absorbers and shutdown rods are held out of the core while the liquid zones are filled to mid-range (about 50%). The adjuster rods in a CANDU fuelled with natural uranium are normally inserted in the core and would be modeled this way for the time-average. The optimized TRUMOX-30 CANDU-900 system operates with the liquid zones at 42% full and adjuster devices fully out of the core. The adjuster rods are removed during normal operations, in contrast to an NU case, because the minor actinides contained in the TRUMOX-30 fuel (especially Pu-240 and Am-241) have high thermal absorption and provide the necessary axial flattening in the core without the use of the adjusters. The removal of the adjusters also increases actinide destruction that can be achieved for a given burnup.

Using the region definitions from the reactor model the specific irradiation levels (based on fuelling frequency) for each region are to be set for the time-average system. The combinations of irradiation levels are selected to produce a system that adheres to a desired power profile, maintains the reactivity and bundle and channel power limits and provides a suitable level of fuel burnup. The determination of an acceptable set of time-average irradiations is iterative and involved. The manipulation of irradiation levels may not be enough to satisfy all the competing criteria and the region definitions made in the reactor model may need to be adjusted. The details of irradiation selection are provided below.

The initial design step is to select irradiations and regional groupings that produce a suitable channel power distribution that meets the channel and bundle power limits. The desired channel power shape is a flattened-cosine, domed with the highest channel power in the inner region of the core with the largest ratio of average to maximum channel power. The symmetry of the power shape is also important to avoid local hot spots or tilting. This power shape aligns with the axial fuelling scheme and desired flux profile in the core with the inner channels operating at higher powers than the outer channels. Once a symmetrical domed power shape has been obtained that meets the channel power limits, the

irradiations in the various inner and outer regions can be adjusted to reach the desired level of radial flatness. The flatter the radial profile, the more even the burnup is over the core and the closer the maximum channel power is to the average value. The flatness of the core is measured by the radial form factor (RFF = Average Channel Power / Maximum Channel Power). The 480 channel CANDU-900 core power is 2, 651MW so average channel power is 5522.91 kW. The reactivity in the core is monitored during the shaping and flattening process to ensure a suitable k-effective value for the core (~1.0) is maintained. To align a proper power shape with the desired core reactivity, all the irradiation values can be scaled up or down proportionally. The process for irradiation region selection as well as setting the target exit irradiations is shown in Figure 5.2.
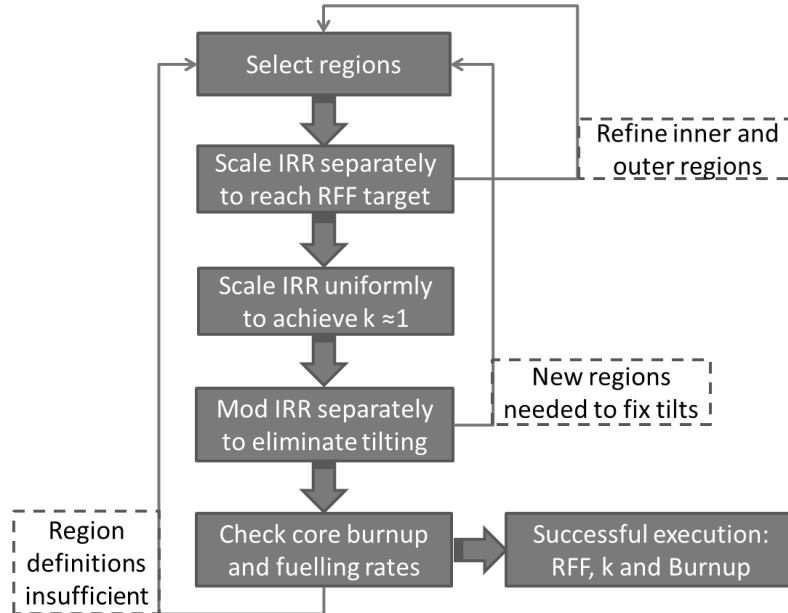
Figure 5.2: Flow chart of region selection and irradiation value definition

Beginning with a set of irradiation regions, the inner and outer irradiation regions are adjusted to achieve a channel power profile with the desired RFF value and then all the irradiations are scaled to produce a suitable value for core reactivity. The irradiations are then modulated slightly to balance out asymmetries across the profile (i.e. tilting). If the perturbations of irradiations seem to be unsuccessful in attaining a high enough RFF while maintaining core reactivity or are unable to correct the tilting in the core, the region definitions are re-evaluated and either redistributed (keeping the number of irradiation regions constant) or subdivided

(increasing the number of irradiation regions). The channel power shape is maintained throughout the design process with the maximum channel power falling in the inner region of the core as designed. After several iterations the outer being on region definition and the inner on irradiations, the desired RFF target is achieved. Following this, the irradiations are perturbed slightly to arrive as near as possible to the proper k-effective value and RFF desired for the given region definition and correct for any tilts in the power shape. At this point the full core burnup levels are evaluated to determine if they are acceptably close to the level prescribed in the lattice calculations. As described in Chapter 4.2.3, the general burnup target is defined based on the fuel activity and the capabilities of the reactor control system. Small burnup gains can be realized by adjusting the level of flattening and irradiation regions but the general burnup target is dictated by fuel activity. The average whole core exit burnup target was 30 MWD/kgHE.

The flatness of the core power profile is important as the maximum channel and bundle power are the primary constraints for reactor operation. A flatter core will have a higher RFF (thus a lower maximum channel power) promoting more even burnup across the core. Flattening of the power profile may cause a reduction in the burnup level which must be taken into account such that the core will achieve both adequate margin to the power limits and an efficient level of burnup.

The goals for this core design were a burnup of about 30MWD/kgHE a k-effective within 1 mk of critical, an RFF of above 0.87. It should be noted that the axial fuelling schemes of one-bundle-shift and two-bundle-shift are in predefined regions that are based on the reactivity injection from the fuelling shift and are not altered during the time-average irradiation region refinement. The fuelling scheme and fuelling regions are consistent with Figure 5.1.

For the TRUMOX-30 CANDU-900 time-average core the process began from a two-region core model. Following from Figure 5.1, the Region 1 included middle and inner while Region 2 was the rest of the core. This model was only able to reach an RFF of about 0.83 but did achieve the desired burnup and reactivity. The irradiations used were 3.773 n/kb for the inner region and 3.255 n/kb for the outer. An additional problem was some asymmetry in the power profile which had a top- to-bottom tilt of 1.92% and a left-to-right tilt of 0.84%.

To correct these deficiencies new regions were created and others were subdivided. First, the original inner and outer regions were each subdivided in two

to allow for further refinement in flattening of the power profile (creating Inner and Outer Ring in Figure 5.1). Then dedicated regions for the top (covering Top, Top-Mid and Top-Ext in Figure 5.1), bottom (covering Bottom, Bottom-Mid and Bottom-Ext in Figure 5.1) and the right edge of the core (Right in Figure 5.1) were added on top of the subdivided four region core. These new regions help to balance the power profile and to adjust for the extra in-core structures that are present in these areas of the core (e.g. LZCRs infrastructure and SDS 2 poison injection nozzles). The result is the seven region core presented in Figure 5.3.
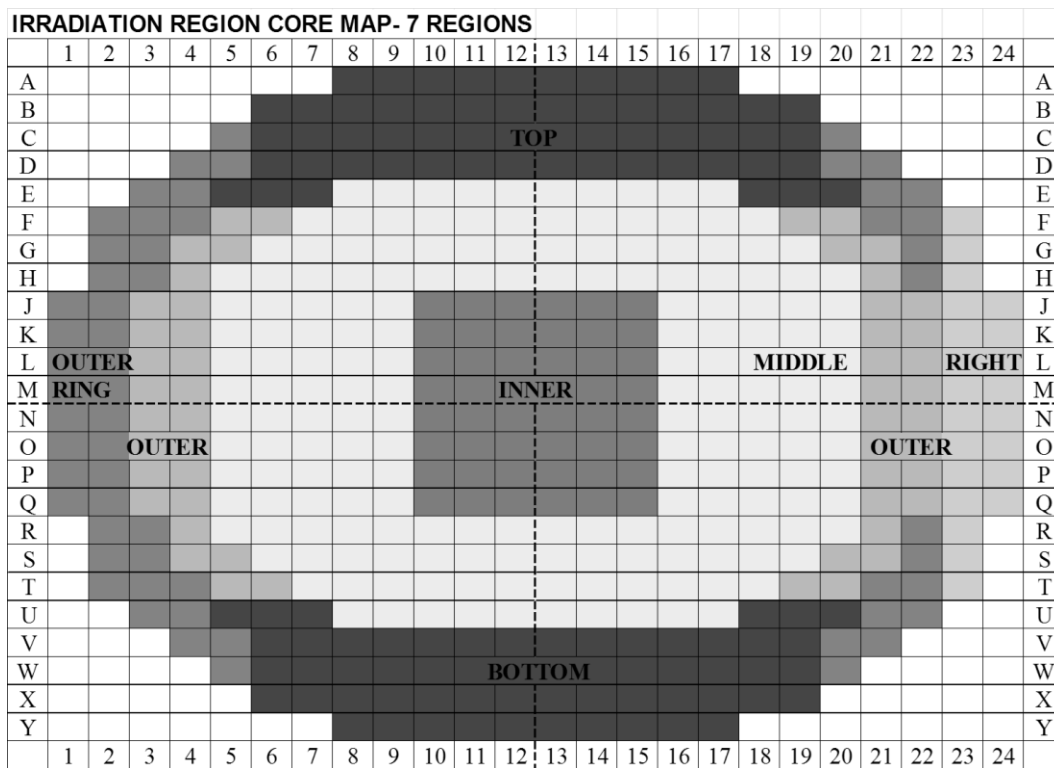
Figure 5.3: Seven irradiation region evolution of the TRUMOX core

These additional regions allowed the correction of some of the tilt problems and assisted in flattening the power profile, achieving an RFF of about 0.863. The symmetry was also enhanced with a top-to-bottom tilt of 0.49% and a left-to-right tilt of only -0.27%. The fuel burnup and reactivity targets were also met. The seven region irradiations and associated burnup values are provided in Table 5.1 and the channel power profile for the seven-region-core is shown in Figure 5.4.

Table 5.1: Seven region core, time-average irradiations and burnups.

Region	Average Exit Irradiation (n/kb)	Burnup (MWD/kgHE)
TOP	3.215	28.36
MIDDLE & INNER	3.810	31.64
OUTER	3.365	29.29
OUTER RING	3.150	27.88
RIGHT	3.110	27.63
BOTTOM	3.185	28.21
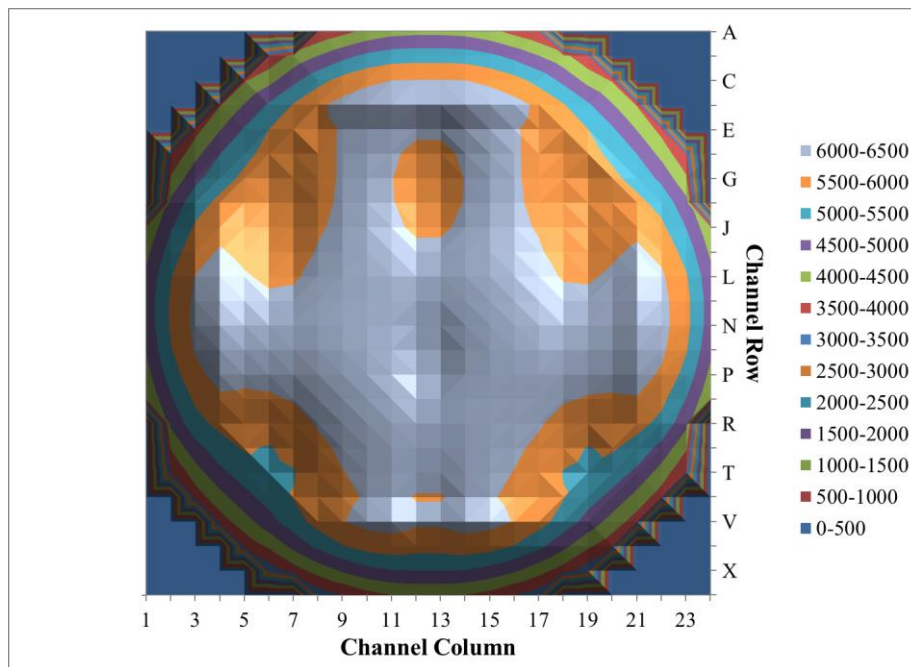
Figure 5.4: Seven region core, time-average channel powers.

The power profile of the seven-region-core can be refined further to account for the depression in the top center of the core. Additionally, subdividing the top and bottom regions will increase the capability for flattening by allowing a graded irradiation that increases the channel powers at the core edges in these zones. The top and bottom regions were split into 3 regions each and the top-cent region was added resulting in the 12 region map originally presented in Figure 5.1.

The additional subdivisions in the top and bottom regions allowed the power profile to reach the desired RFF target and produce a symmetric power profile. The finalized time-average exit irradiations for the 12-region refined TRUMOX-

30 CANDU-900 core are provided in Table 5.2 along with their associated regional burnup values. This configuration was able to achieve an average full core exit burnup of 29.98 MWD/kgHE. The time-average parameters including the powers and form factors are provided in Table 5.3 while a plot of the channel power distribution for the core is shown in Figure 5.5. The channel power distribution has a top-to-bottom tilt of 0.49% and a left-to-right tilt of 0.09%.

Table 5.2: Time-average exit irradiation values.

Region	Average Exit Irradiation (n/kb) [Burnup (MWD/kgHE)]	Region	Average Exit Irradiation (n/kb) [Burnup (MWD/kgHE)]
TOP EXT	3.12 [27.58]	TOP CENT	3.54 [30.26]
TOP MID	3.17 [28.07]	MIDDLE	3.82 [31.69]
TOP	3.40 [29.48]	INNER	3.82 [31.69]
OUTER	3.61 [30.60]	BOTTOM	3.32 [29.05]
OUTER RING	2.90 [26.45]	BOTTOM MID	3.09 [27.63]
RIGHT	2.87 [26.27]	BOTTOM EXT	3.03 [27.13]

Table 5.3: Time-average model characteristics.

Characteristic	TRUMOX Value	Standard CANDU-900 Value [55]
k-effective	0.999086	~1
Max BP (kW)	778	700-800
Max CP (kW)	6320	6400-6500
Whole Core Exit Burnup (MWd/kgHE)	29.98	9.1
Maximum Exit Burnup (MWd/kgHE)	31.69	~ 11.3
Radial Form Factor*	0.874	0.85-0.87
Axial Form Factor**	0.625	0.625
Overall Form Factor***	0.546	0.54

*Radial Form Factor = Average Channel Power / Maximum Channel Power

**Axial Form Factor = Max Channel Power / (Max Bundle Power x 13 bundles)

***Overall Form Factor = Average Bundle Power / Maximum Bundle Power
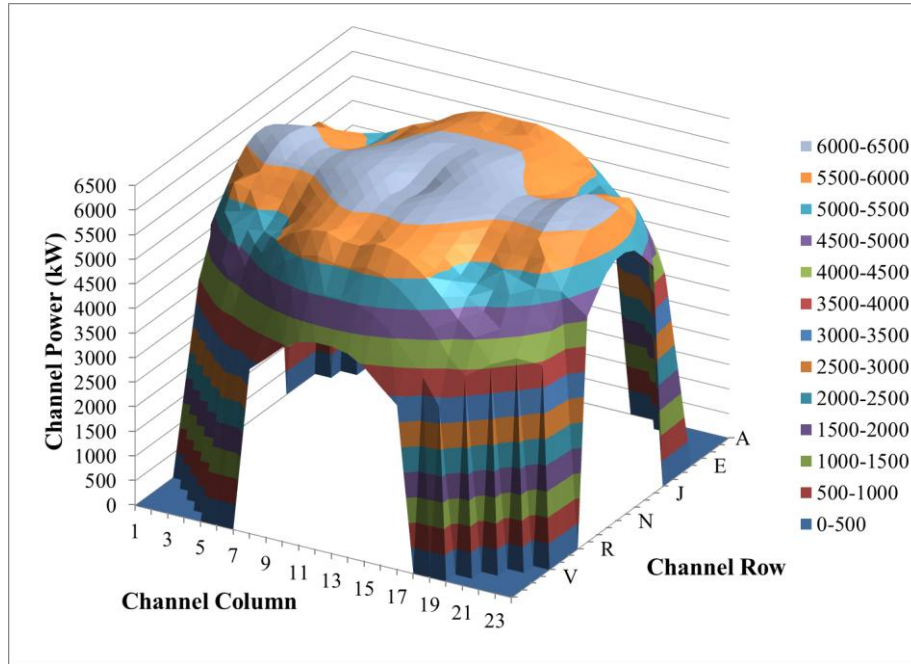
Figure 5.5: Time-average core channel powers, 100% FP.

Given the full core average exit burnup, the actinide destruction level for the core was computed. The TRUMOX-30 fuel is 3.10 wt% actinide oxide and 96.90 wt% natural uranium with a mass of 17.383 kgHE per bundle. The composition of the actinide mixture was described earlier in Table 4.1. The initial and final concentrations of the actinides in g/bundle of fuel are provided in Table 5.4 for the average whole core exit burnup value of 29.98 MWD/kgHE.

Table 5.4: Actinide Destruction (Burnup = 29.98 MWD/kgHE).

Concentration (g/bundle)	U 235	Np Total	Pu Total	Am Total	Cm Total	Total Actinides
Initial	119.88	24.43	439.23	55.48	0.45	519.58
Final	24.55	13.47	293.09	20.80	11.62	338.99
Final-Initial	-95.34	-10.96	-146.13	-34.68	11.17	-180.59
% change	-79.53%	-44.86%	-33.27%	-62.51%	2491.04%	-34.76%

The actinide destruction potential of the TRUMOX-30 CANDU-900 system is quite good with an overall actinide destruction level of 34.76% or 180.6 g/bundle. For a full core load of 6240 bundles, this results in a net burnup of about 1127 kg

of the initial 3242 kg of actinide material[10]. The goal of using the TRUMOX fuel is to remove the actinides from spent fuel and reduce the long term heat loads and reactivity that they produce in the spent fuel. As discussed previously in Chapter 2.2, the decay heat power profile in spent nuclear fuel is dominated by fission products in the short term (< 100 years) and by actinides in the longer term [14].

Looking only at burning actinides from spent fuel in a thermal reactor, such as the TRUMOX-30 CANDU-900 approach, there is a significant level of transmutation (~35%) that reduces the volumes of spent fuel and the actinide load that must be eventually handled by fast reactor systems. However, as seen in Table 5.3, not all the actinides are reduced during the burnup cycle, there is a net production of curium isotopes (98% of which are Cm-244 and lower) in the fuel equivalent to 11 g/bundle which comes from the transmutation of neptunium, plutonium and americium isotopes. However, as discussed in Chapter 2.2, this production of curium is not a significant problem when it comes to the spent fuel decay heat load. Although it is an actinide, curium behaves similarly to the fission products with regards to long term radio toxicity and heat load with both contributions being quite small after 100 years. Curium could be extracted from spent fuel individually and vitrified along with the fission products as waste but such additional reprocessing complexity goes beyond the grouped actinide extraction proposed here. Thus it is simpler to send the curium along with the other actinides to the fast reactor cycle that follows.

The time-average model utilized here could be optimized further with more irradiation regions but for the purposes of this feasibility study the current model achieves a suitable balance between analysis complexity and the desired fidelity (accuracy) of the results.

5.2.1 Axial power distribution

The actinide content within the fuel introduces a large amount of material that absorbs thermal flux and burns up as the fuel passes through the core. This actinide content therefore results in a lower flux level in the TRUMOX-30 CANDU-900 system than in an NU CANDU. The axial flux is also flatter along the channel as the actinides absorb the flux and are depleted at a similar rate to the

---

[10] The accumulation of curium isotopes is expected in any thermal reactor system and can only be fully addressed with the use of fast-neutron spectrum reactor designs.

fissile material. The flattening is accomplished without the use of the adjuster rods which are held out of the core during normal operations. The resultant TRUMOX-30 CANDU-900 axial flux profile is provided in Figure 5.6 and is compared with a standard NU CANDU axial thermal flux profile (with adjusters inserted) for a central channel in the core (M12).
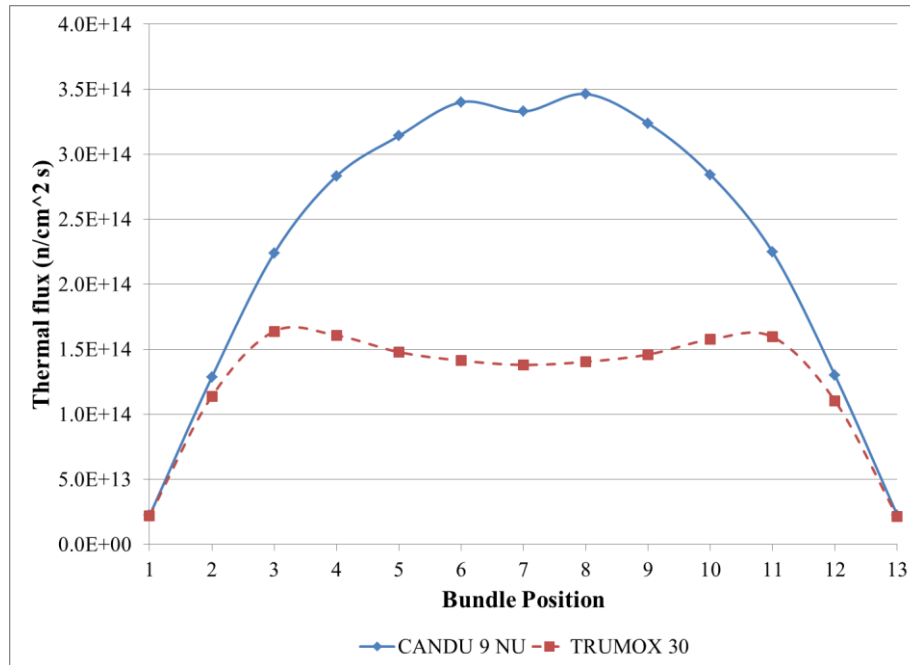
Figure 5.6: Axial thermal flux profile in channel M12.

The axial thermal flux is much flatter and lower for the TRUMOX fuel as compared to NU due to the actinide presence, harder spectrum and plutonium content reducing the amount of thermal flux in the core. The axial thermal flux flattening due to the actinides in the fuel and the BNA in the central pin precludes the need for adjuster rods in the core to flatten the axial profile. The rational for removing the adjusters from the core during normal operations is as follows:

a) If the adjusters were inserted into the TRUMOX-30 core a flux depression would occur in the center of the channel and the ends would be pushed up due to flux displacement, causing higher peak powers which may not provide sufficient margin to the bundle and channel power limits.

b) The adjusters, if inserted, would reduce the neutron economy in the core and hence reduce the levels of actinide transmutation.

c) CANDU-900 reactors can operate successfully without adjusters as demonstrated by the Bruce-A 900 MWe reactor units [71].

The axial flattening is consistent across the core since the actinides are present in the fuel mixture. The axial flux is examined for several channels across the core and is consistently flatter and lower than the natural uranium case. In the CANDU-900 there are 13 bundles arranged in the channel with ½ of a bundle extending outside the active area of the core on either end. The peak flux in a central channel occurs at about 1 to 1.5 meters into the channel from each end due to the one and two bundle shift bidirectional fuelling scheme employed. Thus the axial flux at the center of the third of the 13 bundles and symmetrically on the other end of the channel at the middle of bundle eleven. The flux between positions 3 and 11 is generally constant with some dishing in the central high power channels due to the presence of the BNA and actinides. The central dishing can be measured as the difference between the peak value at position 3 or 11 and the flux value at the center of the channel in position 7 and is generally 10-15% for most channels but is as low as 4.4% in the channels on the periphery of the core. The increases in dishing can be seen by examining the axial flux profiles across the core in the x and y directions. The axial flux in several channels across the central x axis along row M is provided in Figure 5.7.
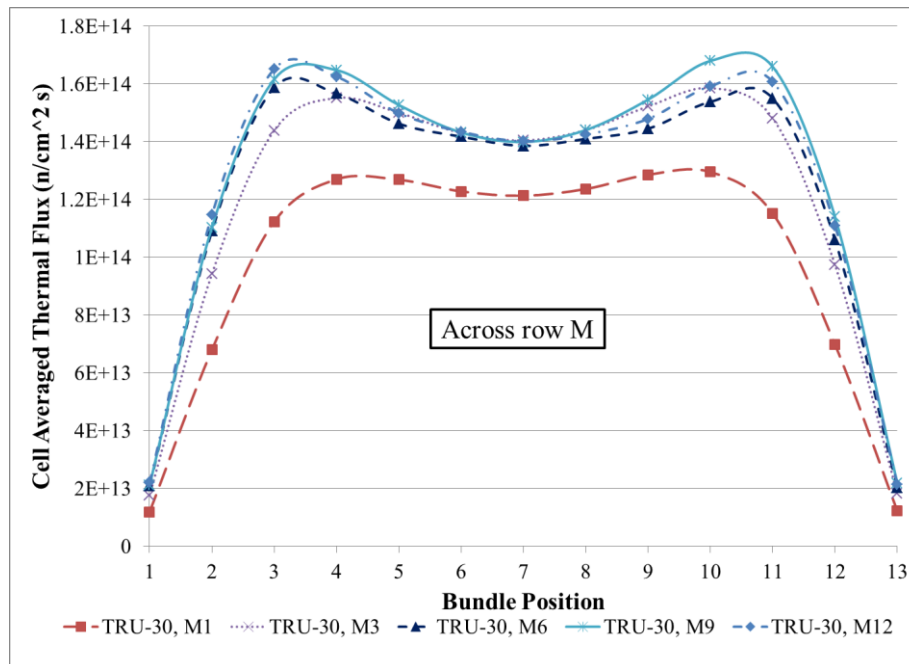
Figure 5.7: Axial thermal flux profile in channels across row M.

There is dishing in the axial flux profiles across row M ranging from 6.4% to 15.0% moving in from channel M1 to channel M12. Row M is at the center of the core and experiences high flux resulting in high absorption from the actinides in the TRUMOX fuel. Similar effects are seen when tracking the axial flux down a column in the y direction as seen in Figure 5.8 where the axial flux profiles down column 12 are displayed. The dishing in column 12 ranges from 4.4% to 15.0% from the outer edge to the center of the core.
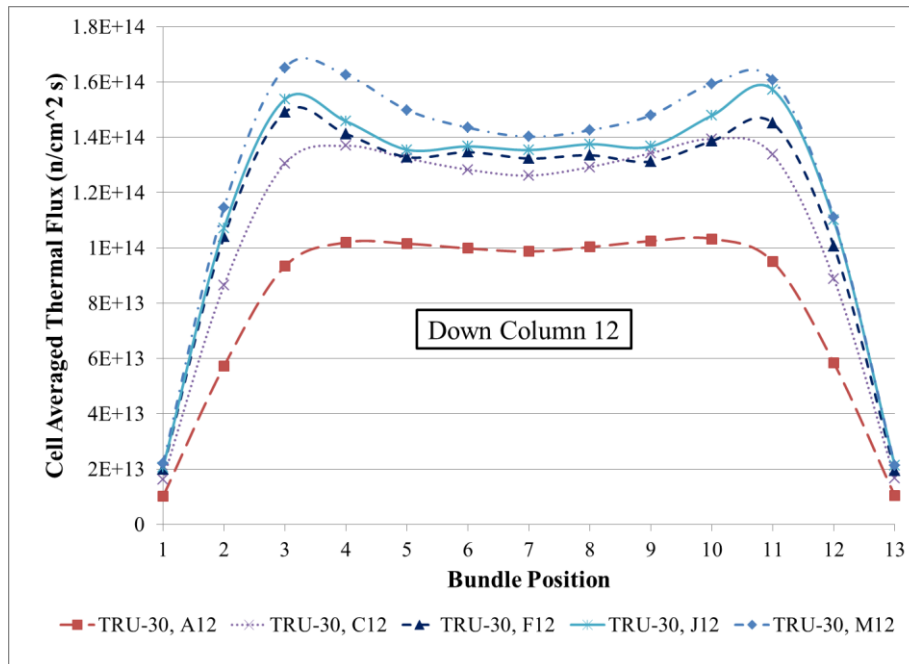
Figure 5.8: Axial thermal flux profile in channels down column 12.

The time-average results provide the quasi-equilibrium channel power behaviour but do not include local spikes which may occur due to fuelling. As a result, the local and instantaneous effects of fuelling must be investigated on the channel and bundle powers to ensure the instantaneous power profiles conform to existing license constraints. This is done by creating an instantaneous snapshot of the core at a single moment in time and comparing the powers to that of the time-average. This comparison is defined as the ripple effect and is analyzed using the INSTANTAN module of RFSP, which generates a core with random channel ages and predicts the core behavior accounting for online refueling effects.

5.3   Instantaneous snapshot simulations

The instantaneous snapshot method seeks to produce a pattern of channel ages that will be more representative of the time dependent specific burnup profiles in the core. This means that some channels will be recently fuelled, some will be in the middle of the burnup cycle and others will be nearing the end of burnup. This instantaneous snapshot simulation provides perturbations from the time-average core which ensures that the criticality and power constraints are maintained. Hence, snapshots are a method for assessing fuelling ripple effects on the core. The methodology for creating the channel ages for the snapshot was described previously in Chapter 3.5.4. A patterned random channel age distribution (PRCAD) is used to assign ages to the channels that are based on an operating history to realistically represent the ages of channels near each other [58].

Multiple random aged cores were created to test the TRUMOX fuel and its associated refueling and irradiation scheme (see Appendix A). In all cases the reactivity was properly maintained and the channel and bundle powers remained below the prescribed limits for CANDU. The simulation results for a selection of the instantaneous cores are provided in Table 5.5.

Table 5.5: TRUMOX-30 CANDU-900 Instantaneous core simulation results

Core (seed matrix size)	k-effective	Max Channel Power (kW) [Location]	Max Bundle Power (kW) [Location]	Over Power Channel (COP)	Over Power Bundle (BOP)
2BT (7x7)	1.00170	6712.31 [K14]	859.53 [K14-B11]	1.206	1.265
2B6T (7x7)	1.00183	6870.71 [O21]	864.97 [P14-B03]	1.208	1.258
2B8T (7x7)	1.00186	6902.95 [L21]	850.44 [P14-B03]	1.261	1.300
2BAT (6x6)	1.00157	6873.86 [N21]	856.85 [Q14-B11]	1.197	1.283
2BBT (6x6)	1.00183	6949.56 [M21]	871.93 [M21-B03]	1.207	1.307

At this stage the completed design satisfies the time-average and fuelling ripple assessments with the specifications and constraints met to a reasonable degree. Further and more detailed testing of the fuelling ripple and the reactor control system response to fuelling is performed using direct operational simulations, described in Chapter 5.8. Following this instantaneous snapshot ripple assessment, the reactor control system capabilities and reactivity coefficients for the TRUMOX CANDU design are explored.

5.4   Reactivity control device worth

The full core response of the reactor control system is an important factor in determining if the fuel design is compatible with the reactor and can operate safely inside the desired envelope. The control devices investigated are the adjuster rods, mechanical control absorbers (MCA), liquid zone controllers (LZCR) and shutdown system 1 rods (SDS 1). The worth of a device is determined using the time-average model. The standard time-average irradiation values are computed for the normal system and the individual bundle irradiations are preserved. The device is then moved and the simulation is run again with the preserved irradiation values. This serves to simulate the insertion or removal of a control device into or out of an equilibrium time-average core.

The CANDU-900 reactor control systems utilize the LZCRs for fine control which consist of 14 vessels of H_2O distributed throughout the core. The water levels in the vessels are altered to control neutron absorption in the core and their distributed nature allows for both bulk and spatial control. The adjuster rods are 24 neutron absorbing rods arranged in (typically) 7 banks and for the TRUMOX-30 CANDU-900 configuration are held out of the core (for an NU core configuration, the adjusters and are usually left inserted in the core to produce a flat flux profile and to provide a positive reactivity reserve to counteract xenon buildup). The MCAs are 4 neutron absorbing rods normally positioned outside the core and driven in to provide additional negative reactivity during conditions where the liquid zone system is either not responding quickly enough or the LZCRs are reaching their fill limits. The MCAs are also used when there is an excessive discrepancy between demanded and actual power or when an adverse condition has been registered by the control system (e.g. set-back or step-back). The adjusters and MCAs are coarse control supplements to the fine control of the LZCRs. SDS 1 is a set of 32 neutron absorbing rods deployed in 4 banks and are poised above the core ready to be released to initiate reactor shutdown. These rods are arrayed across the core and are designed to provide rapid shutdown even if the two strongest rods are unavailable.

The TRUMOX-30 CANDU-900 configuration maintains the normal operating procedures of CANDU with respect to the control systems except for the removal of the adjusters from the core. As described earlier, the presence of actinides in the TRUMOX-30 fuel along with the burnable poison in the central pin of the bundles provide burnable neutron absorption throughout the core that produces a

flat flux profile that peaks much closer to the edges of the core than regular fuel. Therefore, the adjusters are not needed to axially flatten flux and if held in would dampen the central flux in the core pushing it further out to the edges.

The control devices were perturbed on a device by device basis in the time-average core to determine the difference in core reactivity caused by each perturbation. The results for the TRUMOX-30 CANDU-900 design are presented in Table 5.6 along with the standard values for natural uranium fuelled CANDU. The absolute reactivity worth for each of the control devices is considerably lower than the typical values for CANDU with natural uranium fuel. The TRUMOX fuel with the high fissile content and actinides has a higher ratio of $\nu\Sigma_f/\Sigma_a$ at thermal energies effectively increasing the number of fissions to be controlled by the control device and reducing the absolute reactivity worth. Additionally, the flatter axial flux profile of the TRUMOX fuel has displaced the flux in some areas of the core where the control devices interact reducing their effectiveness.

Table 5.6: Approximate reactivity worth of control devices.

Device	TRUMOX Worth (mk), ($)	NU fuel Worth[55] (mk), ($)*
(LZCRs) 0% to 100% Full	3.90, $1.01	~7.00, $1.20
0% to 42% Full	2.01, $0.52	~3.40, $0.59
42% to 100% Full	1.89, $0.49	~3.60, $0.61
Adjuster Rods	3.14, $0.81	~ 15.00, $2.58
Mechanical Absorbers (MCAs)	4.38, $1.13	~ 10.00, $1.72
Shutdown System (SDS 1)	60.27, $15.61	~80.00, $13.75
Strongest rod held out	58.73, $15.22	~77.40, $13.30
Two strongest rods held out	57.37, $14.86	~74.20, $12.75

*Approximate worth, slight variations between reactors
Note: NU runs with adjusters in core during normal operations, TRUMOX does not. Exit burnup for TRUMOX = 30.0MWd/kgHE, NU fuel =9.0MWd/kgHE

The TRUMOX fuel has a lower delayed neutron fraction, β value, than natural uranium (~34%), as detailed in Chapter 4.1.4, due to the larger plutonium content. The full core delayed neutron fractions for the two core types are NU CANDU $\beta_{Full\ Core} = 5.82\ mk$ [61]; TRUMOX-30 $\beta_{Full\ Core} \sim 3.86\ mk$. Using the delayed neutron fractions, the relative dollar worth, ($\Delta\rho/\beta$ in $) of the control

devices was also computed and provided in Table 5.6. The relative worth values are much closer for the LZCRs and MCAs as the differences in delayed fraction offset the lower absolute worth.

The adjusters are significantly affected by the change to the axial flux shape seen with TRUMOX fuel resulting in the worth being much lower (relative worth is more that 65% lower than NU). The flux where the adjusters interact is lower, having already been flattened by the presence of the actinides in the fuel. However, since the adjusters are now designed to be positioned outside the core during operations they can be repurposed to provide negative reactivity to the core supplementing the LZCRs and MCAs. Therefore, the combined relative worth of the adjusters and MCAs in the TRUMOX case can compared to the MCA worth in the NU case. The combined worth of inserting the adjusters and absorbers into the TRUMOX core is about \$1.78 which is quite comparable to the NU core absorber worth of \$1.72. Additionally, as described in Chapter 4.1.5, the prompt generation time, Λ, for the TRUMOX core is about 38% lower than the standard NU value and the neutron lifetime is about 35% lower meaning that the core responds more quickly to reactivity changes.   The lower generation/lifetime impacts reactor control as the standard NU system lags are the same but the core response is faster.

The delayed neutron fraction and the prompt neutron generation time for the NU and TRUMOX-30 cores provide information on the reactor kinetics of the two cores. The point kinetics equations, shown below with 6 delayed neutron groups, help to estimate the kinetic response of a specific core configuration [44].

$$\frac{dn}{dt} = \left[\frac{\rho(t) - \beta}{\Lambda}\right] n(t) + \sum_{i=1}^{6} \lambda_i C_i$$

$$\frac{dC_i}{dt} = \frac{\beta}{\Lambda} n(t) - \lambda_i C_i(t), \quad i = 1, \dots, 6 \quad [44]$$

(48)

From the point kinetics equations it is evident that the ratio of delayed neutron fraction over prompt generation time, β/Λ, is an important factor in the kinetics response of the core. When the generation time and delayed fraction values for the NU and TRUMOX-30 cores are combined we find an interesting similarity between the ratios. For NU, the delayed fraction of 5.82 mk and generation time of 0.688 ms results in a β/Λ ratio of 8.46 mk/ms. In the case of TRUMOX-30, the delayed fraction of 3.86 mk and generation time of 0.427 ms results in a β/Λ

ratio of 9.04 mk/ms. Thus the β/Λ ratio is only about 6.9% higher for the TRUMOX-30 case than for NU, indicating a similar kinetic response not seen as clearly from comparing the delayed fraction and generation times independently.

Though it is beyond the scope of this study, it may be prudent in future investigations to explore the possibility of increasing the worth of the liquid zones through the use of neutron poisons in the LZCR water (e.g. boron) and the possibility of moving the adjuster and MCA locations such that they interact closer to the axial flux peaking near the ends of the channels. These measures would increase the capabilities of the reactor control system and could mitigate differences in the worth and response times.

5.5   Reactivity coefficients

The response of the reactor to changes in the physical properties of the fuel coolant and moderator are important indicators of the response of the system to abnormal and accident scenarios. Reactivity coefficients are used to quantify the effect of the variations in certain parameters on the reactivity of the core. An accident condition involving a reactivity insertion will lead to increased fission and thus higher fuel and coolant temperatures which will generate a reactor response dictated by the reactivity coefficients. Thus the coefficients of reactivity central to the accident response include the coolant temperature, fuel temperature, moderator temperature and the moderator purity. The coefficients are computed for the full core TRUMOX-30 in CANDU-900 system and are provided in Table 5.7 along with the standard values for a natural uranium fuelled CANDU system.

Table 5.7: Reactivity coefficients

Reactor Coefficient	TRUMOX	NU Value [55, 72]
Coolant Temperature	0.025 mk/°C	~ 0.035 mk/°C
Fuel Temperature	-0.003 mk/°C	~ -0.010 mk/°C
Small perturbations (± 5°C)	-0.003 mk/°C	~ -0.002 mk/°C
Moderator Temperature	-0.046 mk/°C	~ 0.080 mk/°C
Small perturbations (± 5°C)	-0.031 mk/°C	~ 0.010 mk/°C
Moderator Purity	1.376 mk/atm%	~ 34 mk/atm%
N. B. All temperature coefficients include the related density changes		

The reactor coefficients are different in the TRUMOX core mostly due to the harder spectrum, increased enrichment and the larger amounts of plutonium in the fuel. The coolant temperature response is about 29% weaker meaning that the heating of the coolant results in a lower reactivity increase. The response to fuel temperature increase is still negative but is 67% lower so the effect of increased fuel temperature on the reactivity is weaker for the TRUMOX core. This is due to the Pu-239 content in the fuel which is the primary fissile element and has a smaller fuel temperature reactivity response than U-235. The net response for fuel and coolant temperature increase is 0.022 mk/°C, which is comparable to the net response of NU (0.025 mk/°C). The moderator temperature response is opposite for the TRUMOX fuel which experiences a negative reactivity insertion when the moderator is heated. The negative moderator temperature coefficient indicates that the system is under moderated while for an equilibrium NU fuelled case the lower fissile content means the reactor is over moderated, hence the positive moderator temperature coefficient. The effects of coolant purity are not discernible in the RFSP simulation due to a narrow range available but simulations in WIMS-AECL show the TRUMOX lattice cell coolant purity coefficient to be approximately 0.38 mk/atm% or about 67% of the NU value. The full core NU CANDU coolant purity coefficient is approximately 0.57 mk/atm% [73]. The moderator and coolant purity effects are much lower for the TRUMOX case due to the higher fissile content of the fuel. These smaller purity coefficients indicate a lower sensitivity to the heavy water content in the coolant and moderator which may reduce the susceptibility of the system to minor purity changes due to contamination.

5.6   Loss of coolant

The pressure tube design of CANDU separates the coolant from the moderator and means that a loss of coolant is not also a loss of moderator. Thus the response of the reactor to the loss of coolant is important in a CANDU system as the coolant void reactivity is generally positive. The concept of coolant voiding was discussed as pertaining to the lattice cell in Chapter 4.1.7. With coolant voiding in the full core diffusion model the core configuration structures and leakage are full accounted for so the response is more realistic.

To recap, there are two sets of changes when the core moves into a state where the moderator is present but the coolant is not. For neutrons born from fission in the fuel the lack of coolant means less of the neutrons are slowed into the

resonance region resulting in more opportunities for fast fission and a higher probability of escaping resonance capture producing a positive effect on reactivity. For thermalized neutrons re-entering the channel from the moderator there is no hot coolant present and thus less up-scatter into resonance energies occurs, this leads to less resonance capture for U-238 but also reduces the resonance fission in Pu-239 producing both a positive and negative reactivity effect. The net result of these four bulk effects within the lattice cell (3 positive and 1 negative) is the coolant void reactivity.

Also, as discussed in Chapter 4.1.7, there is a local effect that is very important to the effectiveness of a central BNA element in the fuel bundle (as is the case with the 43 element TRUMOX-30 fuel design). Upon voiding of the coolant, there is an increase in the thermal flux in the center of the fuel channel and a decrease at the outer edge and in the moderator. This displacement of flux results in larger absorption (and fission for fuel material) in the center of the channel. If there is a BNA located in the center, this flux displacement will produce a negative effect on the reactivity. As discussed in Chapter 4.2, the TRUMOX-30 bundle contains a strong BNA in the central element that impacts the coolant voiding response of the TRUMOX-30 CANDU-900 system.

Analogous to the complete and instantaneous voiding of the lattice cell, the coolant in each channel in the full core model can be voided (by reducing the coolant density by a factor of $\rho_{liquid}/\rho_{vapour} \approx 1000$, as discussed in Chapter 3.5.5) to obtain a value for the full core instantaneous CVR. The TRUMOX-30 case has a much lower full core instantaneous CVR of 1.79 mk than the natural uranium CANDU-900 system at 12.57 mk (the reference value is between 10-15 mk [55]), primarily due to the strong BNA in the TRUMOX-30 fuel design. This concept of instantaneous uniform full core coolant voiding is not physically plausible due to the primary heat transport system design but it provides a means of comparison between the two reactor designs (TRUMOX and NU).

The CANDU-900 primary heat transport system (PHTS) has a two loop design where each half of the core (240 channels: within grid A1-Y12 for the left hand side, LHS, and within grid A13-Y13 for the right hand side, RHS, as in Figure 5.1) is serviced by a separate system of a large header connected to each channel by a feeder pipe and to two steam generators with the flow driven by two heat transport pumps. A simplified depiction of the PHTS is seen in Figure 5.9 [74].
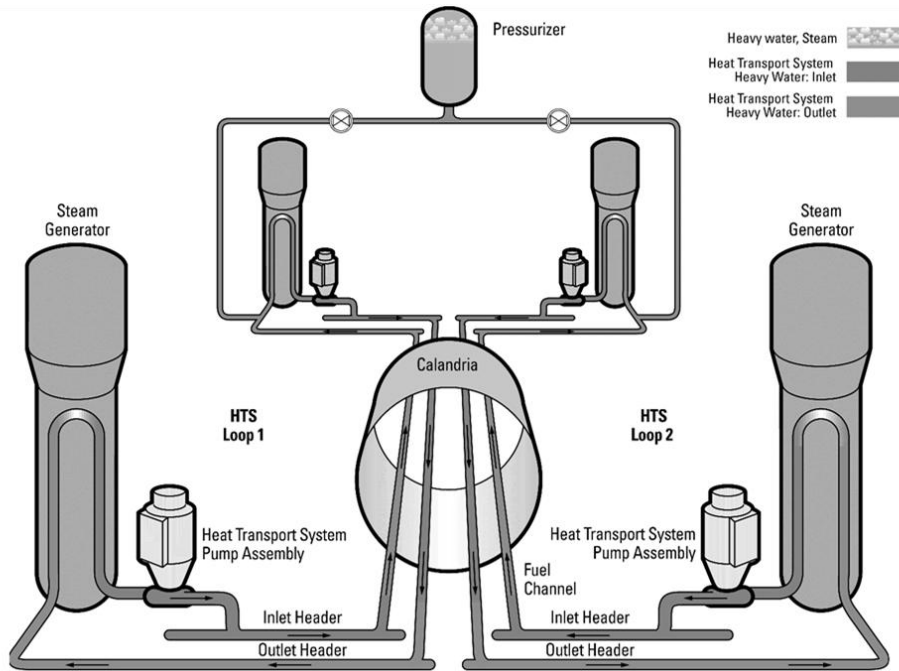
Figure 5.9: CANDU-900 Primary Heat Transport System Diagram [74]

A large loss of coolant in a CANDU-900 system is consistent with a single header break which quickly voids one coolant loop and the 240 associated fuel channels on that side of the core (e.g. the LHS of the core). The other side of the core (e.g. the RHS), which is fed by the other coolant loop that is still intact, would experience a small break loss of coolant through the loop interconnect piping that is a much slower transient. The result is one side of the core being fully voided while the other side still contains a nearly full coolant load. The CVR for this half core case will be larger than 50% the full core CVR due to the flux tilt caused from the coolant imbalance (the cooled side of the core has increased fission).

A simulation of full and half core instantaneous coolant voiding in a standard NU fuelled CANDU-900 configuration was performed using RFSP to more closely compare with the TRUMOX values. The half core void response for the TRUMOX CANDU-900 is 0.97 mk (~46% lower than full core void) while the NU core response is 8.81 mk (~30% lower than the full core void of ~12.57 mk). As before, the TRUMOX CVR response is significantly lower than NU due to the BNA loaded in the center pin of the TRUMOX fuel assembly. The flux tilt effect of the half core voiding is also lower with the TRUMOX fuel being ~16% closer to one half of the full CVR than for the NU case.

As discussed in Chapter 4.1.7, it is useful to factor in the delayed neutron fraction of the fuel into the coolant void reactivity. The full core delayed neutron fraction for the TRUMOX-30 CANDU-900 as discussed in Chapter 5.4 is $\beta_{Full\ Core\ TRUMOX}$ = 3.86 mk. Thus the full core CVR of 1.79 mk is has a relative value, $(\Delta\rho/\beta)$, of $0.46 and the half core void case CVR of 0.97 mk has a relative value of $0.25. In the case of NU CANDU-900, the delayed neutron fraction is higher with $\beta_{Full\ Core\ NU}$ = 5.82 mk. Thus the full core CVR response of 12.57 mk has a relative value of $2.16 and the half core CVR of 8.81 mk has a relative value of $1.51. These instantaneous simulations are not realistic and do not include any action on the part of the reactor control or shutdown systems. Loss of coolant accidents may involve a nearly instantaneous break but the voiding transient for the loop and thus the reactivity transient within the core take time to propagate to such a point of total half core coolant voiding.

The instantaneous coolant voiding simulations explored provide useful information on the general core behaviour but more specific information on the full core neutronic responses to a loss of coolant transient can be obtained. Using a density transient that simulates a loss of coolant event more closely, the reactor system response can be evaluated and the TRUMOX and NU systems can be compared. A density transient for a 100% pump discharge loss of coolant accident in a CANDU reactor (Bruce-A, a 900 MWe CANDU type reactor) is utilized for this study. The Bruce-A reactors use a single coolant loop so this pump discharge LOCA event would result in a symmetric full core coolant voiding response. However, as explained earlier, the CANDU-900 uses a two loop coolant system and thus the pump discharge LOCA will only affect one side of the core. The other side of the core will experience a depressurization through the loop interconnect piping but this transient is much slower so the large break transient will run almost completely through on the left hand side of the core while the right hand side channel coolant densities remain near nominal values, resulting in a voiding of one half of the core.

A density transient for the first 2.5 seconds of a 100% pump discharge LOCA in the CANDU-900 was adopted to produce a simulated loss of coolant event in RFSP for both the TRUMOX and NU fuel configurations in a standard CANDU-900 system [25]. This simulated transient does not include any power change effects or shutdown system actions. While it is expected that the density transient may be different and power change, control system and fuel temperature

properties will impact the outcome, a full scope LOCA analysis is beyond the scope of this study. The coolant void reactivity inserted due to the density transient is presented in Figure 5.10 for each fuel case. The left hand side of the core experiences the density transient in the figure while the right hand side of the core maintains the nominal coolant density of about 0.8 g/cm^3.
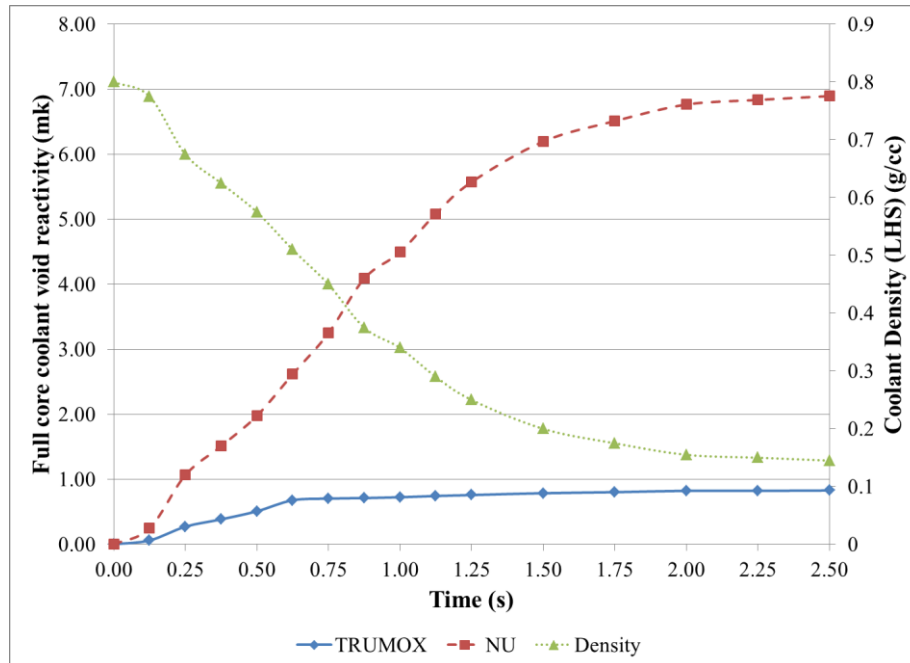
Figure 5.10: 100% Pump Discharge LOCA density transient effects on coolant void reactivity for TRUMOX-30 and NU (Left hand side of core is being voided)

As expected from the previous studies, the response of the TRUMOX fuel is more favourable for this case than NU. The peak void reactivity is 0.83 mk for TRUMOX and 6.90 mk for the NU case. It should also be noted that the TRUMOX void reactivity transient plateaus much faster than the NU case resulting is a smoother response. As discussed earlier, the inclusion of the BNA in the TRUMOX fuel bundle is the main cause of the reduced CVR response. For relative reactivity change, the largest CVR encountered here of 0.83 mk is only about \$0.21. For the NU case, the maximum CVR in this study of 6.90 mk has a relative value of \$1.18.

Overall the TRUMOX core has CVR values about 80% lower than NU CANDU. These represent a potential improvement in loss of coolant accident (LOCA) response since lower CVR will lead to lower predicted fuel centerline and sheath
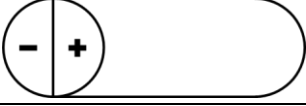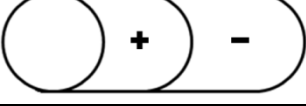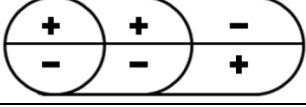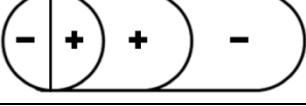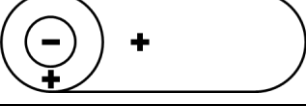
temperatures. However, full coupled code accident analysis was not performed as part of this study. In addition to the neutronics characteristics of voiding, the response of the flux shape to various core configurations provides further information on the response of the reactor to perturbations that can be caused by abnormal or accident conditions.

5.7   Harmonic mode analysis

The harmonic modes of the neutron diffusion equation are powerful tools for evaluating and comparing the flux shapes and neutronics behaviour of different reactor configurations. The lowest level harmonic or "Fundamental" mode is the flux shape calculated by solving the neutron diffusion equation as a critical system. This harmonic has the largest value of k-effective and hence the smallest eigenvalue for the given set of nuclear properties. The higher harmonics have smaller k-effective values (larger eigenvalues) and thus represent sub-critical flux shapes. These cannot exist as a "self-standing" reactor state due to the regions of negative flux (which is non-physical). The harmonics are labeled as per the geometric regions of positive and negative flux that are present. The first 10 harmonic modes are illustrated with the specific flux zones and labels in Table 5.8. These labels and shapes are defined for a clean homogenous bare cylindrical reactor core. Real reactor cores are more heterogeneous and may have more complex harmonic shapes that are harder to specify.

The harmonic modes are assessed using the MONIC module of RFSP. The input is the fundamental flux distribution that is the solution of the diffusion equation for the time-average core configuration. The module then sequentially calculates each of the harmonic modes of the diffusion equation by removing all the components of the previously calculated modes from the flux distribution. Thus each higher mode is computed based on the modes below it that were previously computed. The fundamental mode is the base and contains no regions of negative flux and thus is the valid solution to the diffusion equation. As the harmonic mode in increased, regions of non-physical negative flux appear in the core in different regions producing the shapes of the harmonic modes shown in Table 5.8.

Table 5.8: Standard harmonic modes for CANDU [75].

Mode	Designation	Shape (Bare Cylindrical Reactor)
1	Fundamental	
2	1st Azimuthal (A)	
3	1st Azimuthal (B)	
4	1st Axial	
5	2nd Azimuthal (A)	
6	2nd Azimuthal (B)	
7	1st Axial / 1st Azimuthal (A)	
8	1st Axial / 1st Azimuthal (B)	
9	1st Radial	
10	3rd Azimuthal (A)	

A comparison of the harmonic modes in the TRUMOX core to that of standard natural uranium fueled CANDU provides insight into the behaviour of the core in response to flux tilts. Lower sub-criticality in a mode is a sign that the core will be more susceptible to tilting in that mode. Additionally, the sub-criticalities of

the harmonic modes describe how tightly coupled the regions of the core are from each other. Regional coupling in the core refers to the extent to which a perturbation in the local flux of one region affects the other regions in the core. In a tightly coupled core, local variations in one region will have a strong effect on the other regions in the core. Smaller cores with tightly packed fuel lattices such as PWRs will tend to have tight coupling between the local regions in the core. Larger cores where the fuel is more distributed will generally be more loosely coupled. For cores with tightly coupled regions, the higher harmonic modes are significantly more subcritical than for a loosely coupled core.

In the case of NU CANDU systems, a comparison can be made between the CANDU 6 (380 fuel channels in 22x22 lattice) and the CANDU-900 system (480 channels in a 24x24 lattice). The CANDU 6 is smaller and more compact than the CANDU-900 and thus has smaller sub-criticalities for its higher modes. For example, the reference sub-criticality for an NU CANDU 6 for the 5th (2nd azimuthal) mode is 44 mk compared to the NU CANDU-900 reference of 34 mk a 23% difference indicating that the larger CANDU-900 core is not as tightly coupled [75, 76]. For a loosely coupled reactor, flux in the local regions can become different from the average flux and that of the other regions due to local variations (e.g. fuelling or change in the level of a single LZCR). This may result in regional over power situations and flux imbalances in the core that must be compensated for by the reactor control systems. The distributed nature of the in core flux detectors and liquid zone controllers in the CANDU design help to control these local variations and avoid instances of regional over power.

The first 10 harmonic modes for the TRUMOX CANDU-900 were calculated and compared to an NU-CANDU-900 model and to CANDU reference values for natural uranium [75]. The sub-criticalities for each of the modes were computed for each design and the sets of harmonic modes were compared in Figure 5.11.
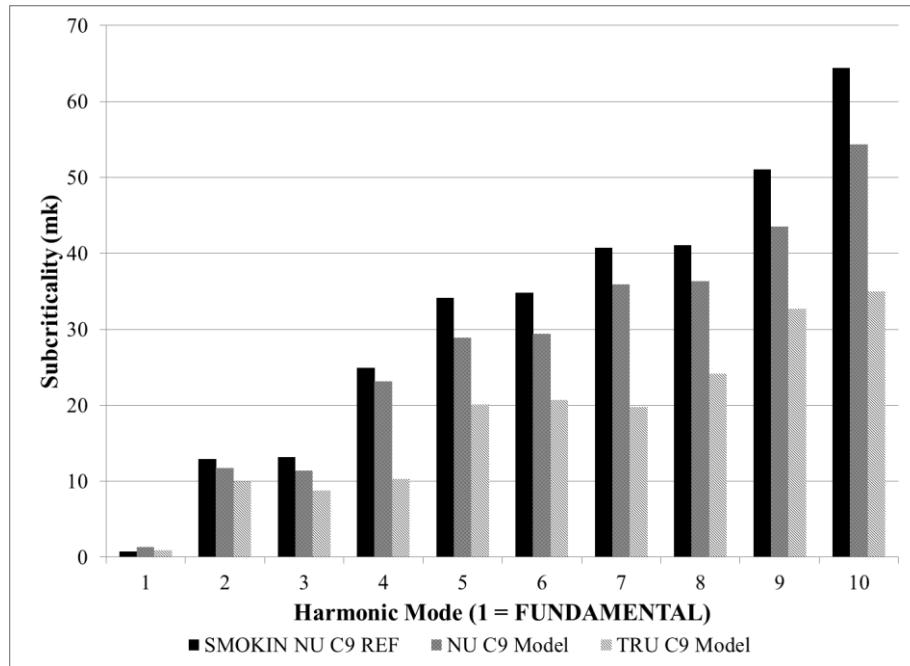
Figure 5.11: Sub-criticalities for the harmonic modes for TRUMOX and NU CANDU.

The sub-criticality of the NU-CANDU-900 model modes follow the trend of the reference values but are lower for the higher modes due to the increased flattening in the core over the base reference model. The NU-CANDU-900 model used here has a radial form factor of 0.869 which is higher than the general value for the reference core which is about 0.85. The flatter the channel power profile is, the lower the sub-criticalities of the higher modes. The TRUMOX core sub-criticalities are lower than both the reference and the NU model but do still follow the trend for most of the modes. The lower modes (1, 2 and 3) are affected by the increased radial flattening as the radial form factor of this core is 0.874. Additionally, the sub-criticality curve is flatter at mode 10 (3rd Azimuthal) for TRUMOX likely due to the increased radial flattening in the core. The axial modes (e.g. 4 and 7) are significantly different primarily due to the fuel composition. An examination of the change in sub-criticality from mode to mode for these cases can help to further detail the differences in the axial modes. The sub-criticality of higher modes builds on the lower modes as such the differences from one mode to the next will provide information on how that mode affects the core. The change in sub-criticality for the two main axial modes in each of the three cases is provided in Figure 5.12.
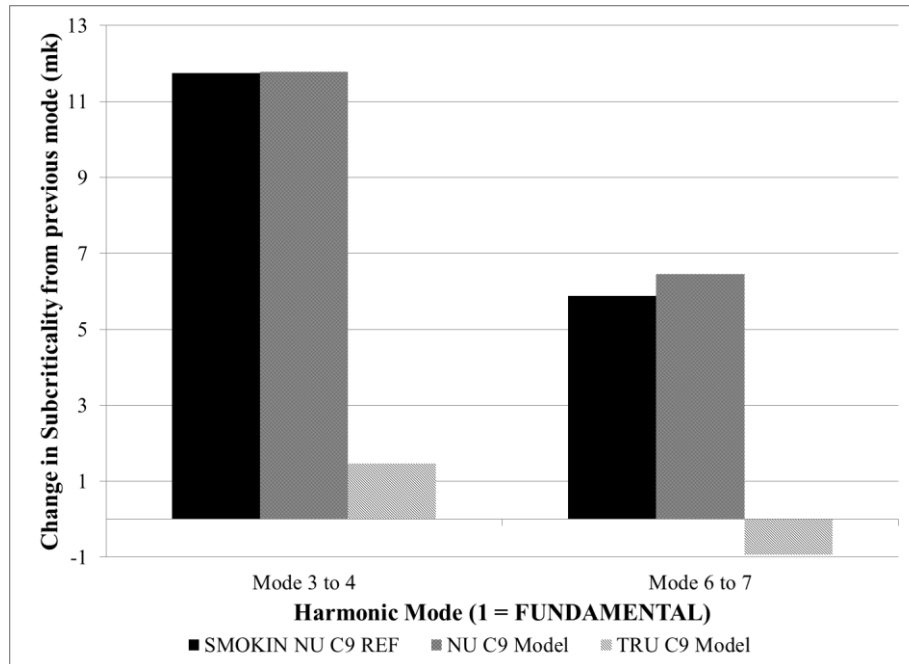
Figure 5.12: Change in sub-criticality between harmonic modes for TRUMOX and NU CANDU

Observing the changes in sub-criticality from mode to mode we see that the changes from mode 3 to 4 and mode 6 to 7 are significantly lower for the TRUMOX compared to NU. These main axial modes indicate the susceptibility to tilting in the axial direction. The flatter axial flux profile in the TRUMOX CANDU-900, caused by the 1 or 2 bundle shift fuelling scheme and minor actinide and BNA presence in the fuel, is much more susceptible to axial tilting resulting in a lower sub-criticality. This effect is somewhat mitigated by the fact that the liquid zone controllers are better able to balance the flatter axial flux and dampen the tilting.

Overall the lower sub-criticalities in the modes for the TRUMOX case indicate that these modes can be more easily excited. This may result in a core that is more susceptible to tilting than an NU core. The response of the control systems and reactor to normal operational conditions such as the effect of fuelling is another important area of investigation.

5.8   Fuelling simulations

The CANDU reactor design uses online fuelling of the channels to maintain the core reactivity over the burnup cycle. These fuelling operations can cause local power peaking and spatial variances in the core reactivity. These fluctuations during fuelling are referred to as the "fuelling ripple" factors in operating reactors and typically vary between 0.9 and 1.1. The ripple is a comparison of the power level of the channel to the time-average target power previously determined. The reactivity insertion from fuelling is controlled by adjusting the liquid zone controller levels in the core to compensate for the local reactivity insertion and maintain the desired bulk power level in the core while avoiding local power spikes that exceed the prescribed limits. The effects of fuelling the core on the control system are very important in determining if the capabilities of the controllers are adequate to handle the fuel, and the power ramp rate that the fuel undergoes. The bundle and channel powers are monitored, along with the fill levels of the liquid zone controllers and power ramps to ensure the reactor remains within operational limits with the TRUMOX fuel.

Online fueling allows the addition of fuel as it is burnt up rather than relying on batch fueling process common in LWR designs which use burnable neutron poisons to hold down the reactivity of fresh fuel and burn off as the fuel burns up and becomes less reactive. The standard CANDU-900 with natural uranium fuel has a reactivity decay rate of -0.42 mk/full power day (FPD) requiring a fuelling rate of about 15-16 bundles/FPD, usually accomplished by fueling 3 to 4 channels with 4 to 8 bundle shifts [55]. The TRUMOX fuel is much more reactive and requires fewer bundles to be fuelled but since it is accomplished by 1 and 2 bundle shifts the fueling rate, in terms of channels visited per day, is higher. The reactivity decay rate of TRUMOX fuel is lower at -0.37 mk/FPD resulting in a fuelling rate of 5.33 bundles/FPD (approximately 1/3 of the daily fuel bundle requirement for NU). Using 1 and 2 bundle shifts this fuelling rate is about 4.63 channel visits/FPD. The reactivity of the fuel dictates the small sized fuelling shifts as a TRUMOX bundle has an average reactivity of 0.069 mk/bundle compared to only 0.026 mk/bundle for NU fuel (reactivity decay rate/fuelling rate in bundles). Considering that the TRUMOX fuel bundle has 2.65 times the average reactivity of the NU bundle the 1 and 2 bundle shift scheme is appropriate. Additionally, the 2 bundle shifts are restricted to the low power channels on the periphery of the core (136 channels in this case). These basic time-average properties are used to produce a realistic single full power day

simulation that will evaluate the fuelling effects on the TRUMOX-30 CANDU-900 core.

The detailed fuelling simulation begins from an instantaneous snapshot created using the method described in Chapter 3.5.4 and Chapter 5.3 and tests the response of the core, fuel and LZCRs. This evaluation is different from the instantaneous snapshot studies as it looks at the direct control responses of the liquid zones to a fuelling event in the core and the ramp rates on the fuel. While the initial core used is one of the snapshots, a time dependent RFSP simulation is performed wherein fuel is inserted into a channel and the direct changes on channel and bundle power and the liquid zone levels across the core are observed. The key objective of these fuelling studies is to ensure that the control system is capable of compensating for the fuelling operations while maintaining the powers and fill levels within their safe operational envelope.

The simulation performed here is one full power day of operation from 9 am to 9 am with 4 fuelling actions that load 5 bundles of TRUMOX into the core. This initial simulation is performed for a front-end heavy fuel loading where the channels are fuelled at 3 hour intervals. The fuelling shifts occur at 9 am, 12 pm, 3 pm and 6 pm. The first shift is a 2 bundle movement into channel P24 followed by three consecutive one-bundle movements into channels E6, M16 and R4. The average zone level for the front-end simulation day is tracked in Figure 5.13.

The average zone level fluctuates through a range of 5.7% from 41.5% to 47.2% which is relatively tame however the maximum and minimum zone levels achieved are 78.0% and 20.0%, a spread of 58.0%. The four individual fuelling events have different effects on the average zone level. The fuelling of M16 has the largest effect increasing the average zone level by 3.04% full or about 0.119 mk of reactivity even more than P24 which, despite being a two bundle shift, affects the average zone level by 2.80% full (0.109mk) since it is in the outer region. The fuelling of E6 has an effect of 1.68% full or 0.066 mk and the fuelling of R4 has an effect of 2.44% full on average liquid zone level (0.095 mk). The bundle and channel powers were maintained below the limits during the full simulation with the maximum channel power of 6.91 MW and the maximum bundle power of 844 kW. The average zone level falls at the end of the simulation as it will soon be time to start fuelling again.
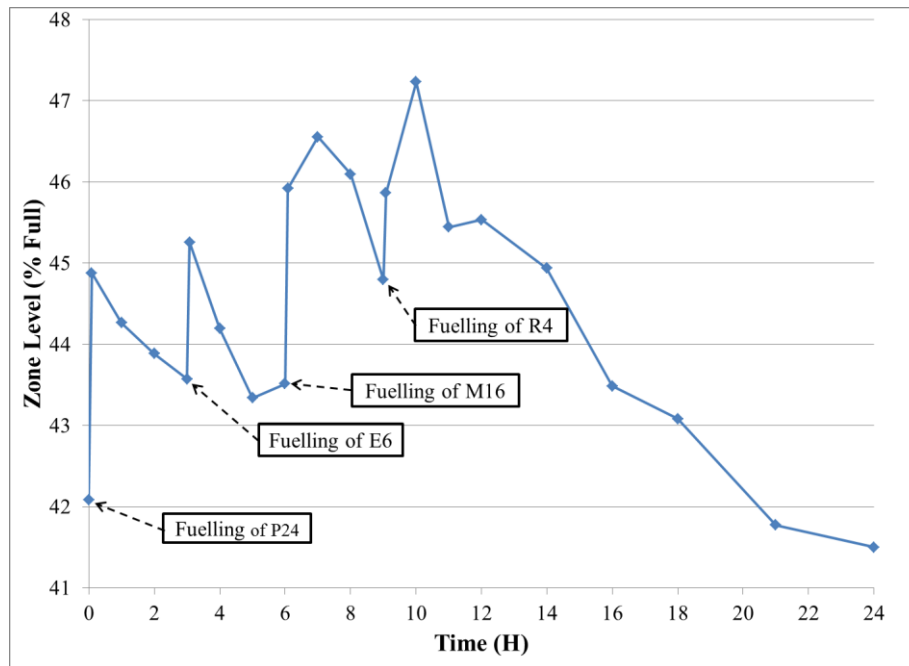
Figure 5.13: Front-end fuelling simulation, average zone level response

The local fuelling effects on a single zone are measured by simulating a fuelling of that zone and performing a duplicate simulation where the channel is not fuelled. This is done for the M16 fuelling at 3 pm which is in Zone 4 and the R4 fuelling at 6pm in Zone 9. The effects on the average zone and local zone level (Zone 4 and 9) for the respective fuelling events are seen in Figure 5.14 and 5.15.

The local zone effect for fuelling M16 at 3pm (Figure 5.14) is a peak zone level change of 17.6% full for the level in LZCR-4 which is adjacent to channel M16 while the core wide average level has a peak change of 4.3% full (~0.170 mk). To examine the local zone effect of a periphery channel, the fuelling of R4 was examined (see Figure 5.15). The effects for the fuelling of R4 are more pronounced with the local peak zone level change in LZCR 9 being 21.1% full while the average zone level effect is smaller with a peak change of 2.1% full (~0.082 mk). The M16 fuelling is at the center of the core so it has less impact on the core power tilt. Channel R4 however, is on the outer edge and can contribute to a tilt if it is not fuelled at appropriate intervals. The tilt effects are seen in the related zone levels for vertical (Zone 8), horizontal (Zone 14), diagonal (Zone 13), axial (Zone 2) and diagonal-axial (Zone 6) tilts. The maximum and minimum differences from fuelling are provided in Table 5.9 for all the zones discussed. The fuelling effect on select zones is tracked in Figure 5.16.

179
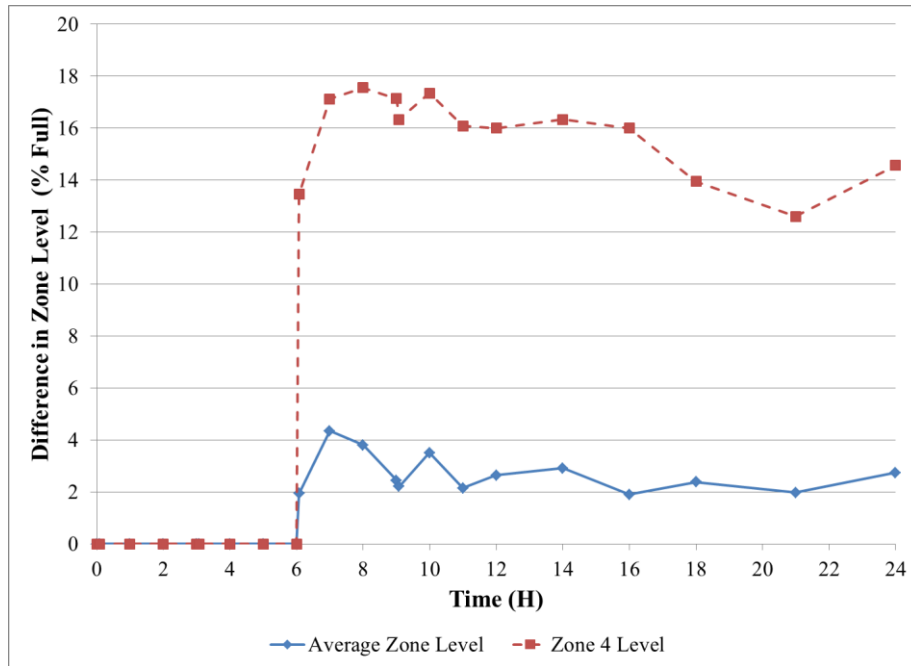
Figure 5.14: Front-end fuelling simulation, local zone fuelling effects (M16).
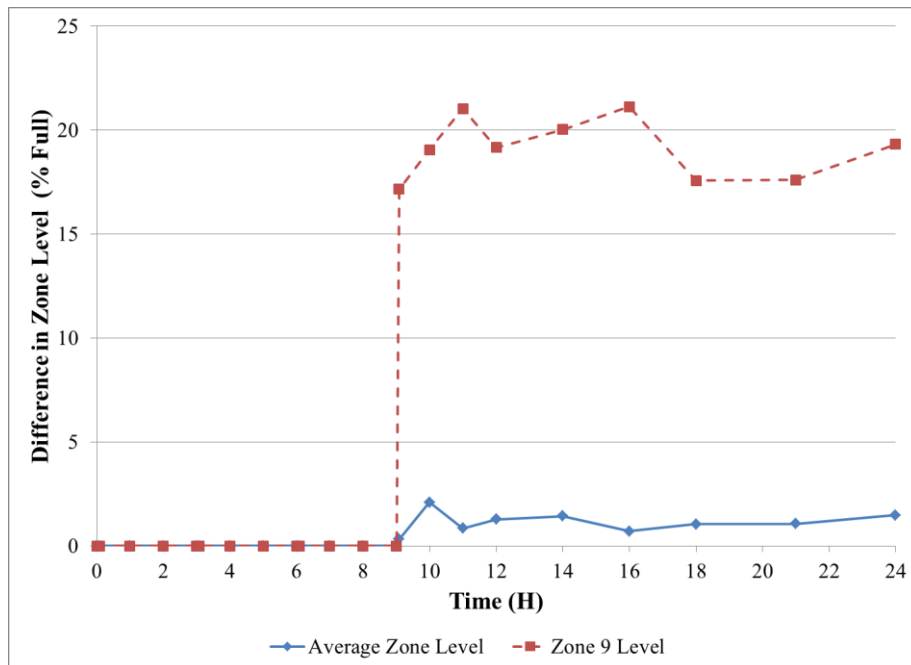
Figure 5.15: Front-end fuelling simulation, local zone fuelling effects (R4).

Table 5.9: Local effects of fuelling channel R4 on liquid zone levels.

Zone (tilt type)	Maximum change (%full)	Minimum change (%full)
9 (local)	21.12	0.00
8 (vertical)	10.42	-4.43
14 (horizontal)	7.77	-10.10
13 (diagonal)	2.44	-5.18
2 (axial)	7.32	-9.77
6 (diagonal-axial)	10.11	-7.40
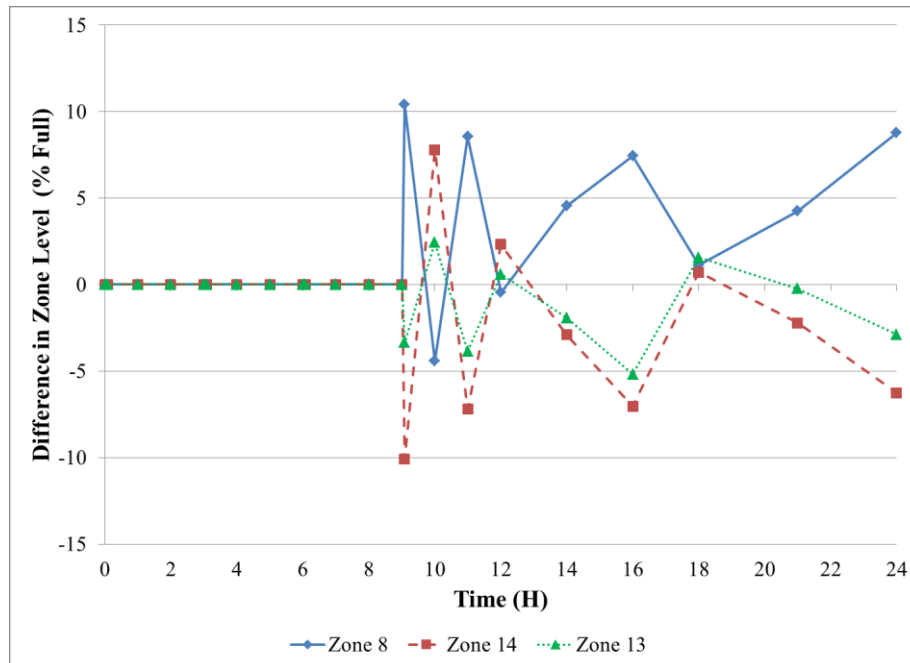
Figure 5.16: Front-end fuelling simulation, local zone fuelling effects 2 (R4).

The effects on the surrounding zones are sporadic causing the zone level to oscillate above and below where it was with the fuelling. The changes in Zones 8 and 6 are similar while changes in Zones 14 and 2 follow similar shapes as does Zone 13 but with a smaller magnitude of change. The tilt effects of the fuelling in R4 on R4 on Zones 8, 14, and 13, seen in Figure 5.16, show how the liquid zones work to provide spatial control. The local effect in Zone 9 is most pronounced but the oscillations in the other zones range as wide as 17.9%. The effect of this fuelling is manageable but care should be taken when fuelling very old channels

in the periphery of the core as these can cause the most tilt. This can be compensated for by fuelling an oppositely located channel soon after.

The previous fuelling simulation is front-end loaded with all the four fuelling shifts coming in the first 9 hours which would place all the fuellings during a regular day shift. It may be desirable to space out the fuellings over the full 24 hour day resulting in one fuelling every 6 hours. This distributed fuelling simulation was performed with the exact same fuellings and is compared to the front-end case in Figure 5.17. As expected, the distributed fuelling case results in lower fluctuations in the average zone level which varies between 40.9% and 44.9%, a range of 4%. This is 30% less fluctuation than seen previously in the front end case and the lower bound of the average zone level is 0.6% lower while the upper bound is 2.3% lower. The distributed fuelling spreads out the fuellings resulting in a flatter zone level response.
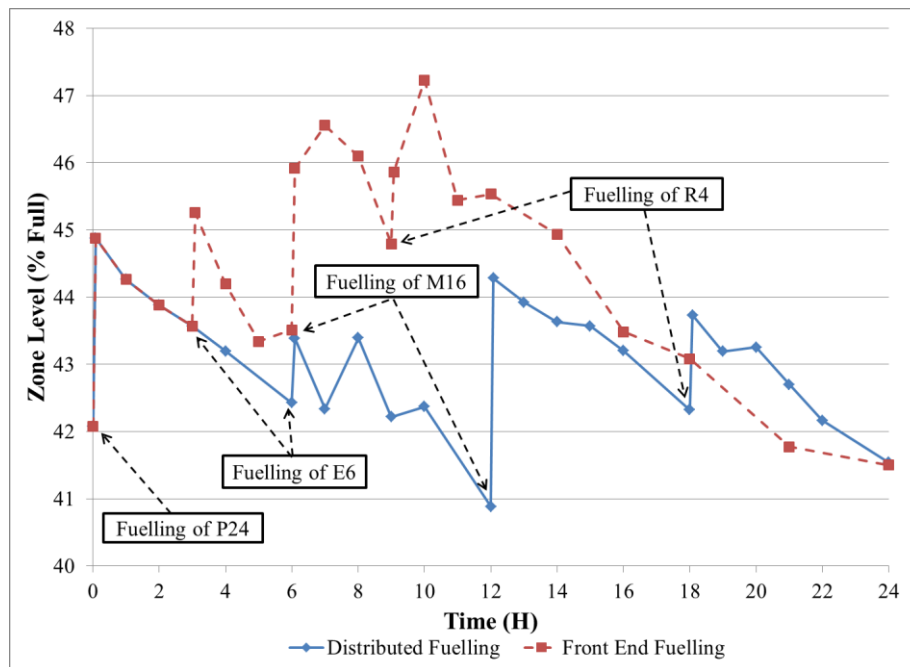
Figure 5.17: Front-end Vs. distributed fuelling simulations, average zone level.

The local impacts of the fuellings are also altered slightly. The individual zone levels fluctuate between 73.7% and 14.1% (a range of 59.6%) which is wider than the front end case by 1.6% with both the upper and lower limits being smaller. This is due to the increased time between fuellings that allows some zones to dip

lower, specifically zone 4 in the case of fuelling channel M16. The initial fuelling of P24 has the same response but the subsequent fuelling events are different. The second fuelling shift into channel E6 has a smaller effect on the zone levels for the distributed case changing the average zone level by 0.97% or a reactivity injection of 0.038 mk this is a 43% reduction in the effect of this fuelling. The third fuelling with a 1 bundle shift into channel M16 actually increases its impact by 11.6% to increase zone level by 3.39% (reactivity insertion of 0.132 mk). The forth fuelling of channel R4 with 1 bundle has a lower effect by 42% reducing the change in zone level to only 1.41% or a reactivity injection of 0.056 mk. It should be also noted that the distributed fuelling shows the change in zone level peaking at 2 hours after the fuelling shift for channel E6 rather than immediately as seen in the front end case. The bundle and channel power limits were respected throughout with maximum channel and bundle power being 6.9 MW and 846 kW.
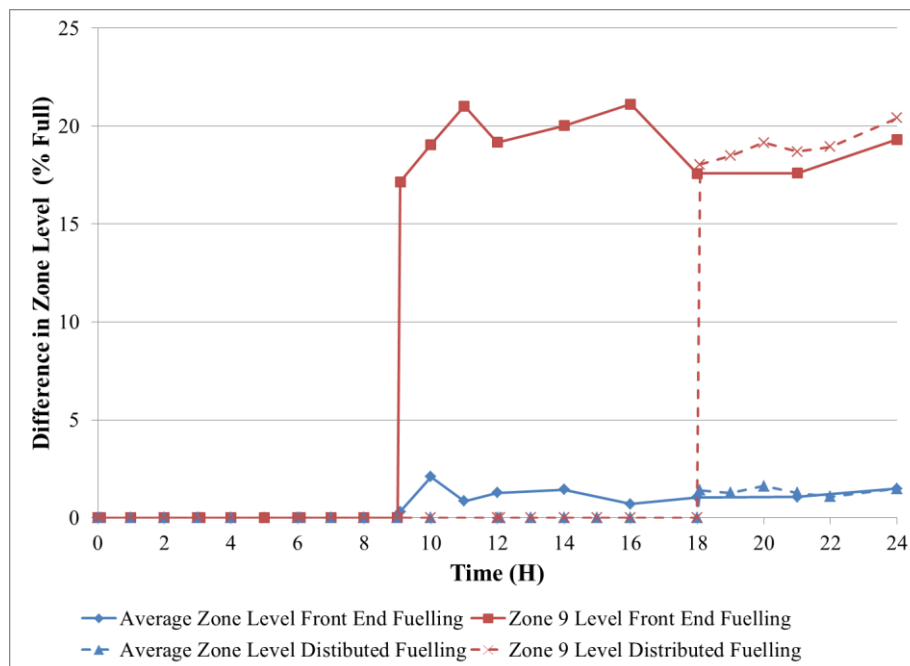
Figure 5.18: Front-end Vs. distributed fuelling, local zone effects (R4).

The local zone effects for the Front-end and Distributed fuelling schemes are compared for the fuelling of channel R4 for both the local (Zone 9) and average levels in Figure 5.18. The response to fuelling R4 for both the front end and distributed cases is quite similar as expected and the differences between the two are small. The peak change in Zone 9 in the distributed case is 20.4% full (a

reduction of 0.7%) while the average zone level peak change is 1.6% full (a reduction of 0.5%). Similar effects will be seen in the levels of adjacent zones with the tilt effects of the fuelling subdued slightly for distributed fuelling.

Although caution should be taken to avoid excessive fuelling in one zone and fuelling induced flux tilts must be monitored, the control system is able to handle the reactivity inputs from fuelling. This fuelling simulation proved that the TRUMOX CANDU was able to handle day-to-day fuelling within the prescribed operational envelope. A major finding in this phase was related to the fuelling strategy for the TRUMOX fuel. In particular, the fuelling rate required for the system is high at 4.66 channel visits per day which will place high demand on the fuelling machine and the associated operations personnel. Changes to the fuelling strategy may be able to reduce this demand to a more reasonable level (e.g. 2-3 channel visits per day) but the reactivity of the fuel may limit the amount of multi-bundle shifting available. Studies done on advanced CANDU systems with dedicated fuelling machines have predicted the need for an average of 5 fuelling visits per day and do not express concern in meeting this requirement [77]. The control system seems capable of handling the fuelling demands of the TRUMOX-30 CANDU-900 system. It is useful now to determine if the power ramps caused by the fuelling transient will have any effects on the integrity of the fuel.

5.9   Fuelling power ramp effects on fuel integrity

The online fuelling nature of the CANDU design which utilizes frequent small fuelling shifts to maintain the reactivity balance, achieve flux profile targets and compensate for fuel burnup has the potential to introduce local power transients which must be limited to ensure fuel sheath integrity. For the TRUMOX-30 CANDU-900 system, approximately 5.33 fuel bundles must be inserted into the core on average during each full power day of operation resulting in approximately 4 to 5 channel visits per full power day. Each fuelling visit will insert 1 to 2 fresh fuel bundles into one end of the channel while removing 1 to 2 spent fuel bundles from the other end of the channel. This fuelling process not only introduces fresh fuel into the core it also shifts low burnup fuel into the higher flux region in the center of the core. The fuelling shift thus produces a local power transient, having an effect on the power level of each of the bundles in the fuelled channel as well as the bundles in the adjacent channels. These local power changes are termed the fuel ramp rate, and if they exceed predetermined

limits there may be a higher probability of fuel defects. The specific limits on power and the ramp rate are based on the linear element rating and changes with fuel burnup. It should be noted that due to the bi-directional fuelling design of CANDU, adjacent channels are fuelled from opposite ends and older fuel bundles with high burnup will be exposed to power transients from fuelling adjacent channels with new fuel.

An in depth analysis of early CANDU fuel performance was performed by Penn et al. [78] to identify the power and ramp limits and the probability of fuel defects derived from operational data of CANDU reactors. The limits derived from this work are considered the standard criterion for power and ramp limits during fuelling for NU CANDU systems. The ramp limits derived from this operational data cover a burnup range from 40 MWh/kgHE to 240 MWh/kgHE which is consistent with the bulk of the CANDU burnup cycle. The limits found are defined by equations 48 and 49 for a given burnup ω in MWh/kgHE and dwell time at the high power, t in hours [78].

$$P > 44.6 + \frac{232}{\omega} - 22[0.5 - e^{-2.3t}] \tag{49}$$

$$\Delta P > 6 + \frac{1460}{\omega} - 24[0.5 - e^{-2.3t}] \tag{50}$$

In a normal NU CANDU system the fuelling shifts of 4 or 8 bundles will push much of the fuel through the high flux central region and out to the lower flux end of the channel. Therefore, there will be a short dwell time during which the bundles will be at the higher power. If the dwell time is more than 2.5 hours the effect of the dwell time is essentially the same as an infinite dwell time at the high power. For an 8 bundle fuelling shift in a CANDU-900, the 5 bundles that remain in the channel are shifted through the high flux region of the core towards the end with the freshest of these sitting in the higher flux positions of 9, 10 and 11 so the dwell time has some effect on the defect probability. However, with a 4 bundle shift the older bundles are shifted into high flux positions and remain there negating the effects of the dwell time. In the case of the TRUMOX-30 fuel, the shifts are 1 or 2 bundles resulting in small incremental movement increasing the dwell time such that the relationships above can be simplified to those presented in equations 50 and 51.

$$P > 33.6 + \frac{232}{\omega} \qquad \qquad \Delta P > \frac{1460}{\omega} - 6 \qquad \qquad (51, 52)$$

In general, the acceptance criteria are satisfied as long as one of the above limits is precluded. This result can be applied to the burnup range to produce the absolute power and ramp limit for fuel in CANDU which is displayed in Figure 5.19.
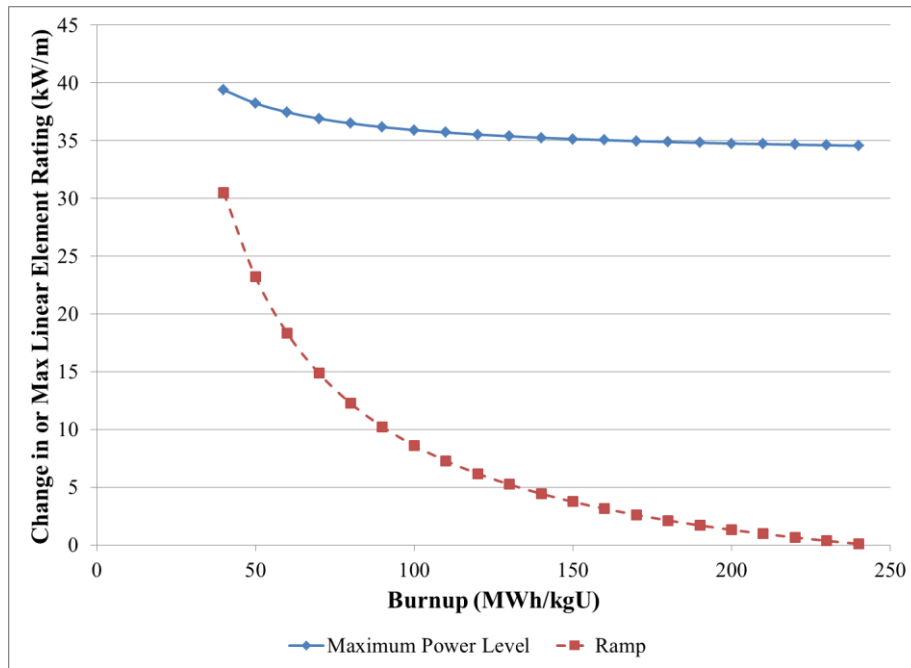
Figure 5.19: Absolute Power limit and ramp limit for CANDU.

These limits on linear element rating are then translated into macroscopic quantities predicted by the RFSP code such as bundle power or bundle power ramp (change in bundle power). The maximum linear element rating in kW/m is converted to kW by multiplying by the bundle length of 0.4953 m and then must be scaled down based on the pin power factors of the fuel. For the TRUMOX-30 fuel the maximum pin powers are experienced in the outer ring with pin power factor (PPF) values of 1.136 to 1.445 over the burnup cycle of 30 MWD/kgHE as shown in Figure 5.20. These values are taken from the WIMS-AECL infinite lattice simulations discussed in Chapter 4.3.
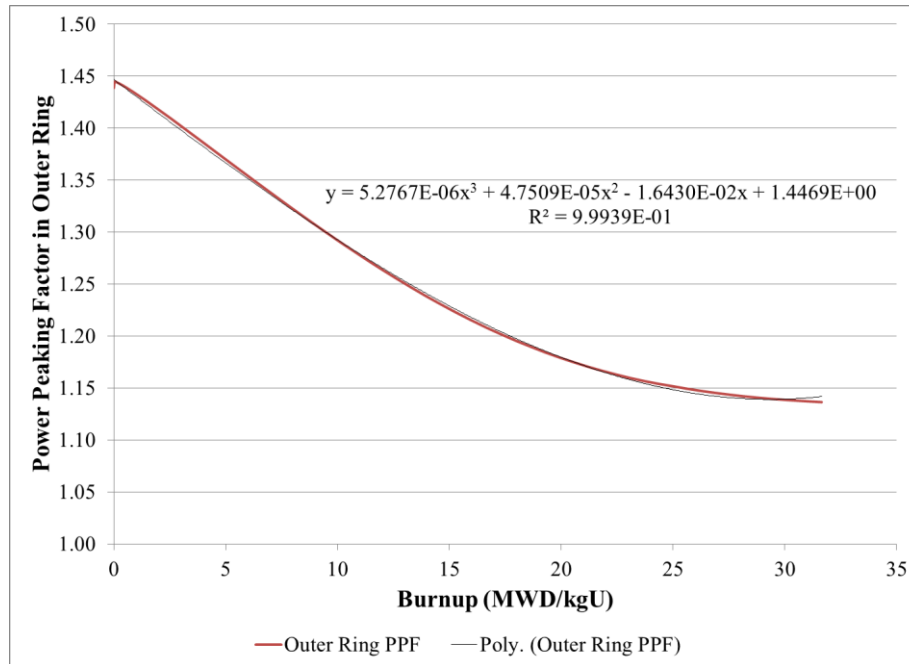
Figure 5.20: Outer ring PPF for TRUMOX-30 Fuel in CANDU 900.

Given the burnup level and the associated PPF value along with the fact that there are 42 fuel elements in the TRUMOX-30 fuel bundle, the limits on absolute bundle power and bundle power change, as dictated by the simplified Penn et al. equations, were calculated. These limits were then applied to the short term fuelling simulations performed in RFSP for the TRUMOX fuel, previously discussed in Chapter 5.8. The fuelling of a central channel in the core will likely cause the largest impacts on bundle power and is thus compared to the derived defect limits. The absolute power reached during the fuelling of channel M16 with one bundle is provided in Figure 5.21.

Channel M16 fuels from the left end of the channel therefore bundle 1 is extracted and a new bundle is placed into position 13. The lowest burnup position is 13 while the highest burnup occurs in is position 1. If we extrapolate the Penn et al. limits and compare them to the pre-fuelled bundle powers and the peak powers after fuelling, we see that all but the first three bundles in the channel (positions 13, 12, 11) exceed the limits for change in bundle power. Additionally, the lower burnup positions of 11, 10, and 9 for both the pre-fuelling power and peak power after fuelling exceed the specified limits for absolute bundle power. Therefore,

there is a probability of defects occurring in the bundles in positions 11, 10 and 9 since these exceed both the absolute and ramp limits for bundle power.
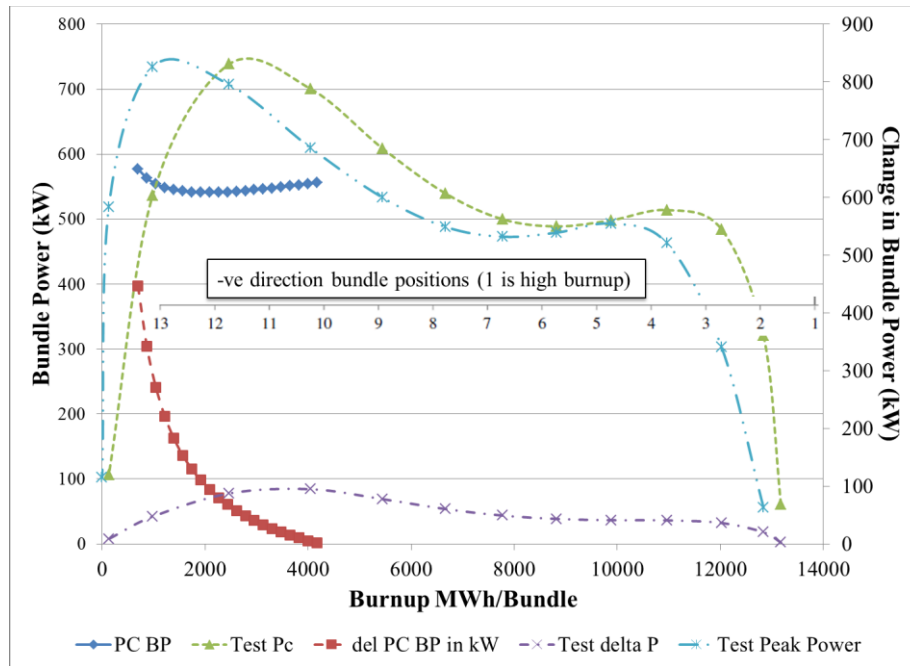
Figure 5.21: Effects of fuelling M16 on Bundle Powers.

The Penn et al. criterion are defined specifically for NU fuelled CANDU systems and as such there are concerns regarding their application to advanced fuel designs that are formulated for long term burnup and have higher enrichments. In these cases, the Penn et al. criterion and limits are conservative in determining the probability for a fuel defect. The operational data for the criteria comes from the earliest CANDU stations, specifically NPD and Pickering. Further literature points out issues such as increased experience in Zircaloy material behavior and higher burnup fuels that provide information that suggests the limits should be shifted [79]. In addition the use of CANLUBE, a graphite lubricant that coats the fuel pellets and remains between the pellet and clad, increases the ability of the fuel elements to withstand fission gas release without developing a defect. These factors are not taken into consideration by the Penn et al. criterion.

The development of the Advanced CANDU Reactor (ACR) included studies to prove the design adequacy of the ACR fuel [80] and to define the operational envelope for the fuel [81] along with simulating refueling transients [82]. The

ACR fuel is very similar to the TRUMOX-30 design both physically, 43 elements with a larger diameter central BNA, and in terms of fissile content (~2.4%) and fuel burnup range (~20-30 MWD/kgU) [80], A comparison is show in Table 5.10.

Table 5.10: Comparison of ACR fuel and TRUMOX-30 Fuel.

Characteristic	ACR Fuel [80]	TRUMOX-30 Fuel
Bundle design	43 Element (large center pin, smaller outer rings)	43 Element (large center pin, smaller outer rings)
BNA	$DyZrO_2$ center element	$DyZrO_2$ center element
Fissile content	2.4 wt%	2.53 wt%
Burnup (average)	~20 MWD/kgHE	~30 MWD/kgHE
Burnup (maximum)	~35 MWD/kgHE	~35 MWD/kgHE

Given the similarities between the two fuel types it is logical to apply the ACR fuel envelope to the TRUMOX-30 fuel in order to determine if the fuelling shifts experienced in the TRUMOX-30 CANDU-900 are within acceptable limits. The ACR fuel operational envelope is provided in Figure 5.22 covering the full burnup cycle of TRUMOX-30 fuel along with the original Penn et al. power limit.
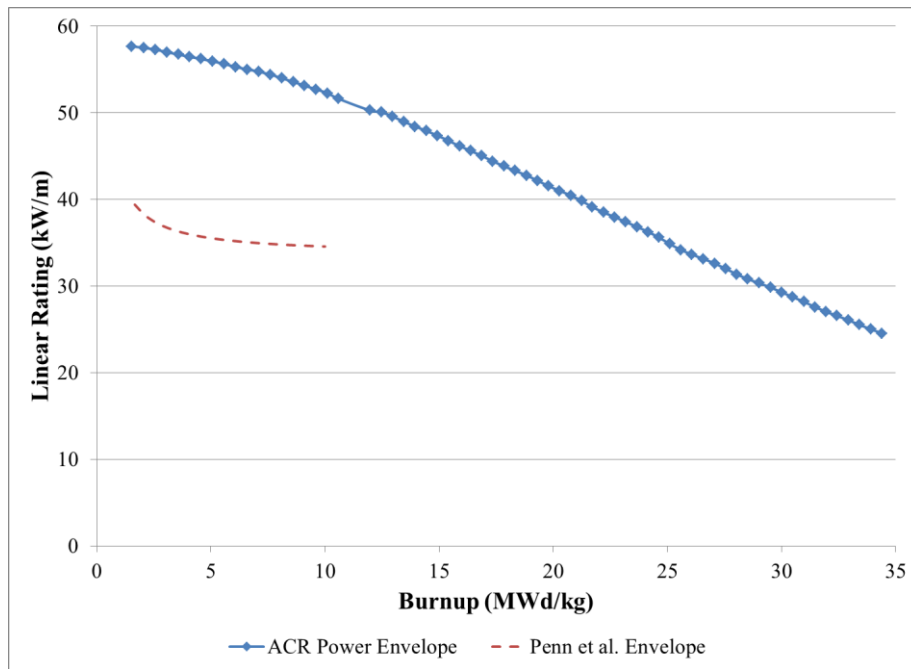
Figure 5.22: ACR Fuel Operational Envelope as compared to the Penn et al. NU criterion [78, 81].

189

The ACR fuel limit is much higher than those adopted for NU fuel based on historical and conservative data. Additionally, the ACR criteria cover a more useful range of burnup for advanced fuels. The transient resulting from the fuelling of channel M16 is compared to the ACR fuel operational envelope in Figure 5.23. The peak bundle powers in M16 during the transient come close to the limit but are still within the envelope. The initial bundle powers in M16 before the fuelling are well within the ACR fuel envelope.
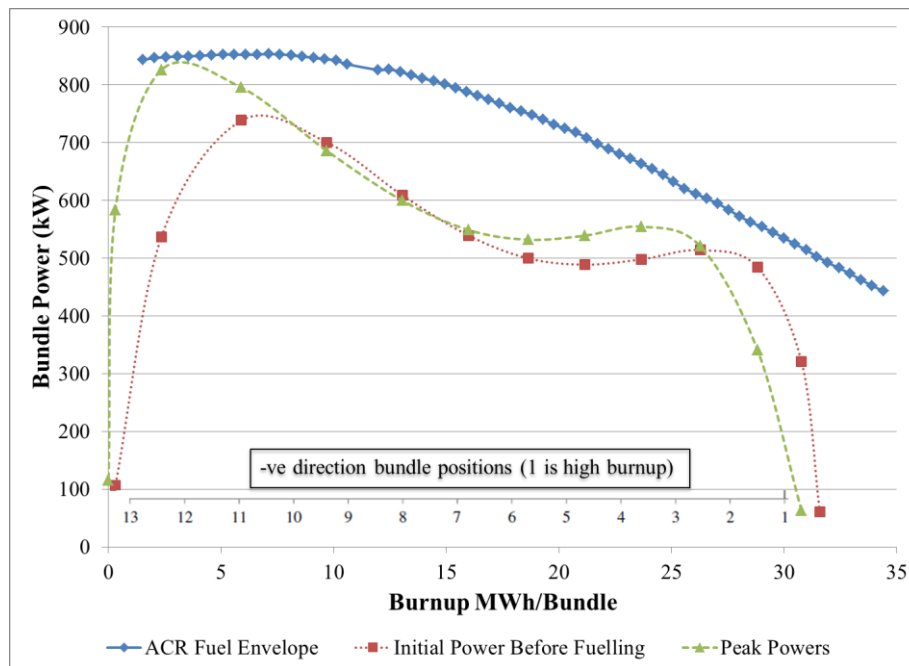
Figure 5.23: Comparison of M16 Fuelling Transient to ACR Fuel Operational Envelope

The peaking bundle powers are the result of two effects, the reactivity insertion from fuelling and the axial flux shape in the core. For TRUMOX, the axial flux shape is peaked at the ends of the core in positions 3 and 11, as discussed in Chapter 5.2.1. This peaking in the ends of the channel means that the fresh fuel is being inserted into higher flux regions than would be the case for NU resulting in larger bundle power ramps. The axial flux profile could be optimized to negate these effects but this would require reconfiguration of the adjuster locations. This is outside the scope of this study as the desire here is to examine the potential for TRUMOX in an existing and unmodified CANDU-900 reactor.

The ACR fuel operational envelope is for sustained power with a maximum linear rating limit of 58 kW/m. The maximum linear ratings during fuelling for ACR are 64 kW/m for fresh fuel and 69 kW/m for irradiated fuel [80]. Using the highest PPF encountered over the TRUMOX-30 fuel burnup cycle, 1.45, the limit on sustained bundle power is 832kW and the limits on bundle power during fueling are 918 kW and 989 kW for fresh and irradiated fuel respectively. These transient fuelling limits are only valid for a short time during and after the fuelling operation (<1 hour) after which the standard fuel envelope applies again.

The bundle power ramp is evaluated based on the original Penn et al. standard in Figure 5.24 and the bundles in positions 10 to 1 exceed the prescribed limit for change in bundle power. However, these bundle positions are safely below the ACR fuel envelope (seen in Figure 5.23) and thus should not experience defects.
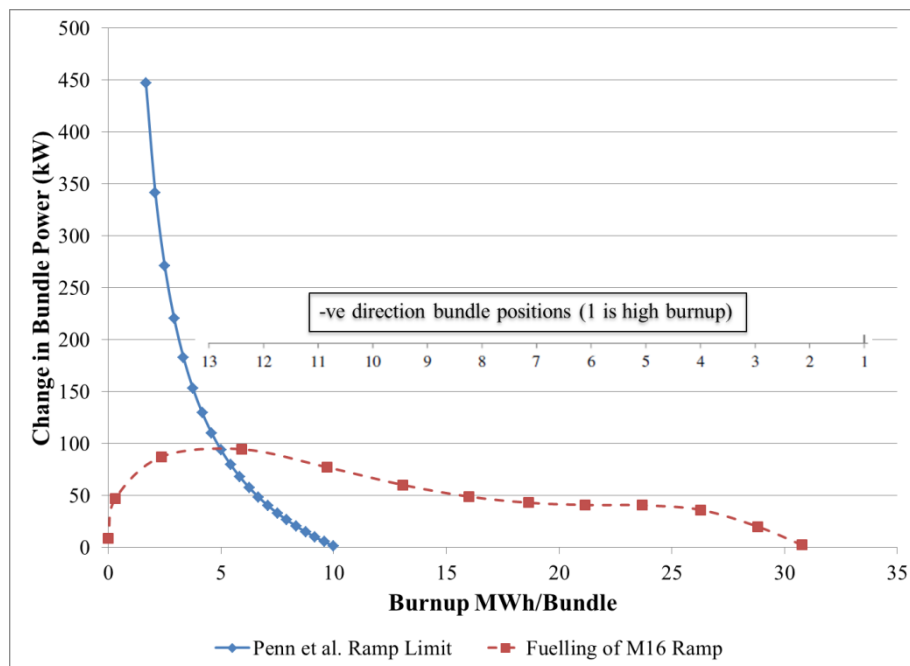
Figure 5.24: Comparison of M16 Fuelling Transient to Penn et al. Ramp.

The channels in proximity to the fuelled channel also see an increase in their bundle powers due to the fuelling. This is less than the power changes seen in the fuelled channel but due to the bi-directional nature of fuelling in CANDU the channels adjacent to the fuelled channel may experience the highest power change in the bundles with the most burnup which can become limiting as the criteria

decreases with burnup. The largest power change in channel M16 when it is fuelled is 94.7 kW at bundle position 10. The adjacent channel fuelled in the opposite direction that experiences the largest associated bundle power change is M-17 which experiences a maximum change of 22.8 kW at bundle position 10. Despite the fact that this bundle is at a higher burnup (26.27 MWD/kg) the peak power is still well within the ACR fuel envelope discussed above. The adjacent channel fuelled in the same direction that experiences the largest power change is N17 which has a maximum change of 28.7 kW in bundle 11. The peak bundle power is still within the envelope and the burnup level is lower for the bundle (5.88 MWD/kg). The peak powers for the two adjacent channels most impacted during the fuelling transient, N17 and M17, are compared to the ACR fuel envelope in Figure 5.25. In all cases adjacent channels show large margins (>78 kW) to the limit.
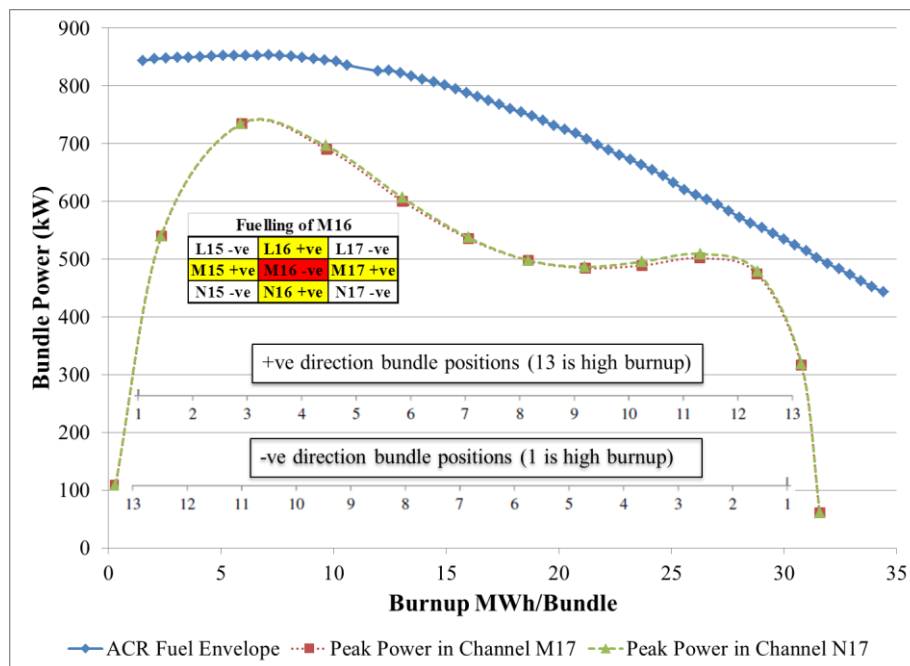
Figure 5.25: Comparison of adjacent channels in the M16 Fuelling Transient to the ACR fuel Envelope.

The channels in the periphery of the core will experience similar transients but with lower initial powers. However, the use of 2 bundle fuelling shifts in the core periphery may result in higher reactivity transients that could produce bundle powers that may exceed the limits. Thus the fuelling of channel P24 is explored

in a similar fashion to that of channel M16. The initial and peak powers during the fuelling transient for P24 are compared to the ACR fuel envelope in Figure 5.26.
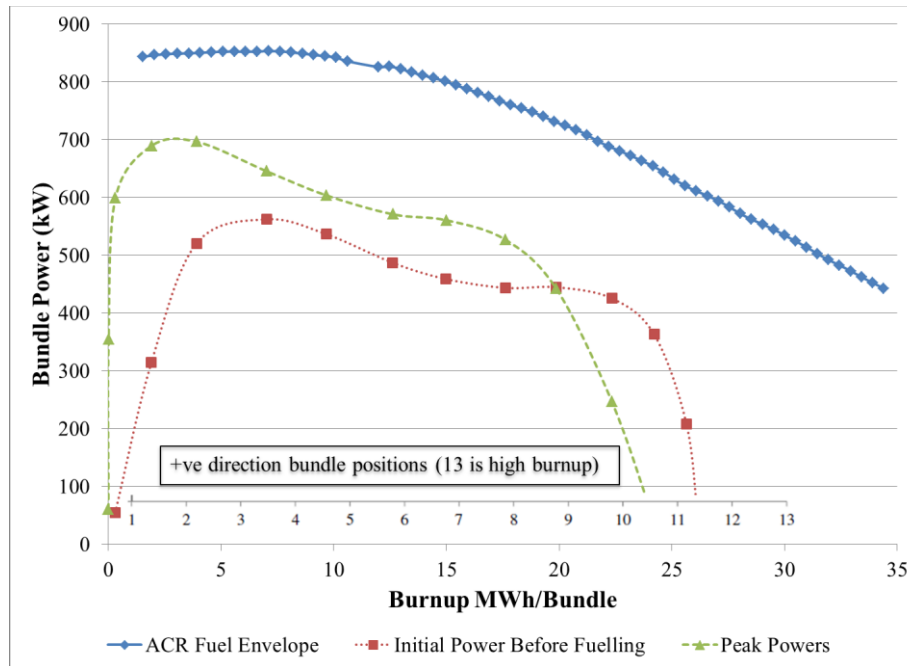
Figure 5.26: Comparison of P24 Fuelling Transient to ACR Fuel Operational Envelope

Channel P24 is fuelled with a 2 bundle shift and experiences a large increase in the bundle powers as a result. The adjacent channels also experience a sizeable bundle power change. The change in bundle power due to fuelling in channel P24 is 159.7 kW at bundle position 5. The adjacent channel fuelled in the opposite direction that experiences the largest bundle power increase due to this fuelling is channel O24 with an increase of 56.2 kW at bundle position 7. The adjacent channel fuelled in the same direction that experiences the largest bundle power increase due to this fuelling is channel O23 with an increase of 55.0 kW at bundle position 5. These changes in bundle power are much higher than for the one bundle shift fuelling for channel M16 but the margin to the top of the fuel envelope is also much higher for the fuelling in the periphery channel P24.

The bundle power ramp experienced in channel P24 during the fuelling event is compared to the Penn et al. criterion in Figure 5.27. Despite the larger bundle power ramp than M16, there is still sufficient margin to the top of the ACR fuel

envelope (>154 kW). The peak powers of the channels in proximity of the P24 fuelling, O23 and O24 are compared to the ACR envelope in Figure 5.28. There is a large margin to the top of the ACR fuel envelope (>152 kW) in both cases.
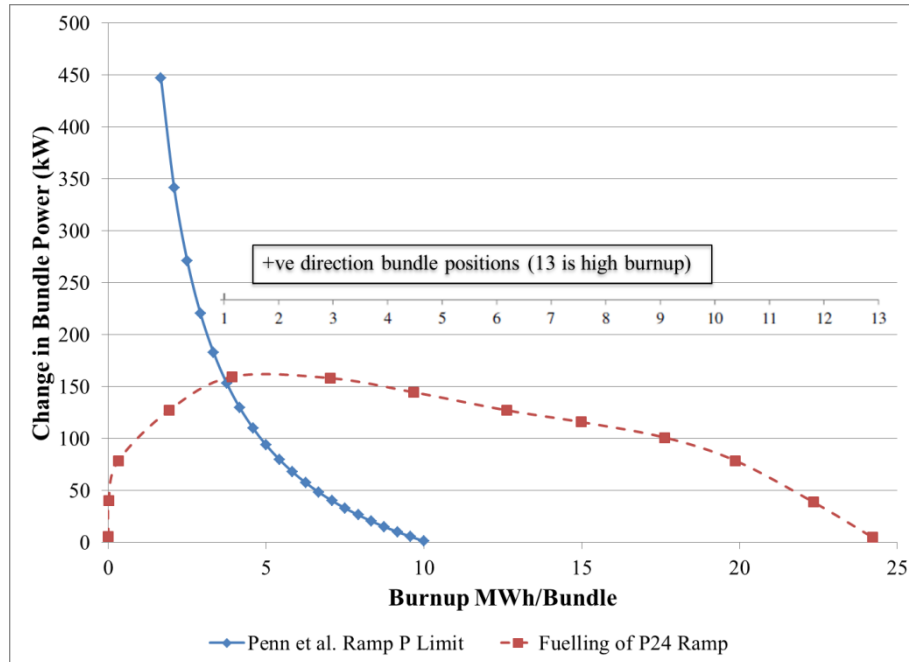
Figure 5.27: Comparison of P24 Fuelling Transient to Penn et al. Ramp.

Since the periphery channels are at much lower powers than the central channels the large changes in bundle power produced by the two-bundle-shift fuelling can be accommodated without stressing the limits dictated by the ACR fuel envelope.

The comparisons above show that during a fuelling transient in both a high power central channel and a lower power periphery channel, the bundle powers in the TRUMOX-30 CANDU-900 core will remain beneath the limits for the ACR fuel operating envelope and the probability for a fuel defect occurring is quite low.
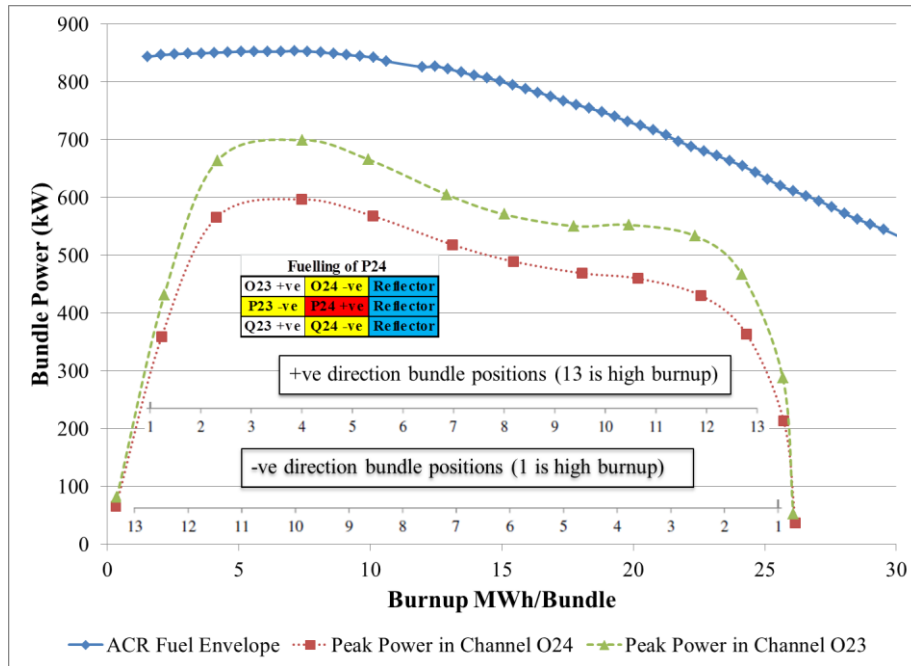
Figure 5.28: Comparison of adjacent channels in the P24 Fuelling Transient to the ACR fuel Envelope

Chapter 6

Conclusion and Discussion

The objective of this dissertation is to present a thorough investigation of the feasibility of actinide transmutation using a new blended oxide fuel design in the proven CANDU reactor system. This capability to reuse once through fuel material further demonstrates the complementary nature of the CANDU system to synergistically interface with LWR designs thereby yielding benefits of increased energy generation from the fuel and reduced legacy impacts of the nuclear fuel cycle. The expansive evaluation of the detailed neutronics behaviour of the actinide fuel and its implications on CANDU reactor operations did not indicate any major complications in the implementation of such an advanced fuel cycle.

The driving force behind using an actinide mixed oxide fuel is the desire to take steps to close the nuclear fuel cycle. This study specifically evaluates the use of current thermal nuclear reactor designs as an intermediary step for burning plutonium and minor actinides before progressing to a fast reactor system that will complete the cycle. The recycle of actinides in spent fuel eliminates much of the long term radiotoxicity and heat load concerns, thereby streamlining the management of spent fuel. Additionally, the reuse of fissile materials increases the energy generated per ton of mined uranium. The use of thermal reactors as an intermediary system to burn actinides provides a significant reduction in the amount of fast reactor infrastructure required to handle the actinides in spent fuel and utilizes proven reactor designs than are currently available.

This thesis presents a unique fuel design using an existing advanced 43 element fuel bundle and a new fuel, TRUMOX-30, composed of a mixture of actinides reprocessed from spent fuels and mined natural uranium that is designed for use in a standard CANDU-900 nuclear power plant. A major underlying criterion of the design and optimization was that the core geometry and physical structures were not to be altered in any way, such that the new fuel could be utilized in an existing reactor with minimal changes.

This fuel design and the analysis performed within this work demonstrated the performance of this actinide mixed oxide (MOX) fuel within the proven CANDU-900 pressurized heavy water reactor system. The 43-element bundle design has a thick central element containing burnable neutron absorber ($DyZrO_2$) which reduces the coolant void reactivity. The TRUMOX-30 fuel is a mixed oxide containing 96.9% natural uranium oxide blended with 3.1% actinide oxide containing neptunium, plutonium, americium, and curium. The actinide isotopes and relative concentrations correspond to used light water reactor fuel that has been cooled for 30 years. The TRUMOX-30 CANDU-900 design is operated with the adjuster rods removed from the core and is able to attain 99.93% of the desired burnup target, 30 MWD/kgHE, while bundle and channel power limits of 935 kW and 7.3 MW are respectively maintained at all times.

Overall it is demonstrated that the TRUMOX-30 CANDU-900 system can provide a significant reduction in the net inventory of actinides. With an initial actinide content of approximately 520 g/bundle, the actinide conversion for this design was approximately 34.76% or 180.6 g/bundle. Thus a full core load of 6240 bundles would result in a net transmutation of about 1127 kg of actinide material. The longer burnup cycle of the TRUMOX-30 fuel reduces the daily fuel bundle requirements for fuelling of the core to 1/3 that of NU CANDU and also provides added efficiency that helps to offset the manufacturing costs of the fuel.

Upon the completion of the fuel design and lattice physics examination, several full core simulations were performed to verify the feasibility of utilizing the TRUMOX-30 fuel in the CANDU-900 system. The items of interest included the reactivity worth of the control devices, the computation of temperature and purity reactivity coefficients, the effects of coolant voiding and short term and long term fuelling effects. The results of these computations were compared to standard values for a natural uranium fuelled CANDU-900. From these studies the following conclusions are drawn:

- TRUMOX CANDU-900 has a more favorable response to coolant voiding
    - The coolant void reactivity for TRUMOX is about 80% lower than the comparable NU values. The reduced reactivity injection, due primarily to the inclusion of the burnable neutron absorber in the center pin of the TRUMOX fuel bundle, puts much less stress on the reactor regulating and shutdown systems in the event of a loss of coolant event.

- The TRUMOX fuelled core has similar controllability to the NU design
    - The relative worth of the reactor control system, $(\Delta\rho/\beta)$, was found to be quite similar between the TRUMOX and NU systems
    - The fuel and coolant temperature reactivity coefficients are both smaller in magnitude for the TRUMOX core but their combined effects are similar to the NU response.

- The TRUMOX fuel design is controllable using the current CANDU-900 control system for normal operations.
    - The fuelling simulations demonstrated that the reactor control system (specifically the liquid zone controllers) was capable of safely managing the core reactivity while maintaining within the standard operational envelope.
    - The channel and bundle powers within the core were maintained below their prescribed limits and the fuelling ripple and local power transients were found to be controllable.
    - The fuelling ramp effects were found to be within the tolerance prescribed for advanced CANDU fuels and should not cause an increase in the amount of fuel defects.
    - The average fuelling rate of 5.33 bundles/FPD is accomplished with 4 to 5 channel visits. This is slightly higher than the standard NU fuelling machine duty requirement of 3-4 channel visits, but is within the capabilities of the reactor fuelling machine[11].

- The TRUMOX core is more responsive to changes in reactivity
    - The delayed neutron fraction and the neutron prompt generation time for the TRUMOX fuel are respectively about 34% and 38% lower than the values for NU, meaning that the core will respond more quickly to changes in reactivity.
    - The flatter axial flux profile of the TRUMOX core produces smaller sub-criticalities for the main axial modes indicating an increased susceptibility to axial tilts.

---

[11] Despite the number of channel visits per day being within the perceived capability of the fuelling machine, a full assessment of its capabilities was not performed here and would be useful to ensure that the system can handle the increased operational demand.

- The coolant and moderator purity is less important in the TRUMOX core
    o The moderator purity coefficient is <5% of the NU value due to the increased fissile content in the TRUMOX fuel.
    o The TRUMOX coolant purity coefficient is about 67% of the value for NU again due to the fissile content.
    o The lower purity coefficients reduce the impact on operations of minor changes in moderator or coolant purity due to contamination.

This dissertation represents the most in depth and detailed analysis and simulation performed for the use of actinide mixed oxide fuel in a CANDU reactor in open literature. Based upon the assessment of lattice and core physics attributes and simulations, the novel fuel design was found to be capable of safe and consistent operation in an existing CANDU reactor with minor changes to operational procedures and could achieve significant actinide destruction (on the order of tons). The TRUMOX-30 fuel design builds on previous experience with plutonium mixed oxide fuels with an evolutionary design that includes minor actinides. This design is easier to manufacture than other types of reprocessed fuels as it uses group extracted actinides thereby reducing the complexity in the partitioning tasks for fuel manufacturing. Additionally, group extraction avoids the proliferation concerns that come with separated extraction processes that produce a pure plutonium stream. The overall conclusion of this work is that the utilization of an actinide mixed oxide fuel in a CANDU reactor is possible and will provide significant benefit to the nuclear fuel cycle. The employment of an actinide burning system, as described herein, is an integral piece to help close the nuclear fuel cycle which will help to reduce the volume and longevity requirements of fuel disposal systems and provide a viable intermediary step of actinide transmutation that can feed into a fast reactor solution.

The closed cycle would include partitioning and transmutation activities at the back end of the current once through fuel cycle such that cooled spent fuel is separated out into three main components which can be reused, recycled and disposed. The uranium inventory of the spent fuel can be partitioned out and reused in light and heavy water reactors through blending with enriched, natural, or depleted uranium to produce a fuel design that is equivalent to the standard fuel used in the design or just used directly in HWRs. The plutonium and minor actinides (neptunium, americium and curium) can be group extracted and recycled using a blended mixed oxide fuel in actinide burning reactors such as the

TRUMOX-30 CANDU-900 examined here. Finally, the fission product waste can be separated out and disposed of safely in a long term repository. Upon the completion of burnup in the thermal systems the reused uranium fuels would be cooled and reenter the cycle at the beginning. The recycled MOX fuel could be reprocessed to extract the uranium content for reuse in thermal systems or as feedstock for fast reactor breeding applications. The actinides content of the MOX fuel would be sent to a fast reactor for ultimate disposal. This multi-stage strategy removes the actinide content from the long term repository stream and through burn steps in both a thermal system (e.g. TRUMOX-30 CANDU-900) and a fast reactor system transmutes the actinides into shorter lived isotopes and fission products. The closing of the nuclear fuel cycle with the assistance of the TRUMOX-30 CANDU-900 will convert the current inventories of spent fuel into a valuable resource that can supplement the mining of new uranium ore. The reuse and recycle of the fuel materials is more efficient and sustainable than the current once through cycle and reduces long term repository costs. Additionally, it ensures that the end waste produced is only the fission products which have little residual value and manageable disposal and monitoring demands.

6.1 Methodology of design and analysis

The design and analysis methodology utilized in this study follows the standard practices for CANDU reactor systems to ensure consistency and enable direct comparison of the TRUMOX-30 fuel performance to that of natural uranium. A major constraint in the study was that changes to the reactor platform and operational procedures be minor, since the desire is to implement an advanced fuel cycle in existing designs. In order to avoid costly design and licensing changes, the reactor systems considered here could not be physically altered in any significant way and the operational procedures must remain largely intact, thus ensuring an easy transition to the new fuel. The most important constraint was that the fuel design utilized must perform within the operational envelope of the existing CANDU-900 reactor system in terms of operational limits (e.g. control system envelopes, temperatures, bundle and channel power limits, fuel ramp rates and burnup limits). These guidelines were adhered to throughout the process and thus the TRUMOX-30 fuel design created is easily implemented into the CANDU reactor.

6.2   Reactor design optimization recommendations

Despite the excellent performance of the TRUMOX-30 CANDU-900 system there are some possible enhancements to the reactor design that can increase the efficiency and optimize the reactor system for actinide transmutation operations. Physical alterations to the CANDU reactor design were constrained in this analysis to ensure a near seamless integration of the actinide fuel into current CANDU units. However, the modeling and simulation efforts performed herein have identified certain reactor systems that can be improved to increase the compatibility of the CANDU design with actinide fuels.

The actinide fuel designs produce a much flatter axial flux profile that is different from the standard NU distribution. As discussed in Chapter 5.2, the axial flux distribution for TRUMOX-30 is flat or dished in the center of the channel and has some peaking at bundle locations 3 and 11 while the NU flux is more cosine shaped and peaks towards the middle of the channel in positions 6 to 8. The flatter profile is the result of neutron absorption by the minor actinides in the fuel and the smaller fuelling shift sizes employed. The control mechanisms used by the reactor regulating system, specifically the adjuster rods and mechanical control absorbers (MCAs) are located primarily in the central area of the core that coincides with the flux peaks of an NU configuration. However, this area is dominated by the flat or dishing flux profile generated by the TRUMOX fuel reducing the effectiveness of the control devices, especially the adjuster rods. Therefore, it may be prudent to investigate the relocation of the adjusters and MCAs to areas of higher flux. The liquid zones are more distributed in the core and are less affected by the flux flattening but are still susceptible and may benefit from modifications to increase their worth (e.g. increasing the size or adding a neutron poison such as boron to the water).

The adjusters in the TRUMOX-30 CANDU-900 design are no longer employed to provide positive reactivity margin to compensate for xenon buildup in the core and are left fully withdrawn from the core during normal operations. They are primarily utilized as supplements to the liquid zone controllers and the MCAs to introduce negative reactivity into the core. The flattened axial flux shape reduces the relative worth of the adjusters significantly (~65%). Repositioning the adjusters closer to the channel ends will place them closer to the areas of peak flux. This relocation would also open up the possibility of keeping the adjusters in core during operations once again. However, this is not a feasible option for an

existing CANDU unit. Although use of the adjusters would impede actinide transmutation it would provide some positive reactivity in the core than can be used to compensate for xenon buildup allowing operational procedures for Xenon override to remain in place.

The flatter flux and lack of a central peak means that the MCAs are similarly affected but to a lesser extent (relative worth is reduced by 34% from NU). However, the lack of the central flux peak may be problematic as the insertion of the MCAs in to the center of the channel causes a significant flux depression and subsequent displacement of flux towards the edges of the core. Thus it is prudent to examine the issue and the possible benefits of spacing out the MCAs in the axial direction.

These recommended changes to the reactor control system will likely be costly and depart from the desire to ensure a simple and easy transition from NU to TRUMOX-30 fuel in a currently operating CANDU-900. Rather than altering the reactor control system for the actinide fuel it may be useful to investigate further refinement of the fuel design. The current TRUMOX-30 fuel design is well tailored for actinide burning while being compatible with the standard CANDU-900 system. Thus modifications to the reactor design should only be undertaken if the reactor is being dedicated to actinide burning and include an exhaustive study of the effects on operations.

6.3   Recommendations for future analysis work

The design and analysis work performed and documented in this dissertation for the TRUMOX-30 CANDU-900 reactor system was extensive. However, there are additional areas of focus that would be necessary to move the design forward towards in-reactor testing and real world trials. This study dealt with steady state near equilibrium operations and did not explore approach to criticality or other lower power configurations. Additionally, the start-up configuration of an actinide core has not been fully explored specifically the loading procedures and subsequent operations to bring an initial full core of fresh actinide fuel to the equilibrium state investigated in this dissertation. The loadings for depleted or natural uranium bundles and the utilization of neutron poisons in the moderator to manage the increased reactivity of a full core of fresh fuel would have to be defined. It would also be beneficial to investigate transition cores and evaluate

the effects of gradually converting an equilibrium NU fuelled core to a full actinide fuel load through small core loadings of actinide fuel, producing sequential transitional mixed fuel cores.

Outside of approach to critical, start-up and transition core analysis, the development of a full thermalhydraulics model that can be coupled to the reactor physics model produced herein would be essential for examining the full safety analysis case. A coupled reactor physics and thermalhydraulics model would be more realistic as it includes the heat transfer characteristics of the fuel and the heat transport system. This would be useful in studying the effects of design basis accidents and will help to determine if the TRUMOX-30 CANDU-900 design would be able to meet the full regulatory requirements necessary to become licensed for operation.

There are certain areas presented here that deserve further investigation that is beyond the scope of the dissertation but important for future implementation efforts. The fuel ramp simulations show a potential area of concern with the fuelling of central high power channels where the peak powers come quite close to the advanced CANDU fuel envelope limits. As discussed in Chapter 5.9, this is primarily due to the axial flux that peaks towards the ends of the channel and warrants further investigation into the possibility of design changes to reposition the adjuster locations in order to reduce this peaking. If this effect remains a significant problem, then a reduction in the fuel reactivity (burnup target) may be required, which would involve reducing the actinide content or using depleted uranium as the carrier material.

The effects of the lower prompt generation time and lower delayed neutron fraction of the TRUMOX-30 CANDU-900 on control system response and effectiveness should be further explored with an integrated coupled code model. The TRUMOX core with its lower generation time responds quicker but the control system still has the same lags and time constants that were designed for the slightly slower NU core. As discussed here, ignoring electronic and actuation delays, the responsiveness of the control systems are similar to NU. However, controllability in the clearest sense must examine the effect of perturbations on the systems. As such, a more detailed analysis evaluating the full control system of detectors, electronics and actuators would be beneficial. This analysis could help to evaluate if the control systems can respond to the same levels of perturbations as it does with NU fuel given the same control system lags (e.g.

actuation, processing and measurement delays) and time constants but the faster responding TRUMOX core. Additionally, the detector systems in the core which provide data to the reactor regulating system may be affected by the change in the flux spectrum caused by the TRUMOX fuel. It would be advantageous to explore the possible effects of this spectrum change on the in core detectors as those which focus on thermal flux would receive less signal due to the harder flux in the TRUMOX core.

A coupled code model would also be very useful in investigating the effects of coolant voiding in a more detailed and accurate fashion. Of particular concern is the effect of a checkerboard voiding condition where fully cooled channels are adjacent to voided channels. The checkerboard void condition has been of concern for other fuel designs with higher fission contents and central burnable absorbers as the void reactivity results for such a configuration have been larger than for a standard full void scenario with all channels in one half or all of the core being voided. Thus an exploration of the checkerboard void effect in the TRUMOX core would be useful in enhancing the understanding of the CVR benefits provided by the central burnable absorber in the fuel.

Furthermore, the increase in required fuelling machine visits per day of the TRUMOX design, while within the expected capabilities of the fuelling machines, suggests that a full assessment of the fuelling machine capabilities be performed to confirm that the system can handle the increased operational demands.

The possible physical changes to the reactor control system (e.g. relocation of the adjusters and MCAs and the possible enhancement of the liquid zones), as discussed in Chapter 6.2, are another area of further investigation. The benefits in terms of controllability will have to be weighed against the costs of implementing such changes. Concurrent further research into modifications of the fuel design to better tailor it to the reactor system may also be useful to examine. These efforts could supplement or possibly replace some of the proposed design changes. However, such design modification studies would be part of a redesign effort to optimize the CANDU reactor design specifically for an actinide mixed oxide fuel design. In such a process, it would be desirable to ensure that the versatility of existing CANDU units to operate with a wide range of alternative fuel designs is not impaired.

Bibliography

[1]   R. A. Weigland, et. al, "Impact on Geologic Repository Usage from Limited Actinide Recycle in Pressurized Light Water Reactors," *Nucl. Sci. and Tech.*, **44-3**, pp. 415-422 (2007).

[2]   T. A. Taiwo, et al, "Comparative Study of Plutonium Burning in Heavy and Light Water Reactors," *Proc. ICAPP-2007: International Conference on Advances in Nuclear Power Plants,* Nice, France, May 13-18, 2007.

[3]   "Status and Advances in MOX Fuel Technology", IAEA TRS-415, International Atomic Energy Agency, Vienna (2003).

[4]   B. Hyland, B. Gihm, "Scenarios for the transmutation of actinides in CANDU reactors" *Nucl. Eng. and Des.*, **241**, 4794-4802 (2011).

[5]   S. Kuran, et. al, "Fuel Cycles—A Key to Future CANDU Success", *Proc. HWR-FUTURE: International Conference on the Future of Heavy Water Reactors*, Ottawa, Ontario, Canada, October 02-05, 2011.

[6]   M. Ovanes, et. al, "Enhanced CANDU6: Reactor and Fuel Cycle Options – Natural Uranium and Beyond", *Proc. PHYSOR-2012: Advances in Reactor Physics – Linking Research, Industry, and Education*, April 15-20, 2012, Knoxville, TN, USA.

[7]   L. H. Baetsle and C. De Raedt, "Limitations of actinide recycle and fuel cycle consequences: a global analysis, Part 1: Global fuel cycle analysis," *Nucl. Eng. and Des.*, **168**, 191-201 (1997).

[8]   "Chart of Nuclides", National Nuclear Data Center – Brookhaven National Laboratory (NNDC), http://www.nndc.bnl.gov/chart/

[9]   R. J. Ellis, "Reactor Physics Assessment of the Inclusion of Unseparated Neptunium in MOX Reactor Fuel", *Proc. ANFM-2009: Advances in Fuel Management IV*, Hilton Head Island, SC, USA, April 12-15, 2009.

[10]   J. C. Kuijper, et. al, "HTGR reactor physics and fuel cycle studies," *Nucl. Eng. and Des.*, **236**, pp. 615-634 (2006).

[11]   M. Miguirditchian, etal, "GANEX: Adaptation of the DIAMEX-SANEX Process for the Group Actinide Separation", *Proc. GLOBAL-2007: Advanced Nuclear Fuel Cycles and Systems*, Boise, Idaho, September 10–14, 2007

[12]   J. C. Luxat, "Nuclear Reactor Dynamics and Control: Chapter 2", McMaster University Courseware: Engineering Physics 710 (2006).

[13]   "Evaluated Nuclear Data File (ENDF) Database", IAEA, 2010, http://www-nds.iaea.org/exfor/endf.htm

[14]   B. R. Bergelson, et. al, "Radiotoxicity and Decay Heat Power of Spent Nuclear Fuel of VVER Type Reactors at Long-Term Storage", *Radiation Protection and Dosimetry*, **115, 1-4**, pp. 445-447, 2005.

[15]   B. R. Bergelson, et. al, "Radiation Characteristics of PWR MOX Spent Fuel After Long-Term Storage Before Transmutation in Accelerator Driven Systems", *Proc. 6th Information Exchange Meeting on Actinide and Fission Product Partitioning and Transmutation*, Madrid, Spain, December 2000.

[16]   J. Hopwood et al., "Fuel Cycles in CANDU: Security of Supply and Reduced Used Fuel Management" *Proc. 32nd Annual Conference of the Canadian Nuclear Society*, June 5-8, 2011, Niagara Falls, ON, Canada.

[17]   T. A. Taiwo, et al, "Assessment of a heterogeneous PWR assembly for plutonium and minor actinide recycle," *Nuclear Technology,* **155**, 34-54 (2006).

[18]   "Viability of inert matrix fuel in reducing plutonium amounts in reactors", IAEA TECDOC-1516, International Atomic Energy Agency, Vienna (2006).

[19]   M. S. Yang, et al, "The Status and Prospect of DUPIC fuel Technology," *Nucl. Eng. and Tech.,* **38-4**, 359-374 (2006).

[20]   G. D. Del Cul, et al, "Analysis of the Reuse of Uranium Recovered from the Reprocessing of Commercial LWR Spent Fuel", ORNL/TM-2007/207 and ORNL/GNEP/LTR-2008-002, Oak Ridge National Laboratory, Oakridge, TN, USA, (2009).

[21]   Y. I. Kim, et al, "BN-600 Full MOX Core Benchmark Analysis" *Proc. PHYSOR-2004: The Physics of Fuel Cycles and Advanced Nuclear Systems: Global Developments,* Chicago, IL, USA, April 25-29, 2004.

[22]   S. Kondo, "History and perspective of fast breeder reactor development in Japan", *Energy*, **23, 7/8**, 619-627 (1998).

[23]   P. Wilson, *The Nuclear Fuel Cycle: From Ore to Waste*, Oxford University Press, Oxford, U.K. (1996).

[24]   "Office of Civilian Radioactive Waste Management, Yucca Mountain Science and Engineering Report, Revision 1", DOE/RW-539-1, United States Department of Energy (2002).

[25]   "Plutonium Consumption Program CANDU Reactor Product, Appendix C: Supplementary Data and Licensing", DE-AC03-94SF20218, AECL Technologies Inc., Rockville, MD, USA (1994).

[26]   C. W. Forsberg, et al, "Can Thermal Reactor Recycle Eliminate the Need for Multiple Repositories?", *Proc. OECD/NEA 8th Information Exchange Meeting on Actinide and Fission Product Partitioning and Transmutation*, Las Vegas, NV, USA, November 2004.

[27]   F. C. Dimayuga, "AECL's Experience in MOX Fuel Fabrication and Irradiation", *Proc. IAEA Technical Committee Meeting, Recycling of Plutonium and Uranium in Water Reactor Fuels, Windermere, U.K.*, July 3-7, 1995.

[28]   F. C. Dimayuga, "Fabrication of Simulated Mid-Burnup CANDU Fuel in the RFFL", *Proc. 5th Intl. Conf. on CANDU Fuel*, Toronto, Canada, September 21-24, 1997.

[29] P. G. Boczar, et al., "Advanced CANDU Systems for Plutonium Destruction", *Proc. NATO Advanced Research Workshop on Advanced Nuclear Systems Consuming Excess Plutonium*, Moscow, Russia, October 1996.

[30] G. Horhoianu and I. Patrulescu, "Technical feasibility of using RU-43 fuel in the CANDU-6 reactors of the Cernavoda NPP" *Kerntechnik,* **73**, (2008).

[31] U. Kasemeyer, et al, "The irradiation test on Inert-Matrix Fuel in comparison to uranium plutonium mixed oxide fuel at the Halden Reactor" *Progress in Nuclear Energy,* **38, 3-4**, 309-312 (2001).

[32] G. M. Thomas, et al., "The Potential of Pressurized Water Reactors for Recycle of Americium-Curium" *Proc. WM2010 Conference,* Phoenix, AZ, USA, March 7-11, 2010.

[33] P. W. Chan, et al., ""CANDU® - A Versatile Reactor for Plutonium Disposition or Actinide Burning", *Proc. Global 97*, Yokohama, Japan September 1997.

[34] D. F. Torgerson, ""CANDU® Development: The Next 25 Years", *Proc. 18th Annual Conference of the Canadian Nuclear Society*, Toronto, ON, Canada, June 8-11, 1997

[35] H. P. Gupta, et al, "Advanced fuel cycles for use in PHWRs", *J. Nuclear Materials*, **383**, 54-62 (2008).

[36] B. R. Bergelson, et al, "Transmutation of Actinides in Power Reactors", *Radiation Protection Dosimetry*, **116, 1-4**, 675-678 (2005).

[37] G. Chang, "Enhancing Advanced CANDU Proliferation Resistance Fuel with Minor Actinides" *Proc. PHYSOR 2010 Advances in Reactor Physics to Power the Nuclear Renaissance*, Pittsburg, PA, USA., May 9-14, 2010.

[38] S. Sahin, et al., "CANDU reactor as minor actinide/thorium burner with uniform power density in the fuel bundle" *Annals of Nuclear Energy*, **35**, 690-703 (2008).

[39]   P. W. Chan, et al., "Plutonium Management and Actinide Burning in CANDU Reactors" *Annals of Nuclear Energy*, **35**, 690-703 (2008).

[40]   R. A. Verrall, et al., "Silicon carbide as an inert-matrix for a thermal reactor fuel" *Journal of Nuclear Materials*, **274, 1-2**, 54-60 (1999).

[41]   A. C. Morreale, W. J. Garland, D. R. Novog, "The reactor physics characteristics of a transuranic mixed oxide fuel in a heavy water moderated reactor" *Nucl. Eng. and Des.*, **241**, 3768-3776 (2011).

[42]   A. C. Morreale, et al., "The behavior of Transuranic Mixed Oxide Fuel in a CANDU-900 Reactor" *Proc. PHYSOR 2012 Advances in Reactor Physics – Linking Research, Industry, and Education*, Knoxville, TN, USA., April 15-20, 2012.

[43]   A. C. Morreale, et al., "The behavior of Transuranic Mixed Oxide Fuel in a CANDU-900 Reactor" *Nuclear Technology*, **In Press**, (2012).

[44]   J. J. Duderstadt, L. J. Hamilton, *Nuclear Reactor Analysis*, John Wiley and Sons, Inc. New York, NY, USA., 1976

[45]   D. V. Altiparmkov, "WIMS-AECL Theory Manual", CANDU Owners Group Protected Document COG-00-077/AECL-S&L-WP-21406**,** Provided under license to McMaster University by Atomic Energy of Canada Ltd, Mississauga, ON, Canada (2001).

[46]   G. Marleau, "DRAGON Theory Manual Part 1: Collision Probability", IGE-236 R1**,** Institut de genie nucleaire Ecole Polytechnique de Montreal, Montreal, Canada (2001)

[47]   A. Buijs, "Advanced Reactor Physics and Analysis, Chapter 4 and 5", McMaster University Courseware Engineering Physics 704 (2009).

[48]   D. Altiparmakov, "New Capabilities of the Lattice Code WIMS-AECL", *Proc. PHYSOR-2008: International Conference on the Physics of Reactors, Nuclear Power: A Sustainable Resource*, Interlaken, Switzerland, September 14-19, 2008.

[49]   G. Marleau, A. Hébert and R. Roy, "A User Guide for DRAGON," IGE-174 Rev.5, École Polytechnique de Montréal, Montreal, Canada (2000).

[50]   M. Dahmani, G. Marleau, R. Le Tellier, "Modeling reactivity devices for advanced CANDU reactors using the code DRAGON", *Annals of Nuclear Energy*, **35**, 804-812 (2008).

[51]   M. R. Ball, et al., "The Effect on Super-cell Calculations due to Modelling CANDU Fuel Pin Clusters as Annuli", *Proc. M&C-2011: International Conference on Mathematics and Computation Methods Applied to Nuclear Science and Engineering*, Rio de Janeiro, RJ, Brazil, May 8-12, 2011.

[52]   W. Shen, "CANDU Three-dimensional Neutron Transport Calculations with DRAGON", *Proc. PHYSOR-2002: International Conference on the New Frontiers of Nuclear Technology: Reactor Physics, Safety and High-Performance Computing*, Seoul, Korea, October 7-10, 2002.

[53]   W. Shen, "RFSP-IST 3.04 Theory Manual", CANDU Owners Group Protected Document COG-SQAD-06-5058/AECL-153-117360-STM-002, Provided under license to McMaster University by Atomic Energy of Canada Ltd, Mississauga, ON, Canada (2006).

[54]   B. Rouben, "RFSP-IST, The Industry Standard Tool Computer Program for CANDU Reactor Core Design and Analysis", *Proc. 13th Pacific Basin Nuclear Conference*, Shenzhen, China, October 21-25, 2002.

[55]   B. Rouben, "Introduction to Reactor Physics", [On-Line], Available: https://canteach.candu.org/Content%20Library/20040502.pdf (2002)

[56]   B. Rouben, "Nuclear Fuel Management, Chapter 11: Time-Average Model", McMaster University Courseware Engineering Physics 704 (2011)

[57]   A. Buijs, "Comparison of Methods to Calculate CANDU-6 Reactivity Coefficients", FFC-RCP-096, Atomic Energy of Canada Limited, Mississauga, ON, Canada (2003).

[58]   Z. Xing Guan, et al., "Physics Codes and Methods for CANDU Reactor." *J. Nucl. Pow. Eng.* **1999-06** (1996)

[59]   F. C. Boyd, "Nuclear Power in Canada: a different approach", *J. Energy Policy*, **2.2**, 126-135 (1974).

[60]   J. C. Luxat, "Advanced Nuclear Engineering: Chapter 3", McMaster University Courseware Engineering Physics 4NE3 (2007).

[61]   P. G. Boczar et al, "Plutonium Dispositioning in CANDU" *Proc. IAEA Technical Committee Meeting on Recycling of Plutonium and Uranium in Water Reactor Fuels*, Newby Bridge, U.K., July, 1995.

[62]   S. S. Alyoshin, et. al, "Characteristics of VVER-1000 with 1/3 Core Loaded by MOX Fuel With Plutonium From Surplus Russian Nuclear Weapons" *Proc. PHYSOR 2002: International Conference on the New Frontiers of Nuclear Technology: Reactor Physics, Safety and High-Performance Computing* , Seoul, Korea, October 7-10, 2002.

[63]   K. O. Ott and R. J. Neuhold, *Nuclear Reactor Dynamics*, American Nuclear Society, Chicago, USA., 1985.

[64]   A. C. Morreale, M.R. Ball, D.R. Novog, J.C. Luxat, "The Effects of Actinide Based Fuels on Incremental Cross Sections in a CANDU Reactor", *Proc. M&C 2011: International Conference on Mathematics and Computational Methods Applied to Nuclear Science and Engineering,* Rio de Janeiro, RJ, Brazil, May 8-12, 2011.

[65]   J. H. Bae and J. H. Park "The effect of a CANDU fuel bundle geometry variation on thermalhydraulic performance", *Annals of Nuclear Energy*, **38**, 1891-1899, (2011).

[66]   P. G. Boczar et al., "Reactor Physics Studies for a Pressure Tube Supercritical Water Reactor (PT-SCWR)" *Proc. CCSC-2010: The 2nd Canada-China Joint Workshop on Supercritical Water-Cooled Reactors*, Toronto, Ontario, Canada, April 25-28, 2010.

[67]   A. C. Morreale D.R. Novog, J. C. Luxat, "Transuranic Mixed Oxide Fuel use in CANDU", *Proc. HWR-FUTURE: International Conference on the Future of Heavy Water Reactors*, Ottawa, Ontario, Canada, October 02-05, 2011.

[68]   V. G. Snell, J. R. Webb, "CANDU 9 – The CANDU Product To Meet Customer and Regulator Requirements Now and In the Future", *Proc. 11th Pacific Basin Nuclear Conference*, Banff, Alberta, Canada, May 3-7, 1998.

[69]   "ACR-1000 Technical Description Summary" AECL-10820-01372-230-002-R1, Atomic Energy of Canada Limited, Toronto, Canada (2010) [On-Line], Available: https://canteach.candu.org/Content%20Library/20100100.pdf

[70]   R. Roy, et. al, "Reactor Core Simulations in Canada" *Proc. PHYSOR 2004: The Physics of Fuel Cycles and Advanced Nuclear Systems: Global Developments*, Chicago, IL, USA, April 25-29, 2004.

[71]   B. Rouben, "CANDU Fuel Management Course", (2003) [On-Line]. Available: https://canteach.candu.org/Content%20Library/20031101.pdf

[72]   "Fundamentals of Power Reactors – Module One: Science and Engineering Fundamentals – Reactivity Effects, Section 4", Atomic Energy of Canada Limited, Toronto (1993), [On-Line], Available: https://canteach.candu.org/Content%20Library/19930201.pdf

[73]   H. C. Chow, "Reactor Physics and Fuelling Strategies 1.4, Role of Physics Analysis in Safety and Licensing (Lecture 9)", Chulalongkorn University, (1996). [On-Line], Available: https://canteach.candu.org/Content%20Library/20042114.pdf

[74]   G. Bereznai, "Nuclear Power Plant Systems and Operations: Chapter 1 Module 1B", McMaster University Courseware Engineering Physics 6P03 (2005).

[75] M. Gold, "SMOKIN-A Family of Codes for Reactor Space-Time Neutronics Calculations Based on Modal Kinetics – Theory Manual" OH-90133, Ontario Hydro, Toronto, Canada (1990).

[76] P. S. Chang, K. T. Tsang, D. B. Buss, "Reactor Physics of NG CANDU" *Proc. 22nd Annual Conference of the Canadian Nuclear Society*, Toronto, ON, Canada, June 10-13, 2001.

[77] R. Farkas, et al., "Simulation of Long-Term Fuelling Operations for the ACR 1000", *Proc. 29th Annual Conference of the Canadian Nuclear Society*, Toronto, ON, Canada, June 2008.

[78] W. J. Penn, R. K. Lo, J. C. Wood, "CANDU Fuel – Power Ramp Performance Criteria", *Nuclear Technology*, **34**, 249-268 (1977).

[79] M. Tayal, G. G. Chassie, "Extrapolating Power Ramp Performance Criteria for Current and Advanced CANDU Fuels", *Proc. 21st Annual Conference of the Canadian Nuclear Society*, Toronto, ON, Canada, June 11-14, 2000.

[80] J. Chang, et al., "Proof of Design Adequacy for the ACR-1000 Fuel Bundle" *Proc. 10th CNS International Conference on CANDU Fuel*, Ottawa, ON, Canada, October 5-8, 2008.

[81] J. Hood, F. Iglesias, "Construction of ACR-1000 Fuel Element Operating Envelopes", *Proc. 10th CNS International Conference on CANDU Fuel*, Ottawa, ON, Canada, October 5-8, 2008.

[82] J. Hu, I. Martchouk, R. Robinson, "RFSP-IST Simulation of Fuel Transient During Refuelling the ACR-1000 Reactor", *Proc. 29th Annual Conference of the Canadian Nuclear Society*, Toronto, ON, Canada, June 1-4, 2008.

Appendix A

Instantaneous Snapshot Cores

This appendix provides a selection of the channel age maps used in the instantaneous snapshot core simulations and the resulting channel power distributions from the application of the age maps to the TRUMOX-30 CANDU-900 core design. The methodology for the creation of instantaneous snapshot cores is discussed in Chapter 3.5.4 while the results of the simulations are discussed in Chapter 5.3. It should be noted that core 2B8T was used for the short term fuelling simulations described in Chapter 5.8. The long term core follow simulations described in Chapter 5.10 start from cores 2BT and 2B8T. The 2BT, 2B8T and 2B8T cores were produced from 7x7 seed matrices while the 2BAT and 2BBT cores were produced from 6x6 seed matrices.

The full core k-effective value and the maximum channel and bundle powers found in each of the instantaneous cores are stated in Chapter 5.3 and in Table A.1 below for easy reference.

Table A.1: TRUMOX-30 CANDU-900 Instantaneous core simulation results

Core (seed matrix size)	k-effective	Max Channel Power (kW) [Location]	Max Bundle Power (kW) [Location]	Over Power Channel (COP)	Bundle (BOP)
2BT (7x7)	1.00170	6712.31 [K14]	859.53 [K14-B11]	1.206	1.265
2B6T (7x7)	1.00183	6870.71 [O21]	864.97 [P14-B03]	1.208	1.258
2B8T (7x7)	1.00186	6902.95 [L21]	850.44 [P14-B03]	1.261	1.300
2BAT (6x6)	1.00157	6873.86 [N21]	856.85 [Q14-B11]	1.197	1.283
2BBT (6x6)	1.00183	6949.56 [M21]	871.93 [M21-B03]	1.207	1.307

A.1 Core 2BT

	1	2	3	4	5	6	7	8	9	10	11	12	13	14	15	16	17	18	19	20	21	22	23	24
A	0	0	0	0	0	0	0	0.14	0.76	0.22	0.68	0.26	0.66	0.04	0.14	0.44	0.82	0	0	0	0	0	0	0
B	0	0	0	0	0	0.72	0.06	0.44	0.54	0.96	0.02	0.48	0.84	0.30	0.76	0.54	0.16	0.70	0.36	0	0	0	0	0
C	0	0	0	0	0.90	0.58	0.28	0.82	0.16	0.42	0.64	0.86	0.38	0.56	0.22	0.96	0.42	0.08	0.90	0.58	0	0	0	0
D	0	0	0	0.18	0.52	0.20	0.94	0.12	0.70	0.08	0.18	0.32	0.92	0.10	0.68	0.02	0.64	0.18	0.52	0.20	0.94	0	0	0
E	0	0	0.86	0.32	0.78	0.74	0.40	0.62	0.36	0.90	0.52	0.78	0.50	0.80	0.26	0.48	0.86	0.32	0.78	0.74	0.40	0.62	0	0
F	0	0.84	0.38	0.92	0.50	0.98	0.60	0.34	0.72	0.58	0.20	0.74	0.98	0.24	0.66	0.84	0.38	0.92	0.50	0.98	0.60	0.34	0.72	0
G	0	0.30	0.56	0.10	0.80	0.24	0.46	0.88	0.06	0.28	0.94	0.40	0.60	0.46	0.04	0.30	0.56	0.10	0.80	0.24	0.46	0.88	0.06	0
H	0	0.76	0.22	0.68	0.26	0.66	0.04	0.14	0.44	0.82	0.12	0.62	0.34	0.88	0.14	0.76	0.22	0.68	0.26	0.66	0.04	0.14	0.44	0
J	0.44	0.54	0.96	0.02	0.48	0.84	0.30	0.76	0.54	0.16	0.70	0.36	0.72	0.06	0.44	0.54	0.96	0.02	0.48	0.84	0.30	0.76	0.54	0.16
K	0.82	0.16	0.42	0.64	0.86	0.38	0.56	0.22	0.96	0.42	0.08	0.90	0.58	0.28	0.82	0.16	0.42	0.64	0.86	0.38	0.56	0.22	0.96	0.42
L	0.12	0.70	0.08	0.18	0.32	0.92	0.10	0.68	0.02	0.64	0.18	0.52	0.20	0.94	0.12	0.70	0.08	0.18	0.32	0.92	0.10	0.68	0.02	0.64
M	0.62	0.36	0.90	0.52	0.78	0.50	0.80	0.26	0.48	0.86	0.32	0.78	0.74	0.40	0.62	0.36	0.90	0.52	0.78	0.50	0.80	0.26	0.48	0.86
N	0.34	0.72	0.58	0.20	0.74	0.98	0.24	0.66	0.84	0.38	0.92	0.50	0.98	0.60	0.34	0.72	0.58	0.20	0.74	0.98	0.24	0.66	0.84	0.38
O	0.88	0.06	0.28	0.94	0.40	0.60	0.46	0.04	0.30	0.56	0.10	0.80	0.24	0.46	0.88	0.06	0.28	0.94	0.40	0.60	0.46	0.04	0.30	0.56
P	0.14	0.44	0.82	0.12	0.62	0.34	0.88	0.14	0.76	0.22	0.68	0.26	0.66	0.04	0.14	0.44	0.82	0.12	0.62	0.34	0.88	0.14	0.76	0.22
Q	0.76	0.54	0.16	0.70	0.36	0.72	0.06	0.44	0.54	0.96	0.02	0.48	0.84	0.30	0.76	0.54	0.16	0.70	0.36	0.72	0.06	0.44	0.54	0.96
R	0	0.96	0.42	0.08	0.90	0.58	0.28	0.82	0.16	0.42	0.64	0.86	0.38	0.56	0.22	0.96	0.42	0.08	0.90	0.58	0.28	0.82	0.16	0
S	0	0.02	0.64	0.18	0.52	0.20	0.94	0.12	0.70	0.08	0.18	0.32	0.92	0.10	0.68	0.02	0.64	0.18	0.52	0.20	0.94	0.12	0.70	0
T	0	0.48	0.86	0.32	0.78	0.74	0.40	0.62	0.36	0.90	0.52	0.78	0.50	0.80	0.26	0.48	0.86	0.32	0.78	0.74	0.40	0.62	0.36	0
U	0	0	0.38	0.92	0.50	0.98	0.60	0.34	0.72	0.58	0.20	0.74	0.98	0.24	0.66	0.84	0.38	0.92	0.50	0.98	0.60	0.34	0	0
V	0	0	0	0.10	0.80	0.24	0.46	0.88	0.06	0.28	0.94	0.40	0.60	0.46	0.04	0.30	0.56	0.10	0.80	0.66	0.04	0	0	0
W	0	0	0	0	0.26	0.66	0.04	0.14	0.44	0.82	0.12	0.62	0.34	0.88	0.14	0.76	0.22	0.68	0.26	0.84	0	0	0	0
X	0	0	0	0	0	0.84	0.30	0.76	0.54	0.16	0.70	0.36	0.72	0.06	0.44	0.54	0.96	0.02	0.48	0	0	0	0	0
Y	0	0	0	0	0	0	0	0.22	0.96	0.42	0.08	0.90	0.58	0.28	0.82	0.16	0.42	0	0	0	0	0	0	0

Figure A.1: Channel age map, instantaneous core 2BT
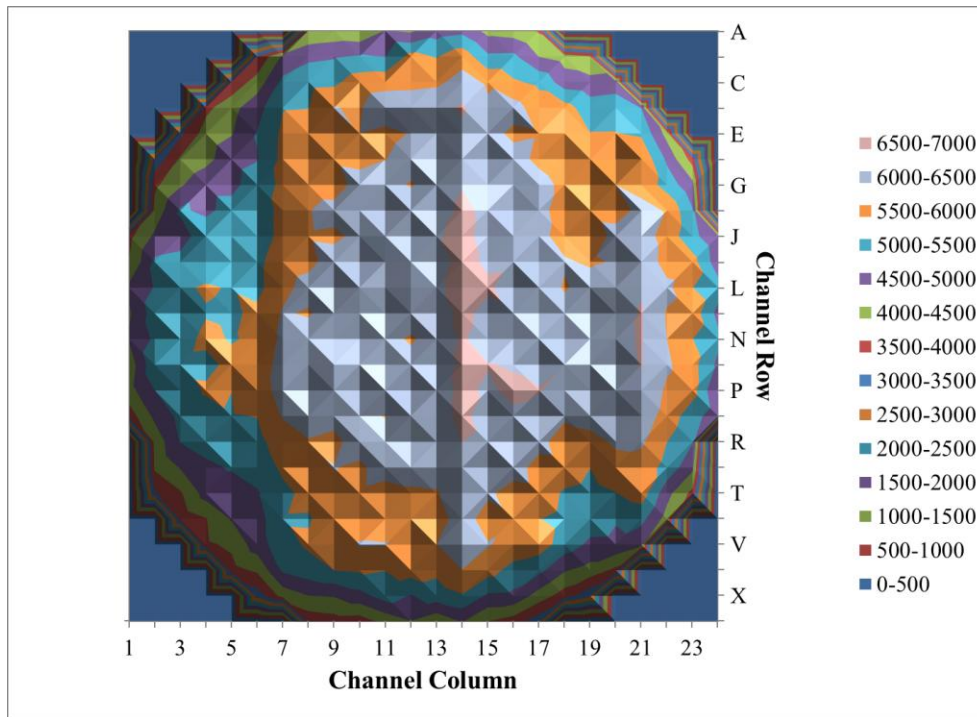
Figure A.2: Channel powers, TRUMOX-30 CANDU-900 core 2BT

215

A.2   Core 2B6T

	1	2	3	4	5	6	7	8	9	10	11	12	13	14	15	16	17	18	19	20	21	22	23	24
A	0	0	0	0	0	0	0	0.76	0.22	0.68	0.26	0.72	0.84	0.30	0.76	0.54	0.16	0	0	0	0	0	0	0
B	0	0	0	0	0	0.06	0.44	0.54	0.96	0.02	0.48	0.58	0.38	0.56	0.22	0.96	0.42	0.08	0.90	0	0	0	0	0
C	0	0	0	0	0.52	0.28	0.82	0.16	0.42	0.64	0.86	0.20	0.92	0.10	0.68	0.02	0.64	0.18	0.52	0.28	0	0	0	0
D	0			0.32	0.78	0.94	0.12	0.70	0.08	0.18	0.32	0.74	0.50	0.80	0.26	0.48	0.86	0.32	0.78	0.94	0.12	0	0	0
E	0		0.20	0.74	0.98	0.40	0.62	0.36	0.90	0.52	0.78	0.98	0.60	0.34	0.72	0.58	0.20	0.74	0.98	0.40	0.62	0.36	0	0
F	0	0.38	0.92	0.50	0.60	0.24	0.46	0.88	0.06	0.28	0.94	0.40	0.24	0.66	0.84	0.38	0.92	0.50	0.60	0.24	0.46	0.88	0.06	0
G	0	0.56	0.10	0.80	0.34	0.66	0.04	0.14	0.44	0.82	0.12	0.62	0.46	0.04	0.30	0.56	0.10	0.80	0.34	0.66	0.04	0.14	0.44	0
H	0	0.22	0.68	0.26	0.72	0.84	0.30	0.76	0.54	0.16	0.70	0.36	0.88	0.14	0.76	0.22	0.68	0.26	0.72	0.84	0.30	0.76	0.54	0
J	0.54	0.96	0.02	0.48	0.58	0.38	0.56	0.22	0.96	0.42	0.08	0.90	0.06	0.44	0.54	0.96	0.02	0.48	0.58	0.38	0.56	0.22	0.96	0.42
K	0.16	0.42	0.64	0.86	0.20	0.92	0.10	0.68	0.02	0.64	0.18	0.52	0.28	0.82	0.16	0.42	0.64	0.86	0.20	0.92	0.10	0.68	0.02	0.64
L	0.70	0.08	0.18	0.32	0.74	0.50	0.80	0.26	0.48	0.86	0.32	0.78	0.94	0.12	0.70	0.08	0.18	0.32	0.74	0.50	0.80	0.26	0.48	0.86
M	0.36	0.90	0.52	0.78	0.98	0.60	0.34	0.72	0.58	0.20	0.74	0.98	0.40	0.62	0.36	0.90	0.52	0.78	0.98	0.60	0.34	0.72	0.58	0.20
N	0.88	0.06	0.28	0.94	0.40	0.24	0.66	0.84	0.38	0.92	0.50	0.60	0.24	0.46	0.88	0.06	0.28	0.94	0.40	0.24	0.66	0.84	0.38	0.92
O	0.14	0.44	0.82	0.12	0.62	0.46	0.04	0.30	0.56	0.10	0.80	0.34	0.66	0.04	0.14	0.44	0.82	0.12	0.62	0.46	0.04	0.30	0.56	0.10
P	0.76	0.54	0.16	0.70	0.36	0.88	0.14	0.76	0.22	0.68	0.26	0.72	0.84	0.30	0.76	0.54	0.16	0.70	0.36	0.88	0.14	0.76	0.22	0.68
Q	0.22	0.96	0.42	0.08	0.90	0.06	0.44	0.54	0.96	0.02	0.48	0.58	0.38	0.56	0.22	0.96	0.42	0.08	0.90	0.06	0.44	0.54	0.96	0.02
R	0	0.02	0.64	0.18	0.52	0.28	0.82	0.16	0.42	0.64	0.86	0.20	0.92	0.10	0.68	0.02	0.64	0.18	0.52	0.28	0.82	0.16	0.42	0
S	0	0.48	0.86	0.32	0.78	0.94	0.12	0.70	0.08	0.18	0.32	0.74	0.50	0.80	0.26	0.48	0.86	0.32	0.78	0.94	0.12	0.70	0.08	0
T	0	0.58	0.20	0.74	0.98	0.40	0.62	0.36	0.90	0.52	0.78	0.98	0.60	0.34	0.72	0.58	0.20	0.74	0.98	0.40	0.62	0.36	0.90	0
U	0	0	0.92	0.50	0.60	0.24	0.46	0.88	0.06	0.28	0.94	0.40	0.24	0.66	0.84	0.38	0.92	0.50	0.60	0.24	0.46	0.88	0	0
V	0	0	0	0.80	0.34	0.66	0.04	0.14	0.44	0.82	0.12	0.62	0.46	0.04	0.30	0.56	0.10	0.80	0.34	0.66	0.04	0	0	0
W	0	0	0	0	0.72	0.84	0.30	0.76	0.54	0.16	0.70	0.36	0.88	0.14	0.76	0.22	0.68	0.26	0.72	0.84	0	0	0	0
X	0	0	0	0	0	0.38	0.56	0.22	0.96	0.42	0.08	0.90	0.06	0.44	0.54	0.96	0.02	0.48	0.58	0	0	0	0	0
Y	0	0	0	0	0	0	0	0.68	0.02	0.64	0.18	0.52	0.28	0.82	0.16	0.42	0.64	0	0	0	0	0	0	0

Figure A.3: Channel age map, instantaneous core 2B6T
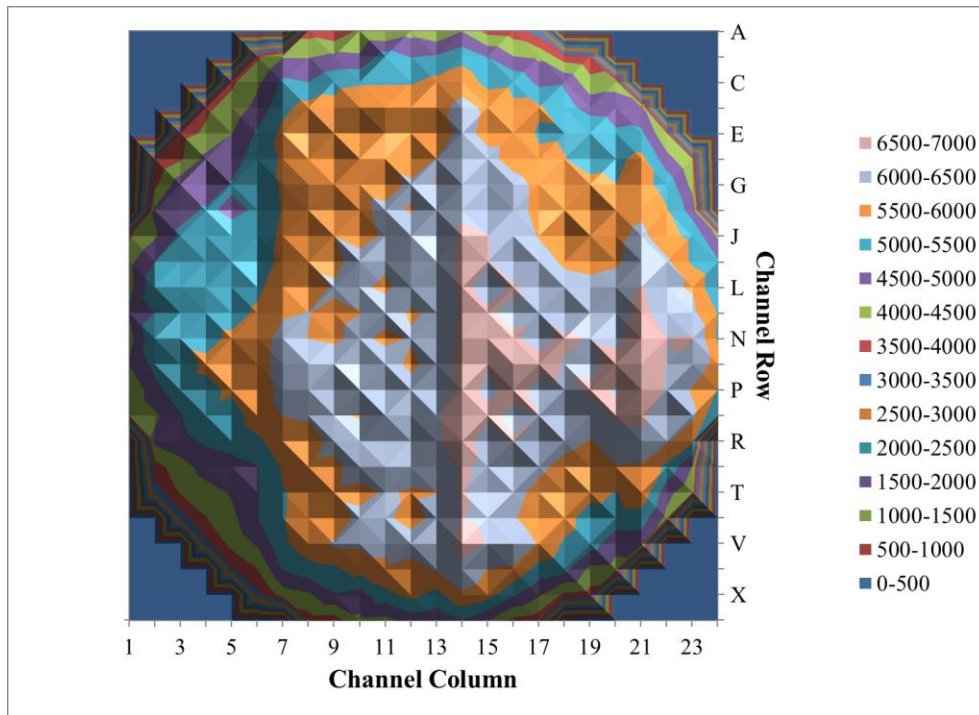
Figure A.4: Channel powers, TRUMOX-30 CANDU-900 core 2B6T

A.3   Core 2B8T

	1	2	3	4	5	6	7	8	9	10	11	12	13	14	15	16	17	18	19	20	21	22	23	24
A	0	0	0	0	0	0	0	0.44	0.54	0.96	0.02	0.48	0.04	0.14	0.44	0.82	0.12	0	0	0	0	0	0	0
B	0	0	0	0	0	0.58	0.28	0.82	0.16	0.42	0.64	0.86	0.30	0.76	0.54	0.16	0.70	0.36	0.84	0	0	0	0	0
C	0	0	0	0	0.38	0.20	0.94	0.12	0.70	0.08	0.18	0.32	0.56	0.22	0.96	0.42	0.08	0.90	0.38	0.20	0	0	0	0
D	0			0.52	0.92	0.74	0.40	0.62	0.36	0.90	0.52	0.78	0.10	0.68	0.02	0.64	0.18	0.52	0.92	0.74	0.40	0	0	0
E	0		0.32	0.78	0.50	0.98	0.24	0.66	0.84	0.38	0.92	0.50	0.80	0.26	0.48	0.86	0.32	0.78	0.50	0.98	0.24	0.66	0	0
F	0	0.30	0.56	0.10	0.80	0.60	0.34	0.72	0.58	0.20	0.74	0.98	0.60	0.46	0.04	0.30	0.56	0.10	0.80	0.60	0.34	0.72	0.58	0
G	0	0.76	0.22	0.68	0.26	0.46	0.88	0.06	0.28	0.94	0.40	0.24	0.34	0.88	0.14	0.76	0.22	0.68	0.26	0.46	0.88	0.06	0.28	0
H	0	0.54	0.96	0.02	0.48	0.04	0.14	0.44	0.82	0.12	0.62	0.66	0.72	0.06	0.44	0.54	0.96	0.02	0.48	0.04	0.14	0.44	0.82	0
J	0.82	0.16	0.42	0.64	0.86	0.30	0.76	0.54	0.16	0.70	0.36	0.84	0.58	0.28	0.82	0.16	0.42	0.64	0.86	0.30	0.76	0.54	0.16	0.70
K	0.12	0.70	0.08	0.18	0.32	0.56	0.22	0.96	0.42	0.08	0.90	0.38	0.20	0.94	0.12	0.70	0.08	0.18	0.32	0.56	0.22	0.96	0.42	0.08
L	0.62	0.36	0.90	0.52	0.78	0.10	0.68	0.02	0.64	0.18	0.52	0.92	0.74	0.40	0.62	0.36	0.90	0.52	0.78	0.10	0.68	0.02	0.64	0.18
M	0.66	0.84	0.38	0.92	0.50	0.80	0.26	0.48	0.86	0.32	0.78	0.50	0.98	0.24	0.66	0.84	0.38	0.92	0.50	0.80	0.26	0.48	0.86	0.32
N	0.72	0.58	0.20	0.74	0.98	0.60	0.46	0.04	0.30	0.56	0.10	0.80	0.60	0.34	0.72	0.58	0.20	0.74	0.98	0.60	0.46	0.04	0.30	0.56
O	0.06	0.28	0.94	0.40	0.24	0.34	0.88	0.14	0.76	0.22	0.68	0.26	0.46	0.88	0.06	0.28	0.94	0.40	0.24	0.34	0.88	0.14	0.76	0.22
P	0.44	0.82	0.12	0.62	0.66	0.72	0.06	0.44	0.54	0.96	0.02	0.48	0.04	0.14	0.44	0.82	0.12	0.62	0.66	0.72	0.06	0.44	0.54	0.96
Q	0.54	0.16	0.70	0.36	0.84	0.58	0.28	0.82	0.16	0.42	0.64	0.86	0.30	0.76	0.54	0.16	0.70	0.36	0.84	0.58	0.28	0.82	0.16	0.42
R	0	0.42	0.08	0.90	0.38	0.20	0.94	0.12	0.70	0.08	0.18	0.32	0.56	0.22	0.96	0.42	0.08	0.90	0.38	0.20	0.94	0.12	0.70	0
S	0	0.64	0.18	0.52	0.92	0.74	0.40	0.62	0.36	0.90	0.52	0.78	0.10	0.68	0.02	0.64	0.18	0.52	0.92	0.74	0.40	0.62	0.36	0
T	0	0.86	0.32	0.78	0.50	0.98	0.24	0.66	0.84	0.38	0.92	0.50	0.80	0.26	0.48	0.86	0.32	0.78	0.50	0.98	0.24	0.66	0.84	0
U	0	0	0.56	0.10	0.80	0.60	0.34	0.72	0.58	0.20	0.74	0.98	0.60	0.46	0.04	0.30	0.56	0.10	0.80	0.60	0.34	0.72	0	0
V	0	0	0	0.68	0.26	0.46	0.88	0.06	0.28	0.94	0.40	0.24	0.34	0.88	0.14	0.76	0.22	0.68	0.26	0.46	0.88	0	0	0
W	0	0	0	0	0.48	0.04	0.14	0.44	0.82	0.12	0.62	0.66	0.72	0.06	0.44	0.54	0.96	0.02	0.48	0.04	0	0	0	0
X	0	0	0	0	0	0.30	0.76	0.54	0.16	0.70	0.36	0.84	0.58	0.28	0.82	0.16	0.42	0.64	0.86	0	0	0	0	0
Y	0	0	0	0	0	0	0	0.96	0.42	0.08	0.90	0.38	0.20	0.94	0.12	0.70	0.08	0	0	0	0	0	0	0

Figure A.5: Channel age map, instantaneous core 2B8T
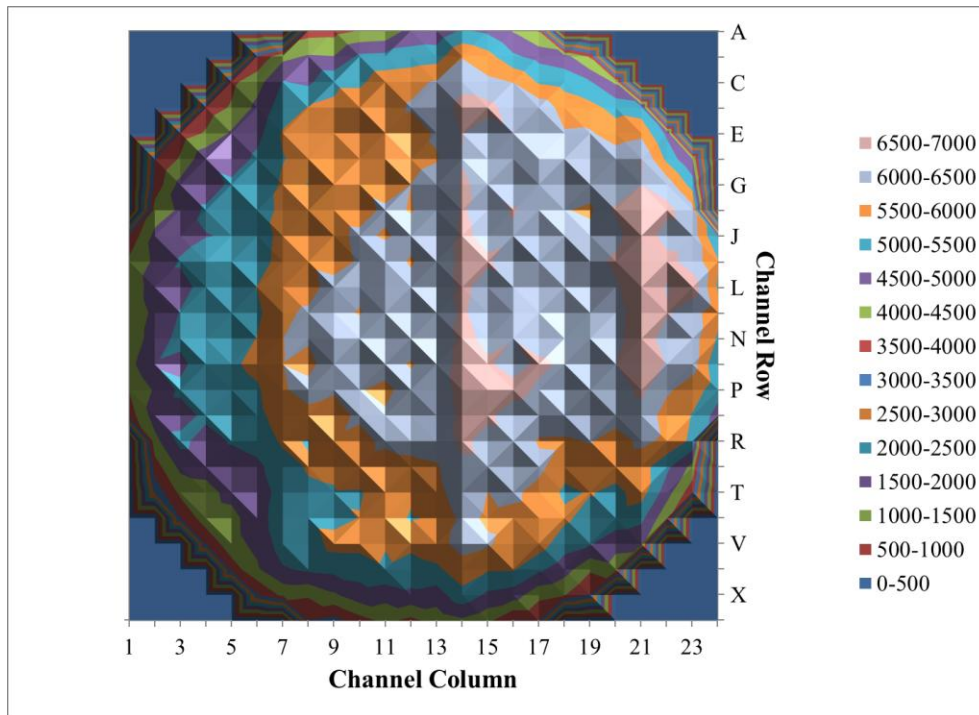
Figure A.6: Channel powers, TRUMOX-30 CANDU-900 core 2B8T

A.4   Core 2BAT

	1	2	3	4	5	6	7	8	9	10	11	12	13	14	15	16	17	18	19	20	21	22	23	24
A	0	0	0	0	0	0	0	0.19	0.82	0.08	0.33	0.14	0.60	0.79	0.22	0.46	0.38	0	0	0	0	0	0	0
B	0	0	0	0	0	0.11	0.79	0.44	0.30	0.54	0.68	0.98	0.19	0.44	0.63	0.93	0.25	0.11	0.79	0	0	0	0	0
C	0	0	0	0	0.65	0.95	0.22	0.63	0.76	0.90	0.27	0.35	0.82	0.30	0.76	0.52	0.65	0.95	0.22	0.63	0	0	0	0
D	0	0	0	0.05	0.57	0.16	0.46	0.93	0.52	0.05	0.41	0.87	0.08	0.54	0.90	0.05	0.57	0.16	0.46	0.93	0.52	0	0	0
E	0	0	0.27	0.41	0.71	0.84	0.38	0.25	0.65	0.57	0.71	0.03	0.33	0.68	0.27	0.41	0.71	0.84	0.38	0.25	0.65	0.57	0	0
F	0	0.98	0.35	0.87	0.03	0.49	0.74	0.11	0.95	0.16	0.84	0.49	0.14	0.98	0.35	0.87	0.03	0.49	0.74	0.11	0.95	0.16	0.84	0
G	0	0.79	0.22	0.46	0.38	0.74	0.60	0.19	0.82	0.08	0.33	0.14	0.60	0.79	0.22	0.46	0.38	0.74	0.60	0.19	0.82	0.08	0.33	0
H	0	0.44	0.63	0.93	0.25	0.11	0.79	0.44	0.30	0.54	0.68	0.98	0.19	0.44	0.63	0.93	0.25	0.11	0.79	0.44	0.30	0.54	0.68	0
J	0.82	0.30	0.76	0.52	0.65	0.95	0.22	0.63	0.76	0.90	0.27	0.35	0.82	0.30	0.76	0.52	0.65	0.95	0.22	0.63	0.76	0.90	0.27	0.35
K	0.08	0.54	0.90	0.05	0.57	0.16	0.46	0.93	0.52	0.05	0.41	0.87	0.08	0.54	0.90	0.05	0.57	0.16	0.46	0.93	0.52	0.05	0.41	0.87
L	0.33	0.68	0.27	0.41	0.71	0.84	0.38	0.25	0.65	0.57	0.71	0.03	0.33	0.68	0.27	0.41	0.71	0.84	0.38	0.25	0.65	0.57	0.71	0.03
M	0.14	0.98	0.35	0.87	0.03	0.49	0.74	0.11	0.95	0.16	0.84	0.49	0.14	0.98	0.35	0.87	0.03	0.49	0.74	0.11	0.95	0.16	0.84	0.49
N	0.60	0.79	0.22	0.46	0.38	0.74	0.60	0.19	0.82	0.08	0.33	0.14	0.60	0.79	0.22	0.46	0.38	0.74	0.60	0.19	0.82	0.08	0.33	0.14
O	0.19	0.44	0.63	0.93	0.25	0.11	0.79	0.44	0.30	0.54	0.68	0.98	0.19	0.44	0.63	0.93	0.25	0.11	0.79	0.44	0.30	0.54	0.68	0.98
P	0.82	0.30	0.76	0.52	0.65	0.95	0.22	0.63	0.76	0.90	0.27	0.35	0.82	0.30	0.76	0.52	0.65	0.95	0.22	0.63	0.76	0.90	0.27	0.35
Q	0.08	0.54	0.90	0.05	0.57	0.16	0.46	0.93	0.52	0.05	0.41	0.87	0.08	0.54	0.90	0.05	0.57	0.16	0.46	0.93	0.52	0.05	0.41	0.87
R	0	0.68	0.27	0.41	0.71	0.84	0.38	0.25	0.65	0.57	0.71	0.03	0.33	0.68	0.27	0.41	0.71	0.84	0.38	0.25	0.65	0.57	0.71	0
S	0	0.98	0.35	0.87	0.03	0.49	0.74	0.11	0.95	0.16	0.84	0.49	0.14	0.98	0.35	0.87	0.03	0.49	0.74	0.11	0.95	0.16	0.84	0
T	0	0.79	0.22	0.46	0.38	0.74	0.60	0.19	0.82	0.08	0.33	0.14	0.60	0.79	0.22	0.46	0.38	0.74	0.60	0.19	0.82	0.08	0.33	0
U	0	0	0.63	0.93	0.25	0.11	0.79	0.44	0.30	0.54	0.68	0.98	0.19	0.44	0.63	0.93	0.25	0.11	0.79	0.44	0.30	0.54	0	0
V	0	0	0	0.52	0.65	0.95	0.22	0.63	0.76	0.90	0.27	0.35	0.82	0.30	0.76	0.52	0.65	0.95	0.22	0.63	0.76	0	0	0
W	0	0	0	0	0.57	0.16	0.46	0.93	0.52	0.05	0.41	0.87	0.08	0.54	0.90	0.05	0.57	0.16	0.46	0.93	0	0	0	0
X	0	0	0	0	0	0.84	0.38	0.25	0.65	0.57	0.71	0.03	0.33	0.68	0.27	0.41	0.71	0.84	0.38	0	0	0	0	0
Y	0	0	0	0	0	0	0	0.11	0.95	0.16	0.84	0.49	0.14	0.98	0.35	0.87	0.03	0	0	0	0	0	0	0

Figure A.7: Channel age map, instantaneous core 2BAT
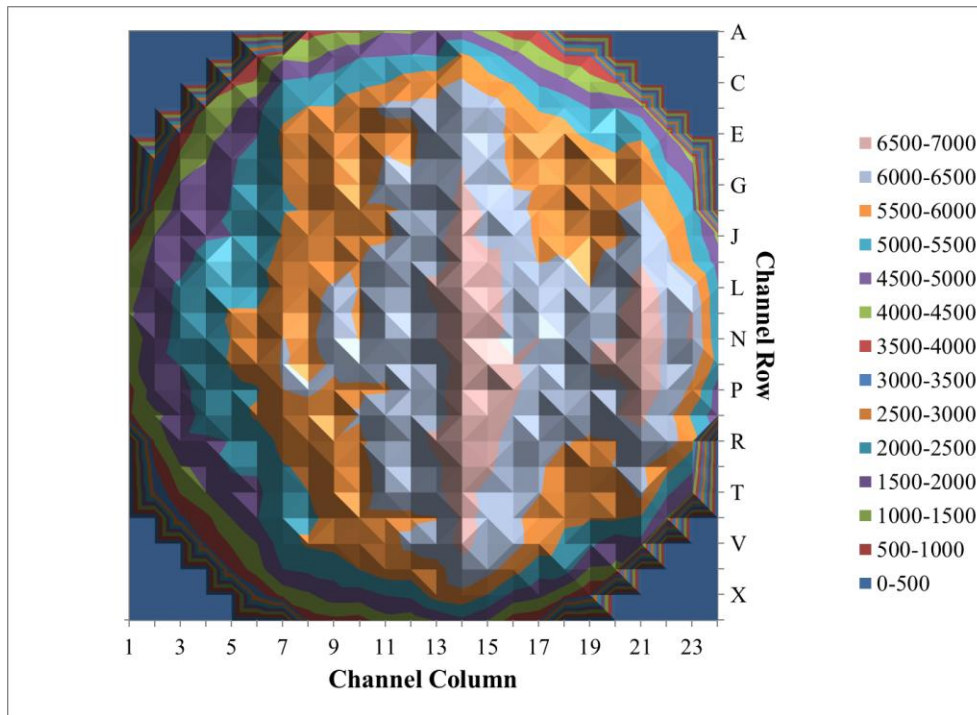
Figure A.8: Channel powers, TRUMOX-30 CANDU-900 core 2BAT

A.5   Core 2BBT

	1	2	3	4	5	6	7	8	9	10	11	12	13	14	15	16	17	18	19	20	21	22	23	24
A	0	0	0	0	0	0	0	0.62	0.38	0.14	0.54	0.98	0.34	0.88	0.14	0.74	0.22	0	0	0	0	0	0	0
B	0	0	0	0	0	0.24	0.88	0.06	0.48	0.94	0.40	0.24	0.62	0.06	0.70	0.42	0.96	0.24	0.88	0	0	0	0	0
C	0	0	0	0	0.46	0.64	0.14	0.70	0.88	0.22	0.28	0.78	0.38	0.48	0.88	0.16	0.46	0.64	0.14	0.70	0	0	0	0
D	0	0	0	0.70	0.08	0.92	0.74	0.42	0.16	0.70	0.36	0.62	0.14	0.94	0.22	0.70	0.08	0.92	0.74	0.42	0.16	0	0	0
E	0	0	0.28	0.36	0.90	0.52	0.22	0.96	0.46	0.08	0.90	0.38	0.54	0.40	0.28	0.36	0.90	0.52	0.22	0.96	0.46	0.08	0	0
F	0	0.24	0.78	0.62	0.38	0.02	0.68	0.24	0.64	0.92	0.52	0.02	0.98	0.24	0.78	0.62	0.38	0.02	0.68	0.24	0.64	0.92	0.52	0
G	0	0.88	0.14	0.74	0.22	0.68	0.34	0.62	0.38	0.14	0.54	0.98	0.34	0.88	0.14	0.74	0.22	0.68	0.34	0.62	0.38	0.14	0.54	0
H	0	0.06	0.70	0.42	0.96	0.24	0.88	0.06	0.48	0.94	0.40	0.24	0.62	0.06	0.70	0.42	0.96	0.24	0.88	0.06	0.48	0.94	0.40	0
J	0.38	0.48	0.88	0.16	0.46	0.64	0.14	0.70	0.88	0.22	0.28	0.78	0.38	0.48	0.88	0.16	0.46	0.64	0.14	0.70	0.88	0.22	0.28	0.78
K	0.14	0.94	0.22	0.70	0.08	0.92	0.74	0.42	0.16	0.70	0.36	0.62	0.14	0.94	0.22	0.70	0.08	0.92	0.74	0.42	0.16	0.70	0.36	0.62
L	0.54	0.40	0.28	0.36	0.90	0.52	0.22	0.96	0.46	0.08	0.90	0.38	0.54	0.40	0.28	0.36	0.90	0.52	0.22	0.96	0.46	0.08	0.90	0.38
M	0.98	0.24	0.78	0.62	0.38	0.02	0.68	0.24	0.64	0.92	0.52	0.02	0.98	0.24	0.78	0.62	0.38	0.02	0.68	0.24	0.64	0.92	0.52	0.02
N	0.34	0.88	0.14	0.74	0.22	0.68	0.34	0.62	0.38	0.14	0.54	0.98	0.34	0.88	0.14	0.74	0.22	0.68	0.34	0.62	0.38	0.14	0.54	0.98
O	0.62	0.06	0.70	0.42	0.96	0.24	0.88	0.06	0.48	0.94	0.40	0.24	0.62	0.06	0.70	0.42	0.96	0.24	0.88	0.06	0.48	0.94	0.40	0.24
P	0.38	0.48	0.88	0.16	0.46	0.64	0.14	0.70	0.88	0.22	0.28	0.78	0.38	0.48	0.88	0.16	0.46	0.64	0.14	0.70	0.88	0.22	0.28	0.78
Q	0.14	0.94	0.22	0.70	0.08	0.92	0.74	0.42	0.16	0.70	0.36	0.62	0.14	0.94	0.22	0.70	0.08	0.92	0.74	0.42	0.16	0.70	0.36	0.62
R	0	0.40	0.28	0.36	0.90	0.52	0.22	0.96	0.46	0.08	0.90	0.38	0.54	0.40	0.28	0.36	0.90	0.52	0.22	0.96	0.46	0.08	0.90	0
S	0	0.24	0.78	0.62	0.38	0.02	0.68	0.24	0.64	0.92	0.52	0.02	0.98	0.24	0.78	0.62	0.38	0.02	0.68	0.24	0.64	0.92	0.52	0
T	0	0.88	0.14	0.74	0.22	0.68	0.34	0.62	0.38	0.14	0.54	0.98	0.34	0.88	0.14	0.74	0.22	0.68	0.34	0.62	0.38	0.14	0.54	0
U	0	0	0.70	0.42	0.96	0.24	0.88	0.06	0.48	0.94	0.40	0.24	0.62	0.06	0.70	0.42	0.96	0.24	0.88	0.06	0.48	0	0	0
V	0	0	0	0.16	0.46	0.64	0.14	0.70	0.88	0.22	0.28	0.78	0.38	0.48	0.88	0.16	0.46	0.64	0.14	0.70	0.88	0	0	0
W	0	0	0	0	0.08	0.92	0.74	0.42	0.16	0.70	0.36	0.62	0.14	0.94	0.22	0.70	0.08	0.92	0.74	0.42	0	0	0	0
X	0	0	0	0	0	0.52	0.22	0.96	0.46	0.08	0.90	0.38	0.54	0.40	0.28	0.36	0.90	0.52	0.22	0	0	0	0	0
Y	0	0	0	0	0	0	0	0.24	0.64	0.92	0.52	0.02	0.98	0.24	0.78	0.62	0.38	0	0	0	0	0	0	0

Figure A.9: Channel age map, instantaneous core 2BBT
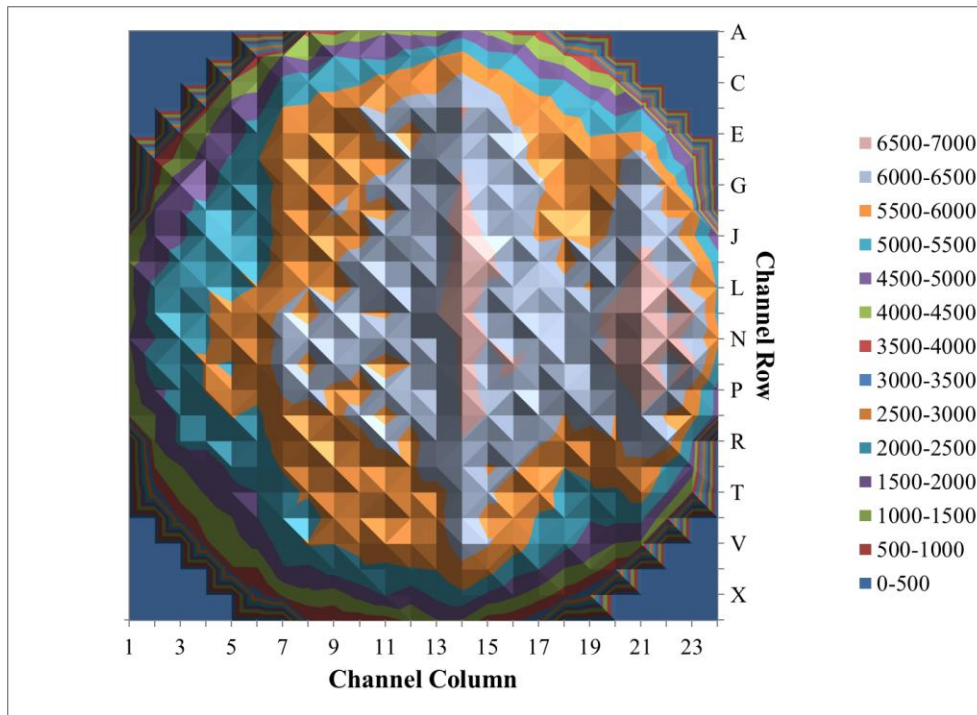
Figure A.10: Channel powers, TRUMOX-30 CANDU-900 core 2BBT

219

Appendix B

Sample Code Input Files

This appendix provides a selection of the input files used for the simulations performed as part of this thesis. The input files are provided for WIMS-AECL and DRAGON lattice cell codes and for select portions of the RFSP full core diffusion code.

B.1   WIMS-AECL 2D lattice cell inputs

```
TITLE "TRUMOX-30 CANDU WIMS-AECL Model, using ENDF/B-VI library"
Cell Cluster
Sequence Pij
Nrods    43  -14
symmetry -14  0.d  25.7142857d
Lines 0      5.190000  53 11
Lines 5.190000 7.787500  11 3
Annulus #   1.317184 Coolant
Annulus #   1.959137 Coolant
Annulus #   2.601089 Coolant
Annulus #   3.243042 Coolant
Annulus #   3.884995 Coolant
Annulus #   4.526947 Coolant
Annulus #   5.190000 Coolant
Annulus #   5.411550 PT
Annulus #   5.633100 PT
Annulus #   6.447800 Gap
Annulus #   6.587500 CT
Annulus #   7.187500 Moder
Annulus #   7.787500 Moder
Npijan #
Polygon #  4 Moder  14.287500
```

** The TRUMOX fuel uses a 43 element bundle with a central pin 17.4 mm in diameter including clad and 3 concentric rings of 7, 14 and 21 elements with diameters of 11.4 mm. Fuel_1 is the central BNA, Fuel_2-4 is MOX. Specifics of the bundle designs could not be fully included due to their proprietary nature.**
*
Power 1   32. 0.2 1   0.0001
Buckling 1.0e-4 1.0e-4 1.0e-5 1.0e-5
*
Tolerance 1.0e-6
FewGroups 1 2 3 4 5 6 7 8 9 $
     10 11 12 13 14 15 16 17 18 19 $
     20 21 22 23 24 25 26 27 28 29 $
     30 31 32 33 34 35 36 37 38 39 $
     40 41 42 43 44 45 46 47 48 49 $
     50 51 52 53 54 55 56 57 58 59 $
     60 61 62 63 64 65 66 67 68 69 $
     70 71 72 73 74 75 76 77 78 79 $
     80 81 82 83 84 85 86 87 88 89 * 89 group
Suppress   1 1 1 1   1 1 1 1   1 1 1 -1   1 1 -1 0
newres 4 0.1 -14 0.d 25.7142857d
*
Water Coolant   .8074   561.285 Cool DD2O=98.764
Water Water1   .000000   336.16 Moder DD2O=99.918
Material boron   1.08875   336.16 Moder b10=199.259 b11=881.821
Material gad 0.32878 336.16 Moder gd155=2292.860 gd157=2455.861
Mixture moder Water1 1 boron 0.1E-06 gad 0 336.16 moder * md=1.08875
noburn moder *To stop burning the Gd in Moderator
*
Material PT 6.5041 561.285 Moder NB93=2.58 FE54=0.00266589864 $
FE56=0.042976786 FE57=0.00100160658 FE58=0.000135886544 $
CR50=0.000337568856 CR52=0.006769656 CR53=0.000782319888 $
CR54=0.00019843099 NI58=0.00248195 NI60=0.00098154 NI64=3.6505e-05 $
b10=.00002431 ZR90=49.34430008 ZR91=10.88052181 ZR92=16.813671028 $
ZR94=17.410197266 ZR96=2.8645910062
Material Gap 0.0012 448.72 Moder C=27.11 O16=72.89 * CO2
Material CT 6.4003 336.16 Moder FE54=0.00769338 FE56=0.1240245 $
  FE57=0.002890485 FE58=0.000392148 NI58=0.03900215 NI60=0.0154242 $
  NI64=0.00057365 CR50=0.0041737 CR52=0.0837 CR53=0.0096726 $

CR54=0.0024534 ZR90=49.798482681 ZR91=10.98067 ZR92=16.96843007 $
ZR94=17.570446953 ZR96=2.8909577271 b10=.00005962

Material DyZr 7.1 859.99 Fuel $ * 67 wt% Dy3O2 -- isotopics corectly in wt%
    Dy160=0.01346 Dy161=0.10943 Dy162= 0.14858 Dy163= 0.14597 $
    Dy164=0.16633 Zr90=0.12388 Zr91= 0.02732 Zr92=0.04221
    Zr94=0.04371 Zr96=0.00719 O16=0.17192 U235=0.00001 U238=0.00001

Material ZrO2 7.1 859.99 Fuel $ *mix with DyZr to dilute Dy
Zr90=37.55163523 Zr91=8.281487523 Zr92=12.7950801 Zr94=13.24977378 $
Zr96=2.179498364 O16=25.94252501 U235=0.00001 U238=0.00001

Mixture DyZrdil DyZr=0.03 ZrO2=0.97 859.99 fuel

Material NUO2 10.5541   859.99 Fuel O16=13.44251 $
  U234=0.0054 U235=0.7110 U238=99.2836

Material PuO2 10.16 859.99 fuel O16=13.361 $
NP237=4.698   Pu238=1.301   Pu239=56.243   Pu240=20.099   Pu241=3.040 $
Pu242=3.800   Am241=9.907   Am243=0.763   Cm243=0.001   Cm244=0.072 $
Cm245=0.012 Cm246=0.001

Mixture MOX NUO2=0.9690 PuO2=0.0310 859.99 fuel

Material Fuel_1 DyZr
Material Fuel_2 MOX
Material Fuel_3 MOX
Material Fuel_4 MOX
*
Material Clad 6.3918 561.285 clad ZR90=49.784791791 ZR91=10.977651153 $
ZR92=16.963765014   ZR94=17.565616383   ZR96=2.8901629281 $
FE54=0.01196748   FE56=0.192927   FE57=0.00449631   FE58=0.00061 $
CR50=0.0041737   CR52=0.0837   CR53=0.0096726   CR54=0.0024534 $
NI58=0.00496391 NI60=0.00196308 NI64=7.301e-05 B10=.00005962

Write 1
Begin
Benoist

222

Buckling 1.0e-4 1.0e-4
Beeone 1
Leakage -6
Cellav
*
Material 0
Begin
write 2
Power 1 -1 0.4 1
Begin
Begin
** burnup time is increased in stages from 0.4 days up to 20 days and extends to 60 burnup steps for a total of 1000 days

* ============== voided case ====================
read 1
Power 1 -1 0.001 1
density 0.001
begin
begin
…
…
read 60
Power 1 -1 0.001 1
density 0.001
begin
begin

The NU input file is the same but the burnup is shorter at 365 days and the bundle design is a 37 element bundle fuelled with NUO2. The 37 element bundle has a center fuel element (Fuel_1) surrounded by concentric rings of 6, 12 and 18 elements (Fuel_2-4). All elements contain NUO2 and are 13.2 mm in diameter including cladding.

B.2   DRAGON 3D super-cell inputs

*-TRUMOX CANDU 43 element bundle calculation

* Annuralized fuel, 3D with adjuster

* TRU-30 fuel, 96.9% NU, 3.1% Actinides

* Adjuster properties for CANDU 9 Reactor Guide tube only Design

* Revised to use Annular Smeared Fuel

* Modified for 1 bundle length spacing (49.53cm)

* therefore Z corordinates use -8.255 and 8.255

* Authors: Matthew Ball, Andrew Morreale

* September 27, 2010

* Revised date December 20, 2011

*-----

LINKED_LIST

  CANDU6S DISCR1 LIBRARY CP CALC OUT

  CANDU6F2D CANDU6S2D DISCRSH ;

SEQ_BINARY

  TRKSPC TRKSPC2D ;

SEQ_ASCII

  RMAP MMAP FLAG_GEO FLAG_TRAK1 FLAG_SH FLAG_TRAK2

  FLAG_ASM FLAG_FLU OUT2 ;

MODULE

  LIB: GEO: EXCELT: SHI: ASM: FLU: EDI:

  DELETE: END: PSP: ;

*----

* Microscopic cross sections from file iaea format WIMSD4

*----

LIBRARY := LIB: ::

  NMIX 22 CTRA WIMS

  MIXS LIB: WIMSD4 FIL: iaea

*Coolant (changed temp and dens) Using atomic 10^24atm/cm^3

  MIX 1 561.285

   O16   = '6016' 2.430907E-2

   D2D2O = '3002' 4.822629E-2

   H1H2O = '3001' 3.781324E-4

*Pressure Tube (Zr 2.5Ni, chnaged temp, dens and comp)

  MIX 2 561.285 6.5041   Nb93   = '93'   2.58000

   BNat   = '1011' 2.4310000E-5

```
  Zr91    = '91'   9.731328117E+1
  FeNAT   = '2056'  0.046780177
  CrNAT   = '52'   8.087975736E-3
  Ni58    = '58'   3.50000E-3
* Gas Gap Co2
 MIX  3  448.72  0.0012        C  = '2012'  2.7110000E+1
  O16     = '6016'  7.289000E+1
* Calandria Tube(change temp, dens and comp)
 MIX  4  336.16  6.4003        Fe56  = '2056'  1.61014878E-1
  Ni58    = '58'   5.50000E-2 Cr52    = '52'   0.09999970
  BNat    = '1011'  5.96200E-5
  Zr91    = '91'   9.96839258E+1
* Moderator(change temp and dens)
 MIX  5  336.16  1.08875       O16     = '6016'  7.98895E+1
  D2D2O   = '3002'  2.01016E+1 H1H2O   = '3001'  8.96000E-3
*Actinide Mixture renormalized to 100% total
  MIX  6  859.99  10.16        O16     = '6016' 13.4970412
   Np237   = '937'   4.0664709 1
   Pu238   = '948'   1.1261129 1
   Pu239   = '6239'  48.6825291 1
   Pu240   = '1240'  17.3971899 1
   Pu241   = '1241'  2.6313477 1
   Pu242   = '1242'   3.2891846 1
   Am241   = '951'   8.5752505 1
   Am243   = '953'   0.6604336 1
   Cm243   = '963'   8.655749E-4 1
*no code for Cm245 (0.12) or Cm246 (0.001) reassigned to cm244
*Cm244 includes the Cm245 and Cm246 = .072+.012+.001=
   Cm244   = '964'   7.35738665E-2  1

*NUO2 fuel at temperature of 860
 MIX  7  859.99  10.5541       O16     = '6016'  1.18502E+1
   Xe135   = '4135'  0.0
   U235    = '2235'  6.267E-1  1
   U238    = '8238'  8.75183E+1 1
   U236    = '236'   0.0      1
   Pu239   = '6239'  0.0      1
   U234    = '234'   4.8E-3    1
```

*Defined fuel mixture for all pins
  MIX 8 COMB 6 3.1 7 96.9
* Sheath mixture, using 10^24atm/cm^3
  MIX 9   561.66
    Fe56   = '2056'   1.447438E-4
    Ni58   = '58'   4.590727E-6
    Cr52   = '52'   7.402933E-5
    BNat   = '1011'   2.122757E-7
    Zr91   = '91'   4.206163E-2

* Duplicate fuel mixes for each ring
* Remixed fuel for use in cluster 2D SS and then into the smeared mix
* ring 2 (O16 is constant)
* Fuel mixtures consistent with mid burnup TRUMOX fuel for MIX 10-12
*as determined by 2D dragon burnup simulation
  MIX 10 859.99 O16 = '6016'   4.722941E-002 1
    ** Mix includes Uranium, transuranics and fission products**
* ring 3
  MIX 11 859.99 O16 = '6016'   4.722941E-002 1
** Mix includes Uranium, transuranics and fission products**
* ring 4
  MIX 12 859.99 O16 = '6016'   4.722941E-002 1
    ** Mix includes Uranium, transuranics and fission products**

* THE SMEARED FUEL MIXES
* Mixture for Annular Smeared fuel in Ring 2 (use fuel mix 10)
* made up of 45.3823% Coolant, 47.7302% Fuel and 6.8875% sheath,
  MIX 13 COMB 1 45.3823 10 47.7302 9 6.8875
* Mixture for Annular Smeared fuel in Ring 3 (use fuel mix 11)
* made up of 34.8602% Coolant, 56.9255% Fuel and 8.2144% sheath,
  MIX 14 COMB 1 34.8602 11 56.9255 9 8.2144

* Mixture for Annular Smeared fuel in Ring 4 (use fuel mix 12)
* made up of 31.4650% Coolant, 59.8925% Fuel and 8.6425% sheath,
  MIX 15 COMB 1 31.4650 12 59.8925 9 8.6425
* Excess mixes for other coolants
  MIX 16 COMB 1 100.0

```
 MIX 17  COMB  1 100.0
 MIX 18  COMB  1 100.0
 MIX 19  COMB  1 100.0

*mixture for the central Dy Pin, DyZr, set at 100%max
*Define a mixture for the Dy2O3 in the center pin
*Changed to 10^24atm/cm^3, with burnup props
 MIX  20  859.99  O16 = '6016'  5.055295E-002
   Dy160   = '160'   3.675412E-004
   Dy161   = '161'   3.006163E-003
   Dy162   = '162'   4.403486E-003
   Dy163   = '163'   4.211039E-003
   Dy164   = '164'   4.525812E-003
   Zr91    = '91'    1.259605E-002
   Ho165   = '165'   3.761375E-004

*  Mix for SS304L from C6 Physics Design Manual
  MIX 21   339.16   7.90
    C  =  '2012'   0.037
    FeNAT = '2056' 72.671
    SiNAT =  '29'  0.46
    NiNAT = '58'   8.43
* MnNAT is Mn + Su + Co
    MnNAT = '55'   1.282
    CrNAT = '52'   17.12

* Guide tube to be 76.4%CT and 23.6%Mod in Vol% using proper wt%
* Density properly computed to 0.764*CT_Dens + 0.236*Mod_Dens
* Dens = 0.764*6.44 +0.236*1.082885 = 5.175720860
* Changed temp, dens and comp
* USING COMB
 MIX 22 COMB 4 76.4 5 23.6
  ;

CANDU6S := GEO: :: CAR3D 3 2 2
  X- REFL X+ SYME
  Y- REFL Y+ SYME
  Z- REFL Z+ SYME
```

```
 CELL   MBLBACK   MBCBACK   MBRBACK   MTLBACK   FPBACK
MTRBACK
    MBLFRNT MBCFRNT ADJBOTT MTLFRNT FPFRNT ADJTOP

 ::: MBLBACK := GEO: CAR3D 1 1 1
   MESHX 0.0 7.14375
   MESHY 0.0 7.14375
   MESHZ -8.255 8.255
   SPLITX 1 SPLITY 1 SPLITZ 1
   MIX 5
;

 ::: MBCBACK := GEO: CAR3D 1 1 1
    MESHX -7.14375 7.14375
    MESHY 0.0 7.14375
    MESHZ -8.255 8.255
    SPLITX 2 SPLITY 1 SPLITZ 1
    MIX 5
;

 ::: MBRBACK := GEO: MBLBACK
    MESHX -7.14375 7.14375
    SPLITX 2
;

 ::: MTLBACK := GEO: CAR3D 1 1 1
    MESHX 0.0 7.14375
    MESHY -7.14375 7.14375
    MESHZ -8.255 8.255
    SPLITX 1 SPLITY 2 SPLITZ 1
    MIX 5
;

 ::: FPBACK := GEO: CARCELZ 12 1
    MESHX -7.14375 7.14375
    MESHY -7.14375 7.14375
    MESHZ -8.255 8.255
```

228

SPLITX 2 SPLITY 2 SPLITZ 1

**Altered to use annularized fuel rings that are the thickness of the fuel elements.
The center pin remains while smeared annuli of fuel, clad and coolant are defined
for the remaining 3 rings of elements centered at the cluster radial locations with a
thickness of 11.4mm**
*This is for TRUMOX 43 element bundle with central burnable poison
* PT IR=5.19 and OR=5.6331, t=0.4431cm
* CT IR=6.4478 and OR=6.5875, t=0.1397cm
    RADIUS 0.00000 ***FUEL BUNDLE DESCRIPTION HERE***
    5.19000 5.63310 6.44780 6.58750
    MIX 20 9 1 13 1 14 1 15 1 2 3 4 5
*DyBNA,sheath,cool,ring2fuel,cool,ring3fuel,cool,ring4fuel,cool,PT,GG,CT
    SPLITR -2 1 1 -2 1 -2 1 -2 1 1 1 1
 ;
   ::: MTRBACK := GEO: MTLBACK
     MESHX -7.14375 7.14375
     SPLITX 2
 ;
   ::: MBLFRNT := GEO: MBLBACK
 ;
   ::: MBCFRNT := GEO: MBCBACK
 ;
   ::: ADJBOTT := GEO: CARCELY 6 1
     MESHX -7.14375 7.14375
     MESHY 0.0 7.14375
     MESHZ -8.255 8.255
     SPLITX 2 SPLITY 1 SPLITZ 1
* The design is a SS pin in tube design with water surrounding the pin
* the guide tube surrounds the outer SS tube
* Guide tube dimensions, ID = 8.89 OD = 9.14, thickness = 0.125cm
    RADIUS 0.0 0.60 1.905 3.6855 3.81 4.445 4.57
    MIX 5 5 5 5 5 22 5
* mod, mod, mod, mod, mod, ZrGT, mod
 ;
   ::: MTLFRNT := GEO: MTLBACK
 ;
   ::: FPFRNT := GEO: FPBACK

```
 ;
  ::: ADJTOP := GEO: ADJBOTT
     MESHY -7.14375 7.14375
     SPLITY 2
 ;
 ;
CANDU6S2D := GEO: ::  CARCEL 4
  X- REFL X+ REFL  MESHX 0.0 28.575
  Y- REFL Y+ REFL  MESHY 0.0 28.575
  RADIUS  0.00000 5.16890 5.60320 6.44780 6.58750
  SPLITR -4 1 1 1
  MIX  1 2 3 4 5
  CLUSTER ROD1 ROD2 ROD3 ROD4
** 43 element bundle as defined for WIMS-AECL models. ROD 1-4
CANDU6F2D := GEO: CANDU6S2D ::
  ::: ROD1 := GEO: ROD1 SPLITR -4 1 ;
  ::: ROD2 := GEO: ROD2 SPLITR -4 1 ;
  ::: ROD3 := GEO: ROD3 SPLITR -4 1 ;
  ::: ROD4 := GEO: ROD4 SPLITR -4 1 ;
 ;
FLAG_GEO := CANDU6F2D ;
RMAP := PSP: CANDU6S2D ::
  FILL RGB
  TYPE REGION
;
MMAP := PSP: CANDU6S2D ::
  FILL RGB
  TYPE MIXTURE
;
DISCRSH TRKSPC2D := EXCELT: CANDU6F2D ::
  TITLE 'CANDU 6 bundle (EXCELL)'
  MAXR 4000
  TRAK TISO 12 20.0
 ;
FLAG_TRAK1 := DISCRSH ;
LIBRARY := SHI: LIBRARY DISCRSH TRKSPC2D :: ;
FLAG_SH := LIBRARY ;
DISCR1 TRKSPC := EXCELT: CANDU6S ::
```

```
 TITLE 'CANDU 6 bundle (EXCELL)'
 MAXR 4000
 TRAK TISO 12 20.0
  ;
FLAG_TRAK2 := DISCR1 ;
CP := ASM: LIBRARY DISCR1 TRKSPC :: ;
FLAG_ASM := CP ;

CALC := FLU: CP LIBRARY DISCR1 ::
 TYPE K ;
FLAG_FLU := CALC ;

OUT := EDI: CALC LIBRARY DISCR1 CP ::
 EDIT 3
 MERG REGI 1 1 2 2
      1 1 1 1 1 1 1 1 1 1 1 1 1 1 1 1 1 1
      2 2 2 2 2 2 2 2 2 2 2 2 2 2 2 2 2 2
      1 1
      2 2 2 2 2 2 2 2
      1 1 1 1 1 1 1 1 1 1 1 1 1 1 1 1 1 1
      2 2 2 2 2 2 2 2 2 2 2 2 2 2 2 2 2 2
      2 2 2 2 2 2 2
```

*REGI matrix, Ln 1 back bottom(4), Ln2 back left top (with fuel) (18), Ln3 back right top (with fuel) (18)
*ln4 Front bottom left(2), Ln5 front bottom right(includes adj) (8)
*ln6 fron top left (with fuel)(18), Ln7 Front top Right (fuel only)(17)
*ln8 front top (adj only)(7)

```
 COND 0.625 SAVE
;
OUT2 := OUT ;
DISCR1 TRKSPC CP := DELETE: DISCR1 TRKSPC CP ;
END: ;
QUIT "LIST" .
```

The above input was for the adjuster guide tube only for the TRUMOX-30 fuel configuration. As with WIMS-AECL, the NU models just use the 37 element bundle in place of the 43 element TRUMOX bundle. The other control devices

have different dimensions defined in the ADJ cells. The 4 types of adjuster are described below.

* The TYPE 1 design, center pin is Titainium
    RADIUS 0.0 0.79 1.905 3.686 3.81 4.445 4.57
    MIX 23 5 5 21 5 22 5
* Ti_rod, mod, mod, SStube, mod, ZrGT, mod

* The TYPE 2 design, Titanium pin in SS tube
    RADIUS 0.0 0.91 1.905 3.6856 3.81 4.445 4.57
    MIX 23 5 5 21 5 22 5
* Ti_rod, mod, mod, SStube, mod, ZrGT, mod

* The TYPE 3 design
    RADIUS 0.0 0.91 1.905 3.7257 3.81 4.445 4.57
    MIX 21 5 5 21 5 22 5
* SSrod, mod, mod, SStube, mod, ZrGT, mod

* The TYPE 4 design
    RADIUS 0.0 0.85 1.905 3.7252 3.81 4.445 4.57
    MIX 21 5 5 21 5 22 5
* SSrod, mod, mod, SStube, mod, ZrGT, mod

The MCA and SDS rods are defined as below.

* The SDS and MCA design
    RADIUS 0.0 5.45448 5.50674 5.59774 5.65 6.225 6.43
    MIX 5 21 23 21 5 22 5
* mod, SStube, Cd, SStube, mod, ZrGT, mod

The liquid zones have the same geometry for all zone types given first but the composition in the smeared annuli are different and are given for the 3 zone types filled with He or Water.

* The ZCR geometry
    RADIUS 0.0 1.293 2.5858 3.63 4.67 5.71 5.837
    MIX 24 24 25 25 25 4 5
* He, He, HeH2OCTsmear, HeH2OCTsmear, HeH2OCTsmear, CT, mod

```
* necessary mixes for the ZCR contents
* mix for the inner contents, He or Water
* Straight water for use in LZCRS
  MIX  23  345.66  1.00799        O16    = '6016'  8.88094799E+1
   D2D2O  = '3002'  8.598768E-4  H1H2O  = '3001'  1.118966022E+1
*Cover gas in the LZCRS is Heilum, not air
  MIX  24  345.66  0.0014         He4    = '4'     1.00000E+2
* mix for the smeared ring composed of He Water and CT
* FOR ZCR1 filled with He, 83.9779 He, 13.5060 H2O, 2.5161 CT
  MIX 25 COMB 24 83.9779 23 13.5060 4 2.5161

* FOR ZCR1 filled with Water, 2.5790 He, 94.9048 H2O, 2.5162 CT
  MIX 25 COMB 24 2.5790 23 94.9048 4 2.5162

* FOR ZCR2 filled with He, 96.8470 He, 2.4935 H2O, 0.6965 CT
  MIX 25 COMB 24 96.8470 23 2.4935 4 0.6965

* FOR ZCR2 filled with Water, 0.2247 He, 99.1159 H2O, 0.6594 CT
  MIX 25 COMB 24 0.2247 23 99.1159 4 0.6594

* FOR ZCR3 filled with He, 71.1087 He, 24.5184 H2O, 4.3729 CT
  MIX 25 COMB 24 71.1087 23 24.5184 4 4.3729

* FOR ZCR3 filled with Water, 4.9334 He, 90.6937 H2O, 4.3729 CT
  MIX 25 COMB 24 4.9334 23 90.6937 4 4.3729
```

B.3   RFSP Inputs

The definitions for the irradiation regions in the time average model for TRUMOX-30 are provided below. The NU case uses the region definitions for the reference CANDU-900 model.

```
$----------------------------------------------------------------------------
$  Define burnup regions for time-average calculations
$  Uses 15 regions here with no further splitting done in the TA
$--------1---------2---------3---------4---------5---------6---------7---------8
J               OUTER RING
$---Defining the top
J        C 8  C17 TOP
J        D 6  D19 TOP
J        E 5  E20 TOP
$--- Defining the bottom
J        W 8  W17 BOTTOM
J        V 6  V19 BOTTOM
J        U 5  U20 BOTTOM
$---- Defining the middle
J        E 8  U17 MIDDLE
$--- Defining the inner region
J        J 9  Q16 INNER
$--- Defining the right side
J        J 3  Q 3 OUTER
J        G 4  S 4 OUTER
J        F 5  T 6 OUTER
$--- Defining the left side
J        J22  Q22 OUTER
J        G21  S21 OUTER
J        F19  T20 OUTER
$--- Defining the Right Region of the ring
J        F23  U23 RIGHT
J        J24  Q24 RIGHT
$--- Defining the Bottom-Mid and Bottom-Ext of the core
J        W 6  W 7 BOTTOM MID
J        W18  W19 BOTTOM MID
J        X 6  X19 BOTTOM MID
J        Y 8  Y17 BOTTOM EXT
```

$--- Redefining the left and right middle
J   H 5 R 5 MIDDLE
J   G 6 S 6 MIDDLE
J   F 7 T 7 MIDDLE
J   F18 T18 MIDDLE
J   G19 S19 MIDDLE
J   H20 R20 MIDDLE
$Defining the top of the core
J   A 8 A17 TOP EXT
J   B 6 B19 TOP MID
J   C 6 C 7 TOP MID
J   C18 C19 TOP MID
$ defining the high channels
J   F 9 T 9 HI
J   F16 T16 HI

The modified incremental cross sections used in the time average model for TRUMOX-30 are provided below for the 4 adjuster types and guide tube, the SDS/MCA and guide tube and the 3 LZCR types for He and Water. The NU case uses the incremental cross sections as defined by the reference CANDU-900 model.

$--- TRU30 fuel using ADJ TYPE 1 and 2 Titanium in DRAGON-
$---- The spacing between adjusters in the model is 2*LP in X and 1*bundle in Z-
MODEL   MOVEPROPS2   ADJ1
2GTR1-1.8789247E-04
2GTR2-7.4885785E-05
2GSA1 2.8232112E-05
2GSA2 7.6185679E-04
2GNF1-2.1276064E-06
2GNF2 1.2548734E-04
2GS12-4.0657818E-05
2GS21 8.1015824E-06
2GF   1.7502900E-03
2GH1 -3.4158800E-04
2GH2 6.5719700E-03
$--------1---------2---------3---------4---------5---------6---------7---------8
MODEL   MOVEPROPS2   ADJ2

2GTR1-2.1275133E-04
2GTR2-8.2403421E-05
2GSA1 3.2193726E-05
2GSA2 8.3648693E-04
2GNF1-2.3649772E-06
2GNF2 1.3936218E-04
2GS12-4.6932138E-05
2GS21 8.8391680E-06
2GF   1.9465390E-03
2GH1 -3.7443000E-04
2GH2 7.1865200E-03
$**
$--------1---------2---------3---------4---------5---------6---------7---------8
$**
$--- TRU30 fuel using ADJ TYPE 3 and 3 SS in DRAGON-------
$---- The spacing between adjusters in the model is 2*LP in X and 1*bundle in Z
MODEL   MOVEPROPS2   ADJ3
2GTR1-1.7818809E-04
2GTR2-8.2470476E-05
2GSA1 2.4161069E-05
2GSA2 6.3740648E-04
2GNF1-1.8877908E-06
2GNF2 1.0631140E-04
2GS12-3.5675242E-05
2GS21 7.2887779E-06
2GF   1.4961660E-03
2GH1 -3.0843400E-04
2GH2 5.8610000E-03
$--------1---------2---------3---------4---------5---------6---------7---------8
$--- TRU30 fuel using ADJ TYPE 4 file in DRAGON-----------
MODEL   MOVEPROPS2   ADJ4
2GTR1-1.6573817E-04
2GTR2-7.7053904E-05
2GSA1 2.2558262E-05
2GSA2 6.0555153E-04
2GNF1-1.7768470E-06
2GNF2 1.0039099E-04
2GS12-3.3088960E-05

```
2GS21 6.9003727E-06
2GF   1.4114680E-03
2GH1 -2.8567200E-04
2GH2  5.4329300E-03
$************************************************************

$--- TRU30 fuel using ADJ GT in DRAGON------------------
$---- The spacing between adjusters in the model is 2*LP in X and 1*Bundle in Z
MODEL   MOVEPROPS2        AJGT1
2GTR1-1.1036172E-04
2GTR2-1.2178719E-04
2GSA1 3.2531098E-06
2GSA2 1.7877668E-05
2GNF1-7.4761920E-07
2GNF2 4.4414773E-06
2GS12-2.0272098E-05
2GS21 3.7158316E-07
2GF   6.0052000E-05
2GH1 -4.4650900E-05
2GH2  2.0738300E-04
$************************************************************

$--- These are updated for TRU30 fuel using SOR in DRAGON------------------
$---- The spacing between SORs in the model is 2*LP in X and Z -----------
MODEL   MOVEPROPS2        SOR
2GTR1-2.7927756E-04
2GTR2 4.1951239E-04
2GSA1 3.6399649E-04
2GSA2 5.5094226E-03
2GNF1-9.7984448E-06
2GNF2 9.0798736E-04
2GS12-2.1282583E-04
2GS21 4.8075890E-05
2GF   7.0754590E-03
2GH1 -1.4817400E-03
2GH2  3.7826200E-02
$************************************************************
$--- TRU30 fuel using SOR GT in DRAGON------------------
```

237

$---- The spacing between SOR GTs in the model is 2*LP in X and Z -----------
MODEL   MOVEPROPS2   SRGT1
2GTR1-2.2635981E-04
2GTR2-2.4272874E-04
2GSA1 5.8249570E-06
2GSA2 3.5157893E-05
2GNF1-2.5972259E-06
2GNF2 8.7274238E-06
2GS12-4.0463172E-05
2GS21 7.8245648E-07
2GF   7.5743000E-05
2GH1 -7.6012000E-05
2GH2 3.1423300E-04
$**

$--- TRU30 fuel using ZCRW 1-3 in DRAGON------------------
$---- The spacing between ZCRs in the model is 2*LP in X and Z -----------
$----Modified for the TRU 30 Fuel---ZC H2O1---top of 2 cell, mid 3 cell---------
MODEL   MOVEPROPS2   ZCR01
2GTR1 1.5039738E-02
2GTR2 4.7058836E-02
2GSA1 6.7445217E-05
2GSA2 1.3377233E-03
2GNF1 6.1916420E-05
2GNF2-2.0444393E-05
2GS12 1.6007135E-03
2GS21-4.7293730E-09
2GF -9.9447300E-04
2GH1 3.8757300E-03
2GH2 1.9824800E-03
$--------1---------2---------3---------4---------5---------6---------7---------8
$----Modified for the TRU 30 Fuel---ZC H2O2---bottom of 2 and 3 cell------------
MODEL   MOVEPROPS2   ZCR02
2GTR1 1.5303802E-02
2GTR2 4.8684672E-02
2GSA1 6.8216119E-05
2GSA2 1.3745320E-03
2GNF1 6.3228537E-05

2GNF2-1.7420854E-05
2GS12 1.6333843E-03
2GS21 9.0287358E-08
2GF -9.5275000E-04
2GH1 4.6320200E-03
2GH2 1.5791000E-03
$-------1---------2---------3---------4---------5---------6---------7---------8
$----Modified for the TRU 30 Fuel---ZC H2O3---top of 3 cell------------
MODEL   MOVEPROPS2   ZCR03
2GTR1 1.4762010E-02
2GTR2 4.5405775E-02
2GSA1 6.6658016E-05
2GSA2 1.3005198E-03
2GNF1 6.0536549E-05
2GNF2-2.3089815E-05
2GS12 1.5663682E-03
2GS21-9.0032700E-08
2GF -1.0298190E-03
2GH1 3.2056700E-03
2GH2 2.2719000E-03
$**
$--- TRU30 fuel using ZCRA 1-3 in DRAGON------------------
$---- The spacing between ZCRs in the model is 2*LP in X and Z -----------
MODEL   MOVEPROPS2   ZCRGT01
2GTR1 4.3810159E-04
2GTR2 1.0107867E-03
2GSA1-7.3106493E-06
2GSA2 1.9604294E-04
2GNF1-9.4748102E-06
2GNF2 4.9930997E-05
2GS12-2.0855013E-04
2GS21-1.0986259E-06
2GF   7.2011400E-04
2GH1 -9.2977100E-04
2GH2 2.9280000E-03
$-------1---------2---------3---------4---------5---------6---------7---------8
MODEL   MOVEPROPS2   ZCRGT02
2GTR1-3.2094046E-03

```
2GTR2-3.0990206E-03
2GSA1-2.6520342E-05
2GSA2 1.1182297E-04
2GNF1-2.6511611E-05
2GNF2 8.6093321E-05
2GS12-6.3663442E-04
2GS21-3.1770469E-07
2GF   1.2540820E-03
2GH1 -1.6464500E-03
2GH2  3.5401300E-03
$-------1---------2---------3---------4---------5---------6---------7--------8
MODEL    MOVEPROPS2       ZCRGT03
2GTR1 3.4931786E-03
2GTR2 5.4572858E-03
2GSA1 7.3777046E-06
2GSA2 2.9124646E-04
2GNF1 4.8065558E-06
2GNF2 1.4667865E-05
2GS12 1.6233698E-04
2GS21-1.8149512E-06
2GF   1.1766000E-04
2GH1 -3.0488200E-04
2GH2  2.4277700E-03
$*****************************************************************
```

The fuelling scheme for each of the defined irradiation regions is provided below.

```
$  Bi-directional fuelling scheme
$-------1---------2---------3---------4---------5---------6---------7--------8
C       A 10      +2
B       OUTER RING     2
B       TOP            1
B       OUTER          1
B       MIDDLE         1
B       INNER          1
B       BOTTOM         1
B       RIGHT          2
```

```
B       BOTTOM MID      2
B       BOTTOM EXT      2
B       TOP EXT       2
B       TOP MID       2
B       HI          1
```

The necessary read cards for the model file are provided below.

```
$----------------------------------------------------------------------------
$  Read 2-group WIMS lattice properties for the fuel
$-------1---------2---------3---------4---------5---------6---------7--------8
*READ CARD
BLOCK    LATPROPS2GTRUMOX
FORMAT   (-A10)
READ     trumox        1       1
FORMAT   (2I10)
READ     trumox        3       4
FORMAT   (6E20.11)
READ     trumox        5     2546
$----------------------------------------------------------------------------
$  Read 2-group WIMS lattice properties for the xenon in the fuel
$-------1---------2---------3---------4---------5---------6---------7--------8
BLOCK    XENONPROP2TRUMOX
FORMAT   (-A10)
READ     trumox        1       1
FORMAT   (2I10)
READ     trumox        3       4
FORMAT   (6E20.11)
READ     trumox        5      698
$----------------------------------------------------------------------------
$  IRRADIATION and BURNUP CORRELATION
$-------1---------2---------3---------4---------5---------6---------7--------8
BLOCK    WIMSBURIRRTRUMOX
FORMAT   (-A10)
READ     trumox        1       1
FORMAT   (I10)
READ     trumox        3       3
FORMAT   (6E20.11)
```

```
READ     trumox        4     158
$-------------------------------------------------------------------------
$-------------------------------------------------------------------------
$ READ LATTICE PROPERTIES FOR THE REFLECTOR (WIMS 2-group)
$--------1---------2---------3---------4---------5---------6---------7---------8
BLOCK    LATPROPS2GREFLECTOR
FORMAT   (2I10)
READ     Reflector     1     2
FORMAT   (6E20.11)
READ     Reflector     3     13
```

The time average model input file is provided below including the MONIC modal analysis simulations.

```
$-------------------------------------------------------------------------
*USE DAF  CANDU-2G2T
*START   A. Morreale
CREATE RFSP SNAPSHOT W/*SIMULATE 0-10 FPD, TEST CASE; USING
RIGHT HANDED MODEL
 FROM DEC. 1998 TEST OF 2-GROUP OPTION
*MODEL   CANDU 9 RFSP - 2-GROUP TIME-AVER
$ CANDU 9 WITH TRUMOX FUELS WITH THE ADJUSTERS OUT
$   Time-Average Calculations for 2-group
$   convergence criteria, number of cycles, underrelaxation factor
$--------1---------2---------3---------4---------5---------6---------7---------8
*TIME-AVER  0.0001    15    0.7          0      0      0
2-GROUP
$  E card defines the iteration data,
E   2 10 2651000.  0.95500    0.0001      1.5          0.01 1 10 999
$  A Card defines the average exit irradiations for a region
A       TOP EXT     3.1500
A       TOP MID     3.1900
A       TOP         3.3400
A       OUTER       3.5700
A       MIDDLE      3.7800
A       INNER       3.7800
A       BOTTOM      3.3000
A       OUTER RING  2.9300
```

```
A      RIGHT     2.9000
A         BOTTOM MID  3.0800
A         BOTTOM EXT  3.0700
A      HI        3.7800
$---------------------------------------------------------------------------
$  C card defines the control device positions, this one all LZCRS at 42%full
C      ADJ**    -1000.0
$  The above should move all the adjusters out of the core
C      ZCR**    0.42
$  XE card defines the xenon parameters
XE           1           1.0          0.001     400
$---------------------------------------------------------------------------
$  S card defines the XE properties, including Xsec
$--------1---------2---------3---------4---------5---------6---------7---------8
S                            .21868E-17
*PRINT   CHANNEL
$---------------------------------------------------------------------------
$  Time-Average Calculations for 2-group
$  convergence criteria, number of cycles, underrelaxation factor
$--------1---------2---------3---------4---------5---------6---------7---------8
*TIME-AVER 0.0001   15     0.7         0     0     0
2-GROUP
$---------------------------------------------------------------------------
$  E card defines the iteration data
E   2 10 2651000.  0.95500   0.0001     1.5           0.01 1  10 400
$---------------------------------------------------------------------------
$  C card defines the control device positions, this one all LZCRS at 42%full
C      ADJ**    -1000.0
$  The above should move all the adjusters out of the core
C      ZCR**    0.42
$  XE card defines the xenon parameters
XE           2           1.0          0.001     400
$---------------------------------------------------------------------------
$  INTREP  interpolates flux to find values at specific points of the core
$--------1---------2---------3---------4---------5---------6---------7---------8
*INTREP
$---------------------------------------------------------------------------
$  A card defines the number of detector groups
```

243

```
$--------1---------2---------3---------4---------5---------6---------7--------8
A   3
$----------------------------------------------------------------------------
$   B card defines the detector group specs
$--------1---------2---------3---------4---------5---------6---------7--------8
B   1    SDS1-NOP    54   3      1      2
B   2    SDS1-ICH    3   1      0      2
B   3    SDS2-NOP    51   3      1      2
$----------------------------------------------------------------------------
$   C card defines the coordinate system for defining detector positions
$--------1---------2---------3---------4---------5---------6---------7--------8
C          0.0  +1        0.0  +1        0.0  +1
$----------------------------------------------------------------------------
$    D card defines the coordinates of the detectors as per CANDU-900 reference
model and is thus not included.
$----------------------------------------------------------------------------
$   F card defines the time constants for ROP detectors
$--------1---------2---------3---------4---------5---------6---------7--------8
F   1       95.24   1538.0  13333.0  333333.0 1000000.0
$----------------------------------------------------------------------------
$   G card defines the ROP delayed component fractions
$--------1---------2---------3---------4---------5---------6---------7--------8
G         -0.01   -0.004   -0.033  -0.0015    0.000
$----------------------------------------------------------------------------
$   H card defines the ROP amplifier and dynamic compensator constants
$--------1---------2---------3---------4---------5---------6---------7--------8
H        0.025    30.0   3000.0    0.032    0.022
$   Reinitialize time average
*TIME-AVER  0.0001    15     0.7        0     0     0
ADJOINT
2-GROUP
$--------1---------2---------3---------4---------5---------6---------7--------8
C      ADJ**    -1000.0
E   2  10  2651000.  0.95500   0.0002    1.5    1.000    0.5 1  10 999
$----------------------------------------------------------------------------
*SUMMARY
2-GROUP
*PRINT    CHANNEL
```

```
$------------------------ MONIC
*STORE
FROM     FLUX/POWERSLOW FLUX
TO       HARMONICS FUNDAMENTLSLOW FLUX
*STORE
FROM     FLUX/POWERFAST FLUX
TO       HARMONICS FUNDAMENTLFAST FLUX
*STORE
FROM     FLUX/POWERFAST FLUXA
TO       FLUX/POWERFAST FLUX
*STORE
FROM     FLUX/POWERSLOW FLUXA
TO       FLUX/POWERSLOW FLUX
$*DELETE   SIMULDATA
$  Adding on the monic analysis commands for 2nd harmonic
*MONIC              2           0
2-GROUP
A            10   1       0.05  10  100  10
$--------1---------2---------3---------4---------5---------6---------7---------8
E   2 10 2651000. 0.95500  0.00002    1.5   1.000     0.5 1 10 999
$ INFORMATION FOR GUESS CARD = col 11-15 is M, col 16-20 is IN, col
$51-60 is Aml  col 61-70 is PHASE
$ M is the order of the azimuthal harmonic, IN is the order of the axial harmonic
$ AlphaML is the value of the Lth zero of the Mth order bessel function
$ Values for AlphaML = 3.832, 7.106 for M = 1
$--------1---------2---------3---------4---------5---------6---------7---------8
GUESS      1   1         0.80   422.90  3.832     0.0
LABEL    MONIC SECOND HARMONIC - 1ST AZIMUTHAL A
*RITE TAPEC9_HARM_02
TITLE    MONIC SECOND HARMONIC - 1ST AZIMUTHAL A
*STORE
FROM     HARMONICS HARMONIC 2SLOW FLUX CELL PHI
TO       FLUX/POWERSLOW FLUX CELL PHI
*PRINT   CELL PHI
*RITE CARD
BLOCK    FLUX/POWERSLOW FLUX CELL PHI
FORMAT    (12E12.5)
WRITE    CELLPHI02 1 6240
```

```
*PRNT MASS
$   Adding on the monic analysis commands for 3rd harmonic
*MONIC               3           0
2-GROUP
A          10   1        0.05   10  100  10
$-------1---------2---------3---------4---------5---------6---------7--------8
E    2  10  2651000.  0.95500   0.00002    1.5    1.000     0.5 1  10 999
$-------1---------2---------3---------4---------5---------6---------7--------8
GUESS      1   1           0.80   422.90   3.832   270.0
LABEL    MONIC THIRD HARMONIC - 1ST AZIMUTHAL B
*RITE TAPEC9_HARM_03
TITLE    MONIC THIRD HARMONIC - 1ST AZIMUTHAL B
*STORE
FROM     HARMONICS HARMONIC 3SLOW FLUX CELL PHI
TO       FLUX/POWERSLOW FLUX CELL PHI
*PRINT    CELL PHI
*RITE CARD
BLOCK    FLUX/POWERSLOW FLUX CELL PHI
FORMAT    (12E12.5)
WRITE     CELLPHI03 1 6240
*PRNT MASS
$   Adding on the monic analysis commands for 4th harmonic
*MONIC               4           0
2-GROUP
A          10   1        0.05   10  100  10
$-------1---------2---------3---------4---------5---------6---------7--------8
E    2  10  2651000.  0.95500   0.00002    1.5    1.000     0.5 1  10 999
$-------1---------2---------3---------4---------5---------6---------7--------8
GUESS      0   1           0.80   422.90   2.405    0.0
LABEL    MONIC FOURTH HARMONIC - 1ST AXIAL
*RITE TAPEC9_HARM_04
TITLE    MONIC FOURTH HARMONIC - 1ST AXIAL
*STORE
FROM     HARMONICS HARMONIC 4SLOW FLUX CELL PHI
TO       FLUX/POWERSLOW FLUX CELL PHI
*PRINT    CELL PHI
*RITE CARD
BLOCK    FLUX/POWERSLOW FLUX CELL PHI
```

246

```
FORMAT    (12E12.5)
WRITE    CELLPHI04 1 6240
*PRNT MASS
$  Adding on the monic analysis commands for 5th harmonic
*MONIC            5          0
2-GROUP
A        10   1      0.05  10  100  10
$-------1---------2---------3---------4---------5---------6---------7---------8
E   2  10  2651000.  0.95500  0.00002    1.5    1.000    0.5 1  10 999
$-------1---------2---------3---------4---------5---------6---------7---------8
GUESS     2   1        0.80   422.90   5.136     0.0
LABEL    MONIC FIFTH HARMONIC - 2ND AZIMUTHAL A
*RITE TAPEC9_HARM_05
TITLE    MONIC FIFTH HARMONIC - 2ND AZIMUTHAL A
*STORE
FROM     HARMONICS HARMONIC 5SLOW FLUX CELL PHI
TO      FLUX/POWERSLOW FLUX CELL PHI
*PRINT    CELL PHI
*RITE CARD
BLOCK    FLUX/POWERSLOW FLUX CELL PHI
FORMAT    (12E12.5)
WRITE    CELLPHI05 1 6240
*PRNT MASS
$  Adding on the monic analysis commands for 6th harmonic
*MONIC            6          0
2-GROUP
A        10   1      0.05  10  100  10
$-------1---------2---------3---------4---------5---------6---------7---------8
E   2  10  2651000.  0.95500  0.00002    1.5    1.000    0.5 1  10 999
$-------1---------2---------3---------4---------5---------6---------7---------8
GUESS     2   1        0.80   422.90   5.136    90.0
LABEL    MONIC SIXTH HARMONIC - 2ND AZIMUTHAL B
*RITE TAPEC9_HARM_06
TITLE    MONIC SIXTH HARMONIC - 2ND AZIMUTHAL B
*STORE
FROM     HARMONICS HARMONIC 6SLOW FLUX CELL PHI
TO      FLUX/POWERSLOW FLUX CELL PHI
*PRINT    CELL PHI
```

```
*RITE CARD
BLOCK    FLUX/POWERSLOW FLUX CELL PHI
FORMAT   (12E12.5)
WRITE    CELLPHI06 1 6240
*PRNT MASS
$  Adding on the monic analysis commands for 7th harmonic
*MONIC            7           0
2-GROUP
A        10   1      0.05  10  100  10
$-------1---------2---------3---------4---------5---------6---------7---------8
E   2  10  2651000.  0.95500  0.00002    1.5   1.000    0.5 1  10 999
$-------1---------2---------3---------4---------5---------6---------7---------8
GUESS     1   2         0.80   422.90   3.832     0.0
LABEL    MONIC SEVENTH HARMONIC - 1ST AZ A 1ST AXIAL
*RITE TAPEC9_HARM_07
TITLE    MONIC SEVENTH HARMONIC - 1ST AZ A 1ST AXIAL
*STORE
FROM     HARMONICS HARMONIC 7SLOW FLUX CELL PHI
TO       FLUX/POWERSLOW FLUX CELL PHI
*PRINT    CELL PHI
*RITE CARD
BLOCK    FLUX/POWERSLOW FLUX CELL PHI
FORMAT   (12E12.5)
WRITE    CELLPHI07 1 6240
*PRNT MASS
$  Adding on the monic analysis commands for 8th harmonic
*MONIC            8           0
2-GROUP
A        10   1      0.05  10  100  10
$-------1---------2---------3---------4---------5---------6---------7---------8
E   2  10  2651000.  0.95500  0.00002    1.5   1.000    0.5 1  10 999
$-------1---------2---------3---------4---------5---------6---------7---------8
GUESS     1   2         0.80   422.90   3.832    90.0
LABEL    MONIC EIGHTH HARMONIC - 1ST AZ B 1ST AXIAL
*RITE TAPEC9_HARM_08
TITLE    MONIC EIGHTH HARMONIC - 1ST AZ B 1ST AXIAL
*STORE
FROM     HARMONICS HARMONIC 8SLOW FLUX CELL PHI
```

```
TO      FLUX/POWERSLOW FLUX CELL PHI
*PRINT   CELL PHI
*RITE CARD
BLOCK    FLUX/POWERSLOW FLUX CELL PHI
FORMAT    (12E12.5)
WRITE    CELLPHI08 1 6240
*PRNT MASS
$  Adding on the monic analysis commands for 9th harmonic
*MONIC              9              0
2-GROUP
A         10   1        0.05  10  100  10
$-------1---------2---------3---------4---------5---------6---------7---------8
E   2  10  2651000.  0.95500  0.00002     1.5    1.000     0.5 1  10 999
$-------1---------2---------3---------4---------5---------6---------7---------8
$GUESS      1   1             0.80   422.90   5.520      0.0
LABEL    MONIC NINTH HARMONIC - 1ST RADIAL
*RITE TAPEC9_HARM_09
TITLE    MONIC NINTH HARMONIC - 1ST RADIAL
*STORE
$-------1---------2---------3---------4---------5---------6---------7---------8
FROM     HARMONICS HARMONIC 9SLOW FLUX CELL PHI
TO      FLUX/POWERSLOW FLUX CELL PHI
*PRINT   CELL PHI
*RITE CARD
BLOCK    FLUX/POWERSLOW FLUX CELL PHI
FORMAT    (12E12.5)
WRITE    CELLPHI09 1 6240
*PRNT MASS
$new monic shit ends--------------------------
$  Adding on the monic analysis commands for 10th harmonic
*MONIC             10              0
2-GROUP
A         10   1        0.05  10  100  10
$-------1---------2---------3---------4---------5---------6---------7---------8
E   2  10  2651000.  0.95500  0.00002     1.5    1.000     0.5 1  10 999
$-------1---------2---------3---------4---------5---------6---------7---------8
$GUESS      3   1             0.80   422.90   6.380      0.0
LABEL    MONIC TENTH HARMONIC - 3RD AZIMUTHAL
```

```
*RITE TAPEC9_HARM_10
TITLE    MONIC TENTH HARMONIC - 3RD AZIMUTHAL
*STORE
FROM     HARMONICS HARMONIC10SLOW FLUX CELL PHI
TO      FLUX/POWERSLOW FLUX CELL PHI
*PRINT   CELL PHI
*RITE CARD
BLOCK    FLUX/POWERSLOW FLUX CELL PHI
FORMAT    (12E12.5)
WRITE    CELLPHI10 1 6240
*PRNT MASS
$   Run a TAV Equivalent
$-------1---------2---------3---------4---------5---------6---------7---------8
*TAVEQUIV       -2
2-GROUP
*PRINT   POWERS
*PRINT   MASS
$  moving power information for use in *PRTPWR module
*STORE
FROM     FLUX/POWERPOWERS
TO      T-AVERAGEDFLUX/POWERPOWERS
*STORE
FROM     FLUX/POWERPOWERS
TO      REFORM   FLUX/POWERPOWERS
$  moving irradiation and burnup data for use in simulate
*STORE
FROM     T-AVERAGE TAEQVIRRAD
TO      IRRADIATONFUEL IRRAD
*STORE
FROM     T-AVERAGE TAEQV BURN
TO      IRRADIATONFUELBURNUP
$*DELETE   SIMULDATA
$  Running simulate to create a good snapshot
$-------1---------2---------3---------4---------5---------6---------7---------8
*simulate C9TRU30        0  0.0       0       40       0
2-GROUP
$-------1---------2---------3---------4---------5---------6---------7---------8
C      ADJ**   -1000.0
```

```
E   2 10 2651000.  0.95500  0.00002     1.5    1.000     0.5 1  10 999
XE          1    0.    1.            0.001      10
PROPXE                        .21868E-17
$-----------------------------------------------------------------------------
$  Standard output
$--------1---------2---------3---------4---------5---------6---------7---------8
*PRINT   POWERS
*PRINT   MASS
*PRINT   FUELBURNUP
*PRINT   CELL PHI
*PRINT   SLOW FLUX
*PRINT   FAST FLUX
$*RITE TAPEdrds.mf
$*RITE TAPETAV_SEQ2G
$ TITLE    CANDU 9 TIME-AVERAGE 2-GROUP with TRU-30 Fuel
*MAKE DAF CANDU-TA2T
 PRINT   REFLECTOR
*CLOSE
EXIT
```

For evaluating control device worth the following simulation code allows the manipulation of devices after a standard time average simulation using the same irradiations.

```
$-----------------------------------------------------------------------------
$  Reinitialize time average
$--------1---------2---------3---------4---------5---------6---------7---------8
*TIME-AVER  .000010  10     .500000            0      0
2-GROUP
C      ADJ**   -1000.0
E   2 10 2651000.  0.95500   0.001     1.5           0.01 1  10 999
*PRINT   CHANNEL
$-----------------------------------------------------------------------------
$ Run a time averag with IPRESERVE =1 to save the irradiations
*TIME-AVER 0.0001    15     0.7          0     1     0
2-GROUP
$--------1---------2---------3---------4---------5---------6---------7---------8
$C      ADJ**    -1000.0
```

```
$  The above should move all the adjusters out of the core
C      ZCR**    0.42
$C     ZCR01   0.42    ZCR02   0.42    ZCR03   0.42
$C     ZCR04   0.42    ZCR05   0.42    ZCR06   0.42
$C     ZCR07   0.42    ZCR08   0.42    ZCR09   0.42
$C     ZCR10   0.42    ZCR11   0.42    ZCR12   0.42
$C     ZCR13   0.42    ZCR14   0.42
$Insertion of MCA (CAR)
$C     CAR01   +575.501
$C     CAR02   +575.501
$C     CAR03   +575.501
$C     CAR04   +575.501
$SDS #1 ROD INSERTION
C      SOR**    +575.501
$SDS #1 ROD INDIVIDUAL ROD INSERTION
$C     SOR01   +575.501
$C     SOR02   +575.501
$C     SOR03   +575.501
$C     SOR04   +575.501
$C     SOR05   +575.501
$C     SOR06   +575.501
$C     SOR07   +575.501
$C     SOR08   +575.501
$C     SOR09   +575.501
$C     SOR10   +575.501
$C     SOR11   +575.501
$C     SOR12   +575.501
$C     SOR13   +575.501
$C     SOR14   +575.501
$C     SOR15   +575.501
$C     SOR16   +575.501
$C     SOR17   +575.501
$C     SOR18   +575.501
$C     SOR19   +575.501
$C     SOR20   +575.501
$C     SOR21   +575.501
$C     SOR22   +575.501
$C     SOR23   +575.501
```

```
$C      SOR24    +575.501
$C      SOR25    +575.501
$C      SOR26    +575.501
$C      SOR27    +575.501
$C      SOR28    +575.501
$C      SOR29    +575.501
$C      SOR30    +575.501
$C      SOR31    +575.501
$C      SOR32    +575.501
E   2  10  2651000.  0.95500   0.0002    1.5    1.000    0.5 1  10 999
$-----------------------------------------------------------------------
```

The simulation input for the Instantaneous snapshot for core ITAN-2B8T is provided below.

```
$-----------------------------------------------------------------------
*USE DAF  CANDU-TA2T
$-----------------------------------------------------------------------
*START   A. Morreale
CREATE RFSP SNAPSHOT W/*SIMULATE 0-10 FPD, TEST CASE; USING
RIGHT HANDED MODEL
 FROM DEC. 1998 TEST OF 2-GROUP OPTION
$-----------------------------------------------------------------------
*MODEL   CANDU 9 RFSP - 2-GROUP INSTANTAN
$ modified Itan to be suitable for the CANDU 9 platform (24x24 channels)
$-----------------------------------------------------------------------
*STORE
FROM     FLUX/POWERPOWERS
TO       T-AVERAGEDFLUX/POWERPOWERS
*INSTANTANINSTANTAN RANDIS 1
2-GROUP
F        00
$Control Statements for devices
C      ZCR**       0.42
C      ADJ** *    -1000.0
$--Row A (4 rows of 6 = 24 channel positions)
G        .0000    .0000    .0000    .0000    .0000    .0000
G        .0000    .4400    .5400    .9600    .0200    .4800
```

```
G         .0400    .1400    .4400    .8200    .1200    .0000
G         .0000    .0000    .0000    .0000    .0000    .0000
$--Row B
G         .0000    .0000    .0000    .0000    .0000    .5800
G         .2800    .8200    .1600    .4200    .6400    .8600
G         .3000    .7600    .5400    .1600    .7000    .3600
G         .8400    .0000    .0000    .0000    .0000    .0000
$--Row C
G         .0000    .0000    .0000    .0000    .3800    .2000
G         .9400    .1200    .7000    .0800    .1800    .3200
G         .5600    .2200    .9600    .4200    .0800    .9000
G         .3800    .2000    .0000    .0000    .0000    .0000
$--Row D
G         .0000    .0000    .0000    .5200    .9200    .7400
G         .4000    .6200    .3600    .9000    .5200    .7800
G         .1000    .6800    .0200    .6400    .1800    .5200
G         .9200    .7400    .4000    .0000    .0000    .0000
$--Row E
G         .0000    .0000    .3200    .7800    .5000    .9800
G         .2400    .6600    .8400    .3800    .9200    .5000
G         .8000    .2600    .4800    .8600    .3200    .7800
G         .5000    .9800    .2400    .6600    .0000    .0000
$--Row F
G         .0000    .3000    .5600    .1000    .8000    .6000
G         .3400    .7200    .5800    .2000    .7400    .9800
G         .6000    .4600    .0400    .3000    .5600    .1000
G         .8000    .6000    .3400    .7200    .5800    .0000
$--Row G
G         .0000    .7600    .2200    .6800    .2600    .4600
G         .8800    .0600    .2800    .9400    .4000    .2400
G         .3400    .8800    .1400    .7600    .2200    .6800
G         .2600    .4600    .8800    .0600    .2800    .0000
$--Row H
G         .0000    .5400    .9600    .0200    .4800    .0400
G         .1400    .4400    .8200    .1200    .6200    .6600
G         .7200    .0600    .4400    .5400    .9600    .0200
G         .4800    .0400    .1400    .4400    .8200    .0000
$--Row J
```

G	.8200	.1600	.4200	.6400	.8600	.3000
G	.7600	.5400	.1600	.7000	.3600	.8400
G	.5800	.2800	.8200	.1600	.4200	.6400
G	.8600	.3000	.7600	.5400	.1600	.7000
$--Row K						
G	.1200	.7000	.0800	.1800	.3200	.5600
G	.2200	.9600	.4200	.0800	.9000	.3800
G	.2000	.9400	.1200	.7000	.0800	.1800
G	.3200	.5600	.2200	.9600	.4200	.0800
$--Row L						
G	.6200	.3600	.9000	.5200	.7800	.1000
G	.6800	.0200	.6400	.1800	.5200	.9200
G	.7400	.4000	.6200	.3600	.9000	.5200
G	.7800	.1000	.6800	.0200	.6400	.1800
$--Row M						
G	.6600	.8400	.3800	.9200	.5000	.8000
G	.2600	.4800	.8600	.3200	.7800	.5000
G	.9800	.2400	.6600	.8400	.3800	.9200
G	.5000	.8000	.2600	.4800	.8600	.3200
$--Row N						
G	.7200	.5800	.2000	.7400	.9800	.6000
G	.4600	.0400	.3000	.5600	.1000	.8000
G	.6000	.3400	.7200	.5800	.2000	.7400
G	.9800	.6000	.4600	.0400	.3000	.5600
$--Row O						
G	.0600	.2800	.9400	.4000	.2400	.3400
G	.8800	.1400	.7600	.2200	.6800	.2600
G	.4600	.8800	.0600	.2800	.9400	.4000
G	.2400	.3400	.8800	.1400	.7600	.2200
$--Row P						
G	.4400	.8200	.1200	.6200	.6600	.7200
G	.0600	.4400	.5400	.9600	.0200	.4800
G	.0400	.1400	.4400	.8200	.1200	.6200
G	.6600	.7200	.0600	.4400	.5400	.9600
$--Row Y						
G	.0000	.0000	.0000	.0000	.0000	.0000
G	.0000	.9600	.4200	.0800	.9000	.3800

```
G          .2000   .9400   .1200   .7000   .0800   .0000
G          .0000   .0000   .0000   .0000   .0000   .0000
```

$$The G cards dictate the channel ages for each of the rows A-Y as per the channel age distributions for the core shown in Appendix A. $$

```
*STORE
FROM    INSTANTAN RANDIS 1  FLUX/POWERPOWERS
TO      FLUX/POWERPOWERS
*PRINT   POWERS
*MAKE DAF CANDU-INST2B8T
$*RITE TAPEC9INST2G
 TITLE    CANDU 9 RFSP INSTANTAN 2 GROUP
*CLOSE   NORMAL TERMINATION
```

The simulation input for a coolant voiding of the time average core is provided below.

```
$----------------------------------------------------------------------------
*USE DAF  CANDU-TA2T
$----------------------------------------------------------------------------
*START   A. Morreale
CREATE RFSP SNAPSHOT W/*SIMULATE 0-10 FPD, TEST CASE; USING
RIGHT HANDED MODEL
 FROM DEC. 1998 TEST OF 2-GROUP OPTION
$----------------------------------------------------------------------------
*MODEL   CANDU 9 RFSP SNAPSHOT TEST CASE 0-10 FPD
$----------------------------------------------------------------------------
$  This code changes the coolant density in order to measure the coolant void
$  reactivity coefficient, each sim is a 0 burn.
$  This code follows 2-Group_Time-Aver2B
$----------------------------------------------------------------------------
$--------1---------2---------3---------4---------5---------6---------7---------8
*READ CARD
BLOCK    WIMSTABLESTRUMOX
FORMAT    (-A10)
READ     fuel.tab        1       1
FORMAT    (1I10)
```

```
READ      fuel.tab       3       3
FORMAT    (6E15.6)
READ      fuel.tab       4    533872
$------------------------------------------------------------------------------
$ SIM 1: NORMAL CORE
$------------------------------------------------------------------------------
$ READ THE MICRO DEPLETION DATA FOR THE REFLECTOR
$-------1---------2---------3---------4--------5---------6--------7--------8
*READ CARD
BLOCK    WIMSTABLESREFLECTOR
FORMAT    (-A10)
READ      refl.tab       1       1
FORMAT    (1I10)
READ      refl.tab       3       3
FORMAT    (6E15.6)
READ      refl.tab       4      300
$------------------------------------------------------------------------------
*READ CARD
BLOCK    LOCAL PARMDENSITY
FORMAT    (8F10.4)
SET           1    6240 0.8074
$-------1---------2---------3---------4--------5---------6--------7--------8
*READ CARD
BLOCK    LOCAL PARMCOOL TEMP
FORMAT    (8F10.4)
SET           1    6240 288.135
$-------1---------2---------3---------4--------5---------6--------7--------8
*READ CARD
BLOCK    LOCAL PARMFUEL TEMP
FORMAT    (8F10.4)
SET           1    6240 586.83
$ SIMULATE with micro depn to simulate the power burnup history
$-------1---------2---------3---------4--------5---------6--------7--------8
*SIMULATE C9TRU30        0  0.0
NUCIRC
FUELTEMP
WIMSHI   ITER 5        \
     NGRO 2        \
```

```
       MODT 63.0    \
       MODP 99.918  \
       MODB 0.0     \
       MODG 0.0     \
       COOLP 98.764 \
       POWR 1.0     \
       STEP 0 S     \
       STOPERR NO   \
       BURNT EQUIL  \
       EDIT 0
$-------------Control card setting device positions ----------------------
C      ADJ** *     -1000.0
$-------1---------2---------3---------4--------5--------6--------7--------8
E   2  10 2651000.0  0.95500  0.00001    1.5   1.000    0.01 0   999
*PRINT   POWERS
$------------------------------------------------------------------------
$ SIM 2: Voided core (change coolant density to represent void)
*READ CARD
BLOCK    LOCAL PARMDENSITY
FORMAT   (8F10.4)
SET         1    6240 0.0008
$-------1---------2---------3---------4--------5--------6--------7--------8
*READ CARD
BLOCK    LOCAL PARMCOOL TEMP
FORMAT   (8F10.4)
SET         1    6240 288.135
$-------1---------2---------3---------4--------5--------6--------7--------8
*READ CARD
BLOCK    LOCAL PARMFUEL TEMP
FORMAT   (8F10.4)
SET         1    6240 586.83
$-------1---------2---------3---------4--------5--------6--------7--------8
*SIMULATE C9TRU30   999999999    0.0     0   1
$  C -> current positions of devices
$  E -> Iteration Data
$-------1---------2---------3---------4--------5--------6--------7--------8
NUCIRC
FUELTEMP
```

```
WIMSHI  ITER 5      \
     NGRO 2       \
     MODT 63.0    \
     MODP 99.918  \
     MODB 0.0     \
     MODG 0.0     \
     COOLP 98.764 \
     POWR 1.0     \
     STEP 0 S     \
     STOPERR NO   \
     BURNT NORM   \
     EDIT 0
$--------------Control card setting device positions -----------------------
C      ADJ** *    -1000.0
$-------1---------2---------3---------4---------5---------6---------7---------8
E   2  10 2651000.0  0.95500  0.00001     1.5    1.000    0.01 0    999
*PRINT   POWERS
*MAKE DAF CANDU-CVR
*CLOSE
```

The initial simulation file for determining reactor coefficients is as follows (2-Group Simulate).

```
$----------------------------------------------------------------------------
*USE DAF  CANDU-TA2T
$----------------------------------------------------------------------------
*START   A. Morreale
CREATE RFSP SNAPSHOT W/*SIMULATE 0-10 FPD, TEST CASE; USING
RIGHT HANDED MODEL
 FROM DEC. 1998 TEST OF 2-GROUP OPTION
$----------------------------------------------------------------------------
*MODEL   CANDU 9 RFSP SNAPSHOT TEST CASE 0-10 FPD
$----------------------------------------------------------------------------
$  READ THE MICRO DEPLETION DATA FOR THE FUEL
$-------1---------2---------3---------4---------5---------6---------7---------8
*READ CARD
BLOCK    WIMSTABLESTRUMOX
```

```
FORMAT    (-A10)
READ    fuel.tab        1       1
FORMAT    (1I10)
READ    fuel.tab        3       3
FORMAT    (6E15.6)
READ    fuel.tab        4    533872
$-------------------------------------------------------------------------
$  READ THE MICRO DEPLETION DATA FOR THE REFLECTOR
$-------1---------2---------3---------4--------5---------6--------7--------8
*READ CARD
BLOCK    WIMSTABLESREFLECTOR
FORMAT    (-A10)
READ    refl.tab        1       1
FORMAT    (1I10)
READ    refl.tab        3       3
FORMAT    (6E15.6)
READ    refl.tab        4     300
$-------------------------------------------------------------------------
*READ CARD
BLOCK    LOCAL PARMDENSITY
FORMAT    (8F10.4)
SET          1    6240 0.8074
$-------1---------2---------3---------4--------5---------6--------7--------8
*READ CARD
BLOCK    LOCAL PARMCOOL TEMP
FORMAT    (8F10.4)
SET          1    6240 288.135
$-------1---------2---------3---------4--------5---------6--------7--------8
*READ CARD
BLOCK    LOCAL PARMFUEL TEMP
FORMAT    (8F10.4)
SET          1    6240 586.83
*PRNT MASS
*SIMULATE C9TRU30          0   0.0
NUCIRC
$FUELTEMP
WIMSHI   ITER 5         \
     NGRO 2       \
```

```
        MODT 63.0    \
        MODP 99.918  \
        MODB 0.0     \
        MODG 0.0     \
        COOLP 98.764 \
        POWR 1.0     \
        STEP 0 S     \
        STOPERR NO   \
        BURNT EQUIL  \
        EDIT 0
$-----control device position settings ------------------------------------------------
C      ZCR**    0.42
C      ADJ**    -1000.0
$-------1---------2---------3---------4---------5---------6---------7---------8
E   2  10 2651000.0  0.95500  0.00001    1.5    1.000    0.01 0    999
*PRINT   POWERS
*PRINT   FUELBURNUP
*MAKE DAF CANDU-SIM
*CLOSE
```

The simulation used for determining reactor coefficients is provided below in the sample case for moderator purity.

```
$-------------------------------------------------------------------------
*USE DAF  CANDU-SIM
$-------------------------------------------------------------------------
*START   A. Morreale
CREATE RFSP SNAPSHOT W/*SIMULATE 0-10 FPD, TEST CASE; USING
RIGHT HANDED MODEL
 FROM DEC. 1998 TEST OF 2-GROUP OPTION
$-------------------------------------------------------------------------
*MODEL   CANDU 9 RFSP SNAPSHOT TEST CASE 0-10 FPD
$-------------------------------------------------------------------------
$  This code varies the Moderator Purity in order to measure the mod purity
$  reactivity coefficient, each sim is a 0 burn. code follows 2-Group_Simulate
$******SIM 1 99%**************
$ Initiate Reactor Local Parameters
$-------1---------2---------3---------4---------5---------6---------7---------8
```

```
*READ CARD
BLOCK    LOCAL PARMDENSITY
FORMAT    (8F10.4)
SET        1    6240 0.8074
$-------1---------2---------3---------4---------5---------6---------7--------8
*READ CARD
BLOCK    LOCAL PARMCOOL TEMP
FORMAT    (8F10.4)
SET        1    6240 288.135
$-------1---------2---------3---------4---------5---------6---------7--------8
*READ CARD
BLOCK    LOCAL PARMFUEL TEMP
FORMAT    (8F10.4)
SET        1    6240 586.83
$ Execution of SIMULATE module
*SIMULATE C9TRU30   9999999990.0              1              20
NUCIRC
FUELTEMP
WIMSHI   ITER 5      \
     NGRO 2      \
     MODT 63.0   \
     MODP 99.000  \
     MODB 0.0     \
     MODG 0.0     \
     COOLP 98.764 \
     POWR 1.0     \
     STEP 0 H     \
     BURNT NORM   \
     EDIT 0
$---------------------------------------------------------------------------
C      ADJ** *    -1000.0
$-------1---------2---------3---------4---------5---------6---------7--------8
E   2 10 2651000.0  0.95500  0.00001    1.5   1.000    0.01 0   999
*PRINT   POWERS
*PRINT   FUELBURNUP
… (continues for different moderator, fuel and coolant properties)
*MAKE DAF CANDU-MP
*CLOSE
```

The precursor to fuelling simulations (Sim-ITAN spatial) is provided below, it follows of an Instantaneous snapshot simulation of one of the cores in Appendix A.

```
$-----------------------------------------------------------------------------
*USE DAF  CANDU-INST2B8T
$-----------------------------------------------------------------------------
*START    A. Morreale
CREATE RFSP SNAPSHOT W/*SIMULATE 0-10 FPD, TEST CASE; USING
RIGHT HANDED MODEL
 FROM DEC. 1998 TEST OF 2-GROUP OPTION
$-----------------------------------------------------------------------------
*MODEL    CANDU 9 RFSP SNAPSHOT TEST CASE 0-10 FPD
$-----------------------------------------------------------------------------
$ Execution of SIMULATE module to simulate the power burnup history
*STORE
FROM     INSTANTAN RANDIS 1  IRRADIATONFUEL IRRAD
TO       IRRADIATONFUEL IRRAD
*DELETE   SIMULDATA
*SIMULATE CANDU 9          0  0.0      0
2-GROUP
C       ADJ**    -1000.0
$-------1---------2---------3---------4---------5---------6---------7--------8
E    2  10 2651000.0  0.95500  0.00001     1.5    1.000    0.01 0   999
*PRINT   POWERS
$-----------------------------------------------------------------------------
$ READ THE MICRO DEPLETION DATA FOR THE FUEL
*READ CARD
BLOCK    WIMSTABLESTRUMOX
FORMAT   (-A10)
READ     fuel.tab       1      1
FORMAT   (1I10)
READ     fuel.tab       3      3
FORMAT   (6E15.6)
READ     fuel.tab       4    533872
$ READ THE MICRO DEPLETION DATA FOR THE REFLECTOR
*READ CARD
```

```
BLOCK    WIMSTABLESREFLECTOR
FORMAT    (-A10)
READ      refl.tab        1       1
FORMAT    (1I10)
READ      refl.tab        3       3
FORMAT    (6E15.6)
READ      refl.tab        4       300
$-------------------------------------------------------------------------------
*READ CARD
BLOCK    LOCAL PARMDENSITY
FORMAT    (8F10.4)
SET          1     6240 0.8074
$-------1---------2---------3---------4--------5--------6--------7--------8
*READ CARD
BLOCK    LOCAL PARMCOOL TEMP
FORMAT    (8F10.4)
SET          1     6240 288.135
$-------1---------2---------3---------4--------5--------6--------7--------8
*READ CARD
BLOCK    LOCAL PARMFUEL TEMP
FORMAT    (8F10.4)
SET          1     6240 586.83
$  SIMULATE module using micro depn to simulate the power burnup history
$-------1---------2---------3---------4--------5--------6--------7--------8
*SIMULATE CANDU 9          0 0.0
NUCIRC
FUELTEMP
WIMSHI   ITER 5        \
      NGRO 2       \
      MODT 63.0    \
      MODP 99.918  \
      MODB 0.0     \
      MODG 0.0     \
      COOLP 98.764 \
      POWR 1.0     \
      STEP 0 S     \
      STOPERR NO   \
      BURNT EQUIL  \
```

```
      EDIT 0
$C      LZCR**        0.50
C       ADJ**    -1000.0
$-------1---------2---------3---------4---------5---------6---------7---------8
E   2 10 2651000.0  0.95500  0.00001    1.5    1.000    0.01 0    999
*PRINT   POWERS
*PRINT   FUELBURNUP
$-------------------------------------------------------------------------------
$  Run the simulate with spatial control
$-------------------------------------------------------------------------------
*READ CARD
BLOCK    LOCAL PARMDENSITY
FORMAT   (8F10.4)
SET          1    6240 0.8074
$-------1---------2---------3---------4---------5---------6---------7---------8
*READ CARD
BLOCK    LOCAL PARMCOOL TEMP
FORMAT   (8F10.4)
SET          1    6240 288.135
$-------1---------2---------3---------4---------5---------6---------7---------8
*READ CARD
BLOCK    LOCAL PARMFUEL TEMP
FORMAT   (8F10.4)
SET          1    6240 586.83
$  SIMULATE module using micro depn to simulate the power burnup history
$-------1---------2---------3---------4---------5---------6---------7---------8
*SIMULATE CANDU 9    9999999990.0                        20
$  C -> current positions of devices
$  E -> Iteration Data
$-------1---------2---------3---------4---------5---------6---------7---------8
NUCIRC
FUELTEMP
WIMSHI   ITER 5       \
     NGRO 2       \
     MODT 63.0    \
     MODP 99.918  \
     MODB 0.0     \
     MODG 0.0     \
```

```
        COOLP 98.764  \
        POWR 1.0      \
        STEP 0 D      \
        STOPERR NO    \
        BURNT NORM    \
        EDIT 0
$------------------------------------------------------------------------
$  SPATIAL AND BULK CONTROL CARDS
$---v----1----v----2----v----3----v----4----v----5----v----6----v----7----v----8
AA       20  1  20  14   1   3   1
BB       0.00001    0.003  1.00150    1.00    0.00    0.95    0.05
CC      ZCR01    ZCR02    ZCR03    ZCR04    ZCR05    ZCR06    ZCR07
CC      ZCR08    ZCR09    ZCR10    ZCR11    ZCR12    ZCR13    ZCR14
DD      ZCR**      300.0
EE      ZCR**    2.0
$*Z_NAME FXLVL X1X2Y1Y2Z1Z2 X1X2Y1Y2Z1Z2   X1X2Y1Y2Z1Z2 **
$** FF FF FF FF FF FF FF FF FF FF FF FF FF FF FF FF FF FF FF FFFF FF FF
FF      ZCR01    0.93146    353607082241   354009102241   354211122241
FF      ZCR01    0.93146    354413132241   354514152241   354616202241
FF      ZCR01    0.93146    354721272241
FF      ZCR02    0.98890    354728342241   354635392241   354540412241
FF      ZCR02    0.98890    354444222241   354243432241   354044452241
FF      ZCR02    0.98890    353646462241
FF      ZCR03    0.97933    193407202241
FF      ZCR04    1.15147    193421342241
FF      ZCR05    1.00941    193435462241
FF      ZCR06    0.97695    171807082241   131809102241   111811122241
FF      ZCR06    0.97695    091813132241   081814152241   071816202241
FF      ZCR06    0.97695    061821272241
FF      ZCR07    0.94726    061828342241   071835392241   081840412241
FF      ZCR07    0.94726    091842422241   111843432241   131844452241
FF      ZCR07    0.94726    171846462241
$****************************************************************
FF      ZCR08    0.94001    171807080121   131809100121   111811120121
FF      ZCR08    0.94001    091813130121   081814150121   071816200121
FF      ZCR08    0.94001    061821270121
FF      ZCR09    0.99325    061828340121   071835390121   081840410121
FF      ZCR09    0.99325    091842420121   111843430121   131844450121
```

```
FF      ZCR09    0.99325    171846460121
FF      ZCR10    0.98381    193407200121
FF      ZCR11    1.15173    193421340121
FF      ZCR12    1.01332    193435460121
FF      ZCR13    0.97941    353607080121   354009100121   354211120121
FF      ZCR13    0.97941    354413130121   354514150121   354616200121
FF      ZCR13    0.97941    354721270121
FF      ZCR14    0.95367    354728340121   354635390121   354540410121
FF      ZCR14    0.95367    354442420121   354243430121   354044450121
FF      ZCR14    0.95367    353646460121
$---v----1----v----2----v----3----v----4----v----5----v----6---v----7----v----8
GG      ZCR**    1.00    0.00    0.95    0.05
$-----------------------------------------------------------------
C       ADJ**    -1000.0
$--------1---------2---------3---------4---------5---------6---------7---------8
E   2  10 2651000.0  0.95500  0.00001     1.5   1.000    0.01 0    999
*PRINT   POWERS
*PRINT   FUELBURNUP
*PRINT   ZC LEVEL
*MAKE DAF CANDU-SITANS
*CLOSE
```

A sample fuelling simulation input file is provided below.

```
$-----------------------------------------------------------------
*USE DAF  CANDU-SITANS
$-----------------------------------------------------------------
*START   A. Morreale
CREATE RFSP SNAPSHOT W/*SIMULATE 0-10 FPD, TEST CASE; USING
RIGHT HANDED MODEL
 FROM DEC. 1998 TEST OF 2-GROUP OPTION
$-----------------------------------------------------------------
*MODEL    CANDU 9 RFSP SNAPSHOT TEST CASE 0-10 FPD
$-----------------------------------------------------------------
$  FUELING SIMULATIONS WITH SPATIAL AND BULK CONTROL
$ PROGRAM FOLLOWS FROM 2-Group_Sim-ITANspatial WITH
$  THE ITAN2B5 CHANNEL AGING SIMULATION
$  THIS IS NOW MODIFIED TO RUN FOR THE CANDU 9 PLATFORM
```

```
$-------------------------------------------------------------------------------
$  BEGIN FUELING DAY 1: MONDAY SEPTEMBER 12 2011
$-------------------------------------------------------------------------------
$ Initiate Reactor Local Parameters
$-------1---------2---------3---------4---------5---------6---------7--------8
*READ CARD
BLOCK    LOCAL PARMDENSITY
FORMAT   (8F10.4)
SET          1    6240 0.8074
$-------1---------2---------3---------4---------5---------6---------7--------8
*READ CARD
BLOCK    LOCAL PARMCOOL TEMP
FORMAT   (8F10.4)
SET          1    6240 288.135
$-------1---------2---------3---------4---------5---------6---------7--------8
*READ CARD
BLOCK    LOCAL PARMFUEL TEMP
FORMAT   (8F10.4)
SET          1    6240 586.83
$  Execution of SIMULATE module
$-------1---------2---------3---------4---------5---------6---------7--------8
*SIMULATE CANDU 9    9999999990.0              1          20
$  C -> current positions of devices
$  E -> Iteration Data
$-------1---------2---------3---------4---------5---------6---------7--------8
NUCIRC
FUELTEMP
WIMSHI   ITER 5      \
     NGRO 2      \
     MODT 63.0    \
     MODP 99.918  \
     MODB 0.0     \
     MODG 0.0     \
     COOLP 98.764 \
     POWR 1.0     \
     STEP 5 M     \
     BURNT NORM   \
     EDIT 0
```

```
$----------------------------------------------------------------------------
C       ADJ**    -1000.0
$----------------------------------------------------------------------------
$ SPATIAL AND BULK CONTROL CARDS
$---v----1----v----2----v----3----v----4----v----5----v----6----v----7----v----8
AA       20  1  20  14   1   3   1
BB       0.00001   0.003  1.00150   1.00    0.00    0.95     0.05
CC       ZCR01    ZCR02    ZCR03    ZCR04    ZCR05    ZCR06    ZCR07
CC       ZCR08    ZCR09    ZCR10    ZCR11    ZCR12    ZCR13    ZCR14
DD       ZCR**        300.0
EE       ZCR**    2.0
$*Z_NAME FXLVL X1X2Y1Y2Z1Z2 X1X2Y1Y2Z1Z2  X1X2Y1Y2Z1Z2 **
$$ (FF cards are the same as in CANDU-SITANS) $$
$---v----1----v----2----v----3----v----4----v----5----v----6----v----7----v----8
GG       ZCR**    1.00    0.00    0.95    0.05
$----------------------------------------------------------------------------
C       ADJ**    -1000.0
$----------------------------------------------------------------------------
$ INITIATE FUELING
$--------1---------2---------3---------4---------5---------6---------7---------8
U       TRUMOX
S      20110912  5  1
$ DECIDE THE PROPER CHANNEL TO REFUEL FOR THE ITAN2B CORE
$--------1---------2---------3---------4---------5---------6---------7---------8
R       T  6   0.001
$--------1---------2---------3---------4---------5---------6---------7---------8
E   2  10 2651000.0  0.95500  0.00001     1.5    1.000    0.01 0    999
$    print out POWERS, FUELBURNUP and FUEL TYPES for subsequent
verification
$
*PRINT   POWERS
*PRINT   FUELBURNUP
*PRINT   ZC LEVEL
*MAKE DAF CANDU-SF8D1
*CLOSE
```